GAS HYDRATE EQUILIBRIA IN THE PRESENCE OF ELECTROLYTE SOLUTIONS

by

Bahman Tohidi Kalorazi

Submitted for the Degree of Doctor of Philosophy

Department of Petroleum Engineering

Heriot-Watt University

Edinburgh, UK

September 1995

Dedicated to my parents, Yahya and Leyla

and my son, Afshin

TABLE OF CONTENTS

LIST OF SYMBOLS

a, b, c	Parameters of equation of state in Equations-2.6 and A.3
a^A	Asymmetric contribution in the non-density dependent mixing rules
a^C	Stands for the classic quadratic mixing rules in the non-density dependent mixing rules
a_w	Activity of water
A, B	Parameters defined by Equations-2.25 and 2.26
A, B, C, D, E	Constants in empirical Equations-2.20, 5.2, 5.4
A, B, n, m	Constants in Equation-3.2
B, C, D	Second, third, and fourth virial coefficients in Equation-A.2
C_{jm}	Langmuir constant for gas component j in cavity type m (Equation-2.11)
C_p	Heat capacity
d_m	Density of the salt free mixture (Equations-2.25 and 2.26)
f	Fugacity
F	Phase fraction
h	Molar enthalpy
h_{gs}	Gas-salt interaction coefficient
h_{ws}	Water-salt interaction coefficient
H	Hydrate phase
I	Ice phase
I	Ionic strength, Equation-2.24
k_{21}, l_{21}^o, l_{21}^1	Binary interaction parameters
L_1	Water-rich phase

L_2	Liquid hydrocarbon phase
m	Coefficient in the temperature function, Equation-2.8 and A.10
M	Molecular weight
n	Hydration number, number of water molecules per gas molecule
N	Number of non-electrolyte components
N	Integer equal to 4, 5, 10, or 11 in Equation-2.14
N	Quantity of material in Equation-A.1
N_A	Avogadro number, 6.02283E23
N_P	Number of data points
P	System pressure
P_3	3-phase (water-liquid hydrocarbon-vapour) equilibrium pressure
P_C	Critical pressure
P^{sat}	Vapour pressure
r	Centre to centre distance between two molecules
r_0	Distance between molecules at minimum potential energy
R	Universal gas constant
R	Cage occupancy ratio, (occupancy of small cavities)/(occupancy of large cavities)
R_c	Cavity radius in hydrate structure
T	Temperature, Kelvin
T_0	Reference temperature, 273.15 K
T_C	Critical temperature
T_r	Reduced temperature
u	Parameter of equation of state in Equations-2.6 and A.3
U	Cell potential in the hydrate model
v	Molar volume
v_c	Critical molar volume
V	Vapour phase
w	Parameter of equation of state in Equations-2.6 and A.3

w	Salt weight percent (Wt%) in Equations-5.2 and 5.4
x	Phase composition, mole fraction
y_i	Ionic strength fraction of electrolyte i
z_c	Coordination no. (no. of oxygen molecules at the periphery of each cavity)
z_i	Mole fraction of component i in the feed
Z	Compressibility factor
Z_c	Critical compressibility factor

Greek Letters

α	Hard core diameter
$\alpha(T_r)$	The temperature function in equation of state, Equation-2.8 and A.10
β	Empty hydrate lattice
γ	Activity coefficient
Γ	The potential energy of interaction between two molecules
Γ_0	Minimum potential energy between two molecules
Γ^*	Overall reduced ionic activity coefficient
δ^N	Polynomial given by Equation-2.14
Δ	Difference between properties
ε	The depth of the energy well, J
ε / κ	Optimisation parameter, K
η_m	Dielectric constant of the salt free mixture (Equations-2.25 and 2.26)
κ	Boltzmann's constant, R / N_A =1.38048E-23 J.K^{-1}
μ	Chemical potential
π	Number of phases in Equations-2.1 to 2.4
π	Constant equal to 3.141592654 in Equation-2.11
σ	Collision diameter
σ^*	Optimisation parameter, $\sigma^* = \sigma - 2\alpha$

θ_m	Number of cavities of type m per water molecule in unit cell (Equation-2.10)
φ	Fugacity coefficient
Ψ	Power in temperature function, Equation-2.8
ω	Acentric factor
Ω_a, Ω_b, Ω_c	Pre-multipliers of a, b, and c in EoS
Ω_u, Ω_w	Pre-multipliers of u and w in EoS

Subscripts and Superscripts

C	Critical
cal	Calculated
DH	Debye-Hückel
EL	Electrostatic contribution
exp	Experimental
gs	Gas-salt
H	Hydrate phase
hc	Hydrocarbon
i	Component index
I	Ice phase
ice	Ice
j	Phase (Equations-2.1 to 2.4) and component index
L_1	Water phase
m	Cavity type in hydrate model
m	The salt-free mixture
ns	Number of salts
o	Reference conditions
p	Index of polar component in Equation-A.18
r	Reduced

r	Reference phase
sat	Saturation
V	Vapour phase
w	Water
ws	Water-salt
β	Empty hydrate lattice
π	Number of phases

Abbreviations

ABS	Absolute value
ALS EoS	Adachi-Lu-Sugie Equation of State
BIP	Binary Interaction Parameters
CH	Cyclohexane
CRC	The Chemical Rubber Company (CRC Press Ltd.)
EoS	Equation of State
EQUIPHASE	Commercial computer package
FFW	Forties Formation Water (Table-6.8)
FOB	Objective function in the optimisation of the Kihara parameters
Frac	Fraction
GPSA	Gas Processors Suppliers Association
HHF	Heavy Hydrate Formers
HYSIM	Commercial computer package
IUPAC	International Union of Pure and Applied Chemistry
L_1-V-H	Liquid water-Vapour-Hydrate
L1-L2-V-H	Liquid water-Liquid hydrocarbon-Vapour-Hydrate
MCH	Methyl-Cyclo-Hexane
MWt	Molecular weight
NDD	Non-Density Dependent Mixing Rules

PIPEPHASE	Commercial computer package
PR EoS	The Peng-Robinson Equation of State
Pred	Predicted
PROCESS	Commercial computer package
SFW	Synthetic Formation Water (Table-6.8)
Sp. Gr.	Specific Gravity
VPT EoS	Valderrama modification of the Patel and Teja Equation of State

LIST OF TABLES

LIST OF FIGURES

ACKNOWLEDGEMENTS

I would like to take this opportunity to express my appreciation to all people both within and outside the Department for their help and encouragement during this study.

I am very much grateful to Professor Ali Danesh for his continuous support, encouragement and invaluable guidelines. I am also deeply grateful to Professor Adrian C. Todd for his constant support, interest and help.

I owe appreciation to my colleague Mr. R. W. Burgass for his close cooperation and fruitful discussions. I am also indebted to other friends and colleagues who helped me in different stages of this work. In particular, to Mr Andrew Kidd and Mr David Parker for their support and help with the computing facilities.

Finally, I wish to express my thanks to the Department of Petroleum Engineering/Heriot-Watt University and the Committee of Vice-Chancellors and Principals of the Universities of the United Kingdom for their financial support.

Gas Hydrate Equilibria in the Presence of Electrolyte Solutions

Bahman Tohidi Kalorazi

ABSTRACT

The application of extended sub-sea gathering networks and the transportation of unprocessed wellstreams are amongst favourable options for reducing field development and operational costs. These lines will convey a mixture of multi-phase fluids, including mixed electrolyte produced water, and liquid and gaseous hydrocarbons. One serious concern in the North Sea is that the above pipelines and process facilities are prone to hydrate formation, giving rise to pipeline blockage, operational problems, and other safety concerns. These can be avoided by either operating outside the hydrate region or transporting hydrates as slurry.

The economics of the first option is largely dependent on the accurate determination of the hydrate phase boundary, whereas the amount of hydrates to be transferred could be the main factor in the success of the second option. In this work both options have been addressed by investigating the effect of intermediate/heavy components of reservoir fluids and electrolyte solutions on the hydrate phase boundary, and the amount and composition of equilibrium phases in the presence of gas hydrates.

At typical pipeline conditions, up to seven phases could be potentially present. A single cubic equation of state has been used in modelling all fluid phases, i.e. vapour, liquid hydrocarbon, and water-rich phases. The ideal solid solution theory with the Kihara potential parameters has been used to model the hydrate phases (structure-I, II, and H), and ice has been treated as a sub-cooled liquid.

Abstract

The reliability of the above hydrate phase equilibria model is heavily dependent on the Kihara potential parameters. In this study, a novel and efficient method has been developed for optimising the Kihara potential parameters from hydrate dissociation pressure data of pure and binary systems for common hydrate formers.

Until recently, n-butane was regarded as the heaviest compound capable of hydrate formation. Now, particularly after the discovery of structure-H gas hydrates, it is known that compounds much heavier than n-butane can form gas hydrates. In this work, the effect of some of these heavy hydrate formers (present in significant quantities in oil and gas-condensate streams), on hydrate phase boundary has been investigated and modelled.

The water-cut in oil production is usually saline water and the salts dissolved in it inhibit hydrate formation to some extent. In this study, a rigorous thermodynamic model for single and mixed electrolyte solutions has been developed and validated. The model is able to predict the phase behaviour (vapour pressure and freezing point depression) of electrolyte solutions and the gas solubility in saline water, as well as the effect of electrolyte solutions on the hydrate phase boundary of synthetic and real reservoir fluids. The model predictions on hydrate phase boundaries of three reservoir fluids have been compared with four leading commercial packages. The results shows that the model is as reliable as, if not superior than, the commercial packages with the extra benefit of thermodynamic consistency. In addition, the model is able to predict the inhibition effect of mixed electrolyte solutions and the combined hydrate inhibition effect of methanol and formation water, which has not been reported by any of the commercial packages.

For systems where the hydrate prevention approach is economically non-viable, such as oil streams with high water-cut, the transfer of hydrates as a slurry in pipelines is an attractive option. In this case, information on the amount and composition of different phases, particularly the amount of hydrates, is a valuable information in the design and operation of the transfer-lines. The model developed in this work has been used to

predict the amount and composition of equilibrium phases in the presence of gas hydrates for synthetic systems and real reservoir fluids in a number of production scenarios. The predictions show good agreement with the experimental data.

In summary, this work presents a reliable thermodynamic model for predicting hydrate phase equilibria for real reservoir fluids in different production scenarios. The developed model could be used as a tool for the economical and safe design and operation of sub-sea transfer lines and production facilities prone to hydrate formation.

CHAPTER-1

INTRODUCTION

Gas hydrates are inclusion compounds in which certain non-polar or slightly polar molecules (guest) of a suitable size stabilise the crystalline structure formed by hydrogen bonded water molecules (host) under favourable conditions of pressure and temperature. The known hydrate structures are those of structure I, II, and the newly discovered H (Ripmeester et al., 1987), where each structure is composed of a certain number of large and small cavities. For hydrate structures to remain stable, a minimum fraction of their cavities have to be filled with the guest molecules. On the other hand, for a molecule to enter a cavity, its size should be smaller than a certain value. Therefore, large molecules which can enter only a limited number of large cavities require smaller molecules "help gas" to mainly fill some smaller cavities to stabilise hydrate crystals.

Gas hydrates resemble ice, but unlike ice they can form at temperatures well above the ice point. They have many applications in science and engineering (Tohidi et al., 1993d) and have recently been receiving attention as a potential energy resource (Sloan, 1990), following the discovery of substantial gas hydrate deposits in permafrost and ocean sediments. However, gas hydrates are considered troublesome for oil and gas industries, because transmission pipelines and hydrocarbon processing facilities could be blocked or damaged by hydrate formation. The hydrate problems can be avoided by either of the following two approaches:

- Preventing the hydrate formation by heating and/or insulating the pipe or by adding chemical inhibitors to operate outside the hydrate zone.
- Allowing the formation of hydrates, but modifying their growth in order to prevent aggregation of hydrate crystals and hence avoiding the blockage by transporting hydrates as slurry.

The first approach which is widely accepted and practised in the industry can become more economical by a more reliable determination of the hydrate free zone (Tohidi et al., 1992). The available information on hydrate formation and prevention have been mostly generated by studies on gaseous systems in pure water. Although the formation of hydrates in oil and gas-condensate systems or in the presence of electrolyte solutions is basically the same as that in gaseous mixtures and can be described similarly by numerical models, there are significant differences between the systems which warrant special considerations for oil transfer lines. Three areas pertinent to oil and/or gas-condensate transportation are as follows:

- The water-cut in oil wellstreams is formation water which inhibits hydrate formation to some extent. Efficient modelling of the inhibition effect of salts on hydrate formation will give the information required for a more economical use of expensive inhibitors.
- Oil and gas-condensate systems contain a significant amount of intermediate hydrocarbon compounds which are currently being considered as non-hydrate formers. Recent results (Ripmeester et al., 1987, 1991) indicate that some of these compounds are indeed strongly hydrate formers. The effect of these compounds on the hydrate boundary can be quite significant.
- Oil wellstreams may contain much higher water-cut than gas systems which can prohibit an economical use of chemical inhibitors to prevent hydrate formation. Furthermore, methanol, which is largely used as the chemical inhibitor, is very harmful for the environment. In these cases, the transfer of hydrates as slurry in pipeline, using low dosage additives, is an attractive option. The success of this option, which is

attracting significant industrial and academic attention, depends on predicting the amount of hydrates present in the pipeline and in equilibrium with other phases.

Both of the above approaches in avoiding hydrate problems are addressed in this study. This work will provide a more reliable prediction for boundary by investigating the effect of heavy hydrate formers (Danesh et al., 1993, 1994, Tohidi et al., 1995d) and electrolyte solutions (Tohidi et al., 1993b, 1994c, 1995a) on the hydrate phase boundary. In relation to the transfer of gas hydrates in the form of slurry, the developed model is able to predict the amount and composition of different phases at any given condition (Tohidi et al., 1993a, 1994b, 1995b)

In a typical hydrate problem a number of phases other than hydrates are potentially present. They are; vapour, liquid hydrocarbon, water-rich phase (with the possible presence of methanol and salts), ice, gas hydrates (structure-I, II, and H). In Chapter-2, the thermodynamic formulations for fugacity calculations in the different phases are detailed.

The hydrate phases have been modelled by the solid solution theory which requires the interaction energy between water and guest molecules in gas hydrates. In this work, the Kihara potential model, which has three parameters, has been used. A novel approach has been employed in the optimisation of the Kihara parameters, and is detailed in Chapter-3.

The phase behaviour modelling and the effect of the heavy hydrate formers on hydrate phase boundary are discussed in Chapter-4.

The produced water with oil is usually formation water and contains salts. In Chapter-5, a rigorous thermodynamic approach has been developed for modelling single and mixed electrolyte solutions, gas solubility in saline water (Tohidi et al., 1995c), and the hydrate inhibition effect of formation water.

Chapter-6 presents the validation and also the comparison of the model with four commercial packages. A wide range of experimental data, including synthetic and real reservoir fluids in different production scenarios, has been used in the validation of the model.

As mentioned earlier, the transportation of gas hydrates as slurry is an attractive option. The information on the amount of hydrates is required for the design and operation of such transfer-lines. As presented in Chapter-6, the developed numerical model is used to predict the amount and composition of different phases and the results are compared with the experimental data.

The conclusions of this work and some recommendations for future work is presented in Chapter-7.

CHAPTER-2

THERMODYNAMIC DESCRIPTION OF THE PHASES

2.1. INTRODUCTION

The term hydrates in inorganic chemistry refers to solid crystalline compounds which have water molecules as an integral part of the crystal e.g. $CuSO_4.5H_2O$. In the oil and gas industries, the term hydrates refers to a different kind of material. For a long time it was thought that they belonged to the above class of compounds and many researchers tried to find the stoichiometric formula. However, it is now understood that these compounds are not stoichiometric and do not have fixed composition.

Gas hydrates are crystalline molecular complexes formed from mixtures of water and suitably sized gas molecules. The water (host) molecules, upon hydrogen bonding, form unstable lattice structures with several interstitial cavities. The gas (guest) molecules can occupy the lattice cavities and when a minimum number of cavities are occupied the crystalline structure will become stable and solid gas hydrates will form, even at temperatures well above the ice point.

Gas hydrates were discovered in 1810 by Sir Humphery Davy (1811). This discovery was the starting point for a period in which the study of gas hydrates was regarded as a means of satisfying a scientific curiosity in which gas and water could be combined into a solid phase. In 1934, gas hydrates were found to be responsible for the blockage in oil and gas transmission lines (Hammerschmidt, 1934), hindering the production,

transportation, and processing of reservoir fluids. This discovery caused a significant increase in gas hydrate research with the aim of finding a solution to the above problems.

The other main milestone in the history of gas hydrates happened in the mid 1960's, when large amounts of gas in the form of gas hydrates were found in permafrost regions and in deep sea sediments. The current estimates show that the amount of energy in the gas hydrates is twice that of the total fossil fuel reserves (Sloan, 1990), indicating a huge source of energy which can be exploited in the right economical conditions. The proven reserves are scattered throughout the world, with particular concentrations in central America, Siberia, Alaska, and Canada. In the past decades gas hydrates have found many useful applications, making this an active research field in Petroleum and Chemical Engineering, as well as, in Geology, Biology, and the Environmental Sciences.

The two common forms of gas hydrates are known as structures-I and II, which have been investigated using X-ray diffraction methods by von Stackelberg and Müller (1954). They found that the unit cell of structure-I (sI) is a 12 Å cube consisting of 46 water molecules which form two types of cavities. The two small cavities are dodecahedra with 12 pentagonal faces (5^{12}), whereas the six large cavities are tetradecanhedra having two opposite hexagonal faces and twelve pentagonal faces ($5^{12}6^2$). The smaller cavities are almost spherical, whereas the larger cavities of structure-I are slightly oblate. Figure-2.1 shows the two types of cavities in structure-I for which the unit cell is presented in Figure-2.2.

The unit cell of structure-II (sII), which is a 17.3 Å cube with 136 water molecules, also contains two types of cavities. The 16 smaller cavities are distorted pentagonal dodecahedra and the 8 larger cavities are hexadecahedra having 4 hexagonal faces and twelve pentagonal faces ($5^{12}6^4$). The latter cavities are almost spherical in shape. The cavities and unit cell of structure-II are presented in Figures-2.1 and 2.3, respectively.

Ripmeester *et al.* (1987) reported a new hexagonal hydrate structure which requires both large and small molecules to stabilise the structure. They proposed that the new structure, due to its hexagonal shape, to be called structure-H (sH). According to the above authors, the unit cell has 34 water molecules forming a hexagonal lattice in which each side of the hexagonal face "a" is 12.26 Å, and the height "c" is 10.17 Å. The sH has three different types of cavities, i.e. three 5^{12} cavities which is common to all known hydrate structures, two new 12 faces $4^3 5^6 6^3$ cavities and one new large $5^{12}6^8$ cavity. The $4^3 5^6 6^3$ cavity has three square faces, six pentagonal faces, and three hexagonal faces, whereas the $5^{12}6^8$ has 12 pentagonal faces and eight hexagonal faces. The first two cavities accommodate the small molecules which act as help gases. The large cavity in this structure can accommodate larger molecules compared to the large cavities of structures-I and II. In fact, molecules in the size range of 7.5 to 8.6 Å can potentially form gas hydrates. The three types of cavities and a view of structure-H hydrates are presented in Figures-2.1 and 2.4, respectively.

A typical hydrate investigation may involve several phases i.e. vapour (V), water rich phase (L_1), liquid hydrocarbon (L_2), hydrate (H), and ice (I), which poses a complex phase equilibrium problem. The possible presence of salts and chemical inhibitors makes it even more complicated. As far as the hydrate phase boundary is concerned, a calculation algorithm was developed by Parrish and Prausnitz (1972), for determining the dissociation curve of a gas hydrate on a water-free basis. The algorithm operates by finding the point at which the chemical potential difference between the water in the hydrate phase and in the coexisting phases is zero. Despite its shortcomings, the above algorithm, which is known as conventional formulation, is still widely used in the industry. Briefly, in this type of calculation it is necessary to specify the number and type of phases present, the hydrocarbon composition on a water free basis, inhibitor concentration, and temperature (or pressure). After performing the calculations, the algorithm will provide values of pressure (or temperature), the composition of all phases and the amount of each hydrocarbon phase (Avlonitis, 1988).

However, there are several calculations that could provide important information regarding gas hydrate phases, in addition to potential hydrate formation conditions. These include the ability to perform flash calculations in the presence of gas hydrates, that is to calculate the amount of hydrate that will form under given circumstances, and the composition of all equilibrium phases. Also in multiphase equilibria, the number and identity of equilibrium phases is not known in advance which can play an important role in hydrate calculations. This has become particularly important after the discovery of structure-H. The appropriate approach to this problem is the minimisation of the Gibbs free energy, since if a system is at true equilibrium the Gibbs free energy is at a global minimum. All of the above calculations are possible when using multi-phase flash calculation procedures based on energy minimisation, such as the method developed by Michelsen (1982a, b) for a combination of vapour and liquid phases, in conjunction with an equation of state or an activity model.

2.2. GENERAL MULTI-PHASE FLASH (GMPF)

Bishnoi *et al.* (1989) adopted the methodology for multiphase equilibrium flash calculations of Gupta for systems containing gas hydrates. Cole and Goodwin (1990) rearranged the hydrate phase model to a form compatible with the Michelsen flash algorithm, to give explicit expressions for the fugacities of all the components of the hydrate lattice as functions of the overall composition of the hydrate phase. Avlonitis (1992) implemented the thermodynamic stability method by starting with all possible phases and eliminating those showing negative mass which is particularly suitable for multiphase equilibria calculations involving solid hydrate phases.

For a system at equilibrium, from a thermodynamic view point, the chemical potential of each component throughout the system must be uniform.

$$\mu_{i1} = \ldots = \mu_{ij} = \ldots = \mu_{i\pi} \qquad i = 1, \ldots, N \qquad (2.1)$$

where μ_{ij} is the chemical potential of component i in phase j, N is the number of components and π the number of phases. For an isothermal system this will reduce to equality of fugacity for each component in different phases.

$$f_{i1} = \ldots = f_{ij} = \ldots = f_{i\pi} \qquad i=1, \ldots, N \qquad (2.2)$$

In the most general case (i.e. when all components are present in all phases) there will be $N(\pi-1)$ such equations. In addition, material balance imposes another set of $N+\pi$ equations:

$$z_i = \sum_j^{\pi} F_j x_{ij} \qquad i=1, \ldots, N \qquad (2.3)$$

and

$$\sum_i^{N} x_{ij} = 1 \qquad j=1, \ldots, \pi \qquad (2.4)$$

where z_i is the specified composition of the feed, F_j the fraction in moles of phase j and x_{ij} the mole fraction of component i in phase j. Totally there are $\pi(N+1)$ equations with an equal number of unknowns, which may be chosen to be either (x_{ij}, F_j) at specified temperature T and pressure P or $(x_{ij}, F_{j=r}, P)$ at specified T with $F_r = 0$. The first is the typical isothermal flash problem and the second is the general phase boundary problem. In summary, the hydrate phase boundary and flash calculation is reduced to finding suitable thermodynamic models for calculating the fugacity in different equilibrium phases. In general more than one model is needed.

2.3. VAPOUR, LIQUID HYDROCARBON, AND SALT FREE WATER PHASES

In this study, the well proven (Danesh *et al.*, 1991) Valderrama (Valderrama, 1990) modification of the Patel and Teja equation of state (VPT EoS) with the non-density dependent (NDD) mixing rules (Avlonitis *et al.*, 1994) as well as the popular Peng-

Robinson (Peng and Robinson, 1976, Robinson and Peng, 1978) equation of state (PR EoS) have been used for the calculation of fugacity in the vapour and liquid hydrocarbon phases. The gas-water Binary Interaction Parameters (BIP) have been determined by matching published binary vapour liquid equilibria data.

The PR and the VPT EoS are explained in Appendix-A. The two mixing rules, namely, classical and non-density dependent mixing rules are also explained in the above appendix. Using the above EoS and associated mixing rules the fugacity of each component in all fluid phases could be calculated from:

$$f_i = x_i \varphi_i P \tag{2.5}$$

where f_i, x_i, and φ_i are the fugacity, the mole fraction, and the fugacity coefficient of component i in vapour or liquid phases. P is the system total pressure.

Optimisation of Water Parameters in EoS

As detailed in Appendix-A, the PR and the VPT EoS can be expressed by the following general form:

$$P = \frac{RT}{v-b} - \frac{a}{v^2 + uv + w} \tag{2.6}$$

where

$$a = \Omega_a \alpha(T_r) \frac{R^2 T_C^2}{P_C} \tag{2.7}$$

The temperature function $\alpha(T_r)$ is generally expressed by:

$$\alpha(T_r) = \{1 + m[1 - (T_r)^{\Psi}]\}^2 \tag{2.8}$$

where ψ=0.5 and other variables in Equations-2.6 through 2.8 are explained in Appendix-A.

Avlonitis *et al.* (1994) relaxed the constrain of ψ=0.5 in the VPT EoS for water and methanol and regressed Equation-2.8 for temperatures up to the critical point to determine m and ψ.

In this work, the Avlonitis *et al.* (1994) approach is extended to the PR EoS. Furthermore, since the above temperature range is beyond the interest of this study, experimental water vapour pressure (P_{exp}^{sat}) data in the range of 258.15 K to 374.15 K were used for determination of m and ψ for water in the PR and the VPT EoS, with $ABS[(P_{cal}^{sat} - P_{exp}^{sat})/P_{exp}^{sat}]$ as objective function.

The above modification significantly improved the prediction of water fugacity, particularly for the PR EoS.

2.4. HYDRATE PHASES

From a modelling view point, the sizes of different cavities in the different hydrate structures are required. This information on structures-I and II are available since the mid 1950s. In relation to structure-H, although powder diffraction studies have identified the structure-H, definitive structural determination needs single-crystal diffraction studies. Recently, Mehta and Sloan (1994b) proposed a thermodynamic model for structure-H and gave approximate values for the sizes of cavities in structure-H. Table-2.1 summarises the unit cell characteristics for the three known hydrate structures of I, II, and H.

Knowing the three types of hydrate structures, the structure formed depends primarily on the size of the molecules involved. Very small molecules, such as helium, hydrogen, and neon do not form gas hydrates, because they are too small to be trapped in any of the

above mentioned cavities. Molecules like nitrogen and oxygen are reported to preferentially form sII gas hydrates (Davidson *et al.*, 1986b, 1987), as this structure contains the smallest size cavities. Slightly larger molecules, such as methane or, ethane, are known to form sI hydrates. The stable hydrate structure for larger molecules such as isobutane is sII, as these molecules cannot enter any of the cavities of sI, but enter the large cavities of sII. For binary and multicomponent systems, generally the size of the largest molecule (with a significant quantity) determines the hydrate structures. Hydrates made of pure compounds are known as simple gas hydrates. However, some large molecules such as normal butane cannot form simple hydrates and they need some smaller molecules, known as help gases, to fill small cavities and stabilise the hydrate structure. These type of hydrates are known as double hydrates. Larger molecules, such as methylcyclohexane can form structure-H double gas hydrates.

van der Waals and Platteeuw (1959) derived the basic statistical thermodynamic equations by using the ideal solution theory. In their approach, hydrate-forming molecules are viewed as adsorbed in the cavity sites which is described by the Langmuir adsorption theory. The fundamental assumptions in developing this theory are:

1. The host molecules contribution to the free energy is independent of the occupation of the cavity. This assumption also implies that the encased molecule does not distort the cavity.
2. Each cavity can contain at most one guest molecule, which cannot diffuse from the cavity.
3. There are no interactions between the guest molecules, i.e. the energy of an encased guest molecule is independent of the number and types of other guest molecules.
4. No quantum effects are needed; classical statistics are valid.

The fugacity of water in the hydrate phase, f_w^H, is given by (Anderson and Prausnitz, 1986):

$$f_w^H = f_w^\beta \exp(-\frac{\Delta\mu_w^{\beta-H}}{RT}) \qquad (2.9)$$

where f_w^β is the fugacity of water in the empty hydrate lattice. $\Delta\mu_w^{\beta-H}$ is the chemical potential difference of water between the empty hydrate lattice, μ_w^β, and the hydrate phase, μ_w^H, and is obtained from the van der Waals and Platteeuw (1959) expression (Parrish and Prausnitz, 1972):

$$\Delta\mu_w^{\beta-H} = \mu_w^\beta - \mu_w^H = RT\sum_m \theta_m \ln(1 + \sum_j C_{jm} f_j) \qquad (2.10)$$

where θ_m is the number of cavities of type m per water molecule in the unit cell (Table-2.1), and f_j is the fugacity of the gas component j. C_{jm} is the Langmuir constant, which accounts for the guest-water interaction in the cavity. Numerical values for the Langmuir constant can be calculated if a model for the guest-host interaction is chosen, as shown by van der Waals and Platteeuw (1959):

$$C_{jm}(T) = \frac{4\pi}{\kappa T}\int_0^\infty \exp(-\frac{U(r)}{kT}) r^2 dr \qquad (2.11)$$

where κ is the Boltzmann's constant and $U(r)$ is the spherically symmetric cell potential in the cavity, with r measured from centre, and depends on the intermolecular potential function chosen for describing the encaged guest-water interaction. Here, the Kihara potential parameters (McKoy and Sinanoglu, 1963) with a spherical core are used:

$$\Gamma(r) = \infty \qquad r = 2\alpha \qquad (2.12a)$$

$$\Gamma(r) = 4\varepsilon[(\frac{\sigma - 2\alpha}{r - 2\alpha})^{12} - (\frac{\sigma - 2\alpha}{r - 2\alpha})^6] \qquad r > 2\alpha \qquad (2.12b)$$

where $\Gamma(r)$ is the potential energy of interaction between two molecules, α is the hard core radius, $\sigma = \sigma^* + 2\alpha$ is the collision diameter and ε is the depth of the energy well. The Kihara model is explained in more details in Chapter-3.

McKoy and Sinanoglu (1963) summed up all these guest-water binary interactions inside the cell to yield an overall cell potential:

$$U(r) = 2z_c\varepsilon[\frac{(\sigma^*)^{12}}{R_c^{11}r}(\delta^{10} + \frac{\alpha}{R_c}\delta^{11}) - \frac{(\sigma^*)^6}{R_c^5 r}(\delta^4 + \frac{\alpha}{R_c}\delta^5)] \qquad (2.13)$$

where z_c is the coordination number of the cavity (Table-2.1), that is, the number of oxygen molecules at the periphery of each cavity, R_c is the radius of the cavity (Table-2.1), and δ^N is a polynomial given by the equation:

$$\delta^N = [(1 - \frac{r}{R_c} - \frac{\alpha}{R_c})^{-N} - (1 + \frac{r}{R_c} - \frac{\alpha}{R_c})^{-N}] \qquad (2.14)$$

here N is an integer equal to 4, 5, 10, or 11. The fugacity of water in the empty hydrate lattice, f_w^β in Equation-2.9, is given by:

$$f_w^\beta = f_w^{I/L_I} exp(\frac{\Delta\mu_w^{\beta-I/L_I}}{RT}) \qquad (2.15)$$

where f_w^{I/L_I} is the fugacity of pure ice or liquid water and the quantity inside the parentheses is given by the following equation:

$$\frac{\Delta\mu_w^{\beta-I/L_I}}{RT} = \frac{\mu_w^\beta(T,P)}{RT} - \frac{\mu_w^{I/L_I}(T,P)}{RT} = \frac{\Delta\mu_w^0}{RT_0} - \int_{T_0}^{T}\frac{\Delta h_w^{\beta-I/L_I}}{RT^2}dT + \int_0^P\frac{\Delta v_w^{\beta-I/L_I}}{RT}dP \qquad (2.16)$$

where $\frac{\mu_w^\beta}{RT}$ and μ_w^{I/L_I} are the chemical potential of the empty hydrate lattice and of pure water in the ice (I) or the liquid (L_I) state, respectively. P is the equilibrium pressure and T_0 is the absolute temperature at the ice point. $\Delta\mu_w^0$ is the reference chemical potential difference between water in the empty hydrate lattice and pure water in the ice phase at 273.15 K (Table-2.2). $\Delta h_w^{\beta-I/L_I}$ and $\Delta v_w^{\beta-I/L_I}$ are the molar enthalpy and molar volume differences between an empty hydrate lattice and ice or liquid water, respectively. Table-2.2 presents the $\Delta v_w^{\beta-I/L_I}$ for different hydrate structures. $\Delta h_w^{\beta-I/L_I}$ is given with the following equation:

$$\Delta h_w^{\beta-I/L_I} = \Delta h_w^0 + \int_{T_0}^{T} \Delta C_{pw} dT \qquad (2.17)$$

where Δh_w^0 is the enthalpy difference between the empty hydrate lattice and ice at the ice point and zero pressure (Table-2.2). The heat capacity difference between the empty hydrate lattice and the pure liquid water phase, ΔC_{pw}, is also temperature dependent and the equation recommended by Holder *et al.* (1980) is used:

$$\Delta C_{pw} = -37.32 + 0.179(T - T_0) \qquad T > T_0 \qquad (2.18)$$

where ΔC_{pw} is in $J.mol^{-1}.K^{-1}$. Furthermore, the heat capacity difference between hydrate structures and is set equal to zero. Table-2.2 presents the reference properties of the hydrate structures used in this work, as reported by Parrish and Prausnitz (1972), Dharmawardhana *et al.* (1980), and Mehta and Sloan (1994b).

Determination of the Kihara Potential Parameters

The main data required by the statistical thermodynamic model is the interaction energy between water and guest molecules in the hydrate. A simplified functional form is adopted for the potential energy of a guest molecule in the hydrate cavity, and the parameters in this potential are then fitted to experimental data. In this work, the Kihara

potential parameters have been used which are determined with a novel approach as detailed in Chapter-3.

2.5. ICE PHASE

The fugacity of a pure solid can be rigorously calculated by correcting the saturation fugacity at the same temperature by an exponential factor (the Poynting correction). The details of the method can be found in Prausnitz et al. (1986) and Anderson and Prausnitz (1986). The above authors regarded ice as a sub-cooled liquid (pure hypothetical-liquid water) and used the following formulation to calculate the fugacity of water in the ice phase:

$$f_w^l = P_{ice}^{sat} \times (\varphi_w^V)_{P_{ice}^{sat}} \times exp((v_{ice}/RT) \times (P - P_{ice}^{sat}) \qquad (2.19)$$

where P is the system pressure and f_w^{ice} stands for the fugacity of water in the ice phase. $(\varphi_w^V)_{P_{ice}^{sat}}$ is water fugacity coefficient in the vapour phase at a pressure equal to the ice vapour pressure. P_{ice}^{sat} and v_{ice} are the ice vapour pressure and the ice molar volume, respectively.

Ice vapour pressure data (CRC handbook of Chemistry and Physics, 1988, 89) in the range of 183.15 to 273.15 K (-90 to 0°C) were used in optimising the parameters of the following empirical equation:

$$P_{ice}^{sat} = Log_{10}(A/T + BLogT + CT + DT^2 + E) \qquad (2.20)$$

where P_{ice}^{sat} is the ice vapour pressure in mmHg absolute. The optimised constants, A, B, C, D, and E are -1.032E3, 5.106, -9.771E-2, 7.036E-5, and -9.851, respectively. The above correlation gave the maximum absolute error of less than 0.25% with the experimental data in the entire temperature range. Experimental and predicted ice vapour pressure is presented in Figure-2.5.

Ice density data as a function of temperature at atmospheric pressure (Hobbs, 1974), were used to calculate the ice molar volume, v_{ice}. Figure-2.6 presents the ice molar volume vs temperature. The best linear fit for the range of interest, as shown in the above figure, is:

$$v_{ice} = 19.655 + (2.2364E-3) \times (T - 273.15) \qquad (2.21)$$

where v_{ice} is ice molar volume in $cm^3.mole^{-1}$.

2.6. SALINE WATER PHASE

In this work, fugacities in the water rich phase are calculated by combining the VPT or the PR EoS with the Debye-Hückel electrostatic contribution for taking into account the effect of salt.

$$ln\,\varphi_i = ln\,\varphi_i^{EOS} + ln\,\gamma_i^{EL} \qquad i=1, \ldots, N \qquad (2.22)$$

where N is the number of non-electrolyte components, φ_i is the fugacity coefficient of component i, φ_i^{EOS} is the fugacity coefficient of component i neglecting the electrostatic effect calculated by an EoS, and γ_i^{EL} is the contribution of the electrostatic term. Using the Debye-Hückel activity coefficient, the final form of the second term in Equation-2.22 would be (Aasberg-Petersen, 1991):

$$ln\,\gamma_i^{DH} = \frac{2AM_m h_{is}}{B^3} f(BI^{1/2}) \qquad (2.23)$$

where M_m is the salt-free mixture molecular weight determined as a molar average and h_{is} is the interaction coefficient between the dissolved salt and a non-electrolytic compound. The optimisation of the water-salt and gas-salt interaction coefficients is detailed in Chapter-4. The function $f(BI^{1/2})$ is obtained from:

$$f(BI^{1/2}) = 1 + BI^{1/2} - 1/(1 + BI^{1/2}) - 2\ln(1 + BI^{1/2}) \qquad (2.24)$$

where I is the ionic strength and the parameters A and B are given by:

$$A = 1.327757 \times 10^5 d_m^{1/2} / (\eta_m T)^{3/2} \qquad (2.25)$$

$$B = 6.359696 \times d_m^{1/2} / (\eta_m T)^{1/2} \qquad (2.26)$$

where η_m is the salt free mixture dielectric constant which can be calculated from:

$$\eta_m = x_w \eta_w \qquad (2.27)$$

x_w and η_w are the salt free mole fraction and dielectric constant of water, respectively. The dielectric constants of dissolved non-electrolyte compounds have been neglected, relative to that of water.

The two equations of state (PR and VPT EoS) used in vapour phase calculations have been employed here as well in the calculation of the fugacity coefficient from EoS in the saline water rich phase.

2.7. CONCLUSIONS

In a typical hydrate problem several phases are potentially present. In this chapter, the requirement for thermodynamic equilibrium and the models to determine fugacities in different phases have been explained. A single EoS has been used for fugacity calculations in all fluid phases, whereas the hydrate phases are described by the solid solution theory and ice is regarded as a sub-cooled liquid. The solid solution theory uses the Kihara potential for expressing the guest-water molecular interaction. The optimisation of the Kihara parameters is detailed in Chapters-3 and 4.

In modelling the water-rich phase, an electrostatic contribution term was added to the fugacity coefficient expression to take into account the effect of salts. This approach uses one adjustable parameter known as the interaction coefficient, and is detailed in Chapter-5.

Three main contributions presented in this chapter are; the optimisation of water parameters in the two EoS, a new correlation for ice vapour pressure, and ice molar volume calculations.

Generally water vapour pressure data from boiling point to critical point are used to optimise the water parameter in EoS. In this work, water vapour pressure data in the temperature range of 258.15 K to 374.15 K (-15 to 101 °C) have been used to optimise the water parameter in the EoS. The above approach has an important impact on the accuracy of calculation, particularly for the PR EoS.

Ice vapour pressure data from the CRC Handbook of Chemistry and Physics (1988, 89) in the temperature range of 183.15 to 273.15 K (-90 to 0°C) were employed in developing a more accurate correlation for ice vapour pressure calculations. The resulting correlation had a maximum error of less than 0.25%. Finally, recent data on the density of ice (Hobbs, 1974) were used to develop a new correlation for calculating ice molar volume. The above data are required in calculating the water fugacity in the ice phase.

Table-2.1. Hydrate unit cell characteristics of structures-I, II, and H.

Structure	I†		II†		H#		
Crystal system	Cubic		Cubic		Hexagonal		
Lattice parameter, Å	12		17.3		a=12.26, c=10.17		
H_2O / unit cell	46		136		34		
Total No. of cavities / unit cell	8		24		6		
Cavity type	5^{12}	$5^{12}6^2$	5^{12}	$5^{12}6^4$	5^{12}	$4^35^66^3$	$5^{12}6^8$
Radius of cavity, Å	3.95	4.3	3.91	4.73	3.91	4.06	5.71
Coordination No.	20	24	20	28	20	20	36
Cavities / unit cell	2	6	16	8	3	2	1

† Avlonitis, (1992).

Mehta and Sloan, (1994b).

Table-2.2. Thermodynamic reference properties for structures-I, II, and H.

	Structure-I	Structure-II	Structure-H
$\Delta\mu_w^0$ (J.mol^{-1})	1297#	937#	914.38¤
Δh_w^0 (J.mol^{-1})†	1389#	1025#	846.57¤
Δv_w (cm^3.mol^{-1})††	3.0§	3.4§	3.85¤

† In the liquid water region subtract 6009.5 J.mol^{-1} from Δh_w^0.

†† In the liquid water region add 1.601 cm^3.mol^{-1} to Δv_w.

Dharmawardhana *et al.*, (1980).

§ Parrish and Prausnitz, (1972).

¤ Mehta and Sloan, (1994b).

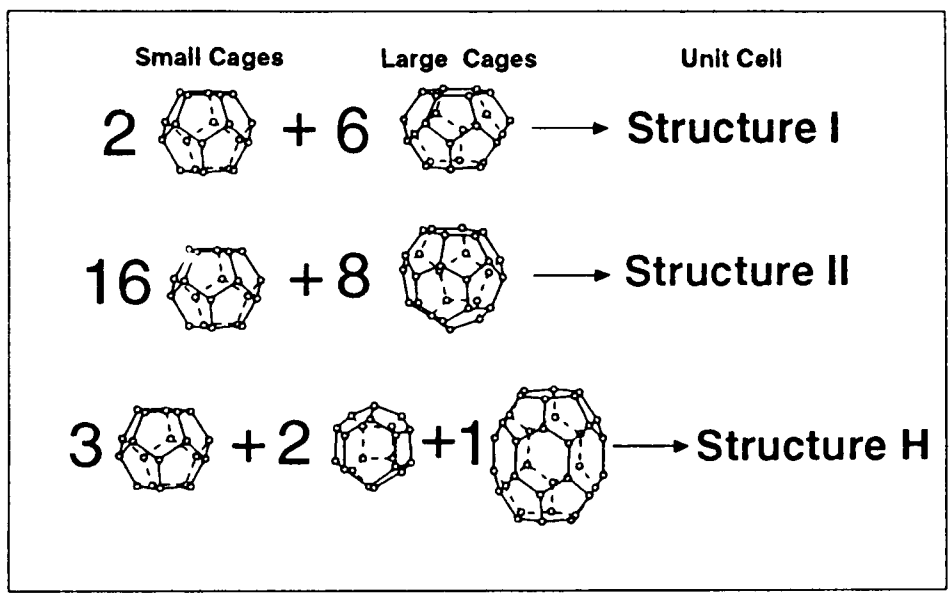

Figure-2.1 Cavities in gas hydrate structures.

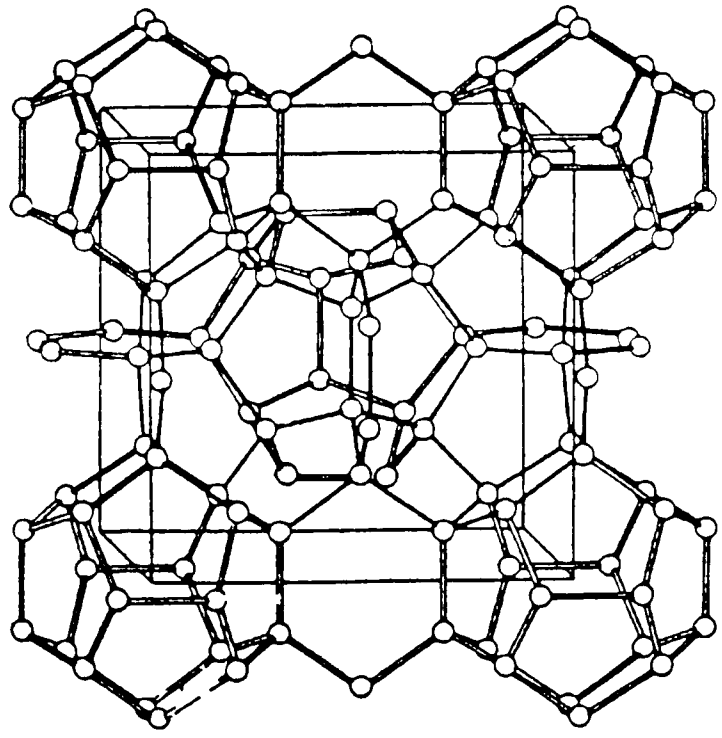

Figure-2.2 Unit cell of structure-I gas hydrates.

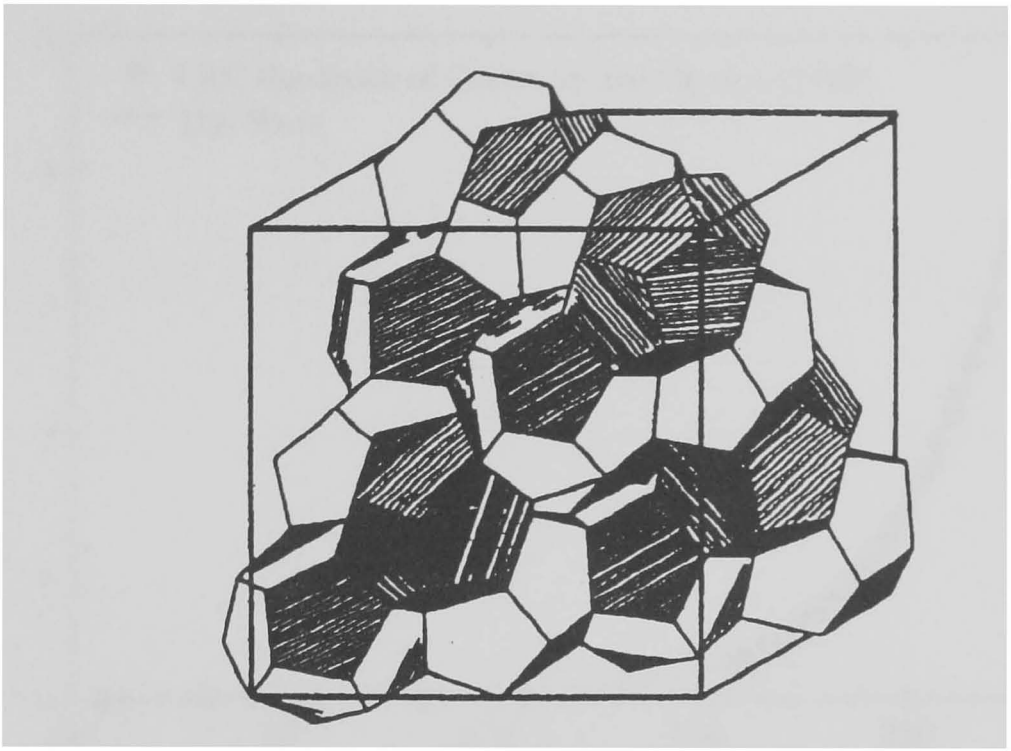

Figure-2.3 Unit cell of structure-II gas hydrates.

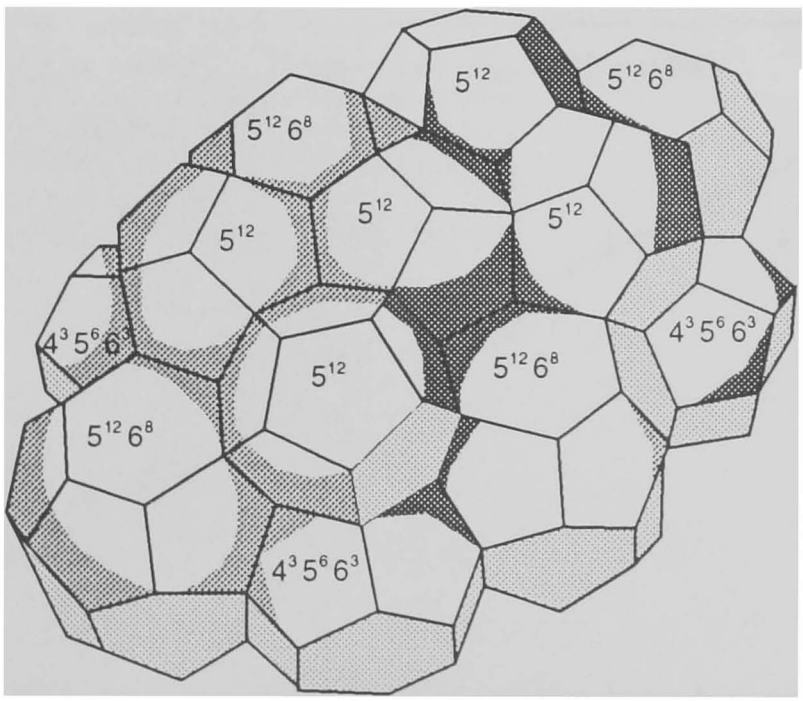

Figure-2.4 A view of structure-H gas hydrates.

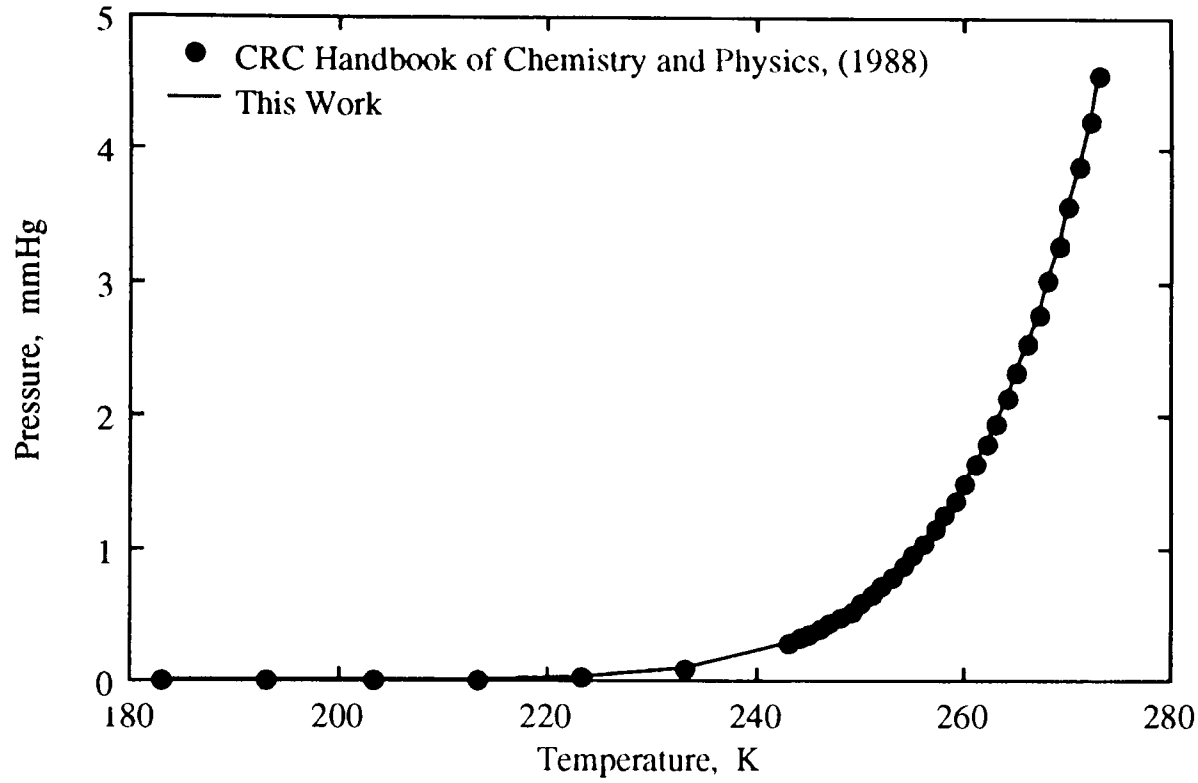

Figure-2.5 Experimental and predicted ice vapour pressure.

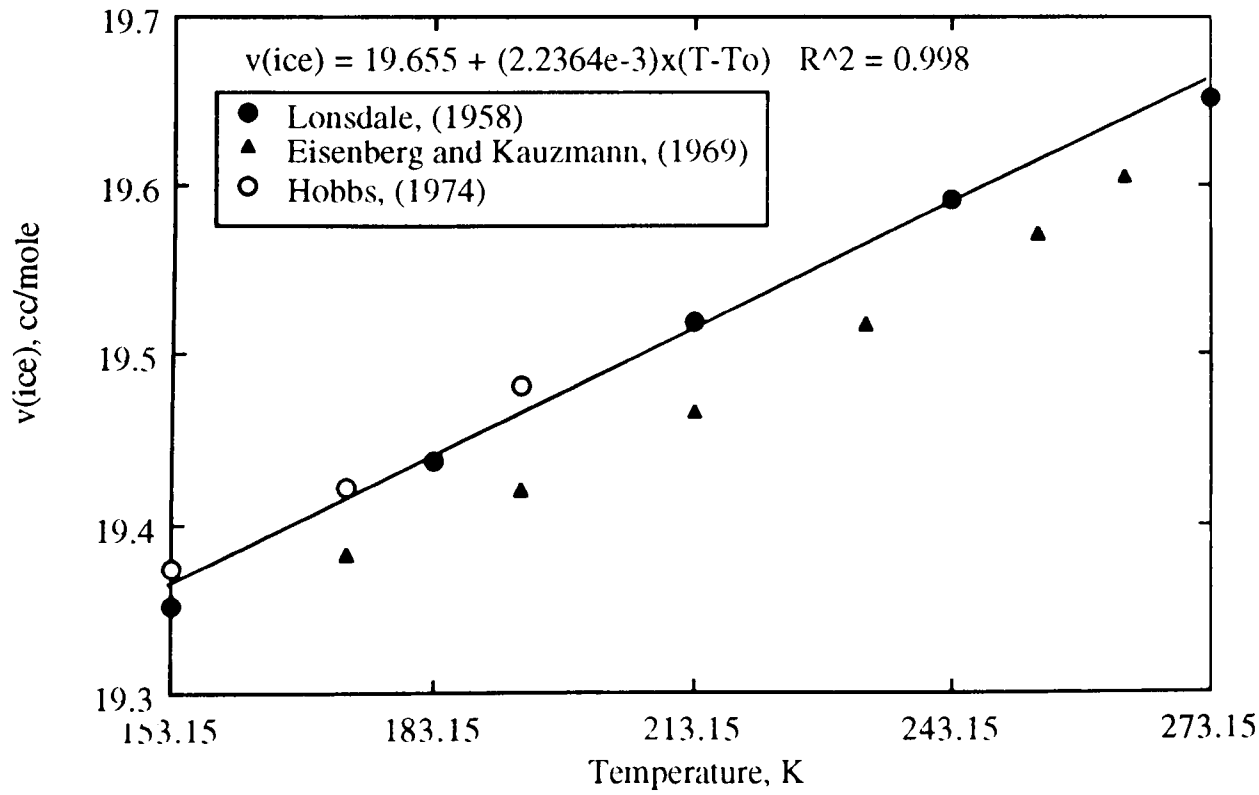

Figure-2.6 Molar volume of ice as a function of temperature.

CHAPTER-3

DETERMINATION OF THE KIHARA PARAMETERS

3.1. INTRODUCTION

After Hammerschmidt's (1934) discovery that gas hydrates are responsible for blockage in natural gas pipelines, prediction of hydrate formation pressure at a given temperature, or vice versa, became an important consideration in the design and operation of pipelines and processing facilities.

The GPSA Engineering Data Book (1981) presents a series of charts for natural gas of varying specific gravities, which may be used for estimating the hydrate formation conditions. However, the classical method for hydrate predictions is based upon empirically determined vapour-solid equilibrium constants (K_{VS} values), as proposed by Katz (Katz and Lee, 1990, Campbell, 1976). The hydrate formation pressure or temperature is then calculated similarly to the conventional saturation pressure K value equilibria. In developing their distribution method, Katz and co-workers noticed that gas hydrates are likely to be solid solutions (Carson and Katz, 1942). After the determination of the hydrate crystal structure in the early 1950's, and the discovery of the fact that gas hydrates are non-stoichiometric compounds, it emerged that gas hydrates are solutions of the hydrate formers in a metastable cage-structure formed by water molecules. van der Waals and Platteeuw (1959) used the statistical thermodynamic method to derive the basic equations, as presented in Chapter-2, to correlate the chemical potential of water in the empty and the filled hydrate lattices .

Determination of the Kihara Parameters

Most of the current numerical models for hydrate equilibria, including this work, are based on the statistical thermodynamic theory of inclusion compounds as presented in Chapter-2. Recalling Equation-2.10:

$$\Delta\mu_w^{\beta-H} = \mu_w^{\beta} - \mu_w^{H} = RT\sum_m \theta_m \ln(1 + \sum_j C_{jm} f_j) \qquad (2.10)$$

C_{jm} is a constant, similar to the Langmuir's constant, taking into account the guest-host interaction in the cavity. Numerical values for C_{jm} can be calculated if a model for the gas-water interaction in the hydrate cavity is chosen. As explained later in this chapter, the Kihara model has been used in this work.

Considering the information in the open literature, all efforts in the optimisation of the potential parameters in the Kihara model are based on using either the second virial coefficient, hydrate dissociation pressure data, heat capacity data, or their combinations. The so-optimised parameters can predict simple hydrate dissociation pressures accurately, but are less accurate in predicting binary and multicomponent systems, particularly those containing heavy compounds.

In this study, it was found that different combinations of the Kihara parameters are able to predict the dissociation pressures. In other words, depending on the number and type of data, the experimental error band, and the EoS used for fugacity calculations, different combinations of the parameters will minimise the objective function. Therefore, it is not strange that different researchers have reported different values for the parameters.

These results lead us to believe that, most probably, by using the above mentioned sets of data, we do not assign proper contributions to different cavity types, and compositional data must be used in the optimisation, to specify the unique set of parameters for each gas.

In this chapter the Kihara parameters for the common hydrate formers, such as, methane, ethane, propane, isobutane, normal butane, carbon dioxide, hydrogen sulphide, and nitrogen are determined. The determination of the Kihara potential parameters for the so-called heavy hydrate formers (HHF), including those forming structure-H, is discussed in the next chapter.

Experimental dissociation pressure and compositional data in the L_1-V-H and L_1-L_2-V-H region, generated in this laboratory, in addition to dissociation pressure data in open literature, have been used in the optimisation of the Kihara parameter and the validation of the model. A complete set of experimental data, equipment, and test procedures are reported by R. W. Burgass, (1995).

In this chapter after describing the Kihara model, two different methods have been used in the optimisation of its parameters. In the first method the aim is to find the Kihara parameters for xenon using the unique available data on cage occupancy and hydration number (Ripmeester *et al.*, 1981 and Davidson *et al.*, 1986a) for xenon gas hydrates, in addition to conventional dissociation pressure data. Then, use xenon as the key compound and determine the Kihara parameters for C_1, C_2, and C_3 from the dissociation pressure and unique *compositional data* of their binaries with xenon (Burgass, 1995).

The second approach is based on the assumption that the Kihara parameters for those compounds which could be trapped in different hydrate structures could be found from the intersection of their ε/κ vs σ^* plots for different structures. In this approach, propane has been selected as the key compound for the reasons detailed later in this chapter. Finally, a method for future work in the optimisation of the Kihara parameters is suggested.

3.2. KIHARA POTENTIAL PARAMETERS

Excluding the reference state parameters for gas hydrates, the main data required by the statistical thermodynamic model is the interaction energy between water and guest

molecules in the hydrate. For calculating the above interaction energy, a molecular potential function for the model is necessary. The simplest of which is a model based on the ideal gas law, which assumes the size of molecules to be equal to zero and there are no attractive or repulsive forces between the molecules. This model is known as the ideal gas potential which has no adjustable parameter. Taking into account the non-zero size of molecules by considering the molecules to be like a billiard ball, the model will change to what is known as the hard-sphere model. This model has one adjustable parameter, α, the hard sphere radius. It neglects the attractive force and assumes that the repulsive force becomes infinitely large when two molecules touch. The potential function $\Gamma(r)$ for this simplistic model is given by:

$$\Gamma(r) = 0 \qquad r > 2\alpha \tag{3.1a}$$

$$\Gamma(r) = \infty \qquad r = 2\alpha \tag{3.1b}$$

Lennard-Jones proposed another model for gas molecules in which each molecule is like a soft sphere. They represented the potential function using the following equation (Prausnitz, 1969) in which both the repulsive and attractive forces between molecules are taken into account :

$$\Gamma_{total} = \Gamma_{repulsive} + \Gamma_{attractive} = \frac{A}{r^n} - \frac{B}{r^m} \tag{3.2}$$

A, B, n, and m are positive constants with $n>m$. Equation-3.2 gives the potential energy of two molecules as a function of their separation. The above potential function passes through a minimum, Γ_0, at some distance r_0. In relation to m and n, London (1937) showed that, according to the theory of dispersion, the value of m is equal to 6. Assuming $\varepsilon=-\Gamma_0$, and $n=12$, and after algebraic rearrangement, the Lennard-Jones potential function becomes:

$$\Gamma(r) = 4\varepsilon[(\frac{\sigma}{r})^{12} - (\frac{\sigma}{r})^{6}] \qquad (3.3)$$

where $\Gamma(r)$ is the potential energy of interaction between two molecules, ε is the minimum potential energy, known as the depth of the energy well, and σ is the collision diameter, the distance where Γ=0. The above equation has two adjustable parameters, namely, σ and ε.

van der Waals and Platteeuw (1959) assumed that the potential energy of a gas molecule is given by the spherically symmetrical potential proposed by the above potential function. McKoy and Sinanoglu (1963) refined the van der Waals and Platteeuw method using the Kihara potential. They concluded that although the Lennard-Jones 12-6 potential is satisfactory for the hydrates of the monatomic gases and CH_4, for the rod-like molecules, the Kihara potential is more suitable.

According to the Kihara's model for spherically symmetric molecules, each molecule has an impenetrable (hard) core surrounded by penetrable (soft) electron clouds. Kihara's potential function is identical to that of Lennard-Jones except that the intermolecular distance is taken not as that between molecular centres but rather as the minimum distance between the surfaces of the molecules cores. Figure-3.1 shows the Kihara's molecular model and the appropriate potential function:

$$\Gamma(r) = \infty \qquad r = 2\alpha \qquad (3.4a)$$

$$\Gamma(r) = 4\varepsilon[(\frac{\sigma - 2\alpha}{r - 2\alpha})^{12} - (\frac{\sigma - 2\alpha}{r - 2\alpha})^{6}] \qquad r > 2\alpha \qquad (3.4b)$$

The Kihara model has three adjustable parameters, namely, α, σ, and ε, which are the hard core radius, collision diameter, and the depth of the potential well, respectively.

Determination of the Kihara Parameters

In the above two works (van der Waals and Platteeuw, 1959 and McKoy and Sinanoglu, 1963), the potential parameters were determined from the second virial coefficient. Parrish and Prausnitz (1972) were the first to develop a computer algorithm for hydrate phase boundary calculations and to extend the statistical thermodynamic method to multicomponent systems. In their work, they also used the Kihara's potential with a spherical core with parameters estimated from second virial coefficient data.

Using Lennard-Jones potential function, Saito *et al.* (1964) were the first to use simple hydrate dissociation pressure data to optimise the potential parameters. Sloan (1990) who used the Kihara potential function, also noticed that the potential parameters from the second virial coefficient and viscosity data are not suitable for hydrate calculations. He used simple hydrate dissociation data to determine the Kihara parameters for seven simple hydrate formers. The approach of optimisation of the Potential parameters showed substantial improvement in predicting the hydrate dissociation pressure.

As mentioned earlier, the Kihara potential function has three adjustable parameters, namely, α, σ, and ε, which are the hard core radius, collision diameter, and the depth of energy well, respectively. However, in this work the optimisation process is restricted to σ and ε, as the dissociation pressure was found to be not very sensitive (Holder and Hand, 1982) to the hard core radius, α. The hard core radii for the compounds in this chapter are fixed to the values calculated from the second virial coefficient (Avlonitis, 1992). Referring to Equations 2.11 to 2.13, for simplicity, σ^* (where $\sigma^*=\sigma-2\alpha$) and ε/κ have been chosen as optimisation parameters, instead of σ and ε, respectively.

3.3. XENON AS THE KEY COMPOUND

As mentioned earlier, the hydrate phase equilibria calculations are very sensitive to the Kihara potential parameters, and the parameters calculated from the second virial coefficient and/or viscosity data are not suitable for hydrate calculations (Sloan, 1990). This and the

fact that compositional data are more sensitive to the Kihara parameters, convinced us to try the use of compositional data for the optimisation of the Kihara parameters.

Current techniques are not very efficient in finding the distribution of guest molecules between cavities for simple gas hydrates of hydrocarbon gases. Whereas, by using the binary systems, comprised of two hydrate formers, the amount and composition of different phases can be measured. In fact, a compositional test in the L_1-V-H region for a binary gas mixture can provide the ratio of the two gases in the hydrate and vapour phases, in addition to the amount of the three phases, which could be used in the optimisation of the Kihara parameters. However, in using the dissociation pressure and compositional data of binary systems for optimisation purposes, it is necessary to know the Kihara parameters of one of the components, which could be called the key compound.

Xenon was chosen as the key compound for the compositional work for both practical and theoretical reasons. From a practical view point, the Xe/Hydrocarbon hydrates are heavier than water and will lie at the base of the water phase. This allows free water (not converted to hydrate) to be sampled and analysed. The change in the concentration of a tracer in water (Burgass, 1995) will indicate the amount of water bonded into the hydrate. From a theoretical view point, the key compound should be the one with enough available information to determine its parameters accurately. Ripmeester and Davidson (1981) and later, Davidson *et al.* (1986a) carried out a comprehensive study using NMR and calorimetry to obtain the cage occupancy ratio, R , and hydration number, n, of xenon hydrates. Knowing the correct values of the Kihara parameters for Xe, it might be possible to find the parameters of C_1, C_2, and C_3 from experimental dissociation pressure data of their binaries with Xe. The compositional data could be used alongside dissociation data or for final adjustment of the parameters.

The initial plan was that, after finding the correct and unique parameters for C_1, C_2, and C_3, proceed and optimise the parameters for other hydrate forming compounds in oil/gas

systems. For this purpose, a plethora of available data in the open literature could be employed.

The following procedure has been employed for optimisation of the Kihara parameters using dissociation pressure data of pure and binary systems:

1. For each system, several experimental dissociation pressure data, P_{exp}, in the L_1-V-H region, particularly in the temperature range of 0-25 °C, were selected.
2. The hard sphere radius, α, was fixed to the value obtained by the second virial coefficient (Avlonitis, 1992).
3. Using an initial guess for ε/κ and σ^*, the hydrate dissociation pressure, P_{cal}, was calculated at each experimental temperature.
4. σ^* was changed in 0.01 Å steps and, at each step the energy parameter, ε/κ was adjusted so as to minimise the following objective function:

$$FOB = \sum_{1}^{N_P} ABS((P_{cal} - P_{exp})/P_{exp})/N_P \qquad (3.5)$$

where P_{cal} and P_{exp} are the calculated and experimental dissociation pressures, respectively. The former is calculated using the equations given in Chapter-2 and the latter is measured experimentally. In order to be able to compare the deviations in different sources of data the objective function is divided to the number of data points, N_P. In the process of optimisation, ε/κ was changed stepwise ($\Delta\varepsilon/\kappa$), and the objective function was calculated and compared with the previous one. If the objective function was higher, the value of the step ($\Delta\varepsilon/\kappa$), were halved. When $\Delta\varepsilon/\kappa<10^{-6}$ the ε/κ and objective function (FOB) were recorded, before changing σ^*.

The above method gives the value of ε/κ as a function of σ^*, with a value of the FOB for each pair of the Kihara parameters. When using the compositional data, the method is essentially the same, except that; instead of dissociation pressure, the mole fraction of

components in vapour and hydrate phases, and the phase mole fraction of hydrate and vapour are calculated. Obviously the objective function is changed accordingly.

Knowing the *n* (hydration number) and *R* (cage occupancy ratio) for Xe, the parameters for this gas are determined first, using the method explained above.

Xenon

Xenon forms structure-I simple gas hydrates. Dissociation points of the xenon hydrate in the three phase L_1-V-H region are reported by Ewing and Ionescu (1974). Figures-3.2 and 3.3 show the optimised ε/κ and the FOB vs σ^* plots obtained using the above mentioned experimental data. Figure-3.3 shows that σ^* is unlikely be higher than 3.40 Å, as the objective function (FOB) increases sharply for higher values of σ^*. A value of σ^*=3.292 Å and the corresponding ε/κ minimise the objective function, but different sets of parameters below σ^*=3.37 Å also give an acceptable fit to the experimental data.

The values of the hydration number and the occupancy ratio of xenon hydrates at 273.15 K have been reported by Davidson *et al.* (1986a) as 6.286±0.03 and 0.73±0.02, respectively. The Kihara parameters of xenon were optimised to match the above experimental hydration number and cage occupancy ratio. The results are shown in Figure-3.4. According to this plot, the intersection is at σ^*=3.292 Å (ε/κ=192.0 K) which can match both sets of data. This value is also in good agreement with the value obtained by the minimisation of the objective function for dissociation pressure data.

Methane

Three sets of data in the L_1-V-H region, all forming structure-I, have been used in the optimisation of the Kihara parameters for methane. They are; dissociation pressure data of methane simple gas hydrates, and its binaries with Xe, as well as C_1/Xe compositional data. Figures-3.5 and 3.6 show the optimised ε/κ vs σ^* and the FOB vs σ^* plots for the three sets of data, respectively. The ε/κ vs σ^* plots are almost parallel and do not have any

intersection, and the FOB vs σ^* plots show minima at different points, so it is not possible to find a unique set of parameters for methane. However, Figure-3.5 shows that the ε/κ vs σ^* plots are approaching each other for 3.2 Ä$<\sigma^*<$3.4 Å, where the FOB vs σ^* plots are also close to their minimum. This could be an indication of an intersection, if there is any. As the possible intersection is on both curves, the set of parameters will fit both sets of data. The compromise would be the point where the curves are as close as possible. In order to find out the above point, the $\Delta\varepsilon/\kappa$ vs σ^* plot for pure and binary dissociation pressures data is depicted in Figure-3.7. The σ^*=3.33 Å, which minimises the value of $\Delta\varepsilon/\kappa$ and the corresponding ε/κ form pure plot were selected as the optimised pairs of parameters for C_1. This will give a perfect match with methane simple gas hydrates and the best possible fit with C_1/Xe binaries.

Ethane

The same procedure, i.e. using the three sets of data, was implemented for C_2. The resulting plots are shown in Figures-3.8 and 3.9. The three plots are almost parallel to each other and it is not possible to specify the correct set of parameters. The FOB vs σ^* plots are not very helpful either. In fact, the optimised σ^* could have any value from 3.1 Å to 3.5 Å. Using any set of parameters in the above range, the prediction for dissociation pressures are good, but they are not accurate for compositional data. If the corresponding ε/κ is chosen from the plot of the C_2/Xe binary, the predictions for the binary will be acceptable but the dissociation pressure prediction of pure C_2 will be in error. Finally, if an average value is selected, all predictions will have some error.

The almost parallel plots in this case showed that this method is not suitable for ethane, because the optimum σ^* could be anywhere in the acceptable error band of C_2 simple gas hydrates. Different weights were assigned to different sets of data, without any significant improvement.

Propane

For propane, the procedure was similar to C_1 and C_2, with the exception that only dissociation pressure data for propane and its binaries with Xe were used in the optimisation of the Kihara data. In this case, the difference between the two ε/κ vs σ^* plots was significant, and it was not possible to find optimised pairs using the two compositional data. The resulting ε/κ and the FOB vs σ^* plots are depicted in Figures-3.10 and 3.11. Again, the two ε/κ vs σ^* plots are parallel and the FOB vs σ^* plot is not helpful either. The large difference between the two curves, means that if a particular value of ε/κ is selected from the plot of one set of data, the error in predicting the results for the other set of data will be significant.

Later, the accuracy of the experimental data was taken into account and different weights were assigned to different elements of the compositional and dissociation data, without any significant improvement

Discussion

After determining the Kihara parameters for xenon, using its simple hydrate dissociation pressure data and cage occupancy and hydration number, xenon was used as the key compound to determine the Kihara parameters for other compounds. The approach was partially successful in determining the Kihara parameters for methane, but it failed for ethane and propane.

Xenon forms structure-I simple gas hydrates and it is small enough to reside in both cavities of structure-I and II. It is known that C_1 and C_2 form structure-I simple gas hydrates, similar to their binaries with Xe. However, C_3 and C_3/Xe form structure-II gas hydrates, as C_3 can only reside in the large cavities of structure-II. It was also noticed that the different plots of ε/κ vs σ^* for simple and binary gas hydrates are more or less parallel to each other. It seems that the ε/κ vs σ^* plot of each gas is a function of hydrate structure, and it is not possible to specify the correct set of potential parameters. This rules out using

xenon as a key compound since it does not cause any change in hydrate structure in the above cases.

Based on the above results it was decided to carry out optimisation with another key compound that will cause change in hydrate structure.

3.4. PROPANE AS THE KEY COMPOUND

As mentioned earlier, the aim is to optimise the Kihara parameters for methane, ethane, propane, i-butane, hydrogen sulphide, n-butane, and carbon dioxide (the heavy hydrate formers, including those forming structure-H are discussed in Chapter-4). These compounds can be classified into three groups:

Group-one, those that can reside in two types of cavities and form structures-I and II as pure or in a mixture with other components, i.e., methane, hydrogen sulphide, nitrogen, and carbon dioxide.

Group-two, ethane, which can reside in the large cavities only and form structures-I and II.

Group-three, those that can reside only in large cavities and form structure-II as pure or in mixture with other gases, i.e. propane, i-butane, and n-butane, where the latter cannot form a simple hydrate.

In the optimisation of the Kihara parameters, the objective is to improve the predictions for multicomponent systems while keeping the accuracy for pure compounds. This is mainly because the experimental data on pure compounds are supposed to be more accurate and the behaviour of these systems are in a better agreement with the assumptions used for the development of the theory, as proposed by van der Waals and Platteeuw (1959).

The main source of experimental data points are those collected by Sloan (1990). The method used in optimising the Kihara parameters for the first and second groups can be summarised as follows:

Determination of the Kihara Parameters

1. See steps 1-4 as described in section 3.3. this gives the value of ε/κ and the FOB (objective function) as a function of σ^*.
2. The ε/κ vs σ^* curve for the pure system (which is structure-I with the exception of nitrogen) is plotted as well as the FOB vs σ^* plot, which could show the range of acceptable pairs of parameters.
3. Steps 1 and 2 are repeated for the same compound in another hydrate structure (which is structure-II with the exception of nitrogen) using binary or ternary dissociation pressure data. The FOB vs σ^* plot will again give an indication of the error.
4. The intersection of the two ε/κ vs σ^* plots determines the optimised set of the Kihara parameters.

To find the ε/κ vs σ^* plot in structure-II for those compounds that form simple gas hydrates of structure-I, binary data of structure-II should be employed. Three compounds form structure-II hydrates with the gases in group one. They are propane, i-butane, and n-butane. Since the accuracy on pure gas hydrates is regarded as a prerequisite in this work, the parameters of all compounds must be selected from the ε/κ vs σ^* plot of pure gas. Therefore, n-butane is rejected, simply because it cannot form a simple gas hydrate. Propane was preferred to i-butane for the following reasons:

1. As a simple hydrate, it covers a wider range of temperature in the L_1-V-H region.
2. It is in a better agreement with the simplified assumptions of the original theory, compared to i-butane.
3. Its binary and ternary data are more available in the L_1-V-H region.
4. Dissociation pressure and compositional data for C_3/Xe binary have been generated in this laboratory (Burgass, 1995). Regarding the unique data on hydration number and cavity occupancy of Xe, it might be possible to specify the correct set of the Kihara parameters for C_3.

6. Holder and Hand (1982) have reported that C_2/C_3 binary form both structures, depending on the concentration and temperature. It may be possible to find the correct set of parameters for C_3 by trial and error calculations.
7. As explained later, the FOB vs σ^* plot for i-C_4 simple gas hydrates does not show any minimum.

Propane

Propane is known to form structure-II simple gas hydrates and does not need any help gas. To reduce the computation time, only 13 dissociation points in the L_1-V-H region of pure propane were selected. The ε/κ vs σ^* and the FOB vs σ^* plots are shown in Figures-3.12 and 3.13. Note that although the objective function is minimum at σ^*=3.49 Å, there is no sharp increase in the FOB vs σ^* plot of pure propane. Therefore, there is no apparent upper limit in the σ^* of propane, and the correct σ^* might be in either side of the minimum FOB (depending on the errors associated with the experimental data). Furthermore, it was noticed that the value of σ^* for a minimum FOB varies if some of the experimental data are rejected, whereas the ε/κ vs σ^* plot does not change significantly. This indicates that errors in the experimental data cannot change the ε/κ vs σ^* plot, and the value of σ^* that minimises the FOB is not necessarily the optimised set of parameters. Two values of σ^* for propane are chosen (3.42 Å and 3.49 Å) to see their effect on the Kihara parameters of other compounds.

Methane

Methane forms structure-I simple gas hydrates. A total of 13 experimental dissociation points in the L_1-V-H region of methane (273.15-305.0 K) were used in the optimisation of the Kihara parameters of methane in structure-I. The ε/κ and the FOB vs σ^* plots of pure methane in structure-I are shown in Figures-3.14 and 3.15.

For drawing the ε/κ vs σ^* of methane in structure-II, propane was used as the key compound. The two values for σ^* of propane (3.42 Å and 3.49 Å) and the corresponding

energy parameters were employed in optimising the Kihara parameters for methane. Different sets of dissociation pressure data of C_1/C_3 were used (to reduce the effect of error in the experimental data) and the results are shown in the above figures.

The intersection between the two plots (determining the Kihara parameters for methane), using the first set of parameters for propane is at σ^*=3.2512 Å, and this point does not change significantly with the other set of parameters. Figure-3.15 shows that the objective functions for pure C_1 and C_1/C_3 binary show the minimum at 3.29 Å and 3.35 Å, respectively. This proves that relying on the objective function as the only measure in determining the optimised set of Kihara parameters could be misleading. In addition, Figure-3.15 shows that the FOB at σ^*=3.2512 Å is also acceptable (this might be the only use of the FOB vs σ^* plot in this approach).

For the rest of this work, the Kihara parameters for propane are fixed with σ^*=3.49 Å and the corresponding value of ε/κ=189.27 K. These values minimise the objective function for C_3 simple gas hydrate dissociation pressure data (as shown in Figure-3.13) and also it seems that a small change in the Kihara parameters of the key compound does not have any significant effect.

Carbon Dioxide

This gas forms structure-I simple gas hydrates. A total of 6 dissociation pressure data points in the L_1-V-H region of pure CO_2 were used in the optimisation of the Kihara parameters in structure-I. The resulting ε/κ and the FOB vs σ^* plots are shown in Figures-3.16 and 3.17. The latter figure shows that the best fit for pure data is achieved at σ^*=2.95 Å, and the error in the objective function increases sharply for σ^* higher than 2.98 Å.

For drawing the ε/κ vs σ^* plot of this gas in structure-II, a set data consisting of 18 dissociation points in the L_1-V-H region of CO_2/C_3 binary were employed. This plot is

also shown in Figure-3.16. The intersection of the plots is at σ^*=2.904 Å (ε/κ=171.97 K) which also gives an acceptable error in the objective function, as presented in Figure-3.17.

Hydrogen Sulphide

Only 6 dissociation pressure data points from the L_1-V-H region of H_2S simple hydrates were used for the optimisation of the Kihara parameters in structure-I. The resulting ε/κ and the FOB vs σ^* plots are depicted in Figures-3.18 and 3.19. The minimum FOB for the above set of data occurs at σ^*=2.94 Å, and σ^*=3.00 Å could be regarded as the upper limit for σ^*. Similar to other group one compounds, starting from low values of σ^*, the FOB changes gradually, passing through a minimum, and rising sharply at the upper limit. As shown in Figure-3.19, different combinations of the parameters below σ^*=3.0 Å can give an acceptable fit to the experimental data of H_2S simple gas hydrates.

Due to the lack of hydrates dissociation pressure data for H_2S/C_3 binary, a ternary system has been used in this case. A set of 13 dissociation pressure data points for a mixture of $C_1/C_3/H_2S$ in the L_1-V-H region has been employed to optimise the Kihara parameters of H_2S in structure-II. The resulting ε/κ vs σ^* plot is shown in the above figures. The intersection of the two plots is at σ^*=2.877 Å and the corresponding value for ε/κ is 210.58 K.

Xenon

Although xenon is not a hydrocarbon gas, an attempt was made to examine the above approach in the optimisation of the Kihara parameters for it. All the available dissociation pressure data of Xe in the L_1-V-H region were used in drawing the ε/κ vs σ^* plot for structure-I, which is shown in Figure-3.20. The Kihara parameters were also optimised according to experimental data of n (hydration number) and R (cage occupancy ratio), as it is depicted in the same figure.

Determination of the Kihara Parameters

The C_3/Xe binary dissociation pressure data (Burgass, 1995), were employed for finding the ε/κ vs σ^* plot of Xe in structure-II. The results are also presented in the above figure. The intersection of the two plots is outside the range specified by *n* (hydration number) and *R* (cage occupancy ratio).

Accordingly, two sets of parameters could be determined for Xe. For the first set, σ^* is equal to 3.286 Å (ε/κ=192.26 K), satisfying the experimental values of *n* and *R*. For the second set, σ^* is determined from the intersection of the ε/κ vs σ^* plots for the two hydrate structures, which is at σ^*=3.2624 Å (ε/κ=193.35 K). The former predicts *n* and *R* to be 6.256 and 0.75, respectively at 273.15 K, whereas the latter predicts *n*=6.168 and *R*=0.809 at the same temperature. Although the deviations in the *n* and *R* are not significant, the latter value of *R* is closer to the cage occupancy ratio of 0.77±0.02 reported by Ripmeester and Davidson in 1981.

Nitrogen

Davidson *et al.* (1986b, 1987) using low-temperature (100 K) X-ray diffraction, found that nitrogen preferentially forms hydrates of structure-II. This is simply because of its affinity for the small cavities which make up two thirds of structure-II cages but only one quarter of the cages of structure-I. In addition, the small cavities in structure-II are smaller than those in structure-I, as shown in Table-2.2.

In order to implement the above method in determining the Kihara parameters, that is, the intersection of ε/κ vs σ^* plots in two different hydrate structures, only gas hydrate dissociation data in structure-I is required for. It is known that N_2/C_1 binary forms structure-I gas hydrates. Figure-3.21 shows the two ε/κ vs σ^* plots with the intersection at σ^*=3.269 Å (ε/κ=134.08 K), without any need to use propane as the key compound. However, the above parameters, do not give good results for nitrogen simple hydrates at pressures above 80 MPa, as presented in Figure-3.22.

Determination of the Kihara Parameters

Figure-3.23 shows the ε/κ vs σ^* plots for three different sets of data, i.e., dissociation pressure data for N_2/C_3 (structure-II), N_2/C_1 (structure-I), and N_2 pure (structure-II?). Although the ε/κ vs σ^* plots are found to be sensitive to the accuracy of the experimental data, the three plots intersect at almost one point. However, we were not expecting any intersection between the two structure-II plots, that is, the ε/κ vs σ^* plots for pure nitrogen and N_2/C_3 binary. We are almost sure about the hydrate structures for N_2/C_1 and N_2/C_3. Is nitrogen forming another structure?

The effect of incorrect assumption for hydrate structure on the ε/κ vs σ^* plot was also investigated in this work. For this purpose, the same sets of dissociation pressure data for nitrogen simple gas hydrates (but assuming structure-I hydrates) were used for optimising the Kihara parameters. Figure-3.24 shows that by assuming structure-I for nitrogen simple gas hydrates, the ε/κ vs σ^* plot is parallel to N_2/C_1 structure-I plot, which is in agreement with our previous observation. This is another indication that N_2 may form structure-I simple gas hydrates.

The results of assuming structure-II (incorrect structure) for N_2/C_1 binary are presented in Figure-3.25, The ε/κ vs σ^* plot is not parallel (based on the earlier experience with Xe as the Key compound) to the one for N_2/C_3 binary, which shows that the assumed structure-II for N_2/C_1 binary is incorrect. This implies that, assigning structure-II for N_2 simple gas hydrates could be equally incorrect. Furthermore, the above observation indicates that, the incorrect assumption in hydrate structure cannot result in a correct trend in the ε/κ vs σ^* plot.

Davidson *et al.* (1986b, 1987) conducted their experiments at 100 K, concluding that N_2 forms structure-II simple gas hydrates. The above observations imply that nitrogen may form structure-I gas hydrates at higher temperatures. This means that nitrogen may change hydrate structure with temperature, which could be the case with some other compounds studied by the above authors.

Assuming structure-I for nitrogen simple gas hydrates, the intersection of the ε/κ vs σ^* plot with that of N_2/C_3 (structure-II) hydrates determines the optimised set of the Kihara parameters for nitrogen. Figure-3.26 shows the above intersection to be at σ^*=3.2171 Å with the corresponding ε/κ=128.39 K. The experimental and predicted hydrate dissociation conditions for nitrogen simple gas hydrates in (assuming structure-I) are presented in Figure-3.27. The results are in good agreement with the experimental data, even at high pressures.

Ethane

Ethane is in group-two since it can enter the large cavities of structure-I as simple gas hydrates. A total of 9 dissociation pressure data points in the whole range of the L_1-V-H region of ethane simple gas hydrates were used to obtain the ε/κ and the FOB vs σ^* plots in structure-I, as is shown in Figures-3.28 and 3.29. Figure-3.29 shows that for ethane simple gas hydrates dissociation pressure data, the objective function reaches a minimum at σ^*=3.32 Å. Unlike the group-1 hydrate formers, the FOB vs σ^* plot does not show any sharp increase to show the upper limit for σ^*. Therefore, the correct σ^* might be on either side of the minimum.

Different sets of C_2/C_3 binary dissociation pressure data were employed for drawing the ε/κ and the FOB vs σ^* plots of C_2 in structure-II, as shown in the above figures. The FOB vs σ^* does not show any minimum to specify the optimised set of parameters. However, as shown in Figure-3.28 the two plots have an intersection at σ^*=3.4315 Å (ε/κ=183.32 K) which could be accepted as the optimised set of parameters.

i-Butane

Iso-butane can only reside in the large cavities of structure-II gas hydrates, so it does not form structure-I gas hydrates. Therefore, the method described previously in this chapter cannot be use for determining its potential parameters. Here, the conventional minimisation of the objective function is used for the optimisation of the Kihara parameters for this

compound. Different sets of dissociation pressure data of i-C_4 as simple hydrate in the L_1-V-H and I-V-H regions are used for optimisation of the Kihara parameters. The ε/κ and the FOB vs σ^* plots are shown in Figures-3.30 and 3.31. The FOB vs σ^* plot in the L_1-V-H region does not show any minimum which may be due to small temperature span (about 2 °C). The FOB vs σ^* plot in the I-V-H region shows that, in the tested interval, increasing σ^* will reduce the error. A value of σ^*=3.60 Å and the corresponding value of ε/κ=209.58 K from the plot in the L_1-V-H region were selected as the optimised set of the Kihara potential parameters.

n-Butane

This component does not form simple gas hydrate, however, it can form structure-II gas hydrates with a help gas. Therefore, it is not possible to plot the ε/κ vs σ^* for pure n-C_4. The Kihara parameters of this compound were optimised using its binaries with C_1, C_3, and i-C_4.

All the potential parameters for gas-water interactions obtained in the course of this study are listed in Table-3.1.

3.5. CONCLUSIONS

Two approaches have been used in this study for optimising the Kihara parameters from gas hydrate data. In the first approach, hydrate dissociation pressure and compositional data for xenon were employed for the optimisation of the Kihara parameters for this gas. Using xenon as a key compound, dissociation pressures and compositional data of Xe/Hydrocarbon were used to specify the Kihara parameters of C_1, C_2, and C_3. Although the first approach was not very successful in determining the Kihara parameters, it confirmed that, for each compound, there are many combinations of the Kihara parameters that can match the experimental data. More importantly, it showed that the ε/κ vs σ^* plot for each guest molecule is a function of hydrate structure. This is an important observation and could be used as a means of confirmation of a hydrate structure.

Determination of the Kihara Parameters

The second approach is based on the above idea, i.e. the shape of the ε/κ vs σ^* plot is a function of hydrate structure. In this approach, the compounds were divided into different groups. For those compounds that can form different structures the optimised set of parameters were determined by finding the intersection between the ε/κ vs σ^* plots for two structures. Propane was employed as the key compound in this method. For optimising the Kihara parameters for those compounds which can form only one structure, the conventional method of minimising the objective function was employed. In both cases a large number of dissociation pressure data were used to reduce the effect of experimental error on the results. Only pure and binary dissociation pressure data are necessary for optimisation. The objective function used in this study is able to specify the range of acceptable pairs. The resulting Kihara parameters are validated against a large number of dissociation pressure and compositional experimental data for synthetic and real systems in Chapter-6.

In the optimisation of the Kihara parameters, the above method showed that nitrogen is likely to form structure-I simple gas hydrates in the L_1-V-H region and in the temperature range of this study (270-294 K). On the other hand, Davidson *et al.* (1986b, 1987) reported that nitrogen forms structure-II gas hydrates (using X-ray diffraction at 100 K). It is thought that nitrogen gas hydrates change structure at higher temperatures. This needs further investigation.

The approach presented in this chapter can be further improved by using compounds that change structure in finding the Kihara parameters for the common hydrate formers. One interesting option is the use of cyclopropane, as its hydrate structure changes from I to II as a function of temperature. Based on the results of this work, it must be possible to optimise the Kihara parameters for cyclopropane by using the dissociation pressure data for the two hydrate structures. The next logical step would be to use the hydrate dissociation pressure data for cyclopropane binaries to find the Kihara parameters for other compounds. There are some other hydrate formers that change structure with temperature. These

compounds could be used for further improvement of the above method, as detailed in Chapter-7.

The subject of optimisation cannot be considered closed and more experimental and theoretical work should be carried out. The work for those compounds that can form only structure-II is not complete, and the Kihara parameters for other potential hydrate forming hydrocarbons must be optimised. In the next chapter, the optimisation of the Kihara parameters for some new hydrate formers forming structure-II and H is detailed.

****

Table-3.1. Kihara potential parameters for gas-water interactions.

Component	α, Å	σ^*, Å	ε/κ, K
Methane	0.2950	3.2512	153.69
Ethane	0.4880	3.4315	183.32
Propane	0.7300	3.4900	189.27
i-Butane	0.7980	3.6000	209.58
n-Butane	1.0290	3.4000	210.58
Xenon, Set-1	0.3270	3.2860	192.26
Set-2	0.3270	3.2624	193.35
Hydrogen Sulphide	0.7178	2.8770	210.58
Carbon Dioxide	0.7530	2.9040	171.97
Nitrogen, sI	0.3350	3.2171	128.39
sII	0.3350	3.2690	134.08

$\sigma=\sigma^*+2\alpha$

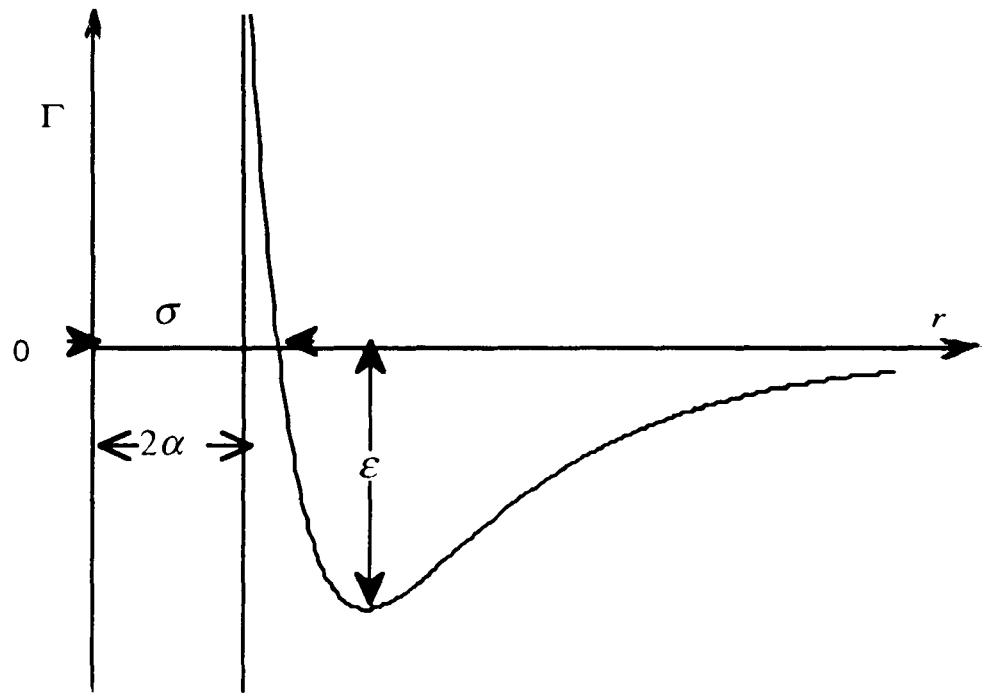

$$\Gamma(r) = \infty \qquad r = 2\alpha$$

$$\Gamma(r) = 4\varepsilon[(\frac{\sigma - 2\alpha}{r - 2\alpha})^{12} - (\frac{\sigma - 2\alpha}{r - 2\alpha})^{6}] \qquad r > 2\alpha$$

Figure-3.1 Potential function in the Kihara model with three adjustable parameters.

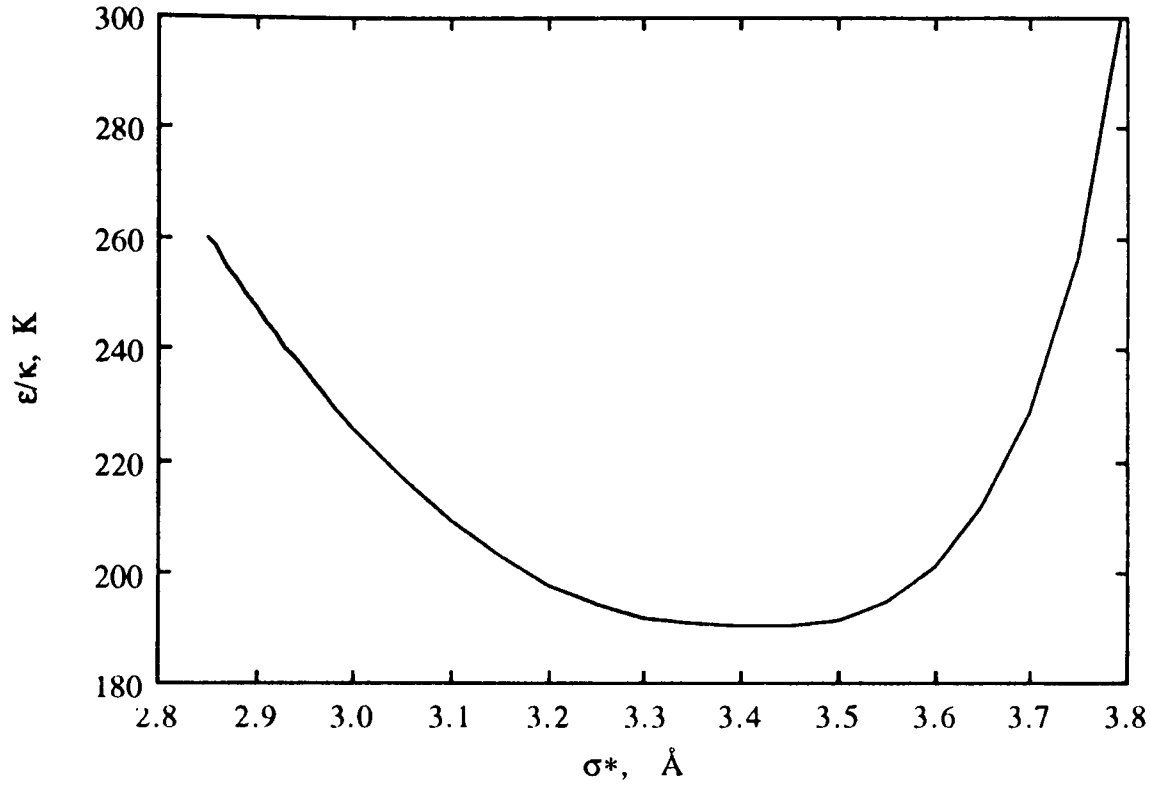

Figure-3.2 Optimised pairs of Kihara parameters for xenon hydrate from dissociation pressure data in the LI-H-V region.

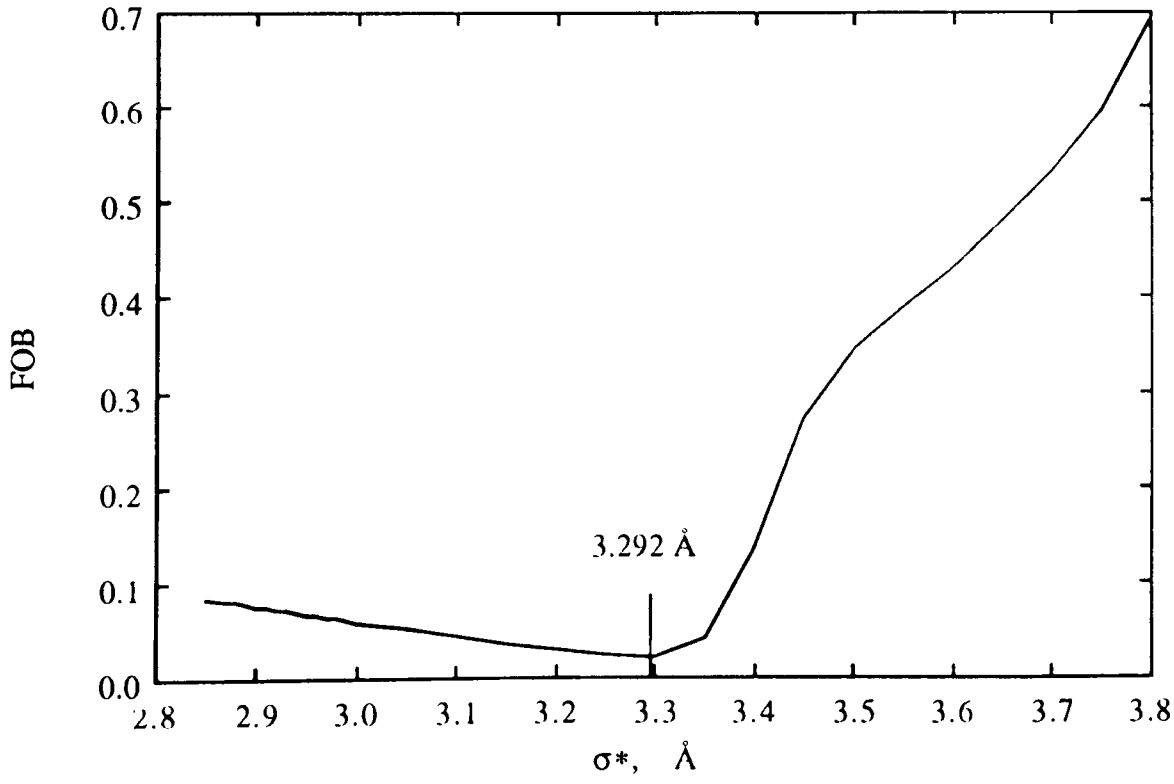

Figure-3.3 Objective Function for different pairs of the Kihara parameters for xenon hydrate.

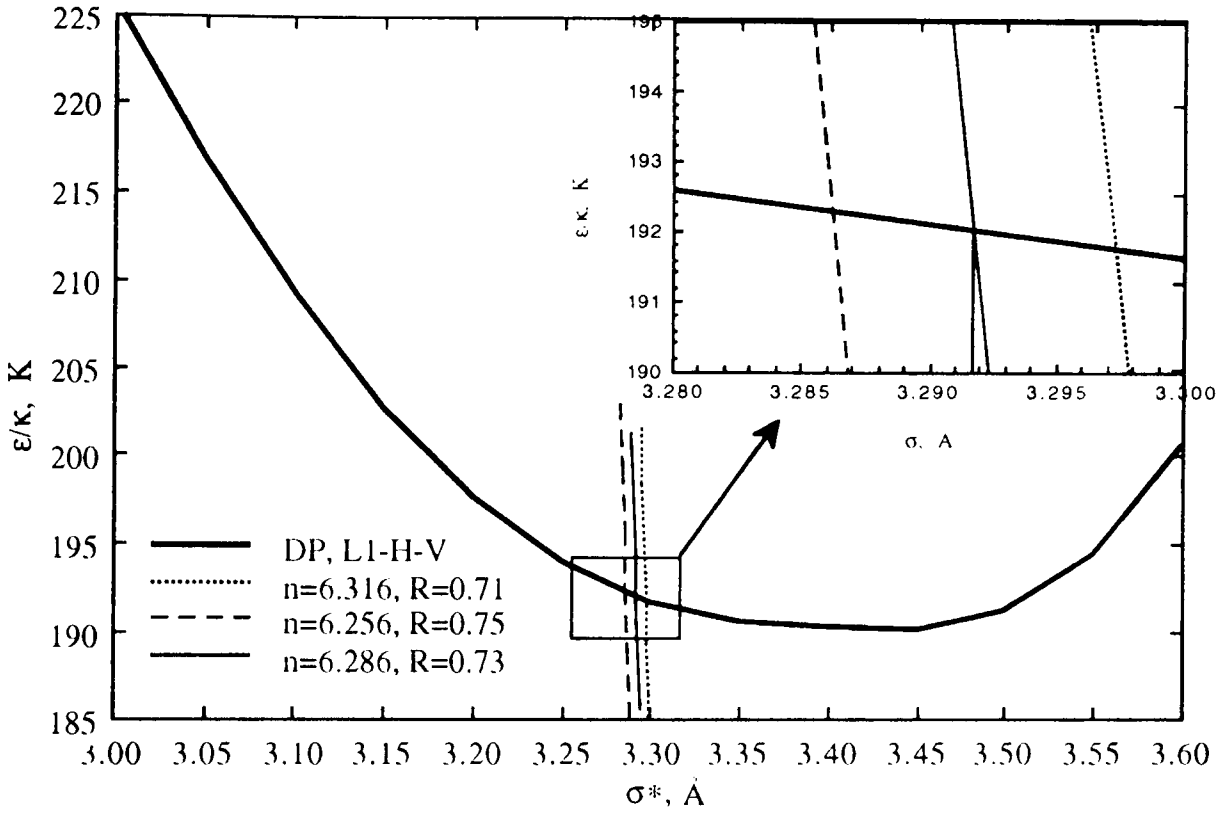

Figure-3.4 Kihara parameters for Xe from data on dissociation pressure, cage occupancy ratio, and hydrate number.

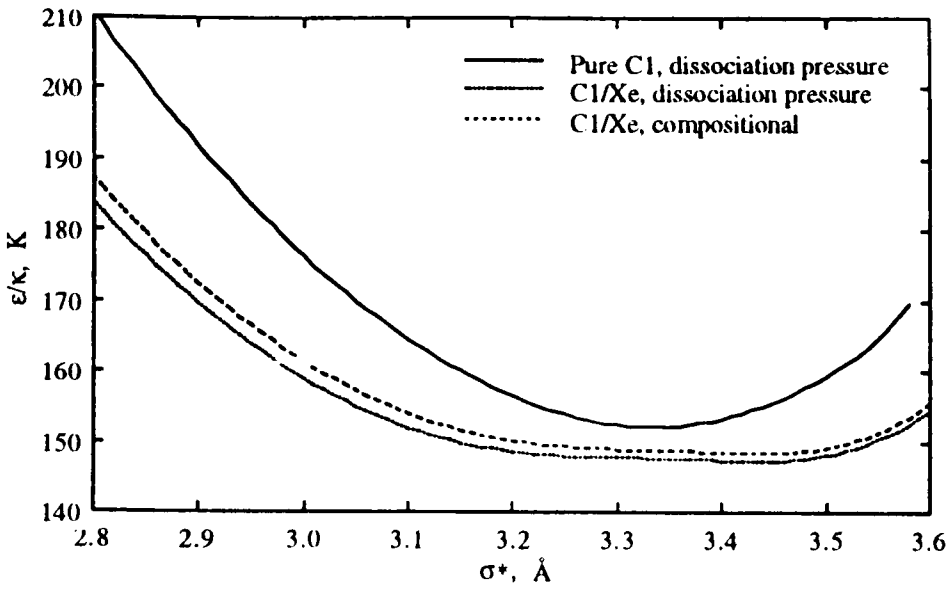

Figure-3.5 Kihara parameters for methane hydrate from different sets of data in the L1-H-V region.

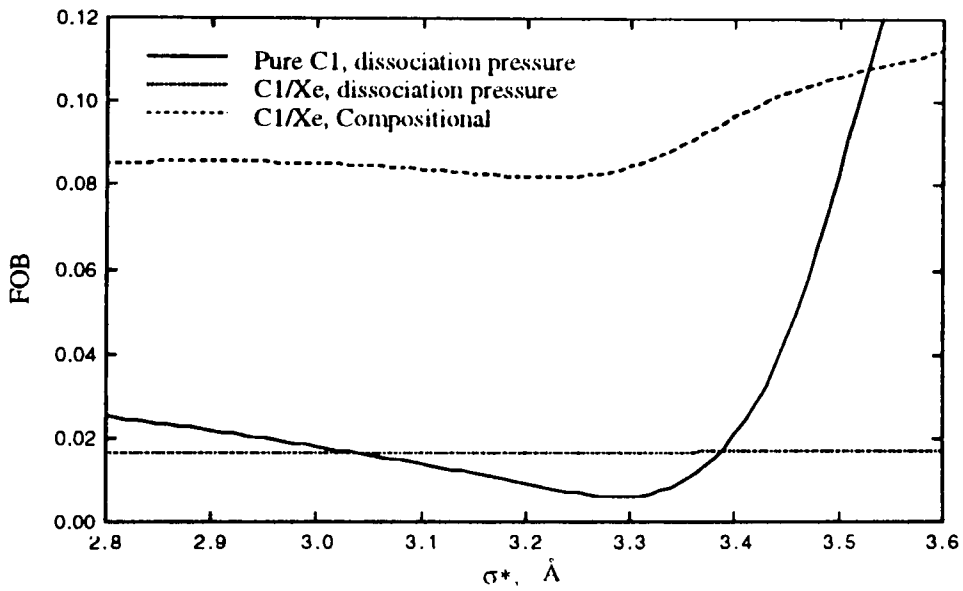

Figure-3.6 Objective Function for optimised pairs of the Kihara parameters in different sets of data.

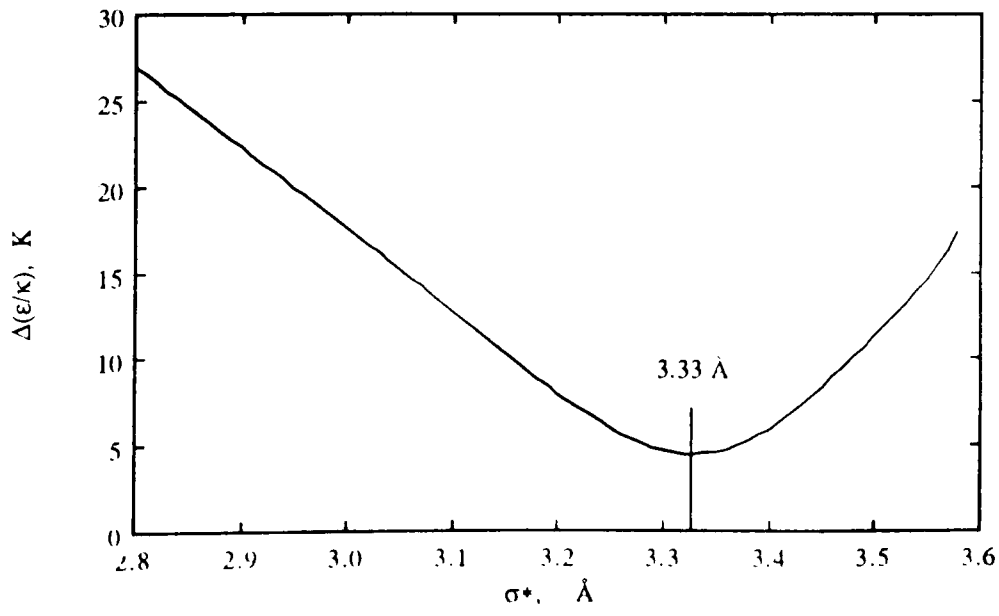

Figure-3.7 Difference between the Kihara energy parameters for methane from pure and C1/Xe binary dissociation pressure data.

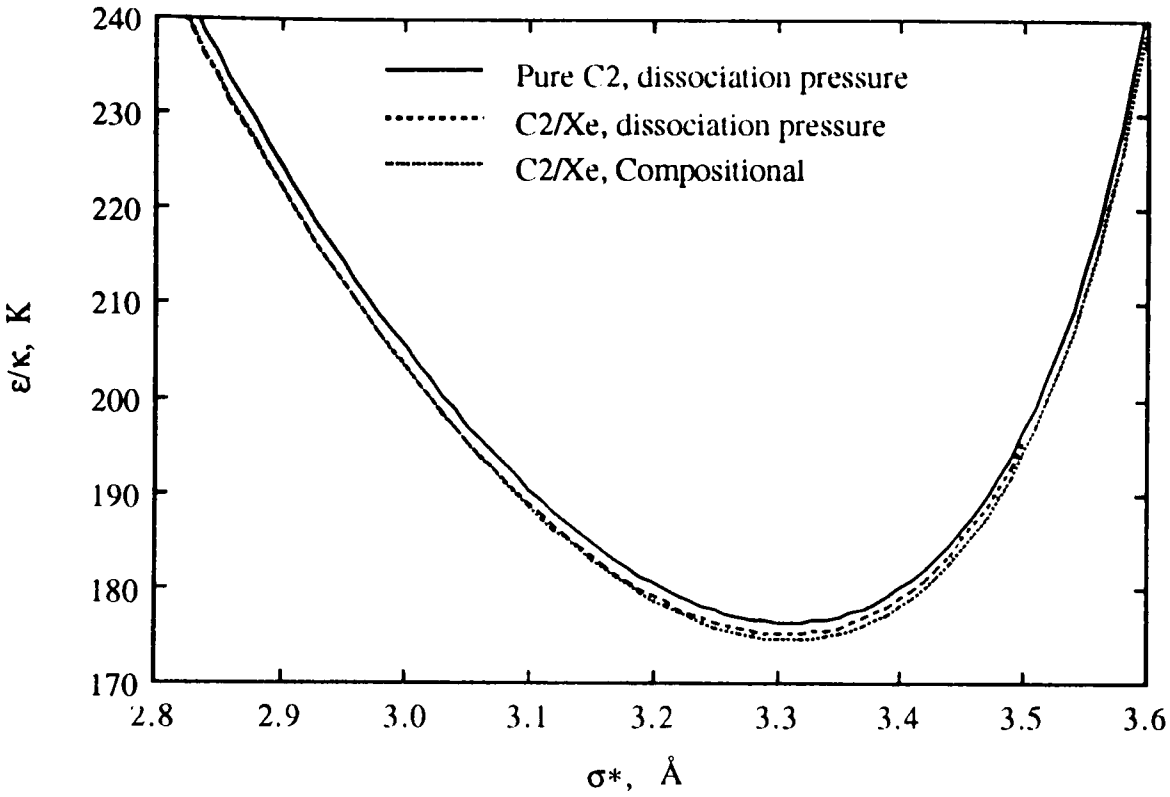

Figure-3.8 Kihara parameters for ethane hydrate from different sets of data in the L1-H-V region.

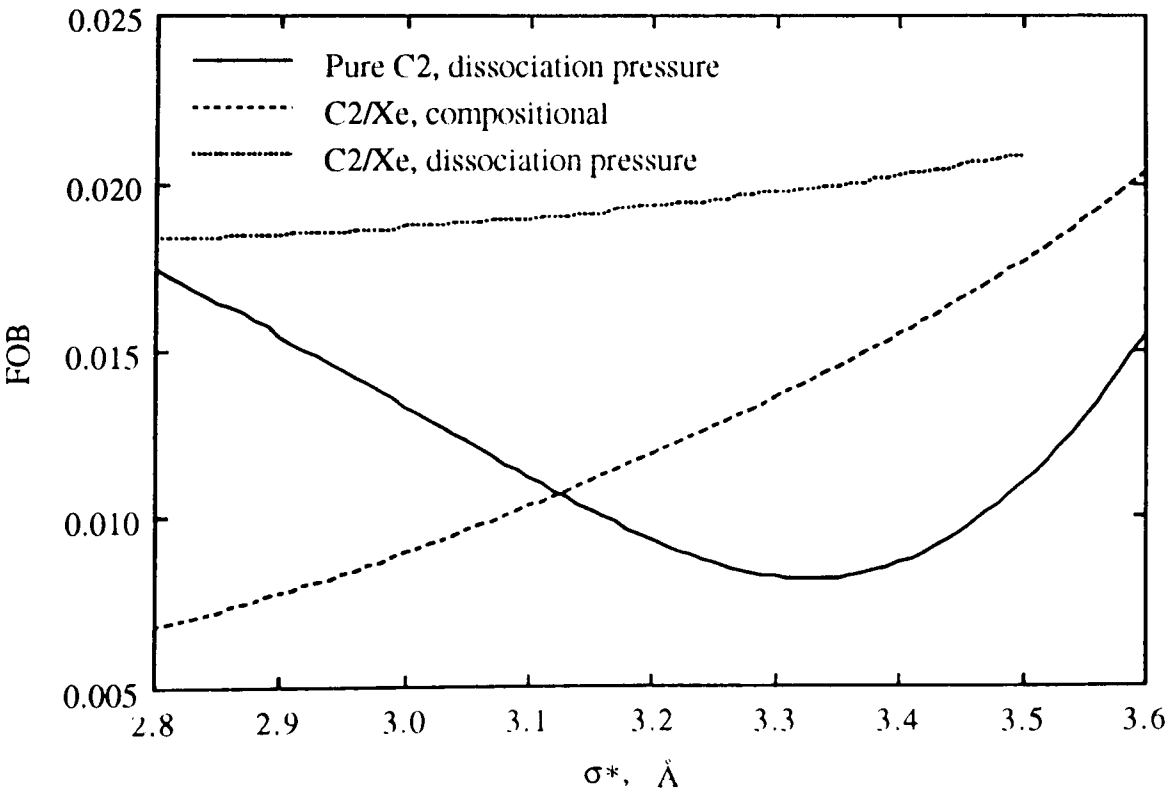

Figure-3.9 Objective Function for pairs of optimised Kihara parameters of ethane for different sets of data.

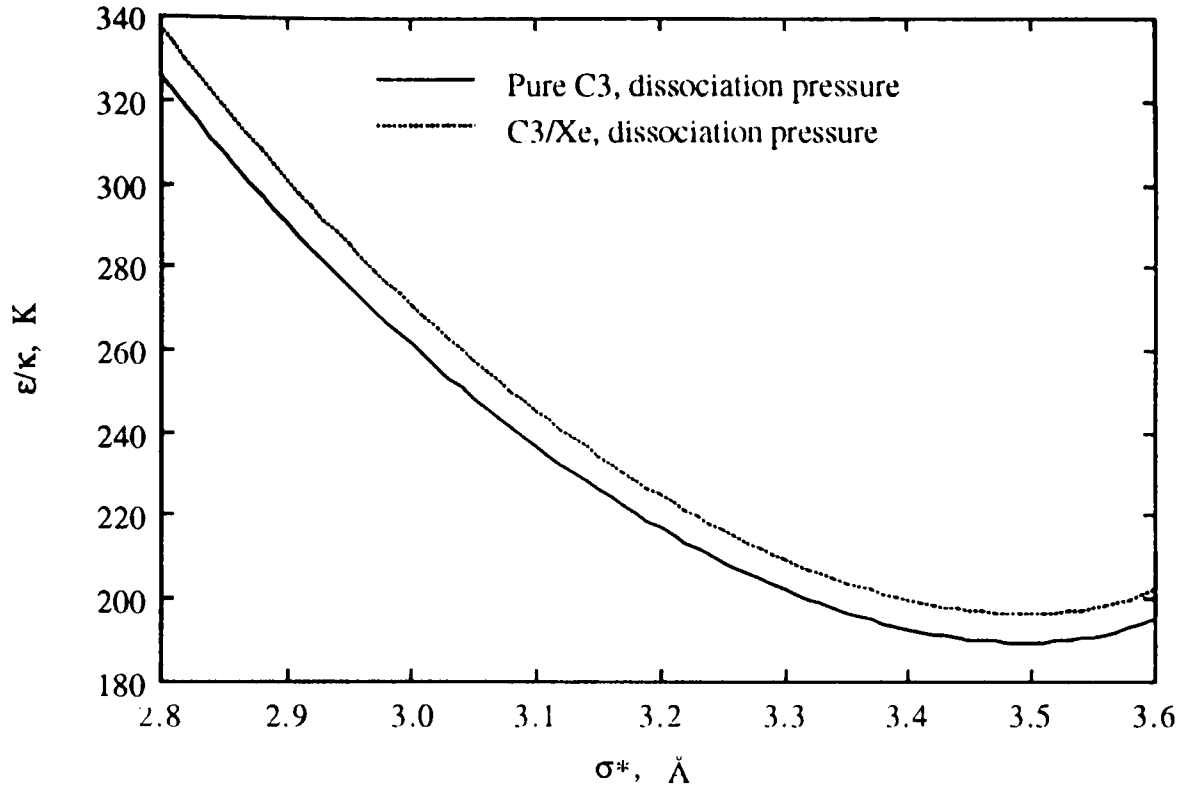

Figure-3.10 Kihara parameters for propane from different sets of data in the L1-H-V region.

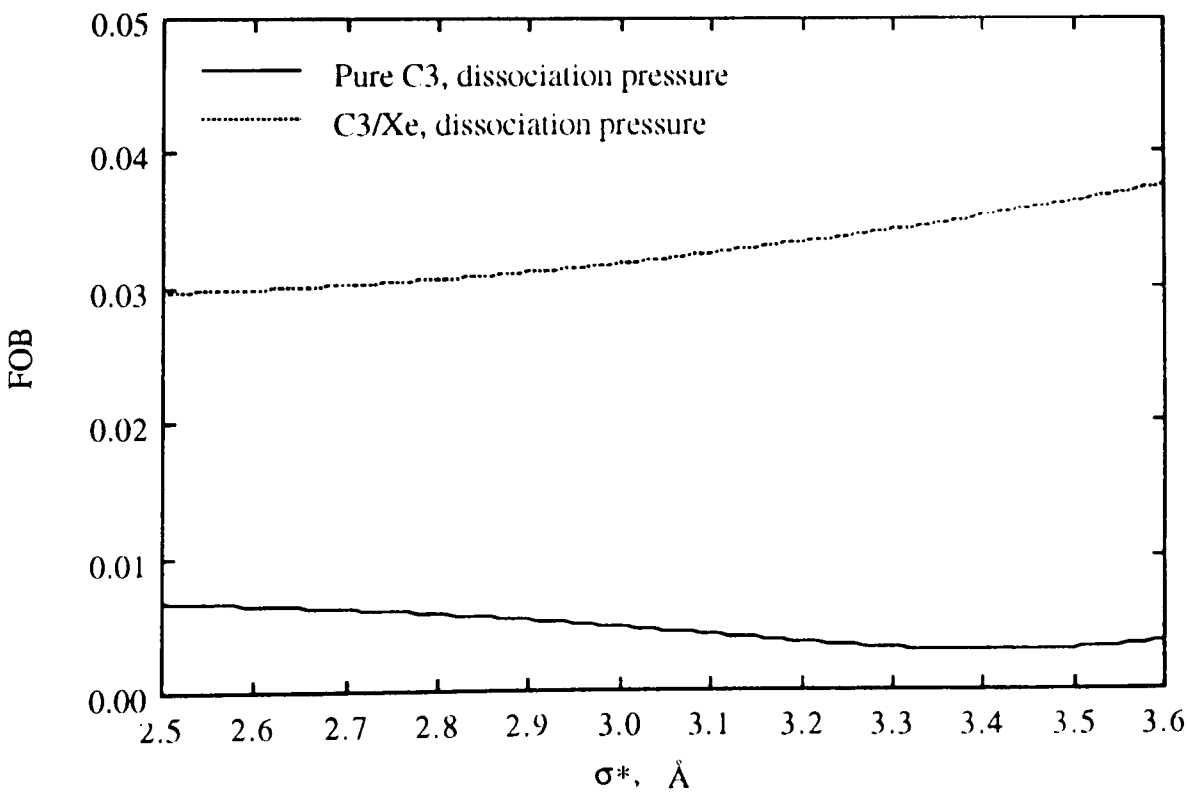

Figure-3.11 Objective Function for pairs of optimised Kihara parameters of propane from different sets of data.

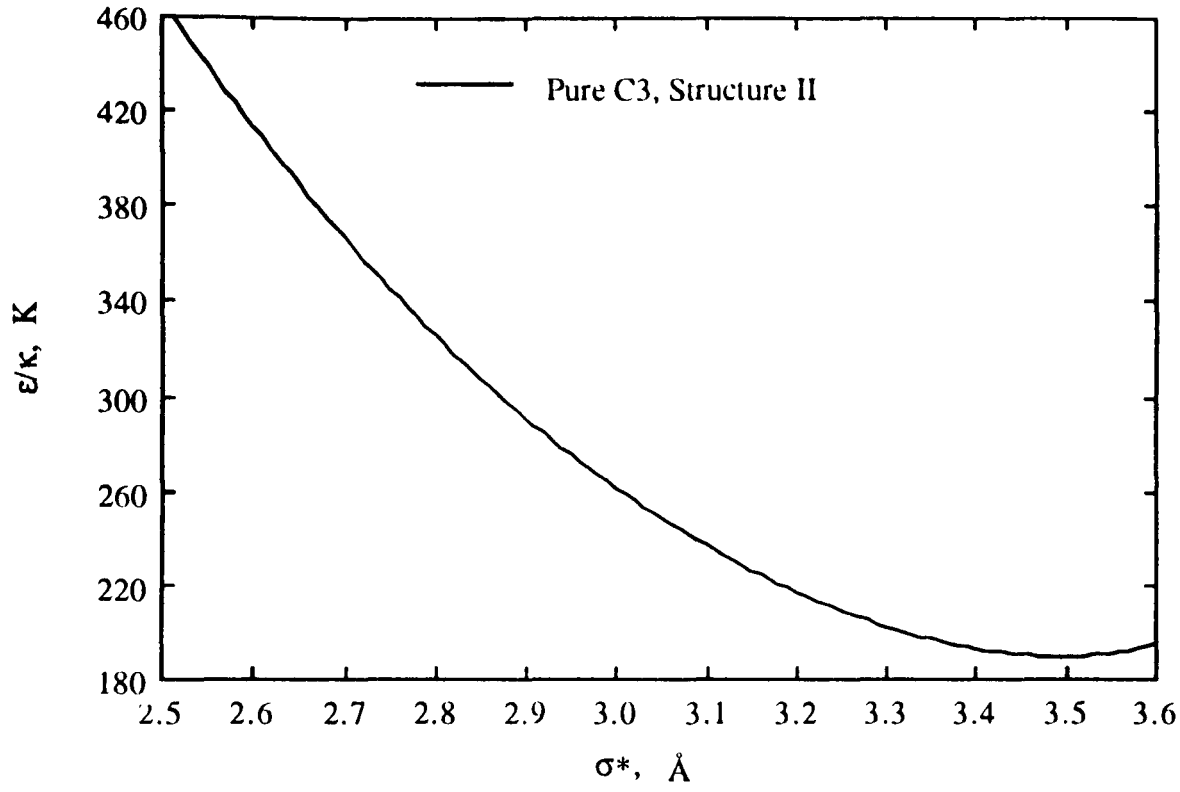

Figure-3.12 Kihara parameters for propane from dissociation pressure data in the L1-H-V region.

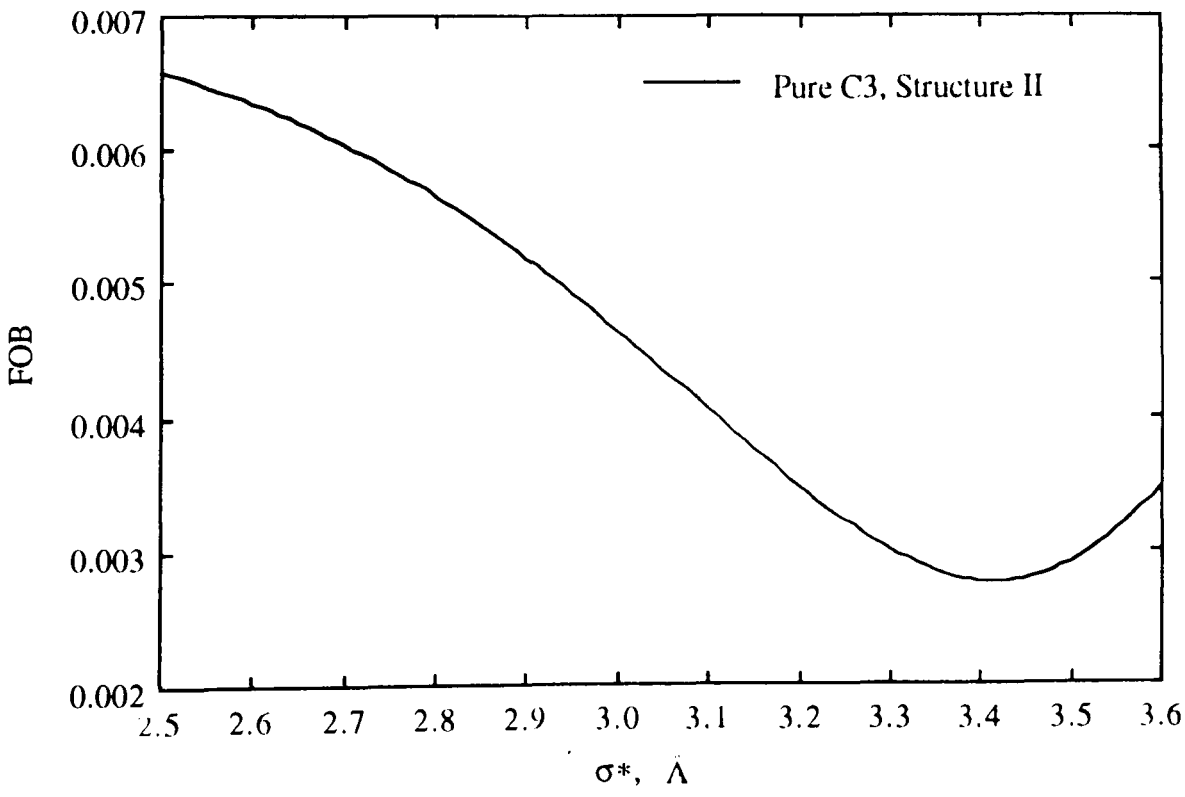

Figure-3.13 Objective Function for optimised pairs of Kihara parameters of propane.

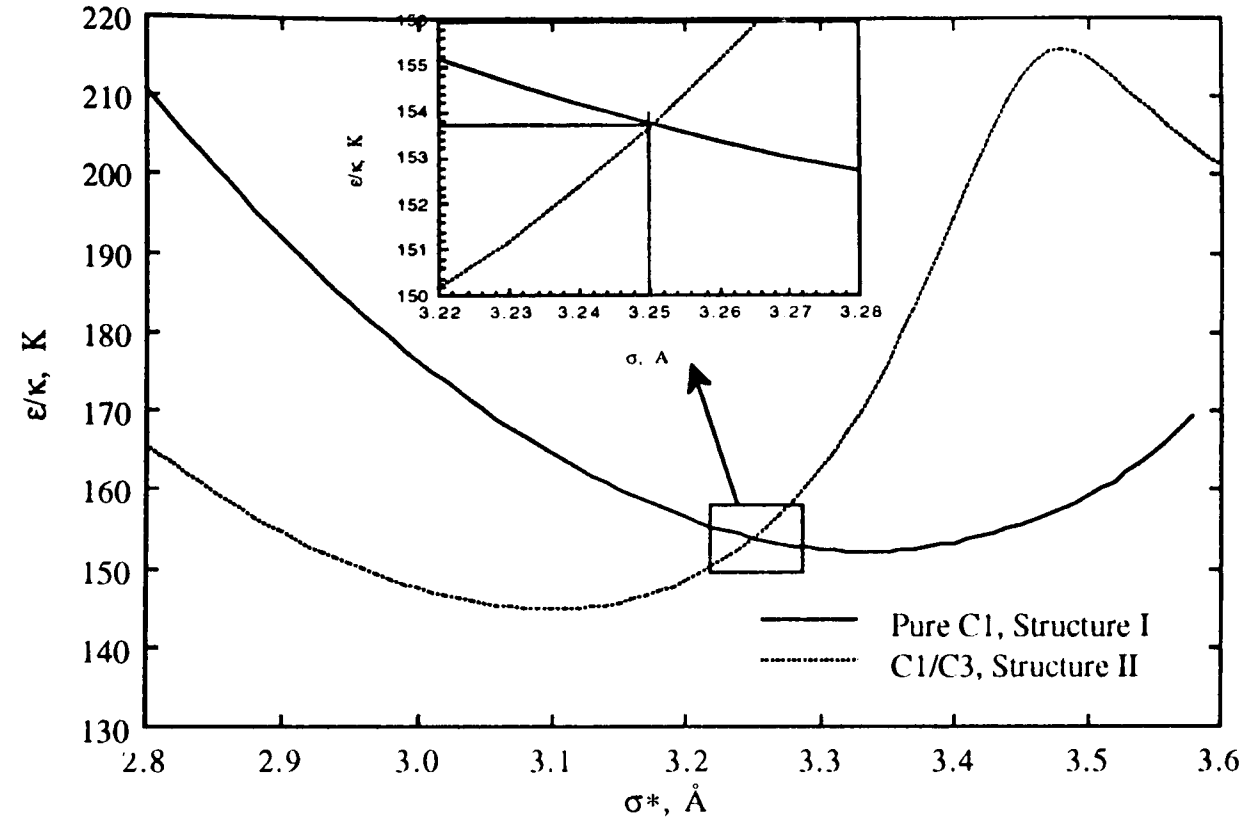

Figure-3.14 Kihara parameters for methane in structures I and II.

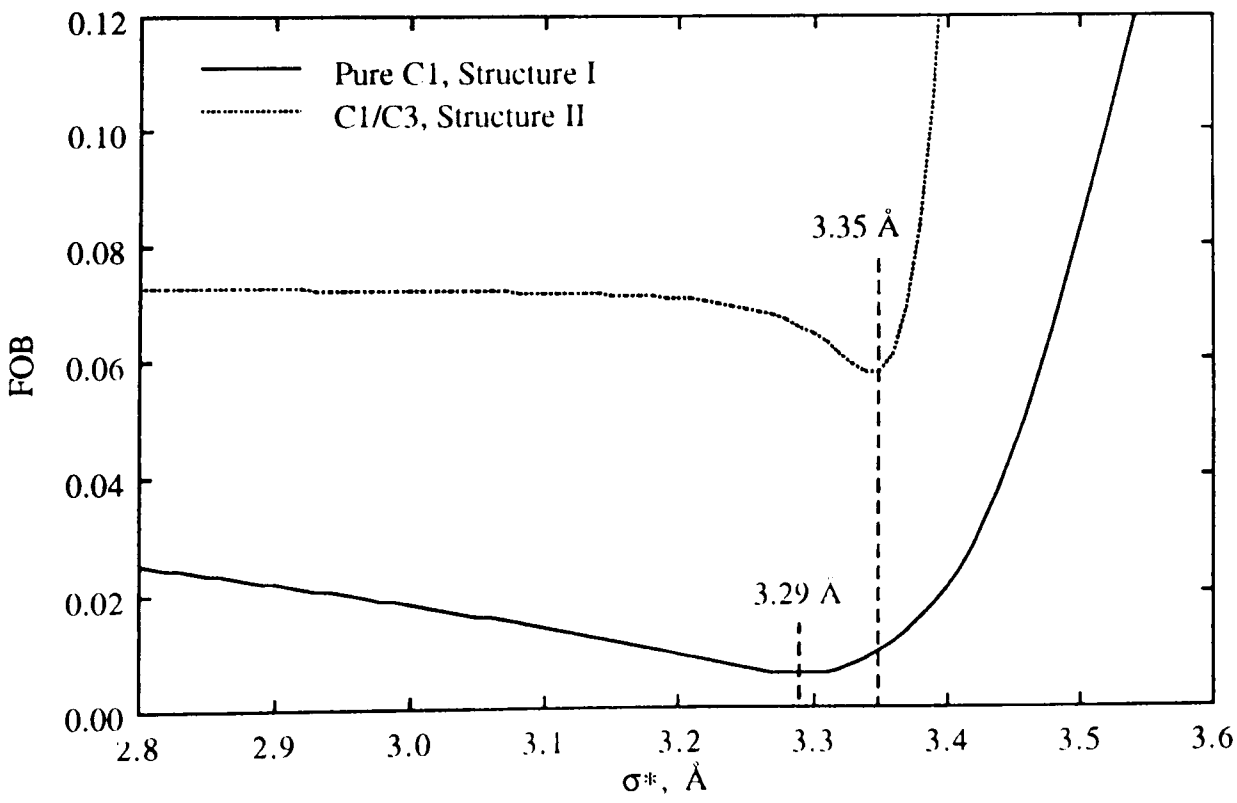

Figure-3.15 Objective Function for optimised pairs of Kihara parameters for methane in structure I and II.

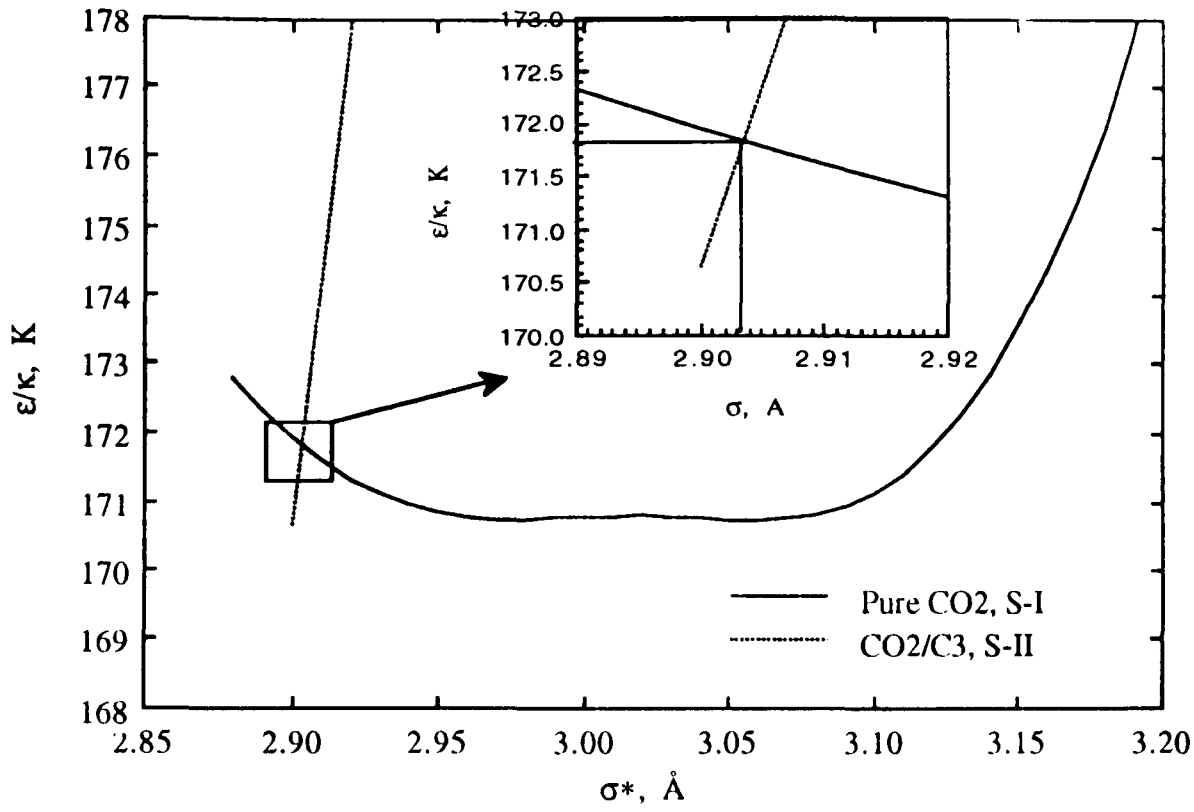

Figure-3.16 Optimised pairs of Kihara parameters for CO2 in structures I and II.

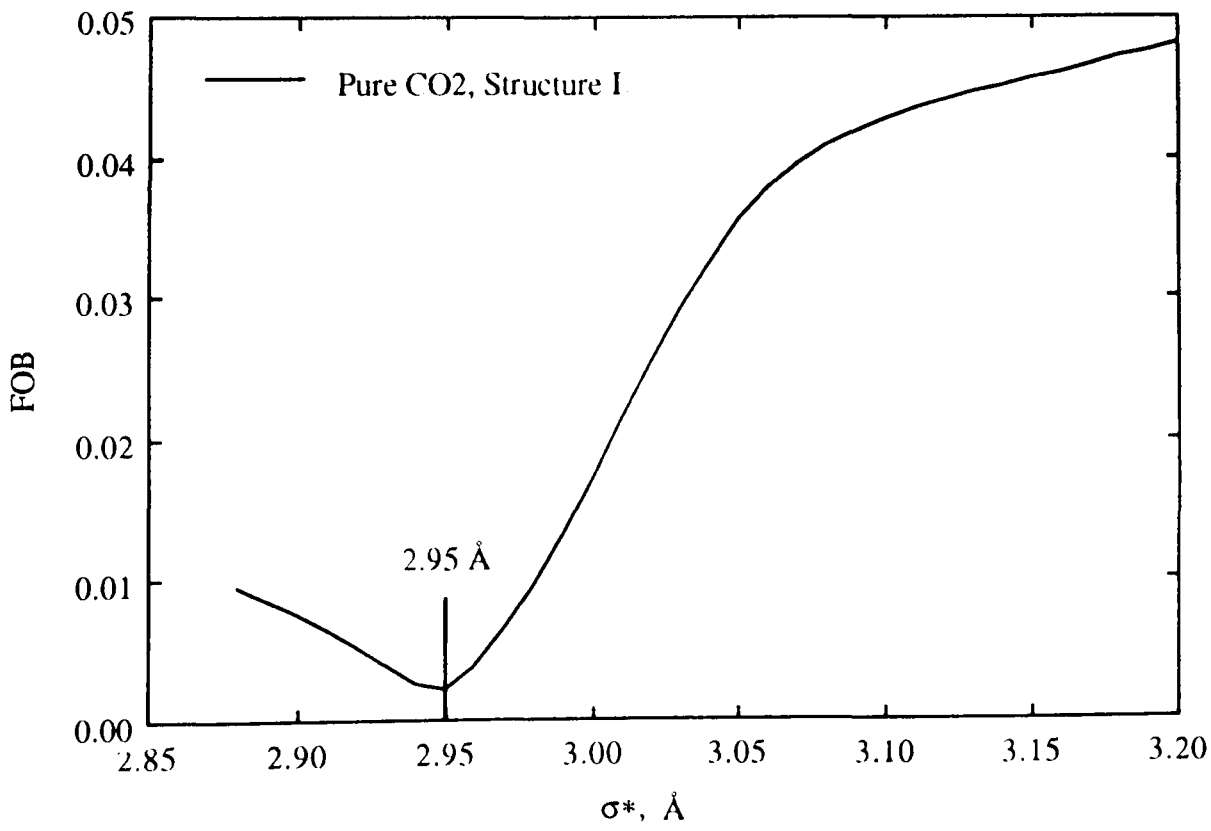

Figure-3.17 Objective Function for optimised pairs of Kihara parameters for CO2 in structure I.

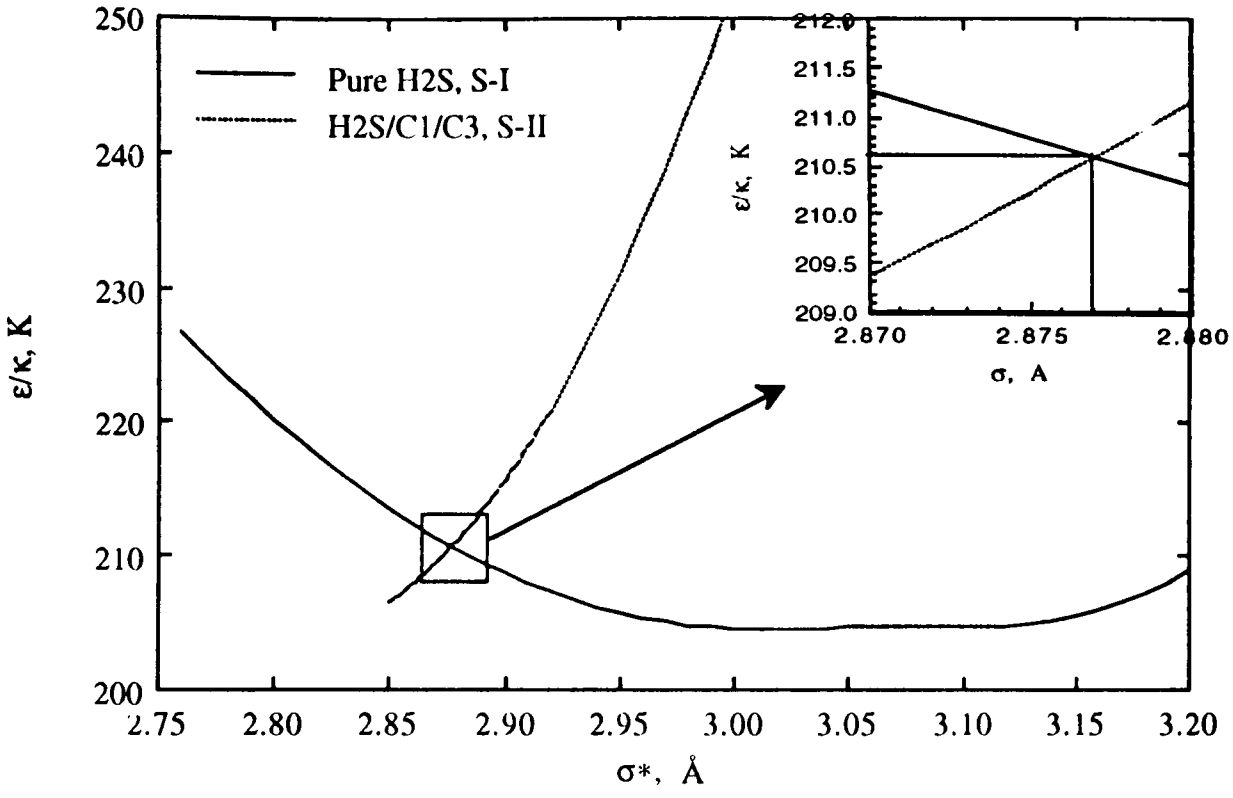

Figure-3.18 Optimised pairs of Kihara parameters for H2S in structures I and II.

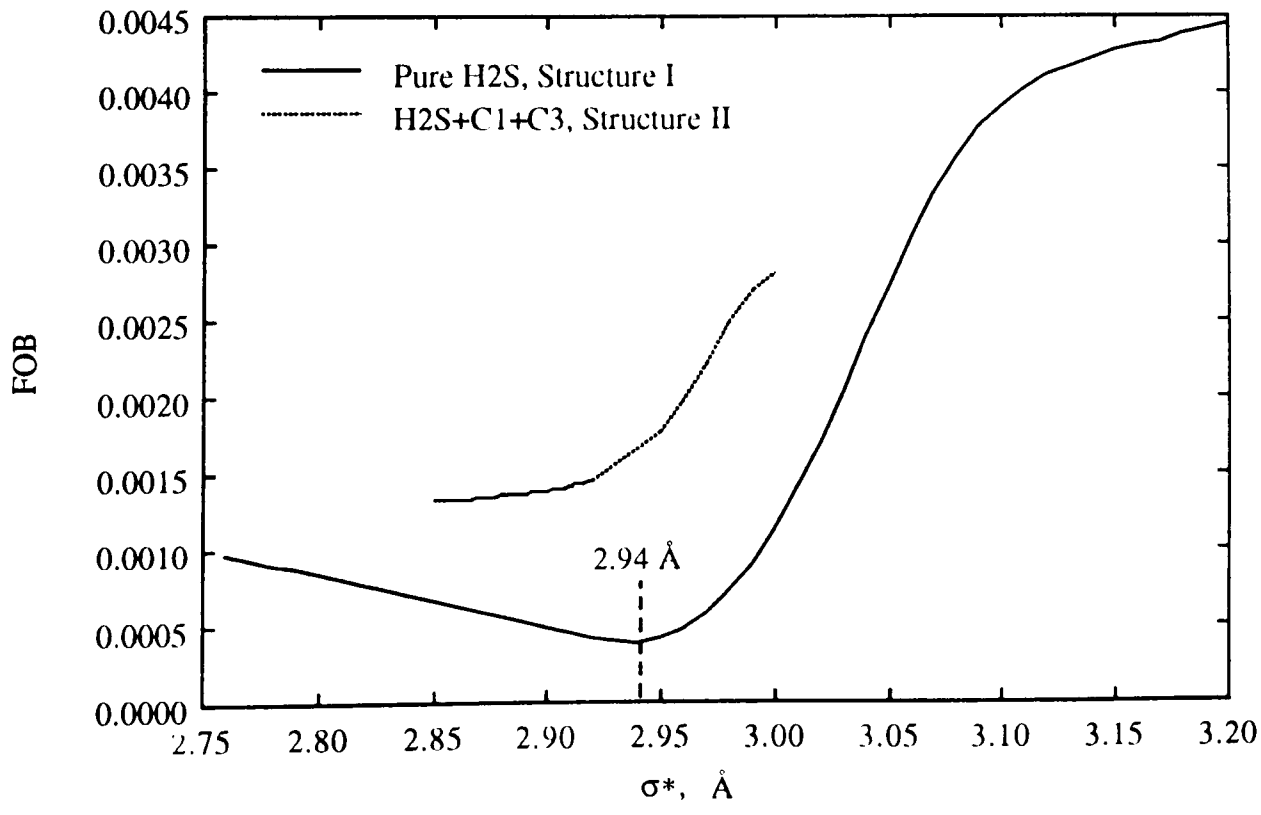

Figure-3.19 Objective Function for optimised pairs of Kihara parameters for H2S in structures I and II.

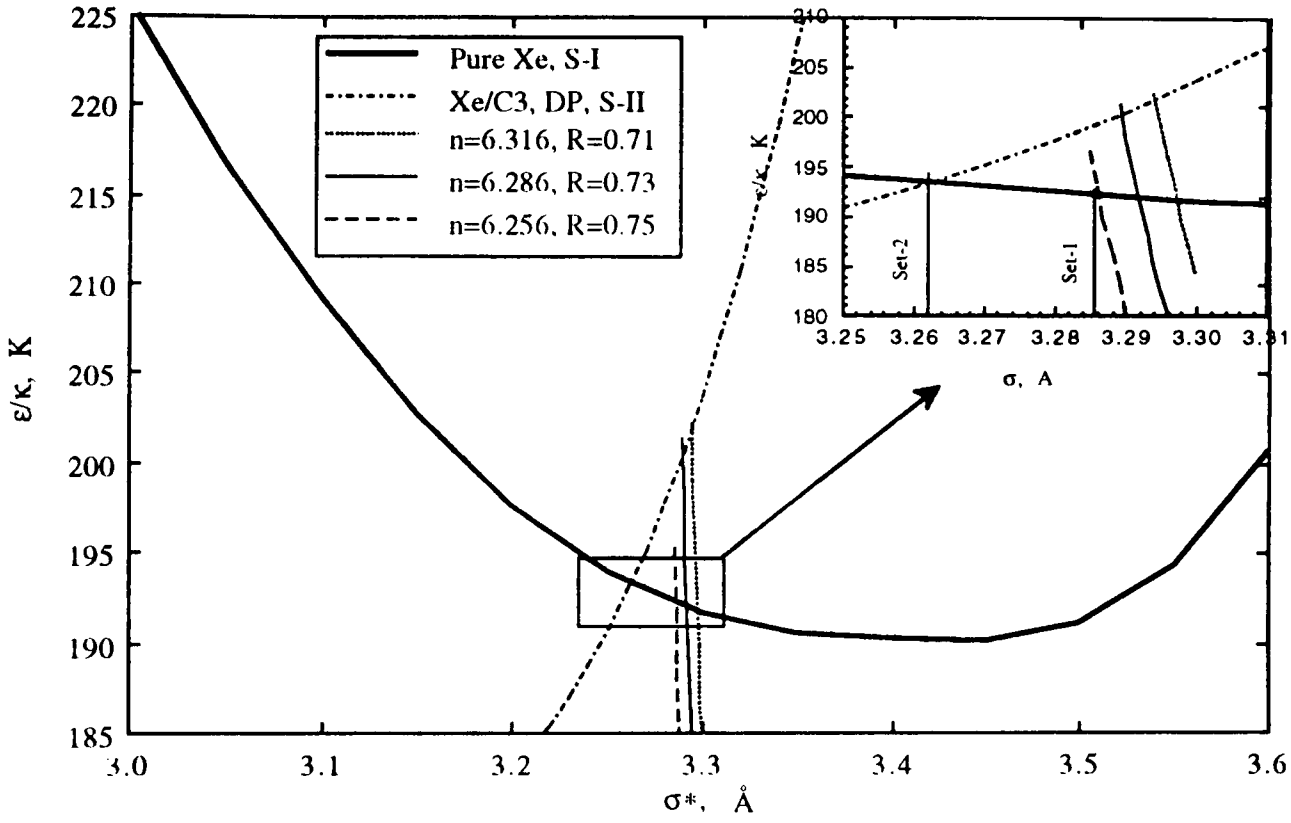

Figure-3.20 Optimised sets of Kihara parameters for xenon.

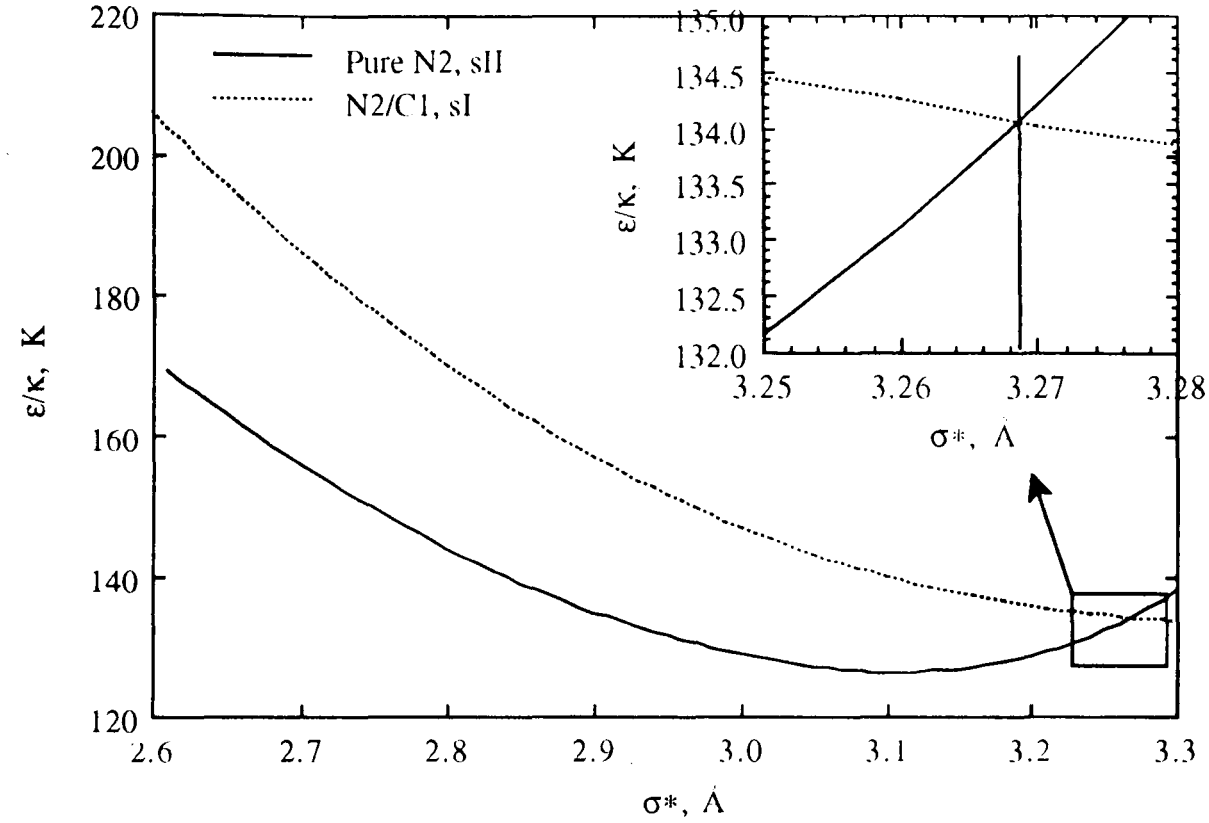

Figure-3.21 Kihara parameters for nitrogen from N2 pure (sII) and N2/C1 (sI) systems.

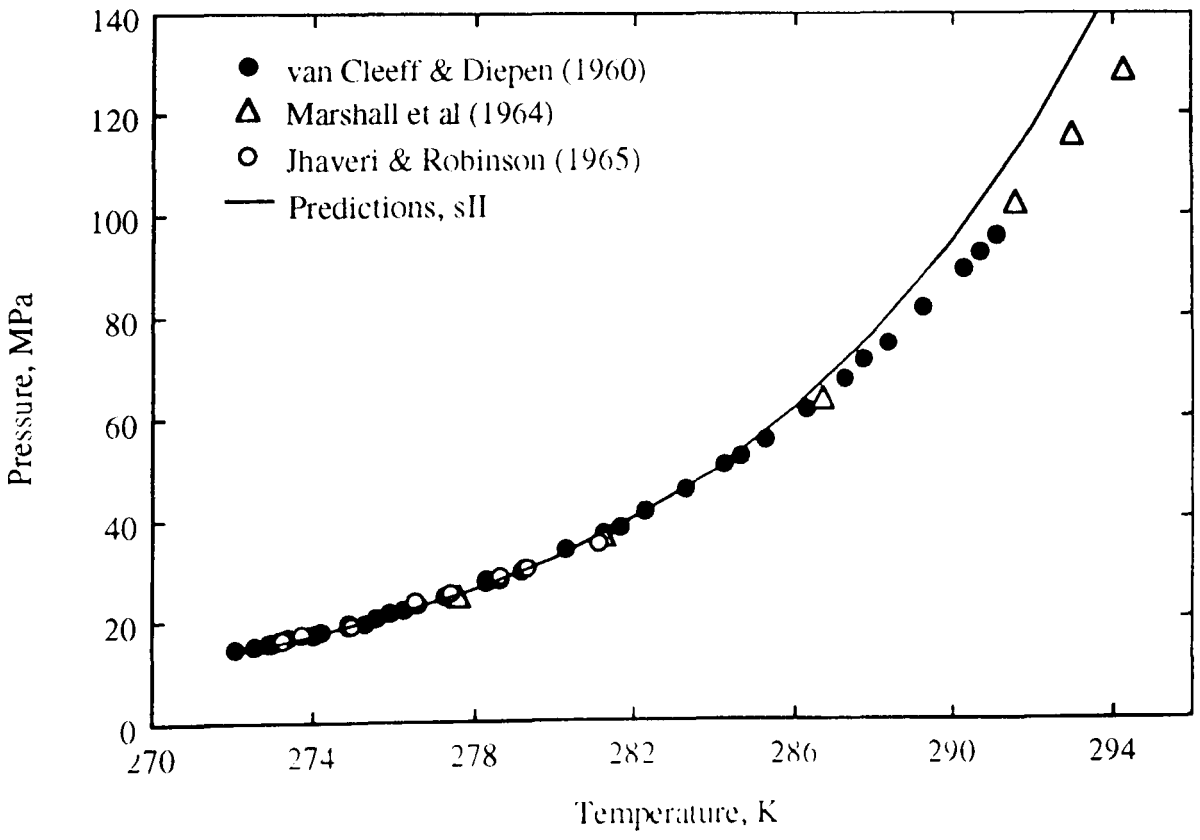

Figure-3.22 Experimental and calculated dissociation pressures of nitrogen (sII) in the L1-H-V region.

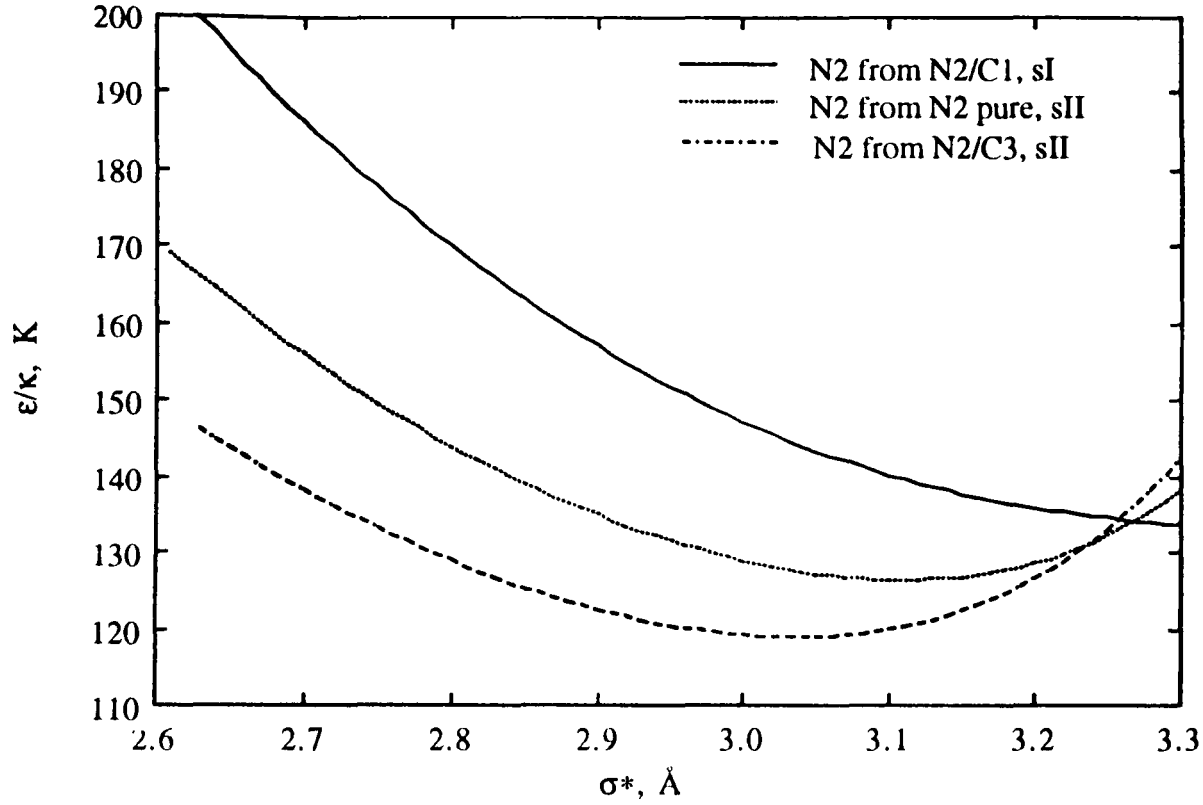

Figure-3.23 Kihara parameters for nitrogen from N2/C1 (sI), N2 pure (sII) and N2/C3 (sII) systems.

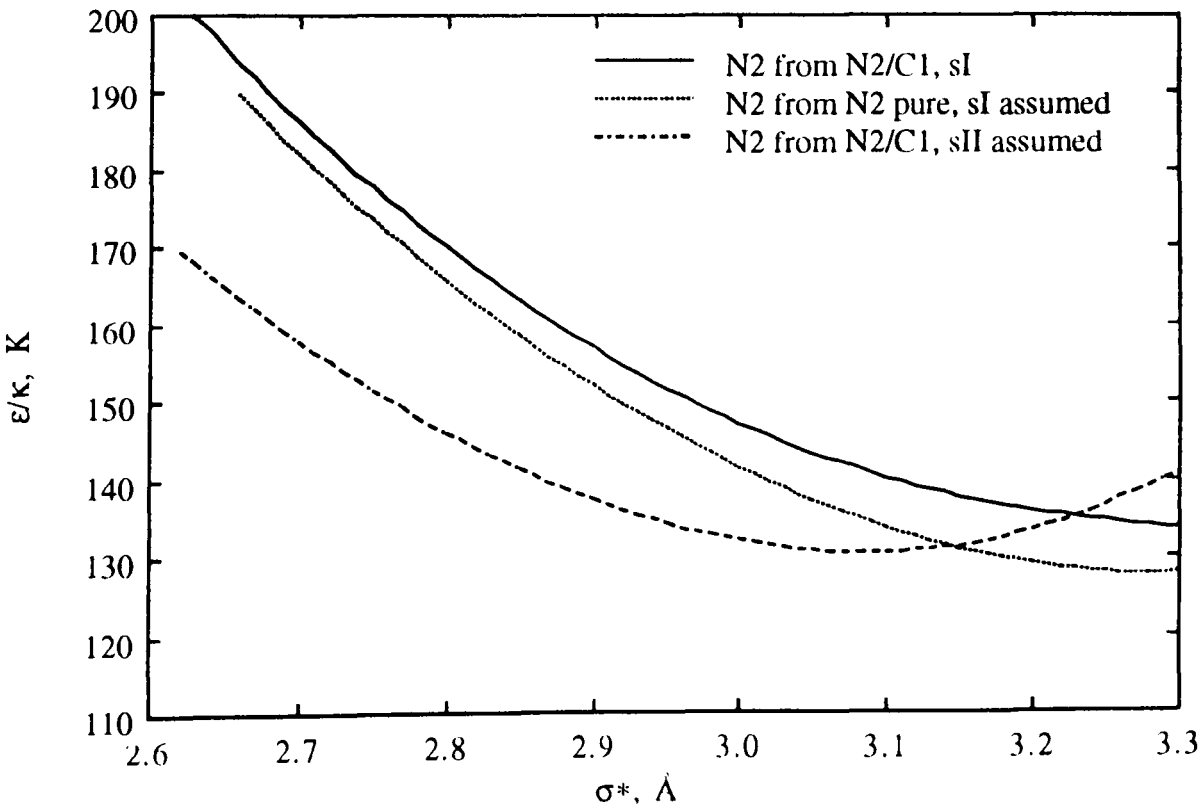

Figure-3.24 Kihara parameters for nitrogen from N2/C1 (sI), N2 pure (sI), N2/C1 (sII) systems.

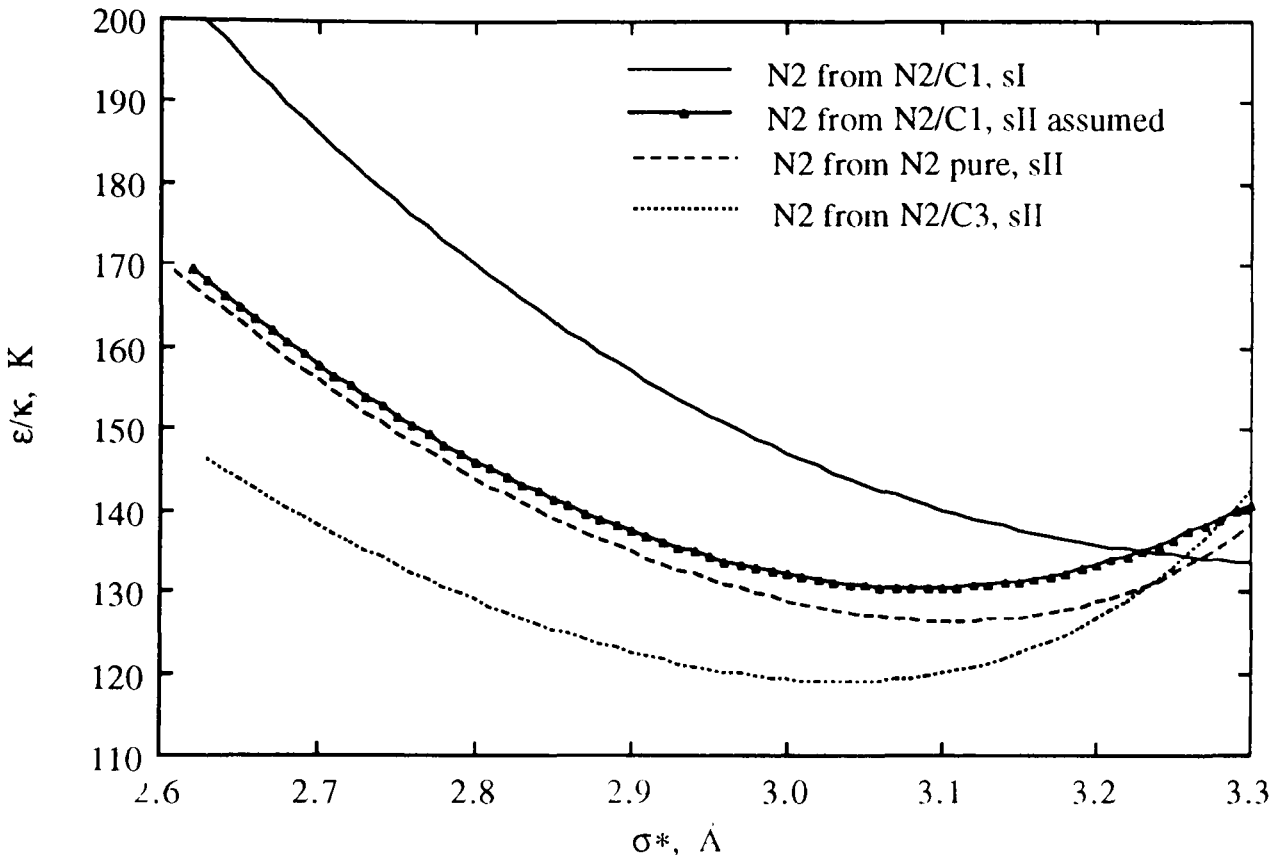

Figure-3.25 Kihara parameters for nitrogen from N2/C1 (sI), N2/C1 (sII), N2 pure (sII), and N2/C3 (sII) systems.

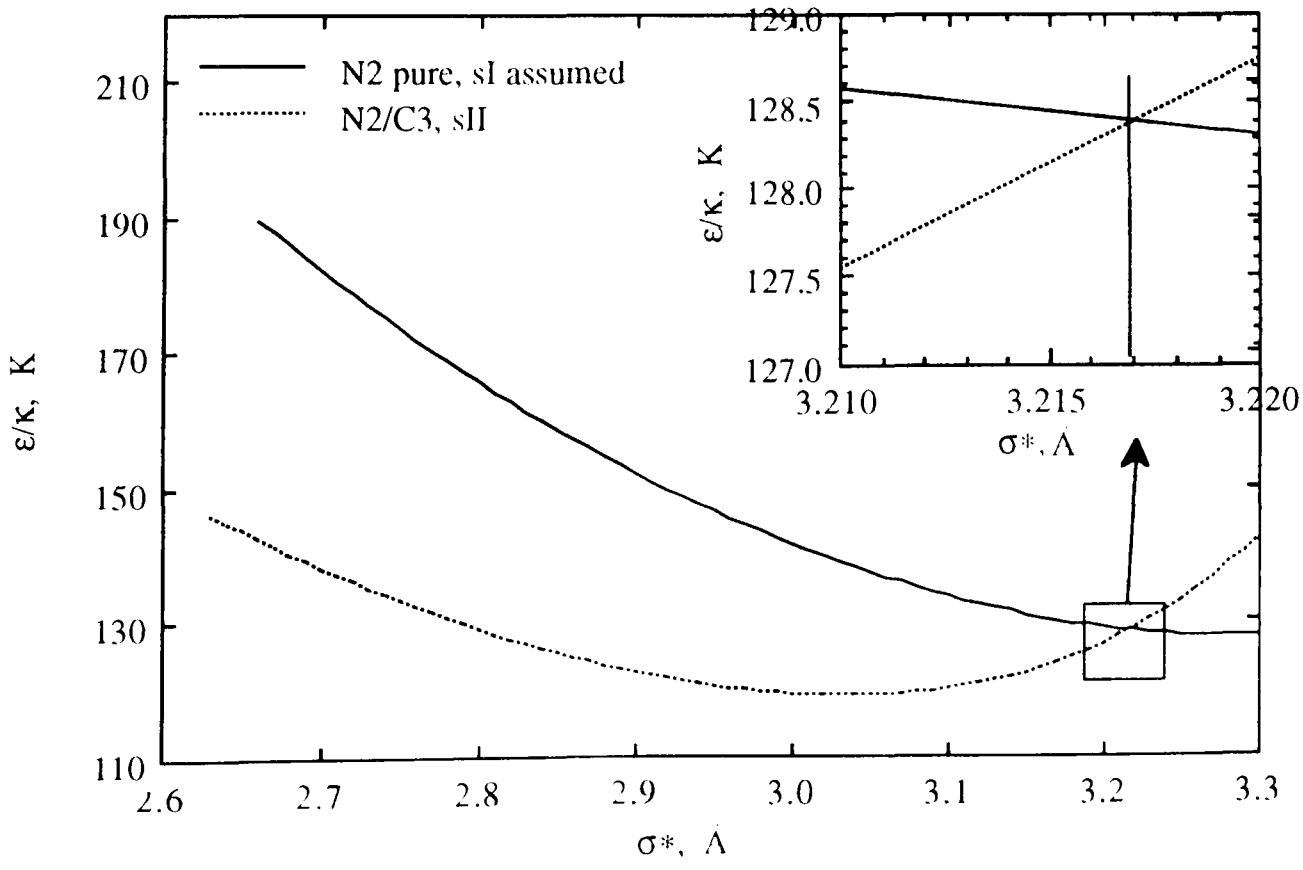

Figure-3.26 Kihara parameters for nitrogen, assuming structure-I for N2 simple gas hydrates.

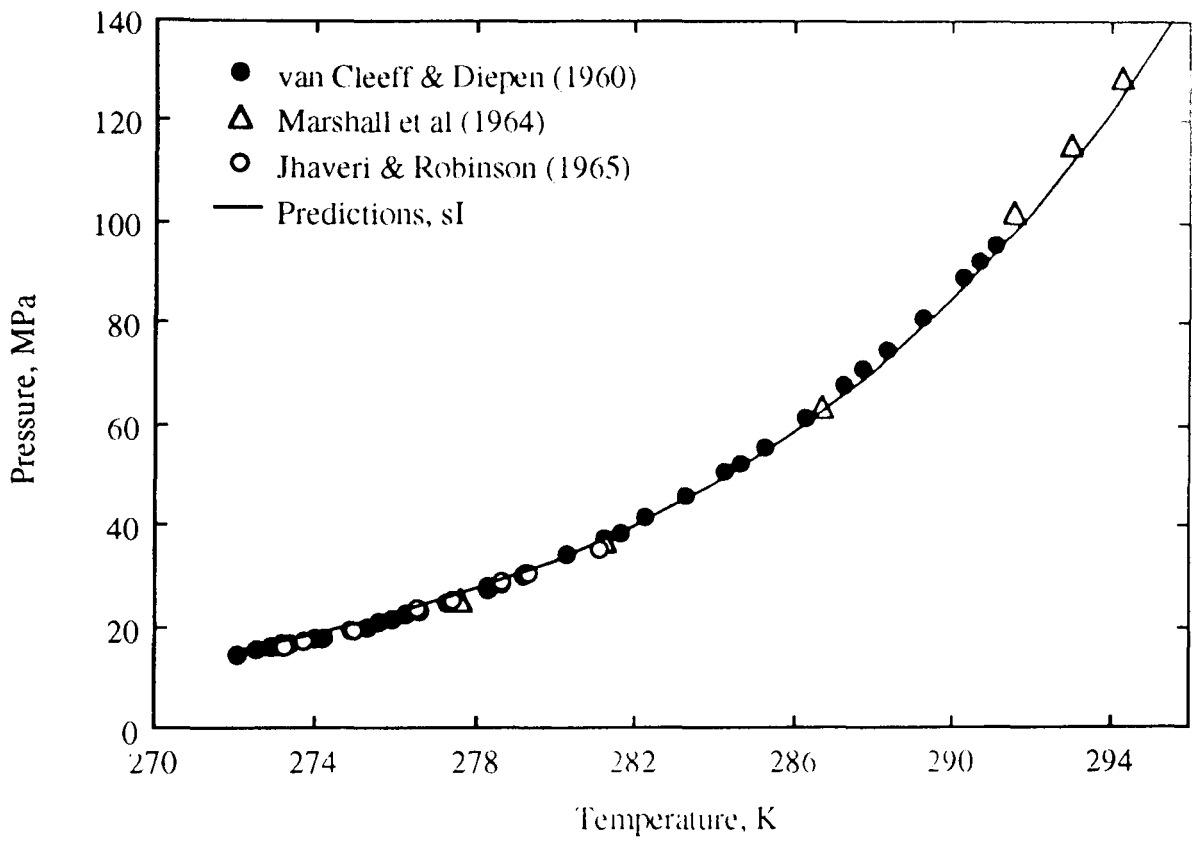

Figure-3.27 Experimental and calculated dissociation pressures of nitrogen (sI) in the L1-H-V region.

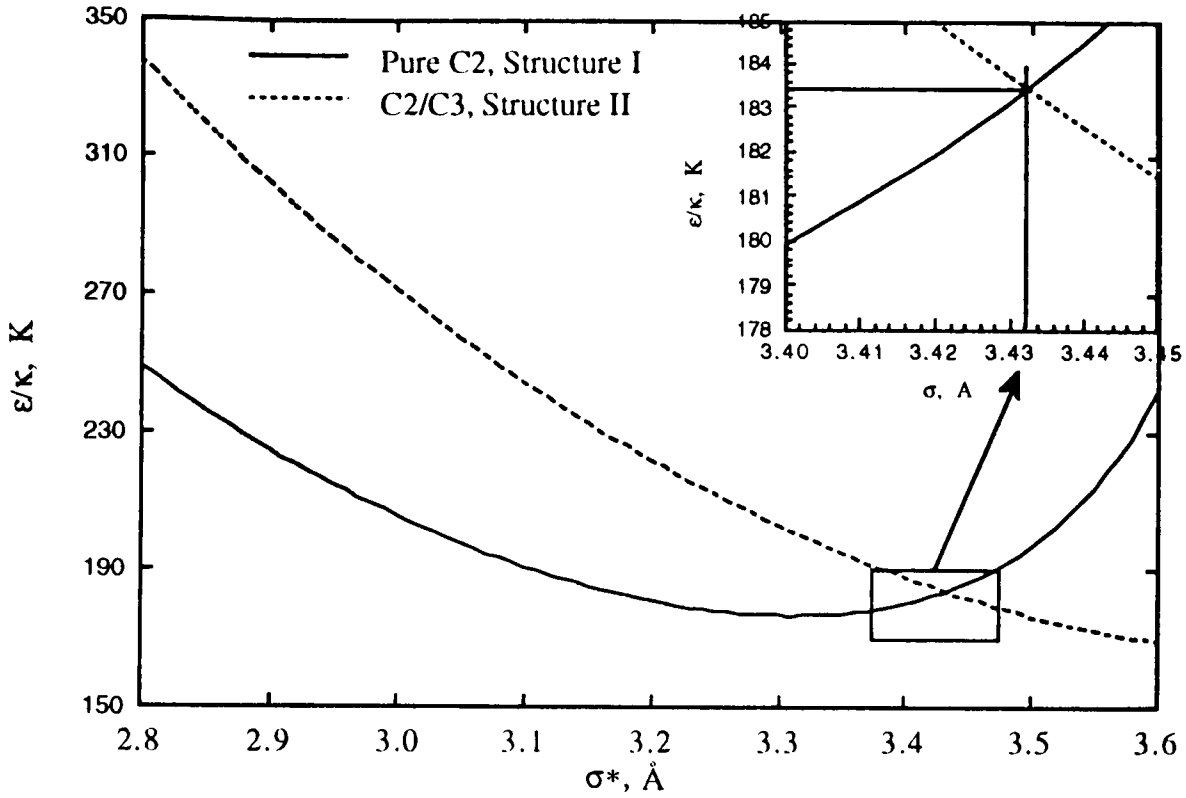

Figure-3.28 Optimised pairs of Kihara parameters for ethane in structures I and II.

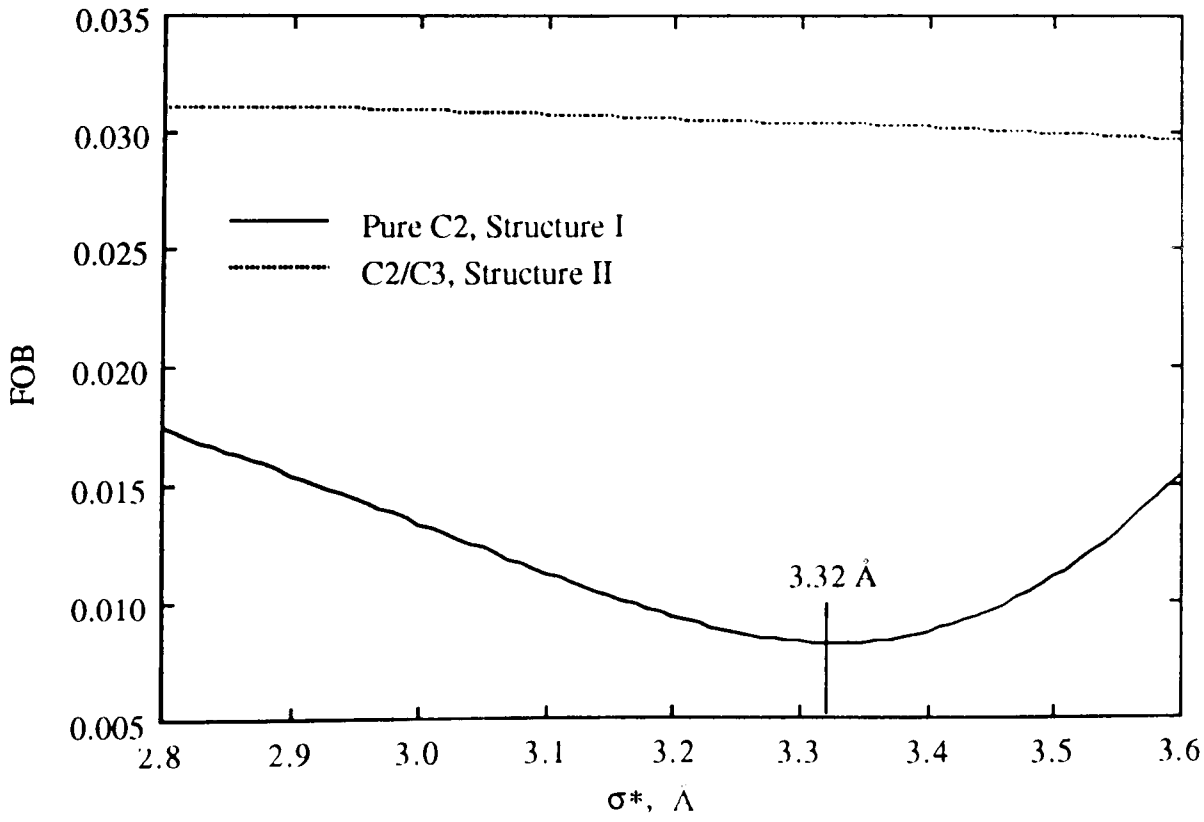

Figure-3.29 Objective Function for optimised pairs of Kihara parameters for ethane in structures I and II.

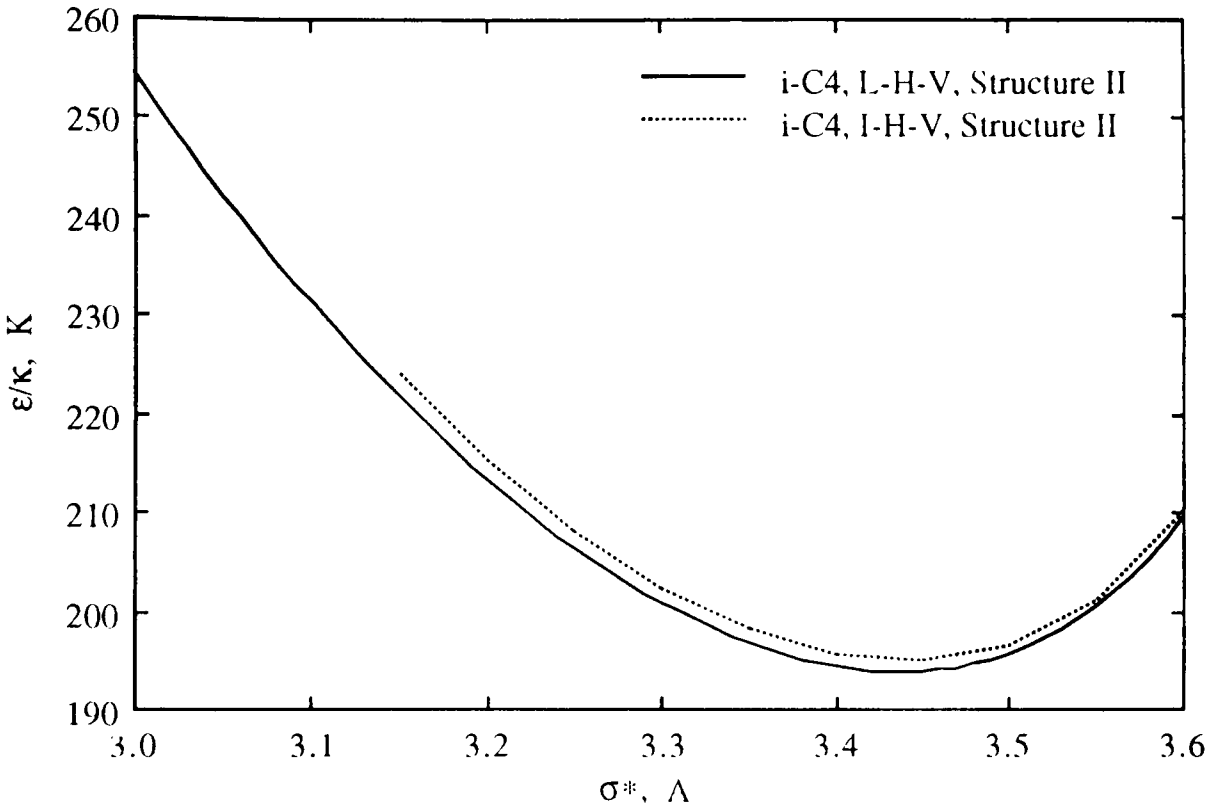

Figure-3.30 Optimised pairs of Kihara parameters for i-butane in the L1-H-V and I-H-V regions.

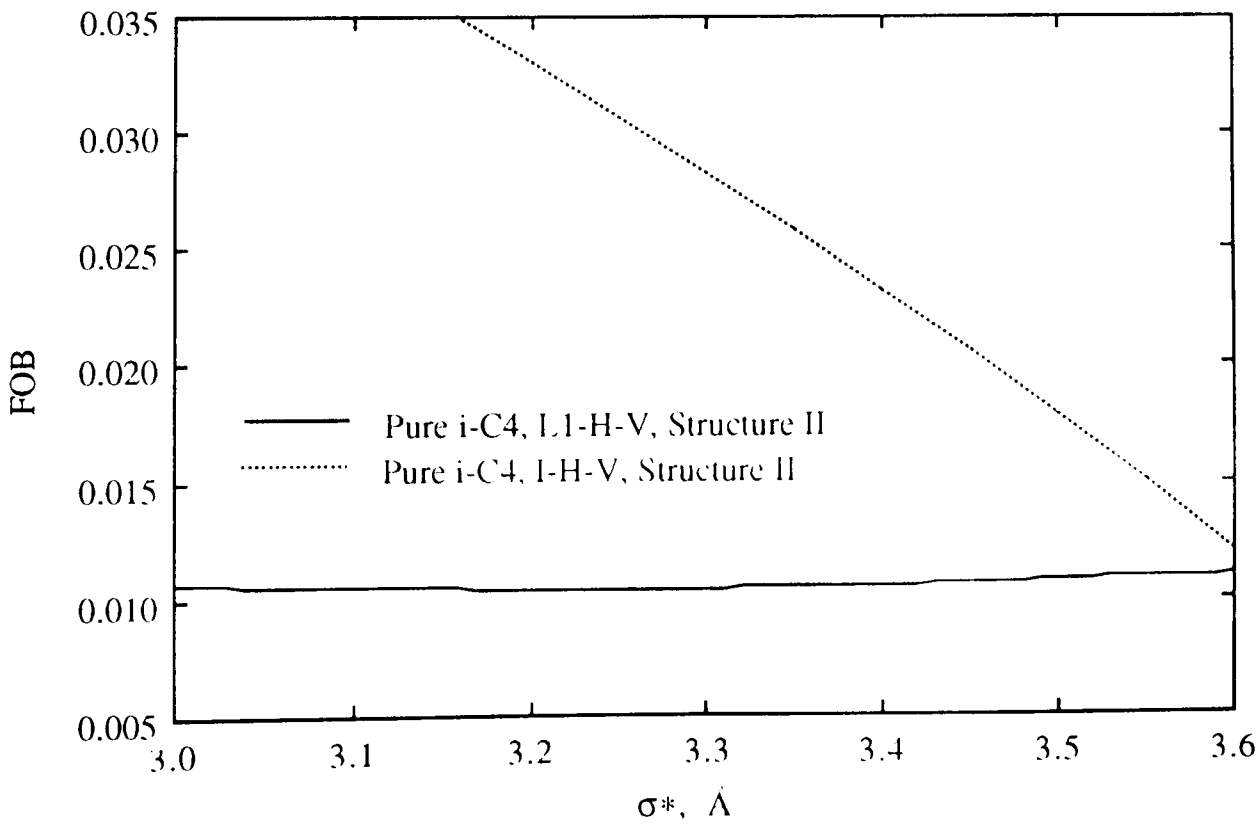

Figure-3.31 Objective Function for optimised pairs of Kihara parameters for i-C4 in the L1-H-V and I-H-V regions.

CHAPTER-4

MODELLING THE HEAVY HYDRATE FORMERS

4.1. INTRODUCTION

The current industrial practice in avoiding hydrate problems is to operate in conditions outside the hydrate phase boundary. This approach can be made more cost effective and efficient by determining the hydrate phase boundary more reliably. Experimental determination of the hydrate phase boundary in different production scenarios could be very expensive, so the industrial trend is in favour of improving the predictive methods. As mentioned previously, the most advanced predictive methods are based on the statistical thermodynamic approach as developed by van der Waals and Platteeuw in 1959. This approach, combined with a phase behaviour model is able to predict the hydrate phase boundary in different production scenarios and feed compositions. The main requirements are the optimisation of the binary interaction parameters (BIP) for the phase behaviour model and the Kihara parameters for the hydrate model.

Until recently in the oil and gas industry, n-butane has been regarded as the heaviest hydrate forming compound, and anything heavier than it was thought to be a non-hydrate former. Although this approach could be adequate for gaseous mixtures, it is not so for all oil and gas condensate systems which contain significant amounts of intermediate/heavy hydrocarbon compounds heavier than n-butane. Some of these compounds have an effective van der Waals' diameter which theoretically should allow them to enter the large cavities of structure-II gas hydrates. Furthermore, Ripmeester *et*

al. (1987, 1991) have suggested the presence of a third structure, called H, with cavities larger than those of structures-I and II. This would allow the formation of hydrates by even larger molecules in the presence of a help gas.

Whilst available models can accurately predict the hydrate equilibria for synthetic and simple mixtures, they are generally optimistic, i.e. under predicting the hydrate zone, for oil and rich gas-condensate (Avlonitis *et al.*, 1989). This could be attributed to the presence of heavy hydrate forming compounds in the fluids. These compounds are commonly regarded as non-hydrate formers, so inhibiting hydrate formation. By taking into account the heavy hydrate formers, more reliable prediction of the hydrate phase boundary (particularly for oil and gas-condensate) is expected.

In this chapter, the phase equilibria modelling and optimisation of the Kihara parameters for some of the Heavy Hydrate Formers (HHF), including, benzene, cyclohexane, and methylcyclohexane are explained. According to Ripmeester *et al.* (1991), the first two compounds form structure-II gas hydrates, whereas the latter forms the newly discovered structure-H gas hydrates. All the above compounds are reported to need help gas to fill and stabilise the smaller cavities. Two different help gases, methane and nitrogen, were used in conducting the experiments (Burgass, 1995). Methane was chosen for several reasons; it is present in large concentrations in reservoir fluids, it can fill all cavities in hydrate structures, and finally the presence of the heavy hydrate formers necessitates a change in the hydrate structure from I to II, or H for methane. Nitrogen is also able to fill all cavities, but there is no change in hydrate structure for its binary with the first three compounds (providing that Davidson *et al.*, 1986b, 1987, are correct in assigning structure-II for nitrogen simple gas hydrates). Finally, its binary with the heavy hydrate formers provides hydrate dissociation data at high pressures, allowing the evaluation of the model at the conditions relevant to pipeline conditions.

al. (1987, 1991) have suggested the presence of a third structure, called H, with cavities larger than those of structures-I and II. This would allow the formation of hydrates by even larger molecules in the presence of a help gas.

Whilst available models can accurately predict the hydrate equilibria for synthetic and simple mixtures, they are generally optimistic, i.e. under predicting the hydrate zone, for oil and rich gas-condensate (Avlonitis *et al.*, 1989). This could be attributed to the presence of heavy hydrate forming compounds in the fluids. These compounds are commonly regarded as non-hydrate formers, so inhibiting hydrate formation. By taking into account the heavy hydrate formers, more reliable prediction of the hydrate phase boundary (particularly for oil and gas-condensate) is expected.

In this chapter, the phase equilibria modelling and optimisation of the Kihara parameters for some of the Heavy Hydrate Formers (HHF), including, benzene, cyclohexane, and methylcyclohexane are explained. According to Ripmeester *et al.* (1991), the first two compounds form structure-II gas hydrates, whereas the latter forms the newly discovered structure-H gas hydrates. All the above compounds are reported to need help gas to fill and stabilise the smaller cavities. Two different help gases, methane and nitrogen, were used in conducting the experiments (Burgass, 1995). Methane was chosen for several reasons; it is present in large concentrations in reservoir fluids, it can fill all cavities in hydrate structures, and finally the presence of the heavy hydrate formers necessitates a change in the hydrate structure from I to II, or H for methane. Nitrogen is also able to fill all cavities, but there is no change in hydrate structure for its binary with the first three compounds (providing that Davidson *et al.*, 1986b, 1987, are correct in assigning structure-II for nitrogen simple gas hydrates). Finally, its binary with the heavy hydrate formers provides hydrate dissociation data at high pressures, allowing the evaluation of the model at the conditions relevant to pipeline conditions.

Three sets of experimental data have been generated for each heavy hydrate former. They are C_1/HHF, N_2/HHF, and C_1/N_2/HHF. Generally, the first set of data, i.e. the dissociation pressure data for the C_1/HHF binaries, have been used in the optimisation of the Kihara potential parameters (Kihara, 1953). The other two sets of experimental data, i.e. the N_2/HHF binaries, and the C_1/N_2/HHF ternaries, have been used in the validation of the model. The experimental data, equipment set-up, and test procedures are presented by Burgass (1995).

It is worth mentioning that, in all binaries (C_1/HHF and N_2/HHF), the system is comprised of three components (methane or nitrogen, new hydrate former, and water) and four phases (water, liquid hydrocarbon, vapour, and gas hydrates). According to the Gibbs phase rule there is only one degree of freedom for the above systems, and therefore, the equilibrium conditions at a given temperature do not depend on the mixture composition.

The fugacity of the heavy hydrate former compounds in fluid phases were calculated using an EoS. Published data on the phase equilibria of the heavy hydrate formers and the mutual solubilities with water have been used in finding the BIP, for the VPT (Valderrama, 1990) EoS with the non-density dependent (NDD) mixing rules (Avlonitis *et al.*, 1994). As mentioned before, the Kihara parameter optimisation has been limited to σ, the collision diameter, and ε, the depth of the energy well. Again, for simplicity, σ^* ($\sigma^*=\sigma-2\alpha$) and ε/κ have been chosen as optimisation parameters, instead of σ and ε, respectively. The hard core radius, α, which does not play an important role in the optimisation process (Holder and Hand, 1982) has been found using the correlations given by Tee *et al.* (1966). For determining the optimised set of parameters, the conventional minimisation of the objective function has been used. The optimisation procedure and the objective function are discussed in Chapter-3.

4.2. STRUCTURE-II HEAVY HYDRATE FORMERS

Structure-II gas hydrates were discovered in the early 1950's (von Stackelberg and Müller, 1954). However, until recently, the general belief in the oil/gas industries was that n-butane is the heaviest hydrocarbon, capable of forming structure-II gas hydrates in the presence of a help gas. All computer programmes or other predictive methods consider any compound heavier that n-butane as a non-hydrate former (Sloan, 1990), which consequently inhibits hydrate formation. In fact, the compositional analysis did not go any further than n-butane for hydrate calculations. Ripmeester *et al.*, (1987, 1991) suggested that benzene and cyclohexane are potential structure-II gas hydrate formers, but this had not been verified by experimental evidence.

4.2.1. Benzene

Critical properties and the acentric factor (Table-4.1) are required to model each compound using the VPT EoS. The model predicts a normal boiling point of 353.18 K against the experimental value of 353.2 K for benzene.

Benzene-water equilibria

The solubility of benzene in water has been extensively investigated. Tsonopoulos and Wilson, (1983) reviewed the available data on the mutual solubilities of several hydrocarbons, including benzene at the three-phase (water-liquid hydrocarbon-vapour) equilibrium pressures. They showed that the liquid mutual solubilities are only weakly pressure-dependent, and therefore, solubilities at pressures greater than the three-phase equilibrium pressures are not drastically different from those at the equilibrium pressures. However, it is important for the system pressures not to be below the three-phase equilibrium pressures, because then the second liquid phase would disappear. After analysing a wide range of experimental data, the above authors presented the following correlation for the three-phase equilibrium pressure of benzene and water:

$$\ln P_s = 10.0774 - 4241.29/T \qquad (4.1)$$

where P_3 is the three-phase equilibrium pressure in MPa and T is the temperature in K. They presented the following equation for calculating the solubility of benzene in water at the three-phase equilibrium pressure:

$$\ln x_{hc} = -170.04018 + 6922.912/T + 24.398795 \ln T \qquad (4.2)$$

where x_{hc} is the mole fraction of benzene in water. The above authors also examined the available data on the solubility of water in benzene and suggested the following equation for calculating the mole fraction of water in benzene at the three-phase equilibrium pressure:

$$\ln x_w = -1.64055 - 2029.41/T + 0.00900544T \qquad (4.3)$$

where x_w is the mole fraction of water in benzene. Equations-4.2 and 4.3 were used to calculate the mutual solubilities of benzene and water for the optimisation of the Binary Interaction Parameters (BIP) in the Non-Density Dependent (NDD) mixing rules (Table-4.2), (Avlonitis *et al.* 1994). Figures-4.1 and 4.2 show the predicted mutual solubilities of benzene and water alongside those calculated from Equations-4.2 and 4.3.

Benzene-methane equilibria

The above system has been studied extensively. In this work the data generated by Elbishlawi and Spencer, (1951) and Lin *et al.*, (1979), as reported in IUPAC Solubility Data Series Volume 27/28, have been used in the optimisation of the binary interaction parameter between methane and benzene (Table-4.2). Figures-4.3 and 4.4 show the experimental and predicted methane-benzene phase equilibria at two different temperatures.

Benzene-nitrogen equilibria

A total of 46 experimental data points (IUPAC Solubility Data Series, Volume 10, 1982) were employed in the optimisation of the nitrogen-benzene binary interaction parameters

(Table-4.2). Figure-4.5 shows the experimental and predicted solubilities of nitrogen in benzene at two different temperatures. Experimental and predicted phase equilibria for the above system is presented in Figure-4.6, as an example. As demonstrated in the above figures, in all cases the predicted solubilities are in good agreement with the experimental data.

Kihara potential parameters for Benzene

Hydrate dissociation points are measured and reported by Burgass (1995) for the methane/benzene and nitrogen/benzene binary systems. The feed compositions and the experimental hydrate dissociation conditions for the methane/benzene gas hydrates are duplicated in Table-4.4. Four sets of dissociation pressure data were generated for the binary with only the first two sets being used in the optimisation of the Kihara potential parameters and the other two sets were employed for validation.

Tee *et al.* (1966) reported two sets of Kihara parameters for benzene (Table-4.5), based on second virial coefficient and viscosity data. In this study, the value of the hard core radius, α, is fixed at 1.2 Å, and the optimisation of the Kihara parameters is restricted to the collision diameter, σ, and the energy parameter, ε.

Figures-4.7 and 4.8 present all the ε/κ and σ^* pairs and the corresponding objective functions (FOB), using the first two sets of experimental data, respectively. Figure-4.8 shows that the objective function reaches a minimum at σ^*=3.16 Å, for which ε/κ is equal to 210.32 K (Table-4.3).

Figure-4.9 shows the experimental and predicted dissociation pressure for methane/benzene gas hydrates. The measured and predicted dissociation conditions of pure methane (Deaton and Frost, 1946, de Roo *et al.*, 1983, Tohidi *et al.*, 1993) are also shown for comparison. *Note the significant shift of the dissociation temperature to higher values due to the presence of benzene.* Experimental data for sets-3 and 4 have not been

used in the optimisation, but the model predictions are in good agreement with them, as is shown in Figure-4.9. Experimental and predicted dissociation conditions for pure nitrogen, and nitrogen/benzene binaries are presented in Figure-4.10. The predictions are in very good agreement with the experimental data. Again, the presence of benzene significantly reduces the hydrate free zone.

4.2.2. Cyclohexane (CH)

Cyclohexane is reported to form structure-II gas hydrates (Ripmeester *et al.*, 1991). Using its physical and critical constants, the phase equilibria of this compound could be modelled by the VPT EoS. The acentric factor has been slightly adjusted to match the vapour data (Table-4.1). Figures-4.11 and 4.12 show the experimental and predicted vapour pressure for cyclohexane in low and high pressure ranges, respectively. The good agreement demonstrates the success of the EoS modelling of pure cyclohexane.

Cyclohexane-water equilibria

The phase equilibria of cyclohexane-water systems could be modelled by optimising the BIP in the NDD mixing rules. The main source of data was the excellent work of Tsonopoulos and Wilson, (1983), in which they suggested the following correlation for calculating the three-phase equilibria pressure for the cyclohexane-water systems:

$$\ln P_3 = 10.0506 - 4229.59/T \qquad (4.4)$$

here P_3 is the three-phase pressure in MPa at any given temperature. T is the equilibrium temperature in K. The solubility of cyclohexane in water x_{hc} and water in cyclohexane x_w at the three-phase pressures could be calculated from the following equations:

$$\ln x_{hc} = -209.11689 + 8325.49/T + 29.8231 \ln T \qquad (4.5)$$

$$\ln x_w = -62.7645 - 654.027/T + 9.99967 \ln T \qquad (4.6)$$

The above equations (4.4 to 4.6) were employed to find the three-phase pressures, the solubilities of cyclohexane in water and water in cyclohexane in the temperature range of 273.15 to 423.15 K in 10 K intervals. The solubility data were used to optimise the binary interaction parameters (Table-4.2). At any given temperature, the equilibrium pressure was assumed 1 atm higher than the three-phase pressure predicted by Equation-4.4 to insure L_1-L_2 equilibria. Experimental and predicted mutual solubilities of cyclohexane and water are presented in Figures-4.13 and 4.14. The solubility of water in cyclohexane is higher than cyclohexane in water and the model predictions are in better agreement with the experimental data for the former. For the latter, the model predictions have significant deviations at high temperatures (i.e. T>370 K). However, considering the fact that hydrate calculations are at relatively low temperatures, it could be concluded that the model predictions for the mutual solubilities are acceptable.

Cyclohexane-methane equilibria

The above system was modelled using the experimental data reported by Reamer *et al.* (1958). A total of 67 data points in the temperature range of 294.3 K to 444.3 K were employed in optimising the methane-cyclohexane BIP (Table-4.2). Experimental and predicted methane-cyclohexane phase equilibria at different temperatures are presented in Figures-4.15 to 4.17, which demonstrate the success of modelling. Figure-4.15 shows that, for the above system assuming a BIP of 0 will still give good results.

Cyclohexane-nitrogen equilibria

A total of 25 solubility data (IUPAC Solubility Data Series, Volume-10) for the above system were employed in the determination of the binary interaction parameter between nitrogen and cyclohexane (Table-4.2). Figure-4.18 shows the experimental and predicted solubilities of nitrogen in cyclohexane.

Kihara potential parameters for Cyclohexane

A total of 9 dissociation points were measured for the methane/cyclohexane system over the temperature range of 275.05 to 290.95 K (Tohidi *et al.*, 1995d). For nitrogen/cyclohexane and methane/nitrogen/cyclohexane systems, 5 and 4 dissociation points were measured over temperature ranges of 277.25 to 288.75 K and 277.95 to 289.95 K, respectively. The three sets of experimental data are reported by Burgass (1995).

Cyclohexane is not among the compounds studied by Tee *et al* (1966) to determine their Kihara potential parameters from viscosity and second virial coefficients. However, they have suggested several correlations to determine the Kihara parameters from the acentric factor, P_C, and T_C . In this work, the appropriate correlations were used resulting in an average hard core diameter, α of 0.975 Å. The other two Kihara parameters for cyclohexane, the collision diameter (σ) and the depth of the energy well (ε) were optimised by minimising the absolute average deviation between the predicted and measured hydrate dissociation pressures of methane-cyclohexane mixtures.

Figures-4.19 and 4.20 show ε/κ vs σ^* and FOB vs σ^* for methane-cyclohexane binary. Figure-4.20 shows that the objective function is minimum at σ^*=2.53 Å with a corresponding value of ε/κ=426.75 K (Table-4.3). The above Kihara potential parameters and those previously determined (Chapter-3) for methane and nitrogen were used in predicting the hydrate dissociation conditions for cyclohexane binaries and ternaries with methane and nitrogen.

Figure-4.21 shows the experimental and predicted dissociation conditions for methane/cyclohexane gas hydrates. As expected, the agreement is excellent, as the data have been used in the optimisation of the Kihara parameters. In the above figure, the experimental and predicted hydrate phase boundaries for methane simple gas hydrates are also presented. The hydrates formed in the presence of cyclohexane are of structure-II,

whereas those formed in the presence of pure methane are structure-I hydrates. Note the significant increase in dissociation temperatures (about 10 K), due to the presence of cyclohexane.

Figure-4.22 presents the experimental and predicted hydrate dissociation conditions for nitrogen/cyclohexane hydrates. Although none of the nitrogen/cyclohexane hydrate dissociation data has been used in the optimisation, the agreement for this high pressure system is very good and the maximum error in predicted potential hydrate formation temperature is about 0.5 K. Experimental and predicted hydrate dissociation conditions for nitrogen simple gas hydrates are also presented in the above figure. As shown in the above figure, the shift in the potential hydrate formation temperature is quite large (about 10 K), which demonstrates the substantial reduction in the hydrate free zone due to the presence of cyclohexane.

Figure-4.23 shows the experimental and predicted hydrate dissociation conditions for methane/nitrogen/cyclohexane. Again, the agreement between the experimental data and predictions is very good. The experimental and predicted hydrate phase boundaries for nitrogen and methane simple hydrates are also presented in the above figure for comparison.

Figure-4.24 presents all the hydrate data generated for cyclohexane by Burgass, (1995). As mentioned before, all the above systems are in the four phase (water, liquid hydrocarbon, vapour, and hydrates) equilibria region. The hydrate phase boundary for methane/nitrogen/cyclohexane is between the phase boundaries for nitrogen/cyclohexane and methane/cyclohexane, depending on the composition of the system.

4.3. STRUCTURE-H HEAVY HYDRATE FORMERS

The first equilibrium data on structure-H gas hydrates was reported for methane/adamantane by Lederhos *et al.* (1992). Mehta and Sloan (1993, 1994a) have

reported structure-H hydrate data for some other heavy compounds with methane. In a recent publication Mehta and Sloan (1994b) presented a statistical thermodynamic model for structure-H hydrates, based on the original work of van der Waals and Platteeuw (1959). They also optimised the Kihara potential parameters for four structure-H hydrate formers.

After modelling the phase equilibria of the heavy hydrate formers, the hydrate model and the optimisation method, proposed in Chapters-2 and 3, were used to optimise the Kihara parameters. The Kihara parameters are determined by minimising the absolute average deviation between the predicted and measured hydrate dissociation pressures.

Three sets of dissociation pressure data have been generated for each of the heavy hydrate formers. Only their binaries with methane have been used for optimising the Kihara parameters. The other two sets of dissociation pressure data, i.e. the binaries with nitrogen, and the ternaries with methane plus nitrogen, have been used in the validation of the model.

4.3.1. Methylcyclohexane (MCH)

Methylcyclohexane is reported to form structure-H gas hydrates (Ripmeester, *et al.*, 1991). This compound is modelled as a pure compound using its physical and critical constants (Table-4.1). The calculated acentric factor is slightly changed to match vapour pressure data. Figure-4.25 shows the experimental and predicted vapour pressures of methylcyclohexane over a wide range of temperature.

Methylcyclohexane-water equilibria

IUPAC solubility data series, Volume-37, has reported some experimental data on the solubility of methylcyclohexane in water, but there is no data on the solubility of water in methylcyclohexane. However, it is known that the solubility of water in the hydrocarbon phase varies only slightly within a class of hydrocarbons (Michel *et al.* 1989). In this

work, the solubility of water in methylcyclohexane is assumed to be the same as the solubility of water in cyclohexane (Equation-4.6). The above data were employed to calculate the BIP between water and methylcyclohexane in the VPT EoS with the NDD mixing rules. The methylcyclohexane-water binary interaction parameters are presented in Table-4.2. Figures-4.26 and 4.27 show the experimental/estimated and predicted mutual solubilities of methylcyclohexane and water.

Methylcyclohexane-methane equilibria

Very limited data is available on the above system. The data generated by Field *et al* (1974), as reported in the IUPAC Solubility Data Series Volume 27/28, were used in optimising the binary interaction parameter between methane and methylcyclohexane (Table-4.2). Experimental and predicted solubilities of methane in methylcyclohexane at 101.325 KPa methane partial pressure are presented in Figure-4.28.

Methylcyclohexane-nitrogen equilibria

Phase equilibria of the above system is reported in the IUPAC Solubility Data Series Volume 10, and were used in the optimisation of the binary interaction parameter (Table-4.2). Experimental and predicted vapour-liquid equilibria for nitrogen methylcyclohexane system at two different temperatures are presented in Figures-4.29 and 4.30.

Kihara potential parameters for Methylcyclohexane

Three sets of experimental dissociation pressure data were generated for C_1/MCH, N_2/MCH, and C_1/N_2/MCH systems, and are reported by Burgass (1995). Again, the first set of data was used in the optimisation of the Kihara parameters for MCH and the other two sets were employed in the validation of the model. Optimisation was restricted to the depth of the energy well, ε, and the collision diameter, σ. The hard core radius, α=1.0693 Å, was calculated from the relations given by Tee *et al.* (1966). Figure-4.31 and 4.32

show the ε/κ vs σ^* and FOB vs σ^* plots. Figure-4.32 shows a sharp minimum at σ^*=4.38 Å with corresponds to ε/κ=230.296 K (Table-4.3).

Figure-4.33 presents experimental and predicted hydrates dissociation conditions for pure methane, and methane/methylcyclohexane systems. The experimental data reported by Mehta and Sloan (1994a) are also presented in the above figure. The model predictions are in good agreement with all experimental data. The reduction in the hydrate free zone due to the presence of methylcyclohexane is significant. Figure-4.34 presents experimental and predicted hydrate dissociation conditions for nitrogen/methylcyclohexane binary. The system is in the L_1-L_2-V-H four phase region. The hydrate dissociation points for pure nitrogen are also presented in Figure-4.34 for comparison. The predictions are in good agreement with the experimental data and the maximum error in predicting the potential hydrate formation temperature is less than 1K.

4.4. CONCLUSIONS

Phase equilibria and hydrate modelling for some intermediate/heavy hydrocarbons have been detailed. In the phase equilibria, three different systems, i.e., HHF-water, HHF-methane, and HHF-nitrogen have been modelled. In the hydrate modelling sections, the Kihara potential parameters have been determined for each of the HHF. In all cases the predictions are compared with the experimental data.

Solubility and phase equilibria data published in the open literature have been used in the vapour-liquid equilibria modelling of the heavy hydrate formers. The overall agreement of the model predictions with the experimental data was good, though in some cases the model was not able to give accurate predictions on the HHF solubilities in water at high temperatures.

Among the HHF discussed in this section, benzene and cyclohexane are reported to form structure-II gas hydrates. Methylcyclohexane is known to for structure-H gas hydrates in

the presence of a help gas. Two different help gases, i.e. methane and nitrogen have been used in performing the experiments (Burgass, 1995). Methane was chosen due to its high concentrations in the reservoir fluids and the choice of nitrogen gives the opportunity of examining the model at higher pressures, relevant to sub-sea transmission lines. For each HHF, three different systems, i.e. HHF/C_1, HHF/N_2, HHF/C_1/N_2 have been studied. Only the hydrate dissociation pressure data point for the HHF/C_1 binaries have been used in the optimisation of the Kihara parameters. The experimental dissociation pressure data points on the other two systems have been used in the validation of the hydrate model, with good results.

The addition of heavy hydrate formers to other recognised hydrate forming compounds is expected to result in a more reliable prediction of hydrate phase boundary of petroleum reservoir fluids. This can play an important role in the design and operation of sub-sea transmission lines.

****

Table-4.1. Physical and critical constants for the heavy hydrate formers.

Component	M, g.mole^{-1}	ω	T_c, K	P_c, MPa	v_c, cm^3.mole-1
Benzene	78.114	0.2120	562.20	4.89	259.10
Cyclohexane	84.160	0.21367	553.50	4.07	308.00
Methylcyclohexane	98.190	0.23680	572.20	3.47	368.00

Table-4.2. Binary interaction parameters between the heavy hydrate formers and methane, nitrogen, or water.

	Methane	Nitrogen	Water (2)*		
Component (1)	k_{21}	k_{21}	k_{21}	l^o_{21}	$l^l_{21} \times 10^4$
Benzene	0.020	0.156	0.638	1.5828	-21.7859
Cyclohexane	0.011	0.123	0.540	1.4432	-29.9036
Methylcyclohexane	0.017	0.071	0.556	1.5959	-29.7648

* BIP for the non-density dependent mixing rules (Appendix-A).

Table-4.3. Kihara potential parameters for gas-water interactions.

Component	α, Å	σ*, Å	ε/κ, K
Benzene	1.200	3.16	210.32
Cyclohexane	0.975	2.53	426.75
Methylcyclohexane	1.069	4.38	230.30

$\sigma=\sigma^*+2\alpha$

Table-4.4. Feed compositions and measured dissociation conditions for methane/benzene gas hydrates.

Feed Composition (Mole%)			Dissociation Conditions	
Methane	Benzene	Water	Temp. (K) (±0.05 K)	Press. (MPa) (±0.007 MPa)
		Set-1		
13.224	8.440	78.336	275.45	1.507
		Set-2		
14.247	8.372	77.381	277.30	2.082
			278.35	2.392
			279.85	2.958
			280.95	3.482
			282.35	4.046
		Set-3		
25.578	1.971	72.451	281.35	3.406
			291.95	3.696
			282.95	4.240
		Set-4		
34.443	6.188	59.369	284.55	5.502
			284.95	5.909
			285.65	6.578
			286.25	7.219
			286.65	7.826
			287.45	8.570

Table-4.5. Benzene Kihara spherical core potential parameters, Tee et al., 1966.

α, Å	σ*, Ä	ε/κ, K	Source of data
1.2397	4.2166	582.62	Second virial coefficient.
1.2054	2.5272	975.37	Viscosity and second virial coefficient.

$\sigma=\sigma^*+2\alpha$

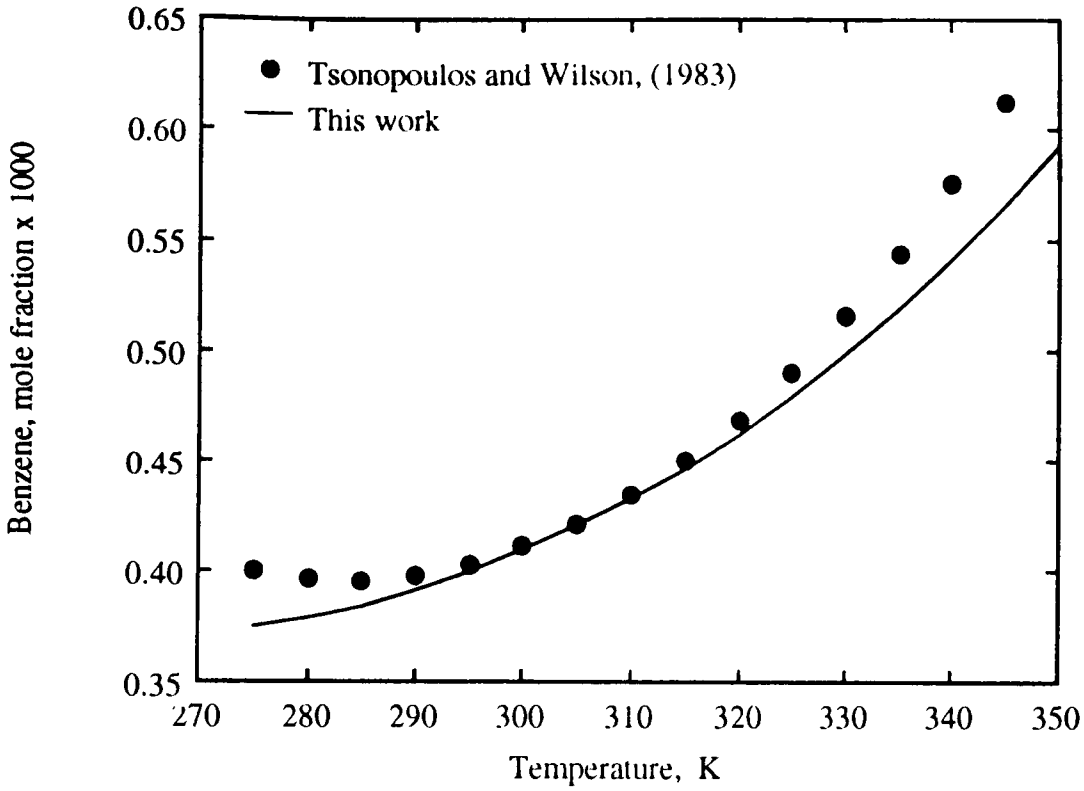

Figure-4.1 Experimental and predicted solubilities of benzene in water, at three-phase equilibrium pressure.

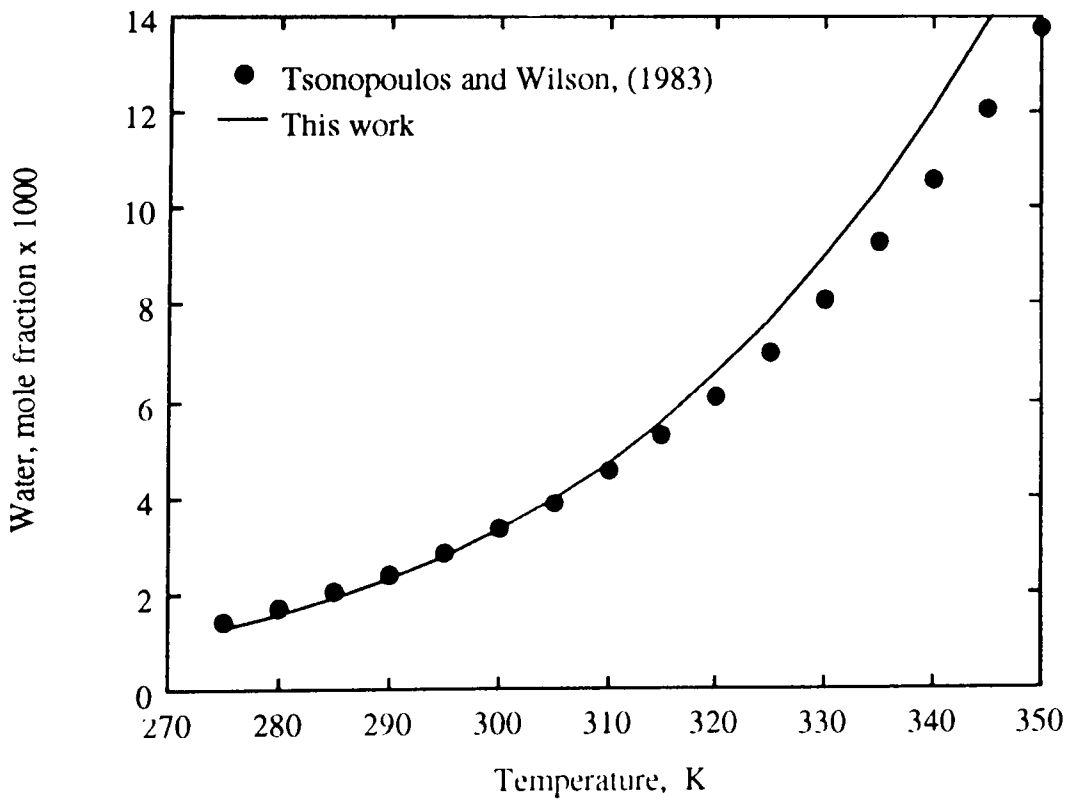

Figure-4.2 Experimental and predicted solubilities of water in benzene, at three-phase equilibrium pressure.

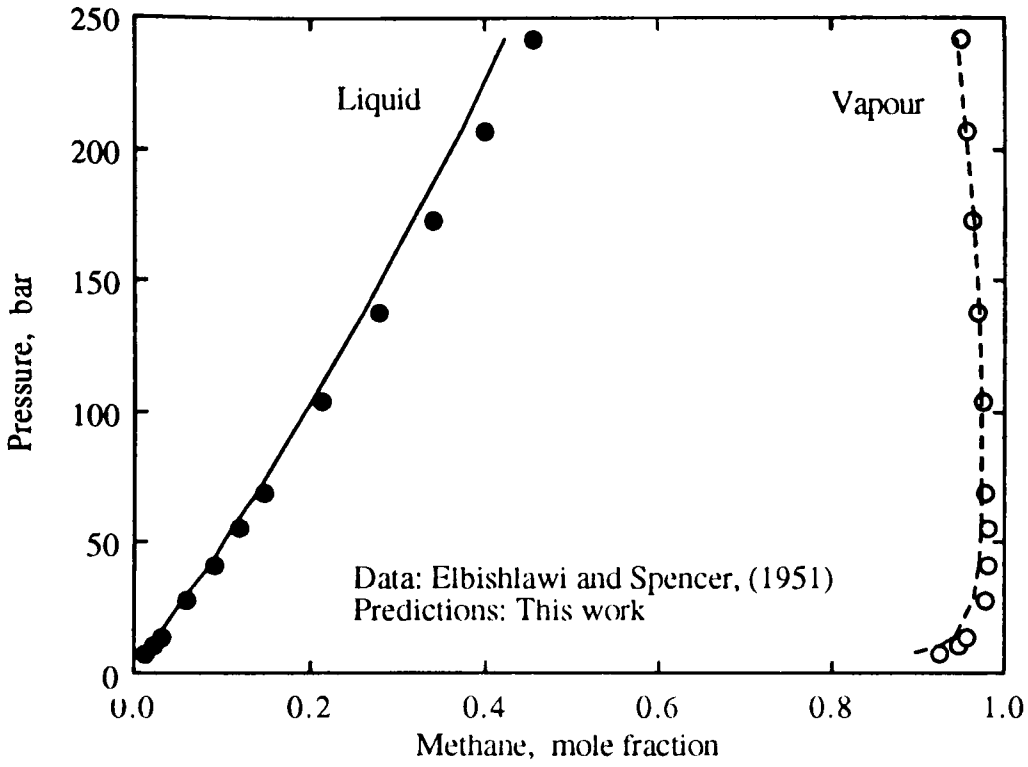

Figure-4.3 Experimental and predicted methane-benzene phase equilibria at 338.71 K.

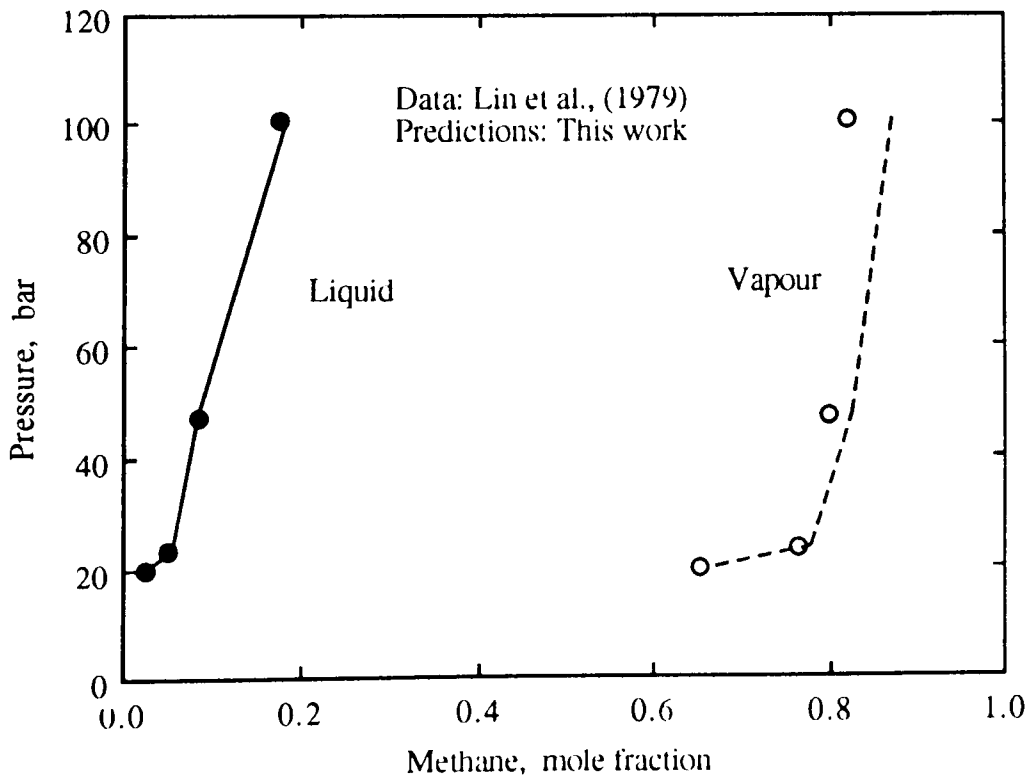

Figure-4.4 Experimental and predicted methane-benzene phase equilibria at 421.05 K.

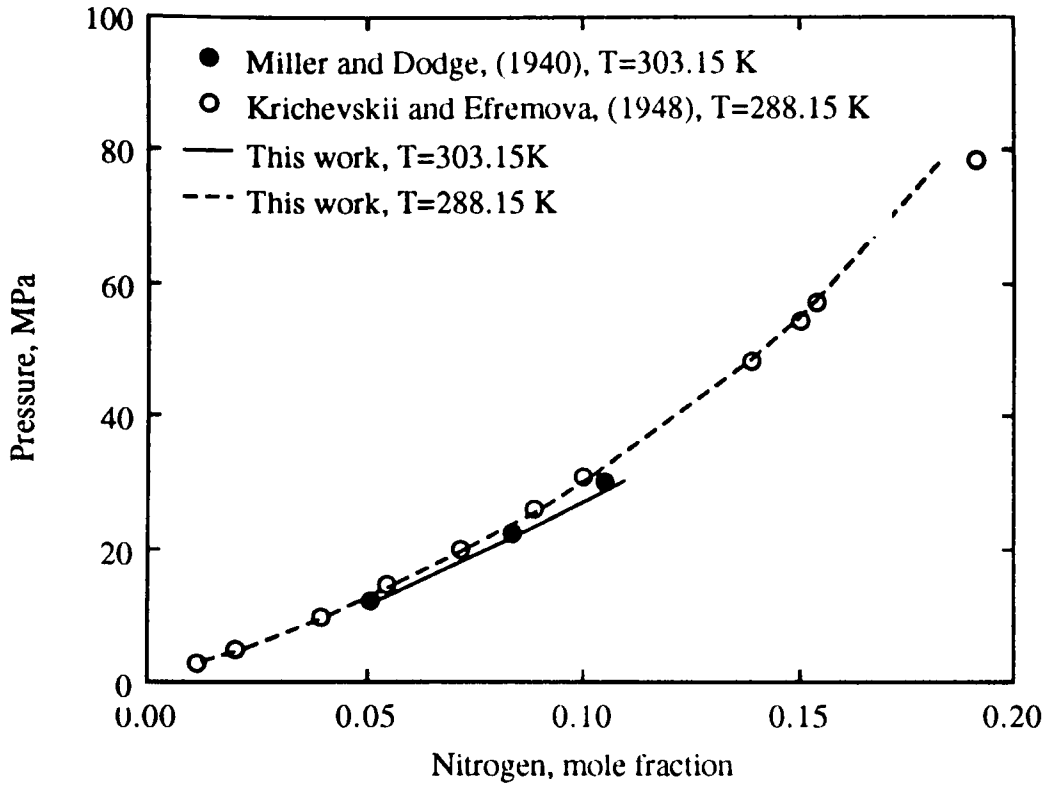

Figure-4.5 Experimental and predicted solubilities of nitrogen in benzene.

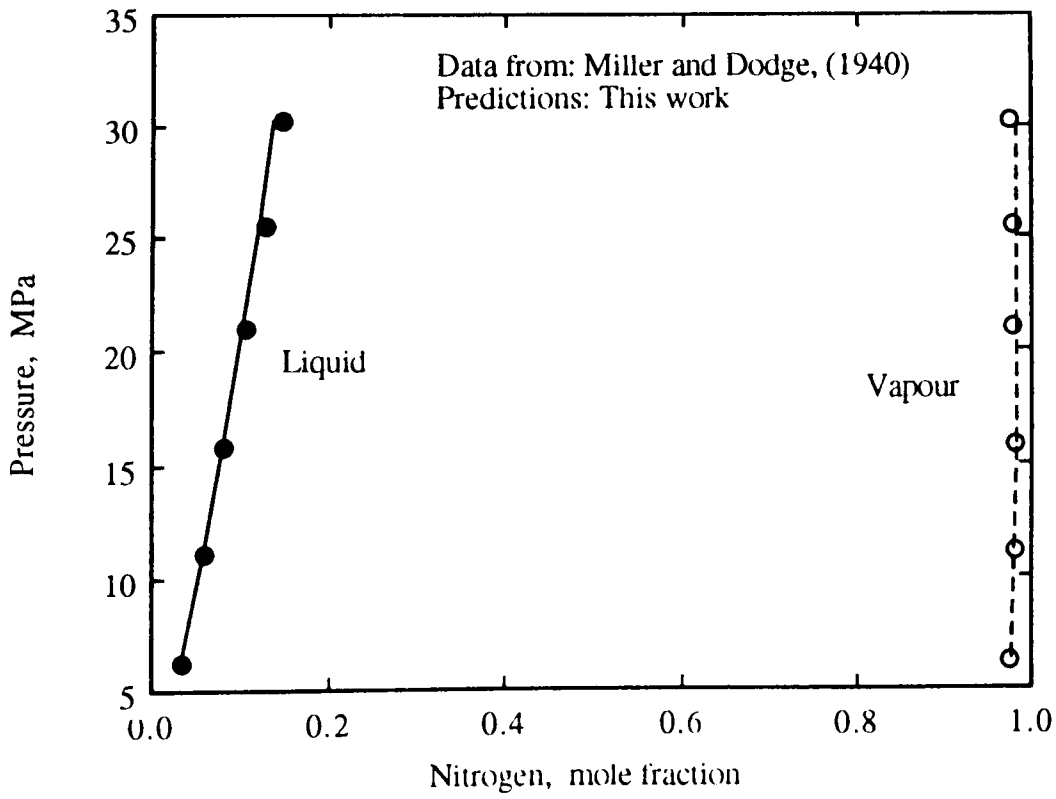

Figure-4.6 Experimental and predicted nitrogen-benzene phase equilibria at 348.15 K.

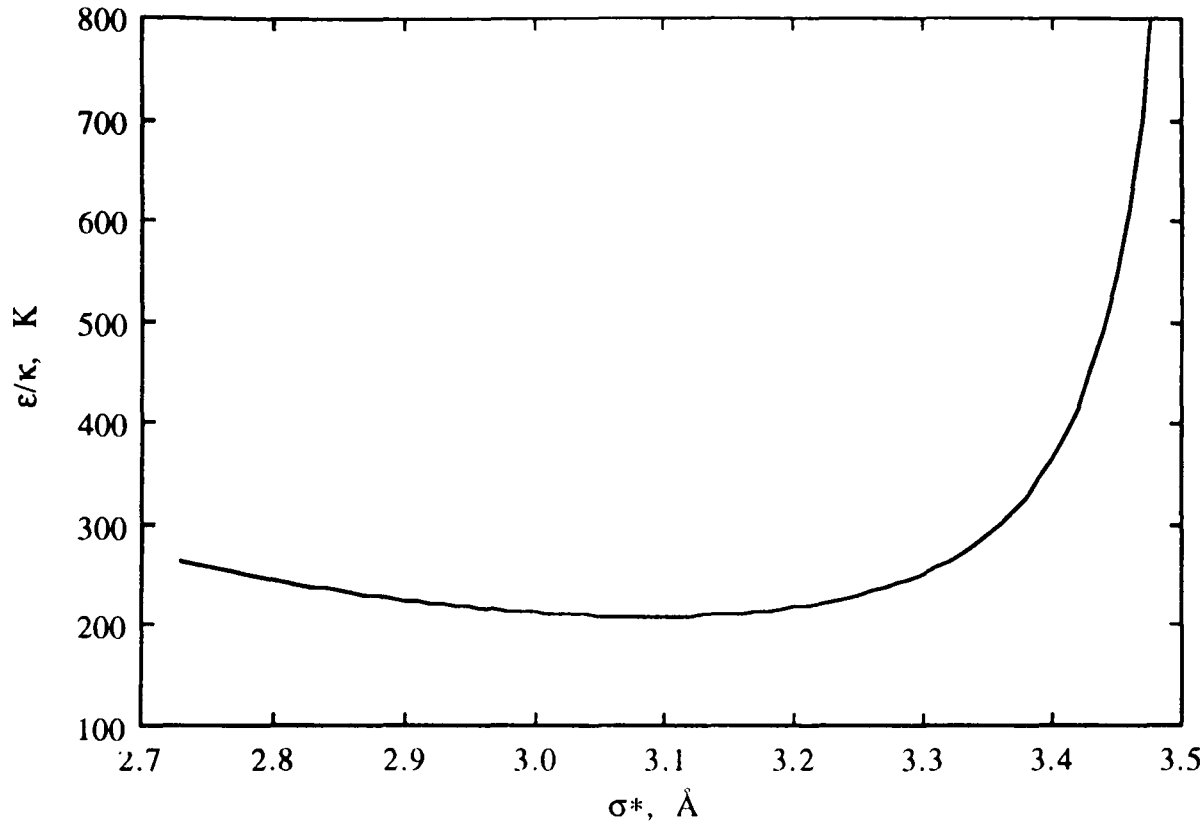

Figure-4.7 Kihara potential parameters for benzene.

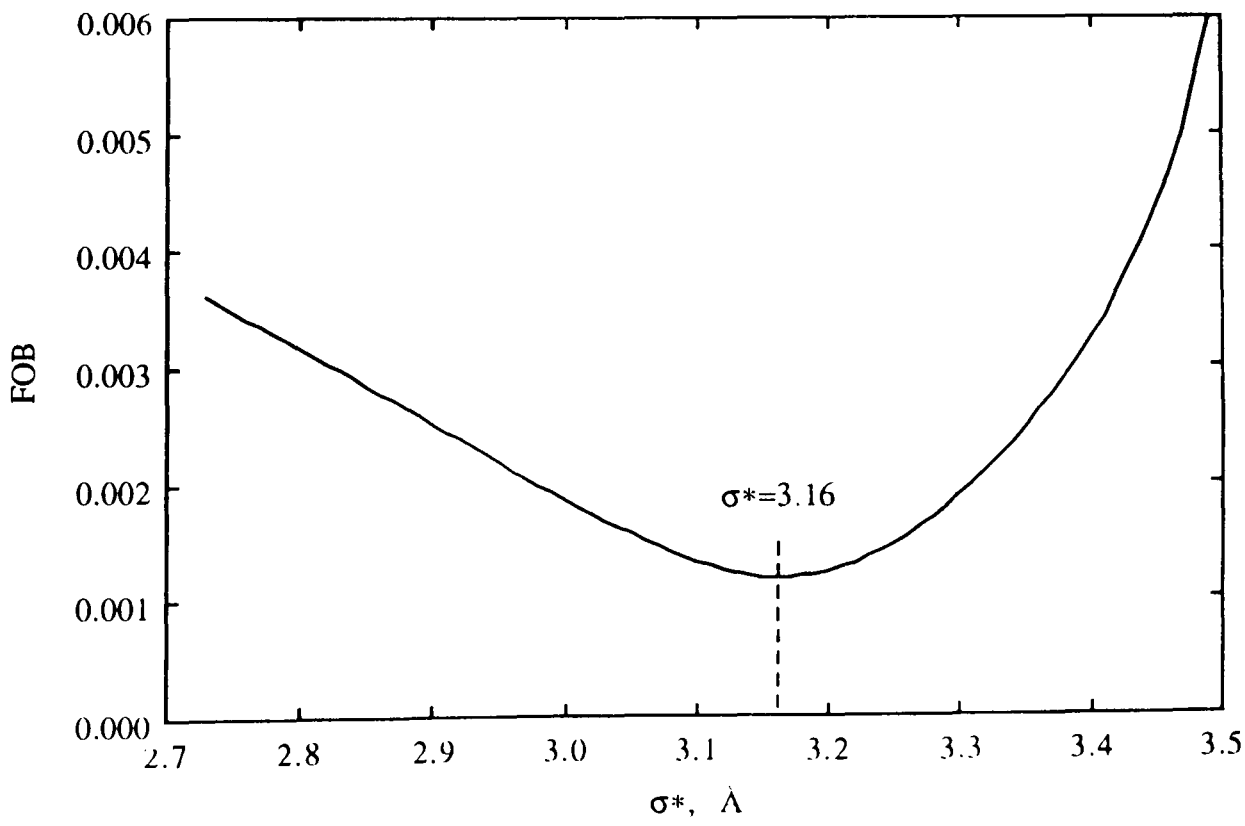

Figure-4.8 Objective function using the first two sets of methane/benzene dissociation pressure data.

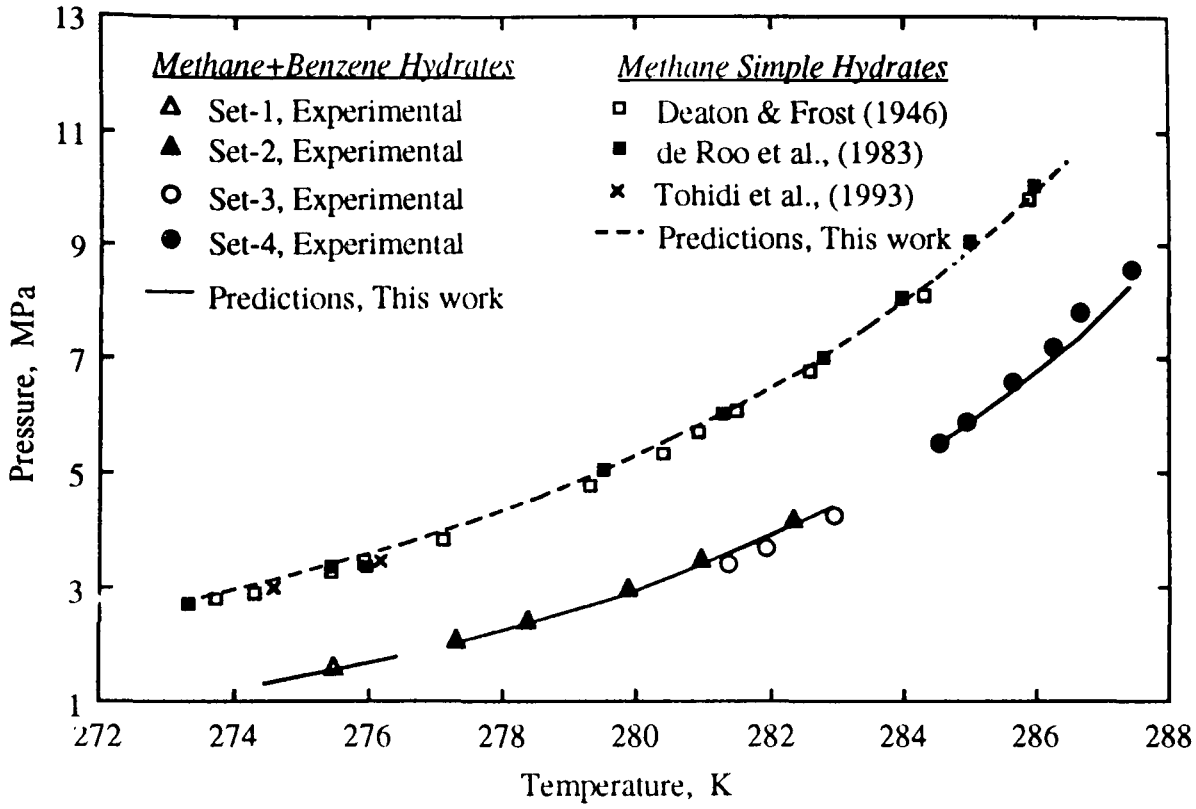

Figure-4.9 Experimental and predicted dissociation conditions of methane and methane+benzene gas hydrates.

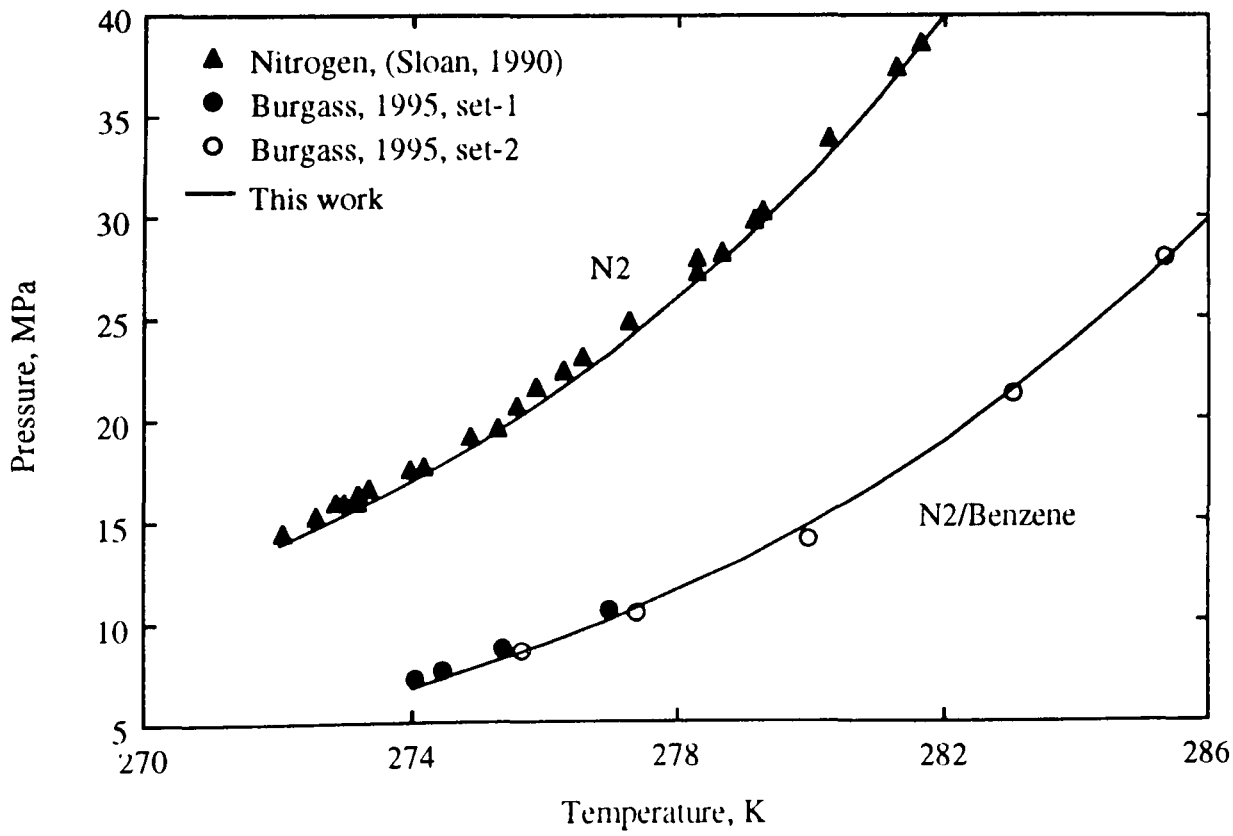

Figure-4.10 Dissociation conditions for nitrogen, and nitrogen+ benzene gas hydrates.

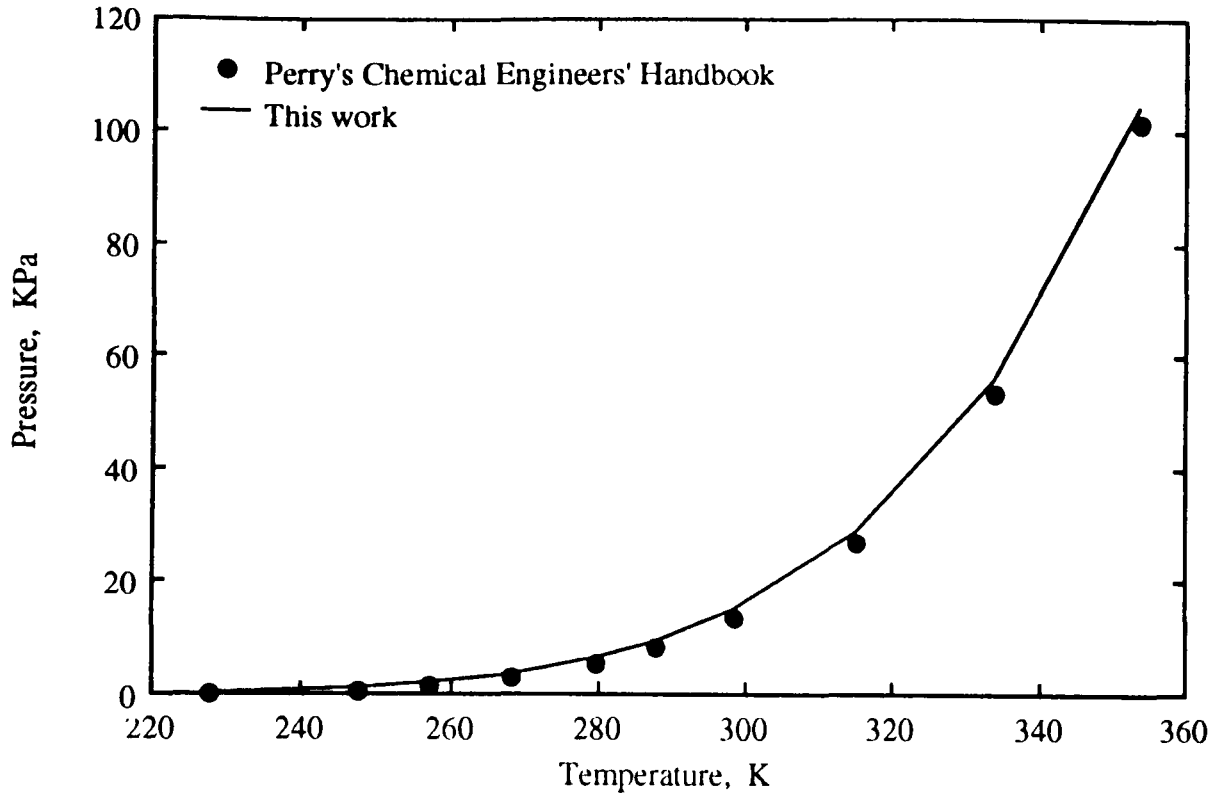

Figure-4.11 Experimental and predicted vapour pressure of cyclohexane, up to 1 atm.

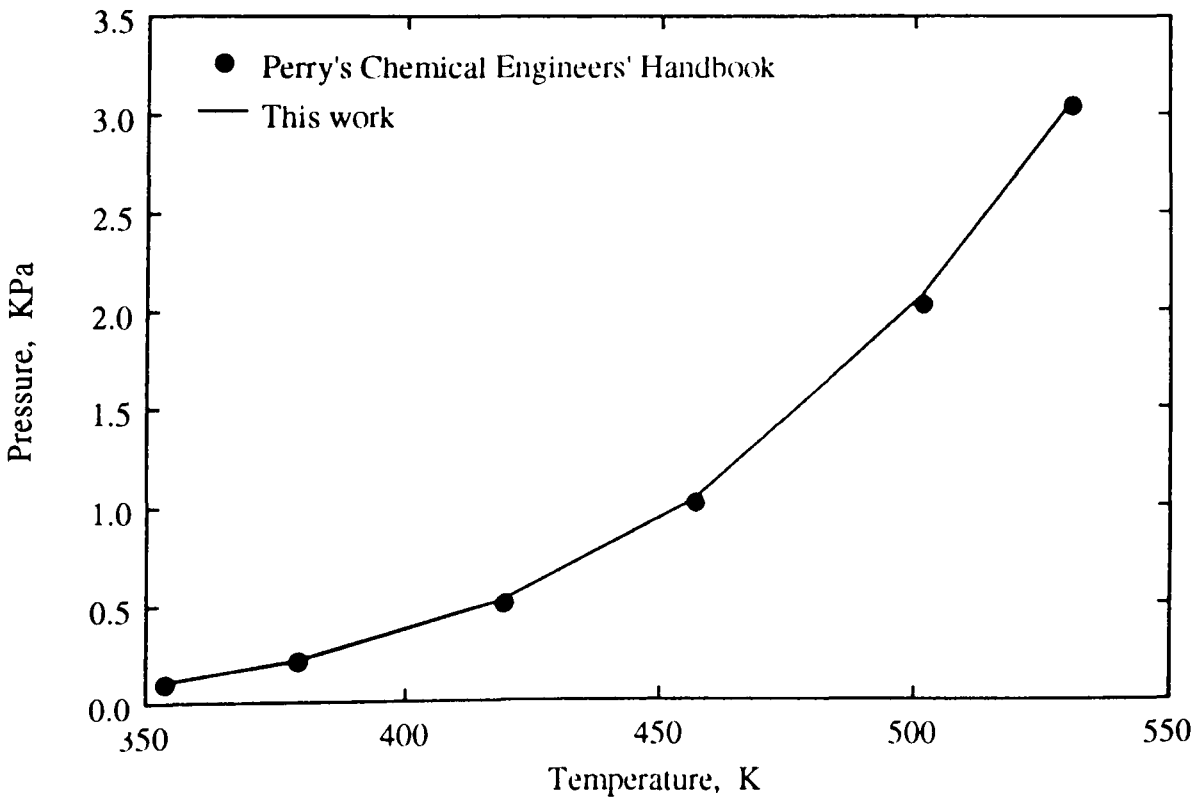

Figure-4.12 Experimental and predicted vapour pressure of cyclohexane, above 1 atm.

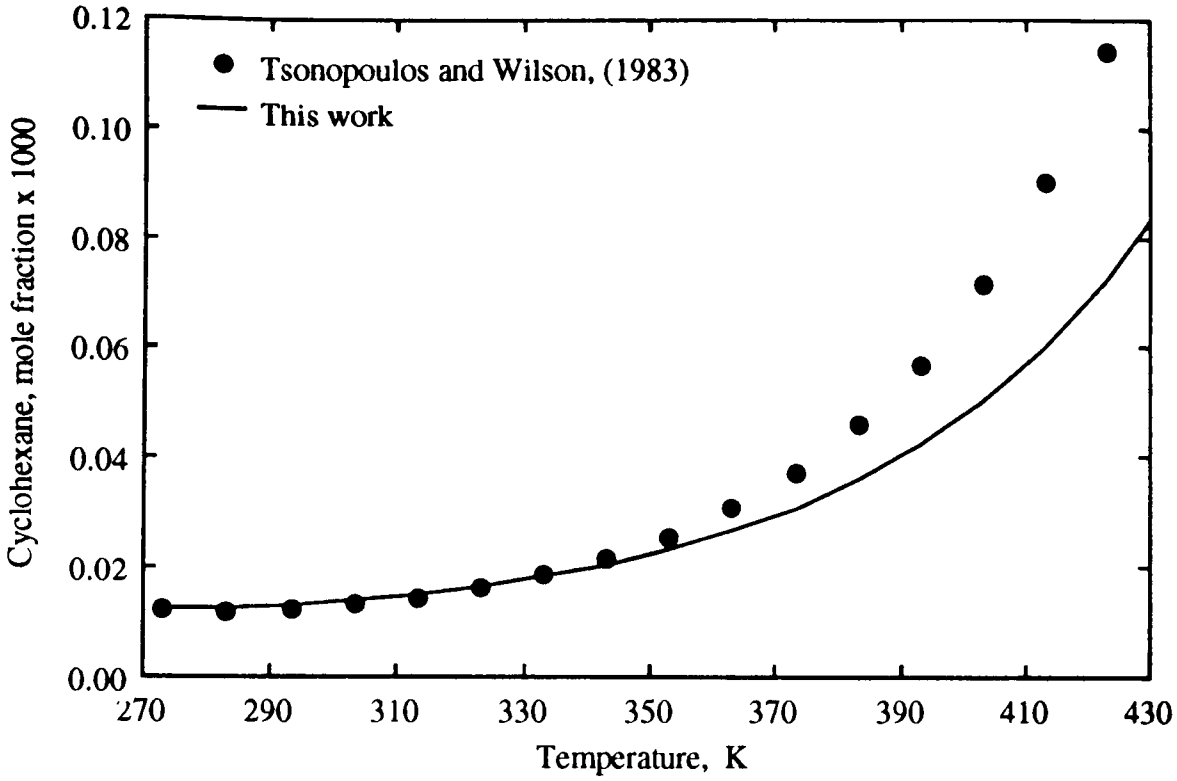

Figure-4.13 Experimental and predicted cyclohexane solubilities in water.

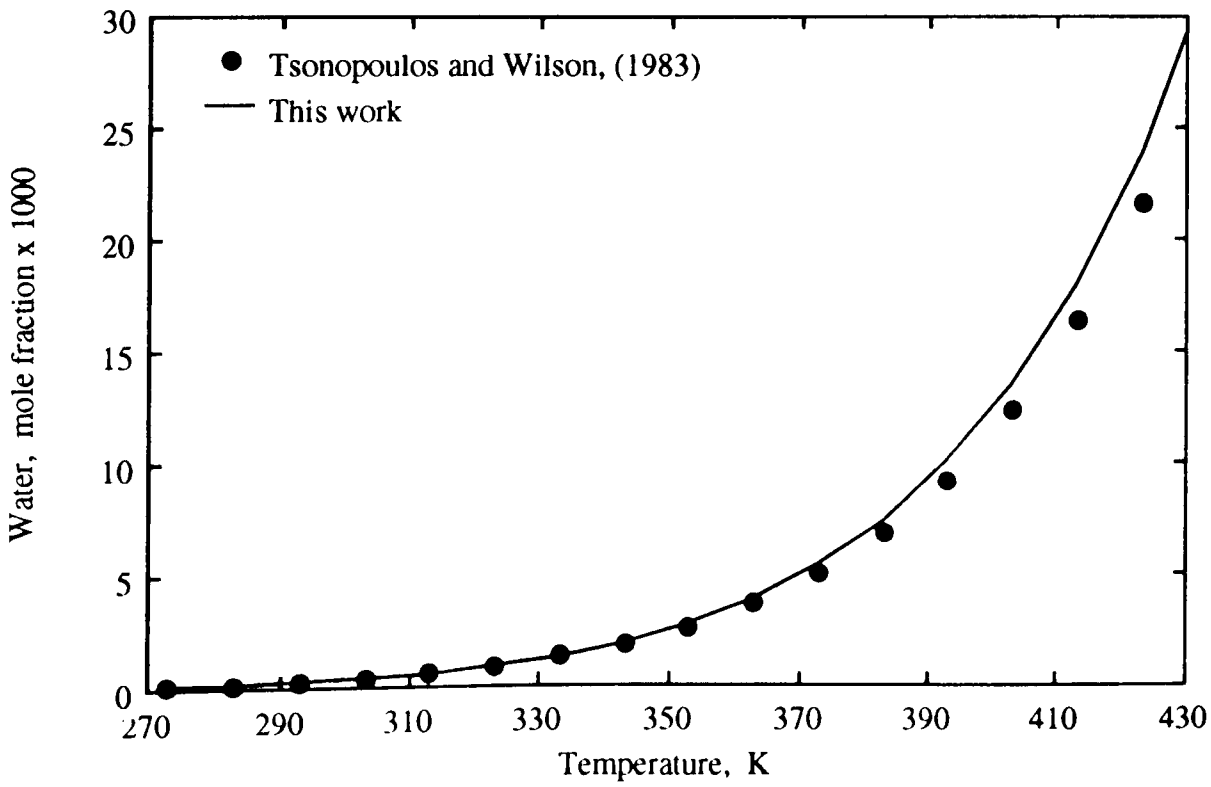

Figure-4.14 Experimental and predicted water solubilities in cyclohexane.

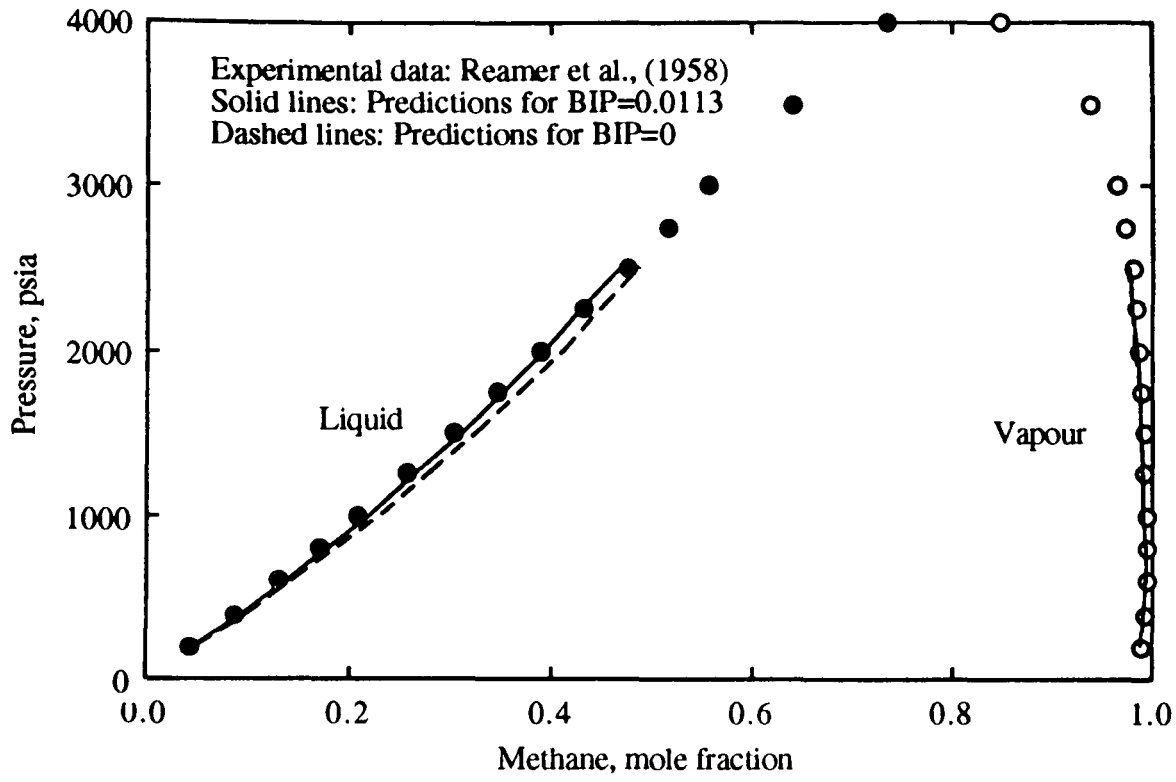

Figure-4.15 Experimental and predicted methane/cyclohexane phase equilibria at 294.3 K.

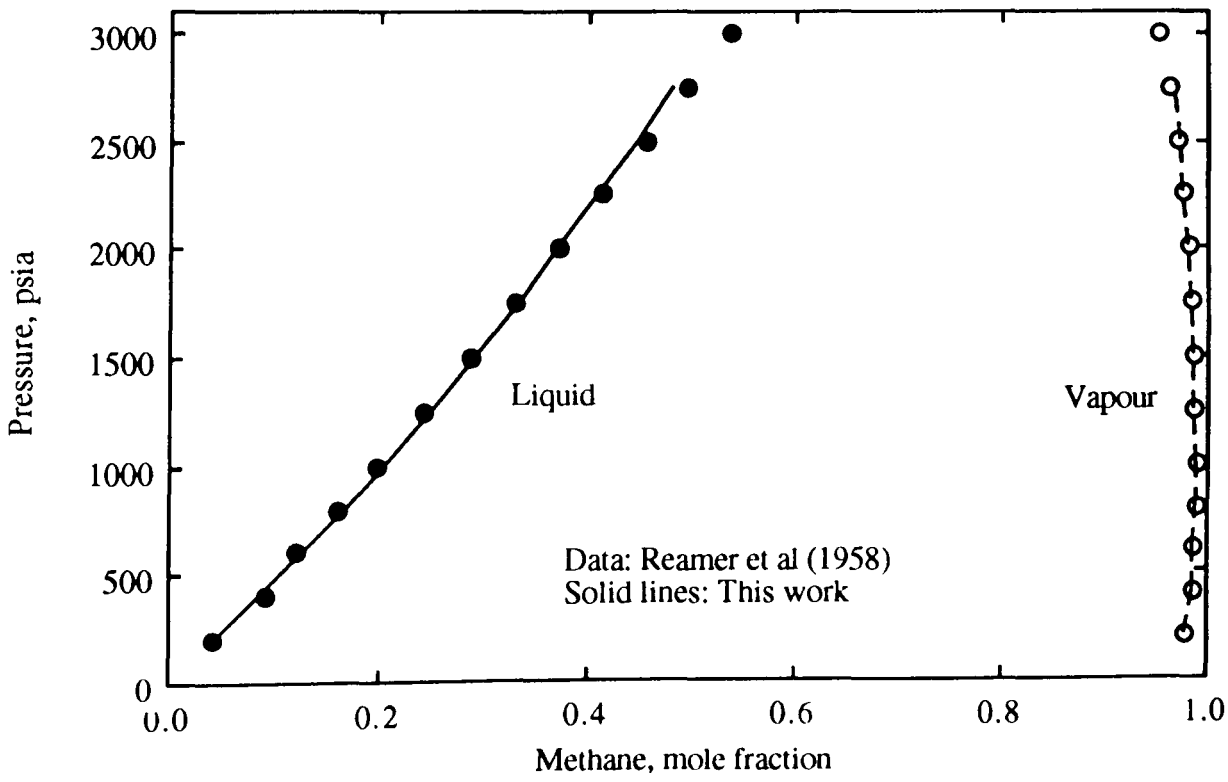

Figure-4.16 Experimental and predicted methane/cyclohexane phase equilibria at 310.9 K.

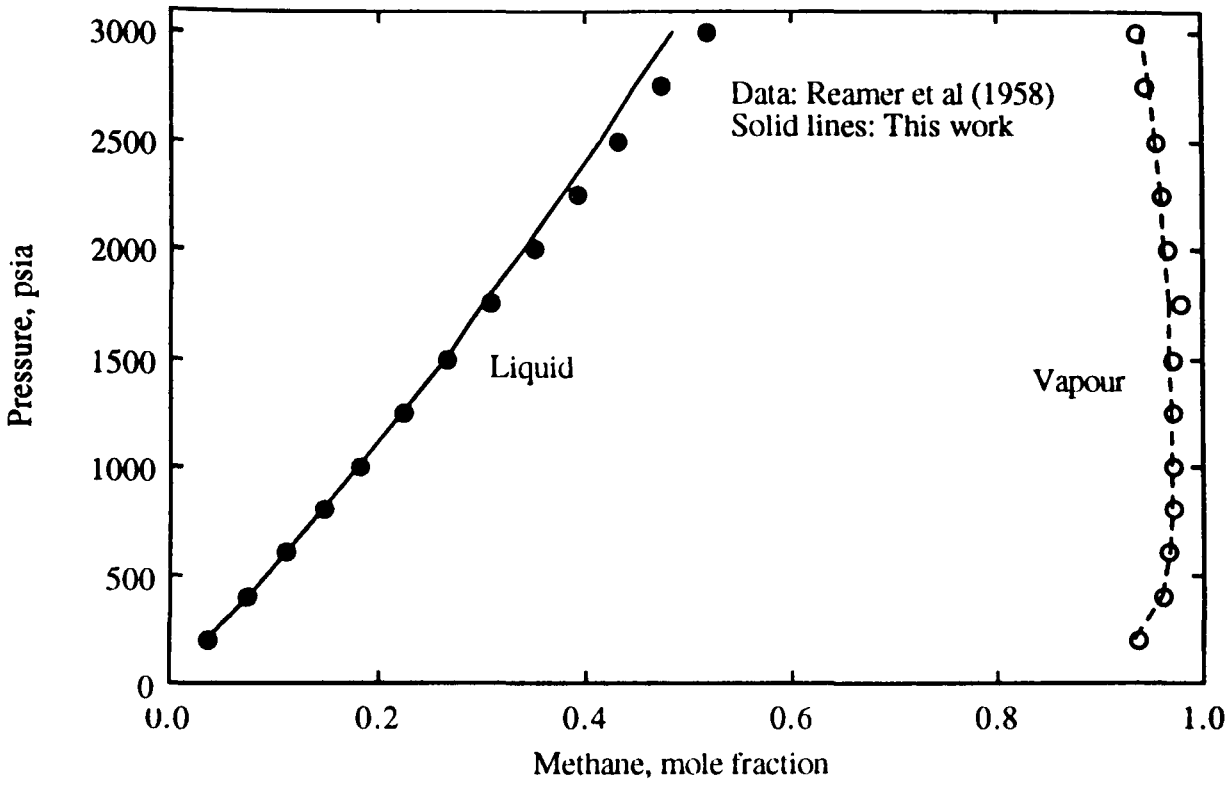

Figure-4.17 Experimental and predicted methane/cyclohexane phase equilibria at 344.3 K.

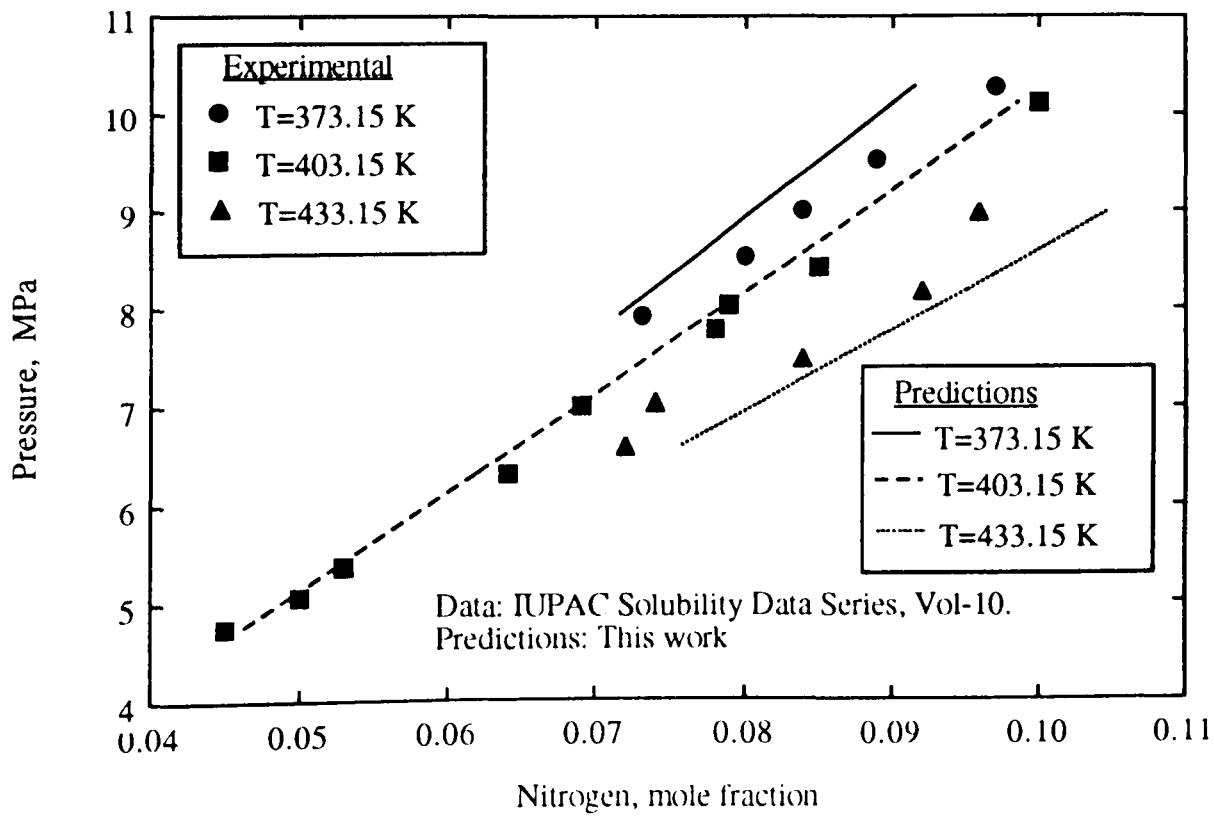

Figure-4.18 Experimental and predicted nitrogen solubilities in cyclohexane.

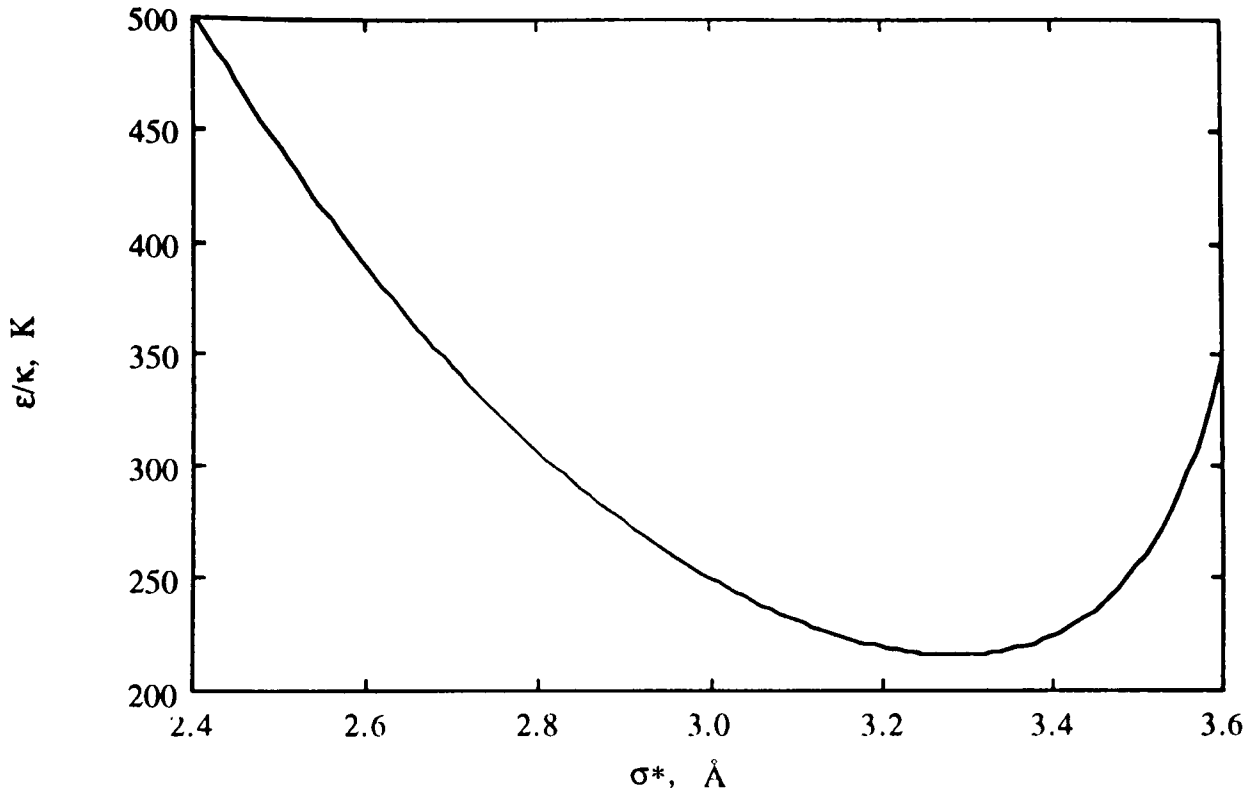

Figure-4.19 Optimised sets of the Kihara parameters for cyclohexane.

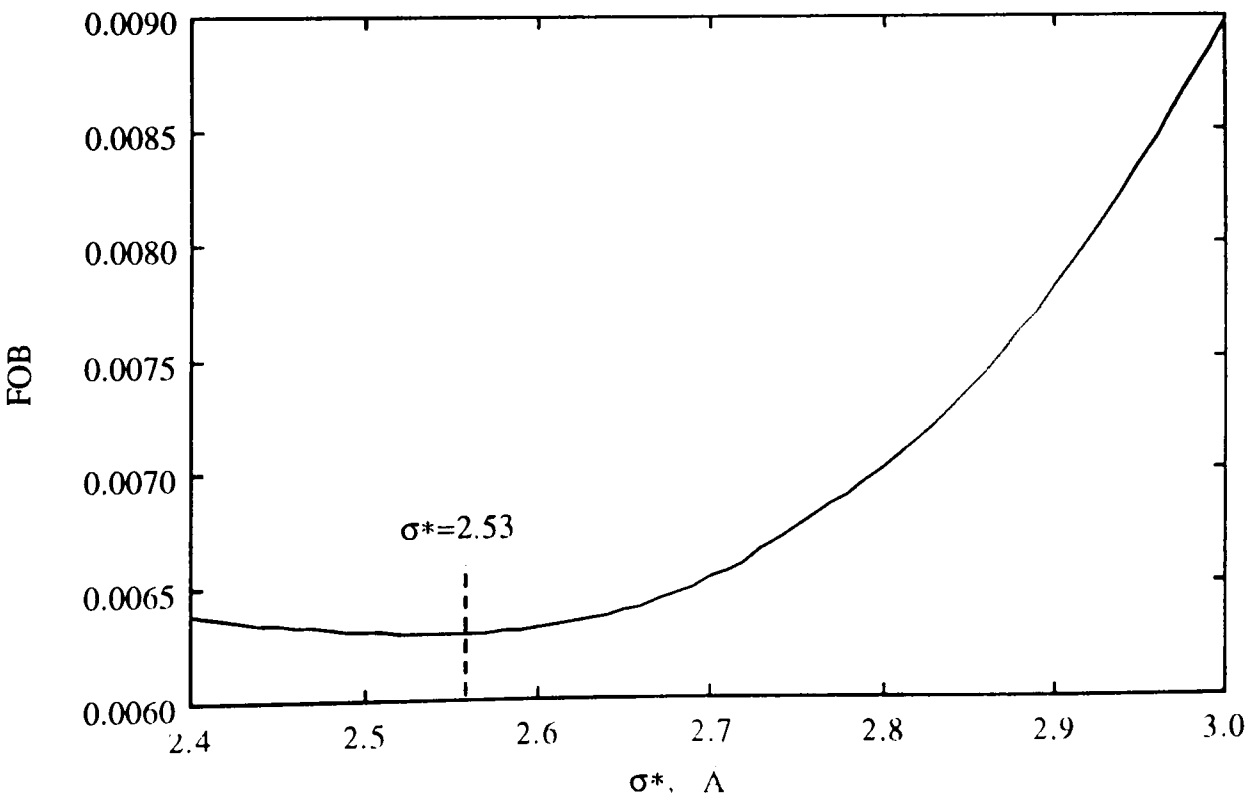

Figure-4.20 Objective function using dissociation pressure data of methane/cyclohexane.

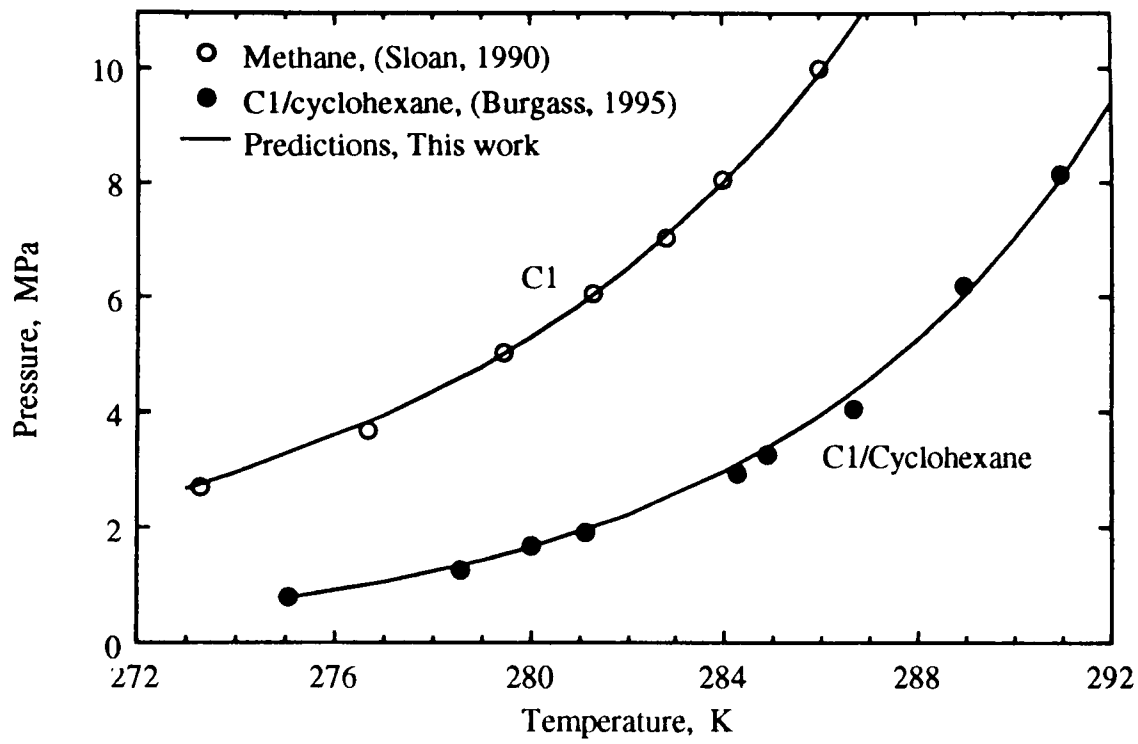

Figure-4.21 Dissociation conditions of methane, and methane+ cyclohexane hydrates.

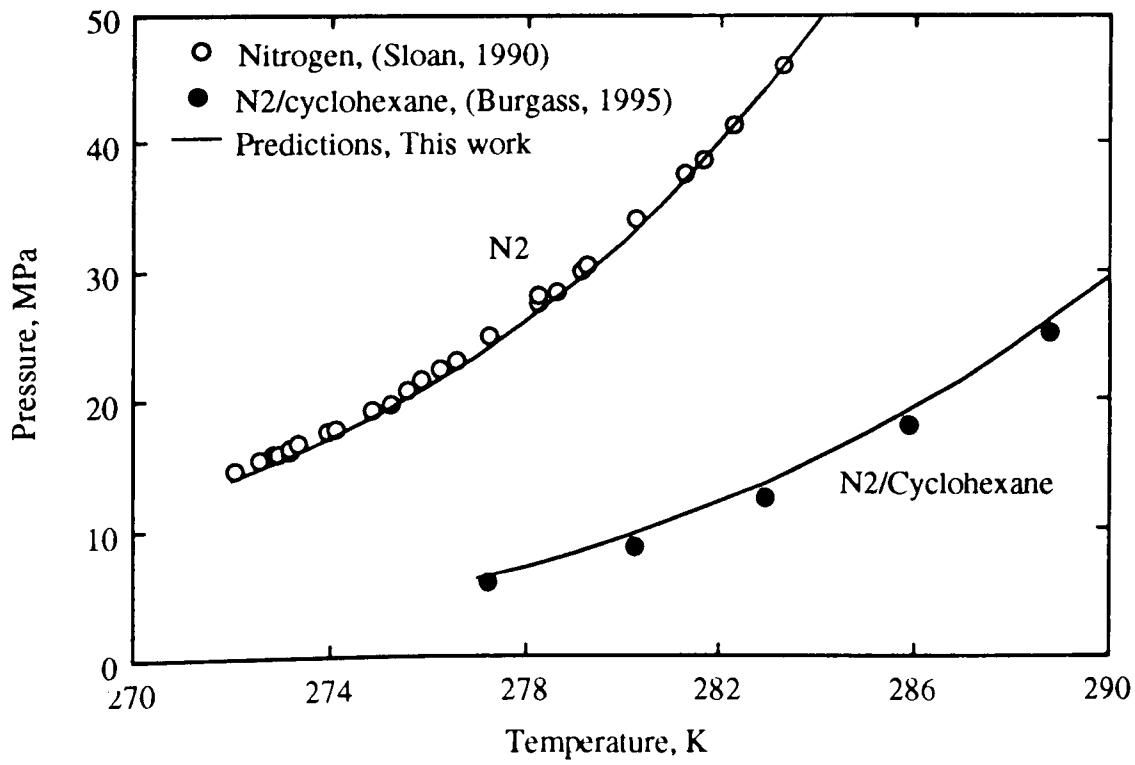

Figure-4.22 Dissociation conditions of nitrogen, and nitrogen+ cyclohexane hydrates.

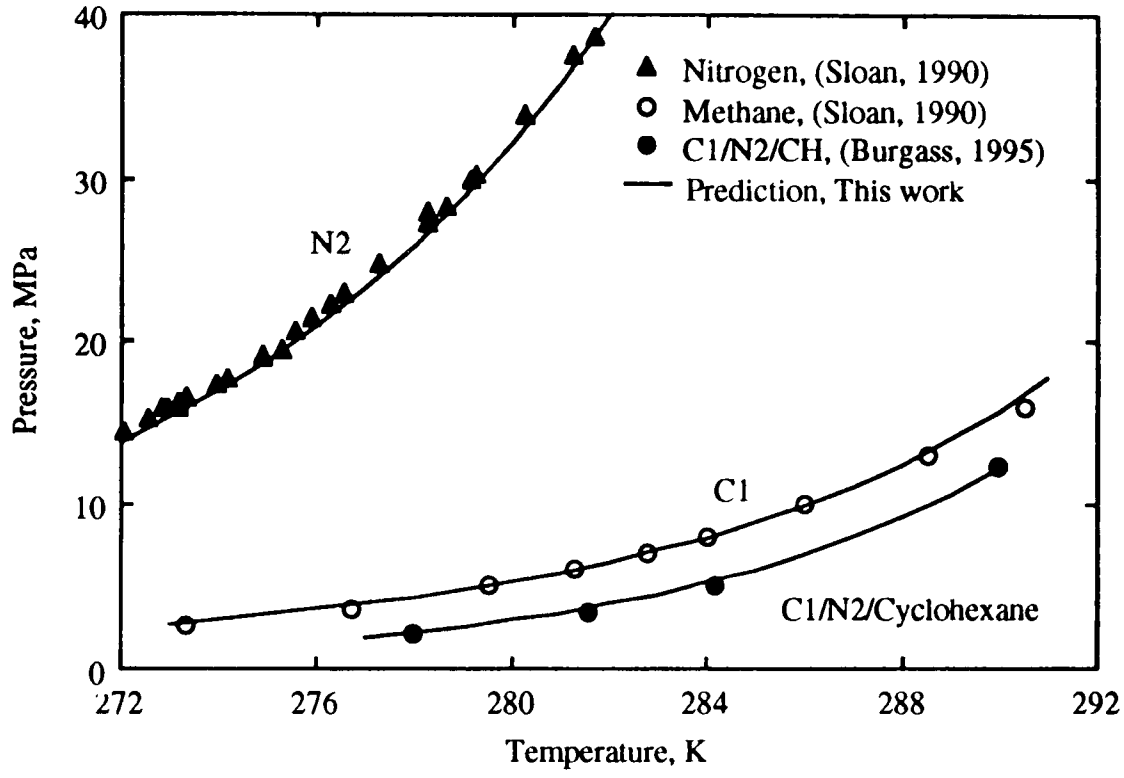

Figure-4.23 Dissociation conditions of nitrogen, methane, and methane+nitrogen+cyclohexane hydrates.

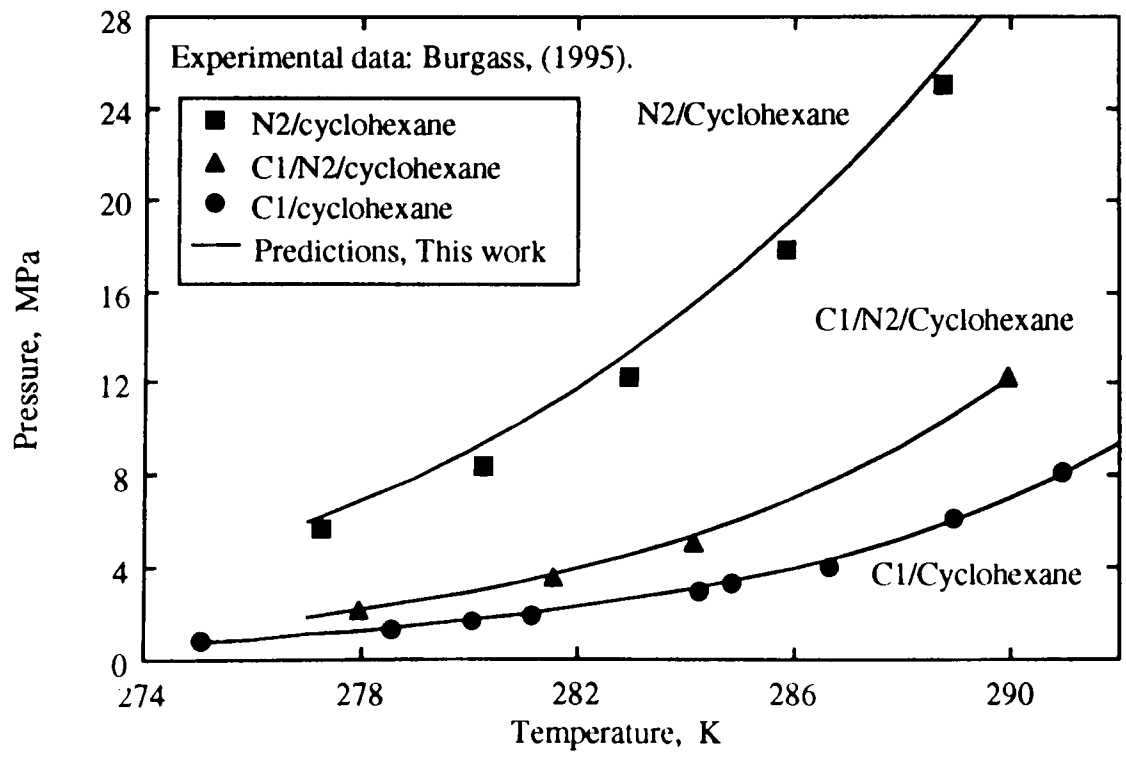

Figure-4.24 Dissociation conditions of methane+cyclohexane, nitrogen+cyclohexane, and methane+nitrogen+cyclohexane hydrates.

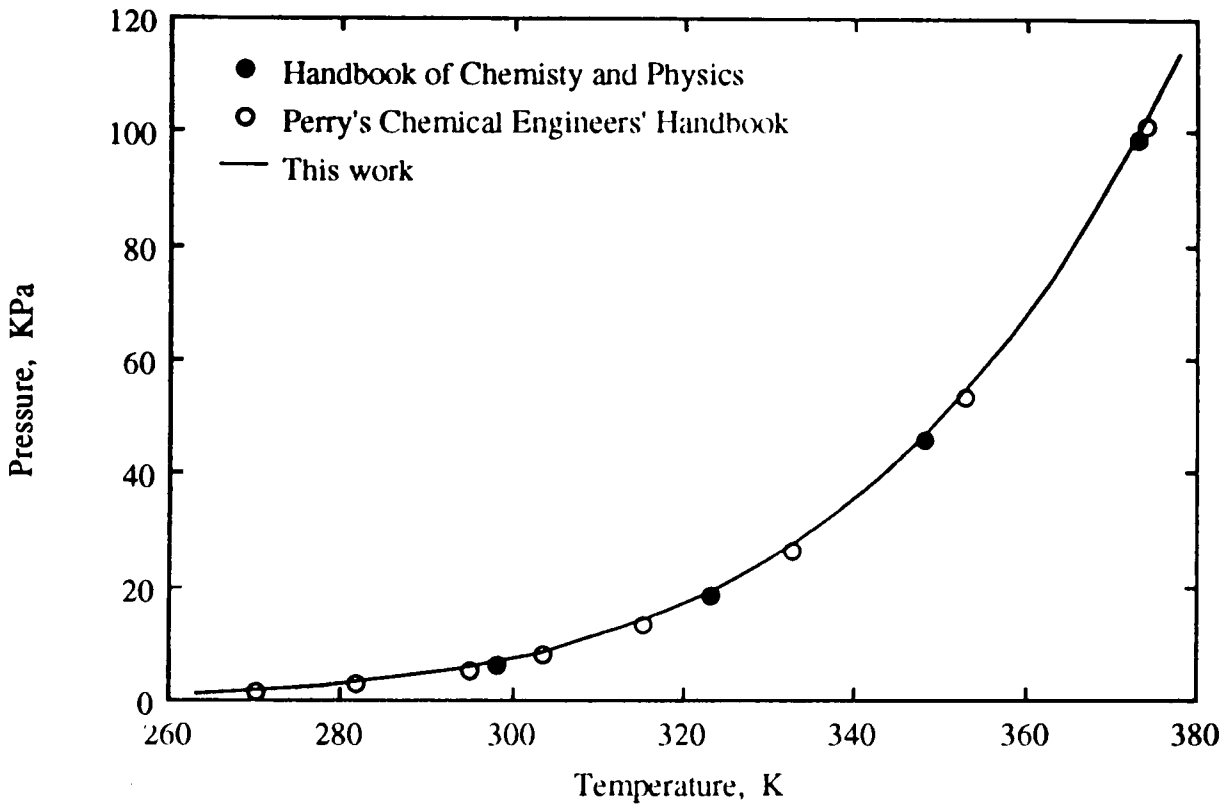

Figure-4.25 Experimental and predicted vapour pressure for methylcyclohexane.

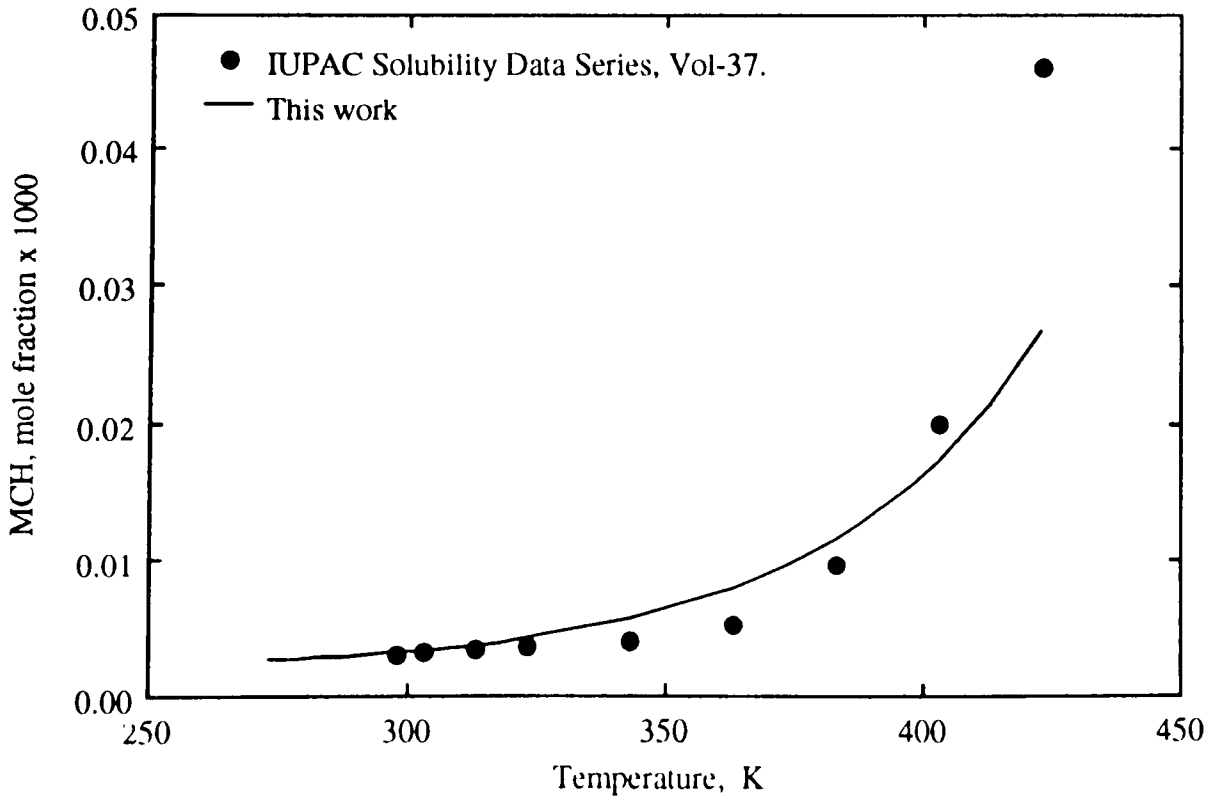

Figure-4.26 Experimental and predicted solubilities of methylcyclohexane (MCH) in water.

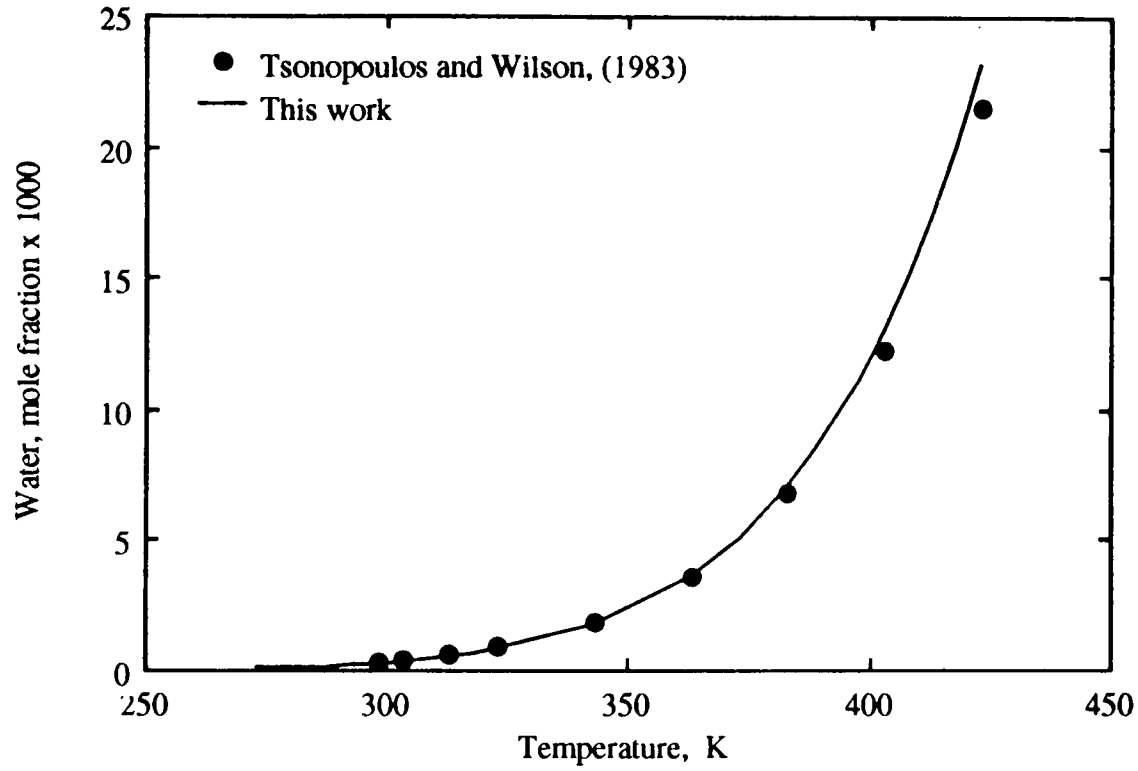

Figure-4.27 Experimental and predicted solubilities of water in methylcyclohexane (cyclohexane).

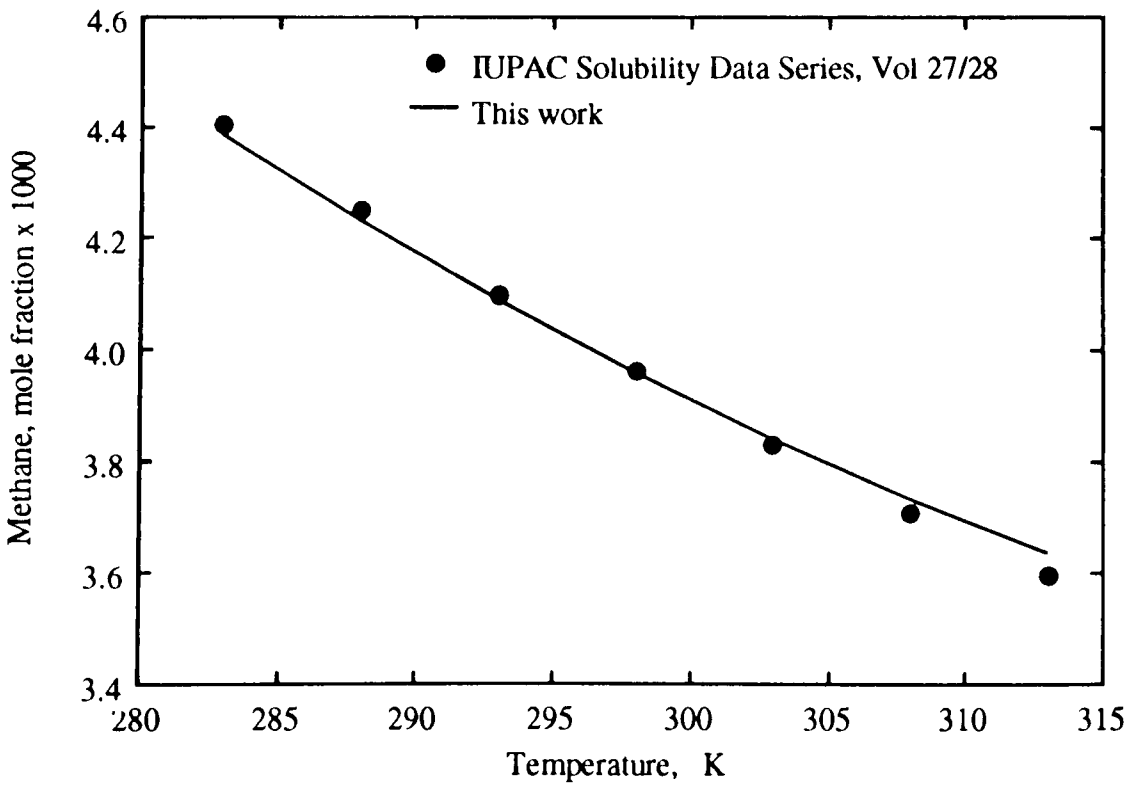

Figure-4.28 Experimental and predicted methane solubilities in methylcyclohexane.

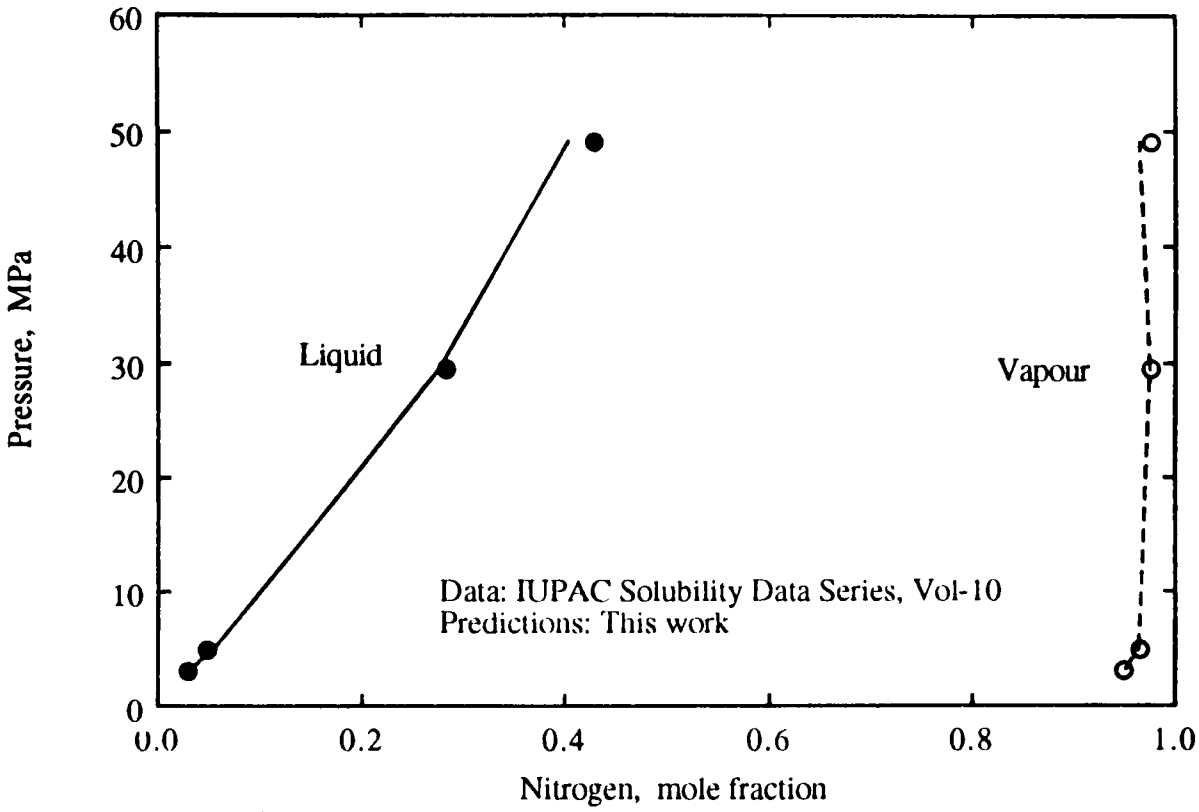

Figure-4.29 Experimental and predicted nitrogen-methylcyclohexane phase equilibria at 376.45 K.

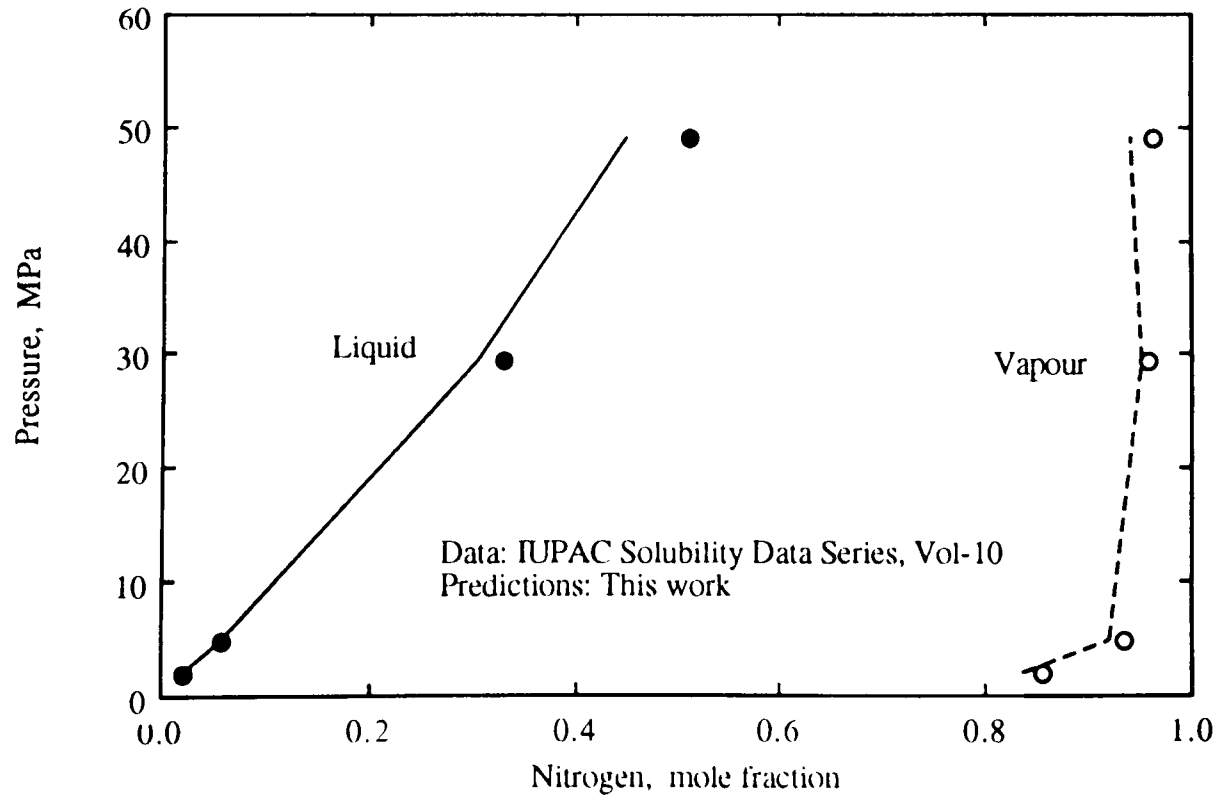

Figure-4.30 Experimental and predicted nitrogen-methylcyclohexane phase equilibria at 413.15 K.

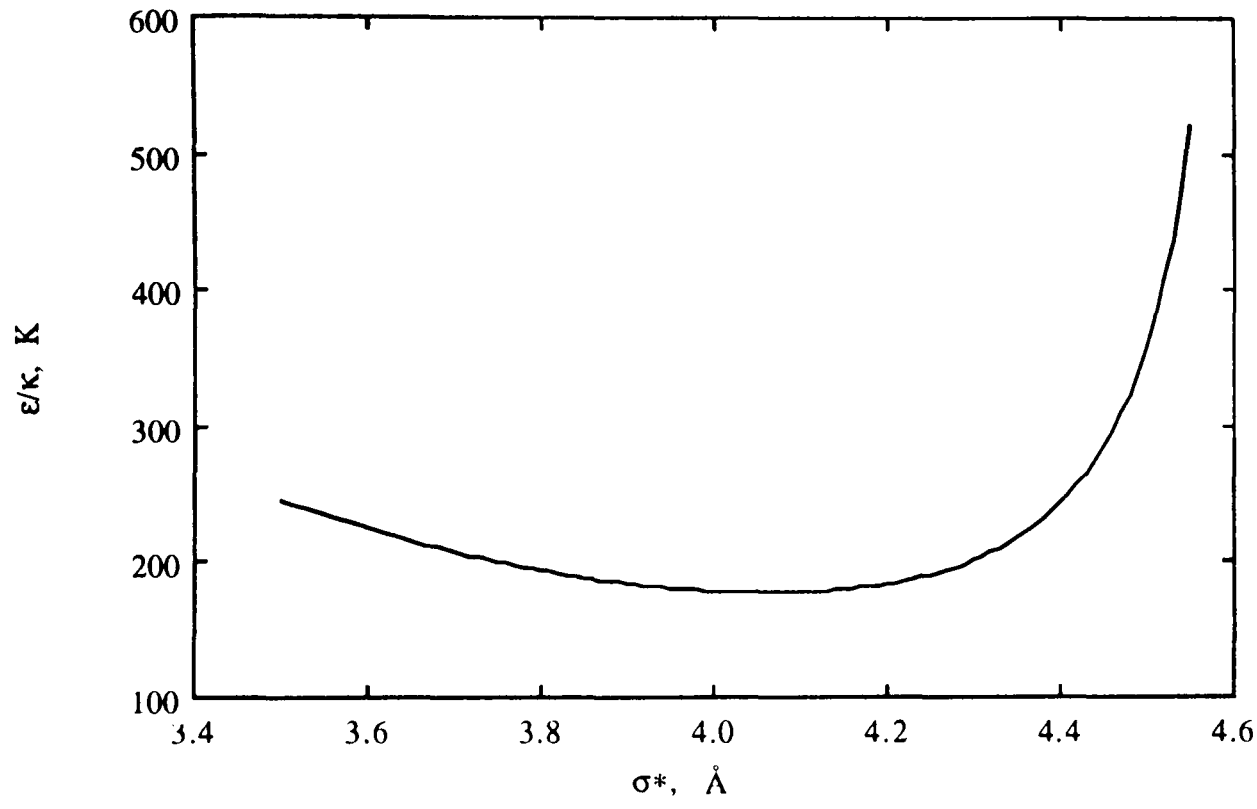

Figure-4.31 Optimised sets of the Kihara parameters for methylcyclohexane.

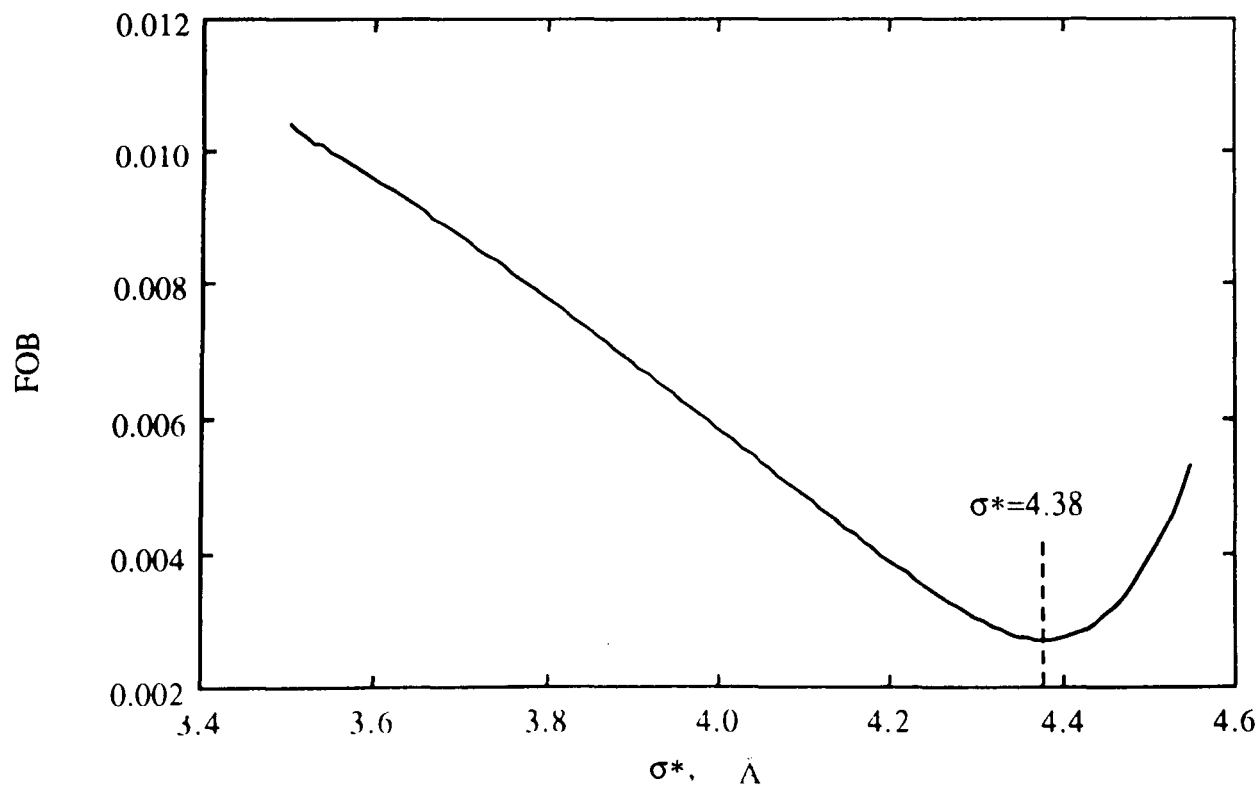

Figure-4.32 Objective function for C1/MCH dissociation pressure data.

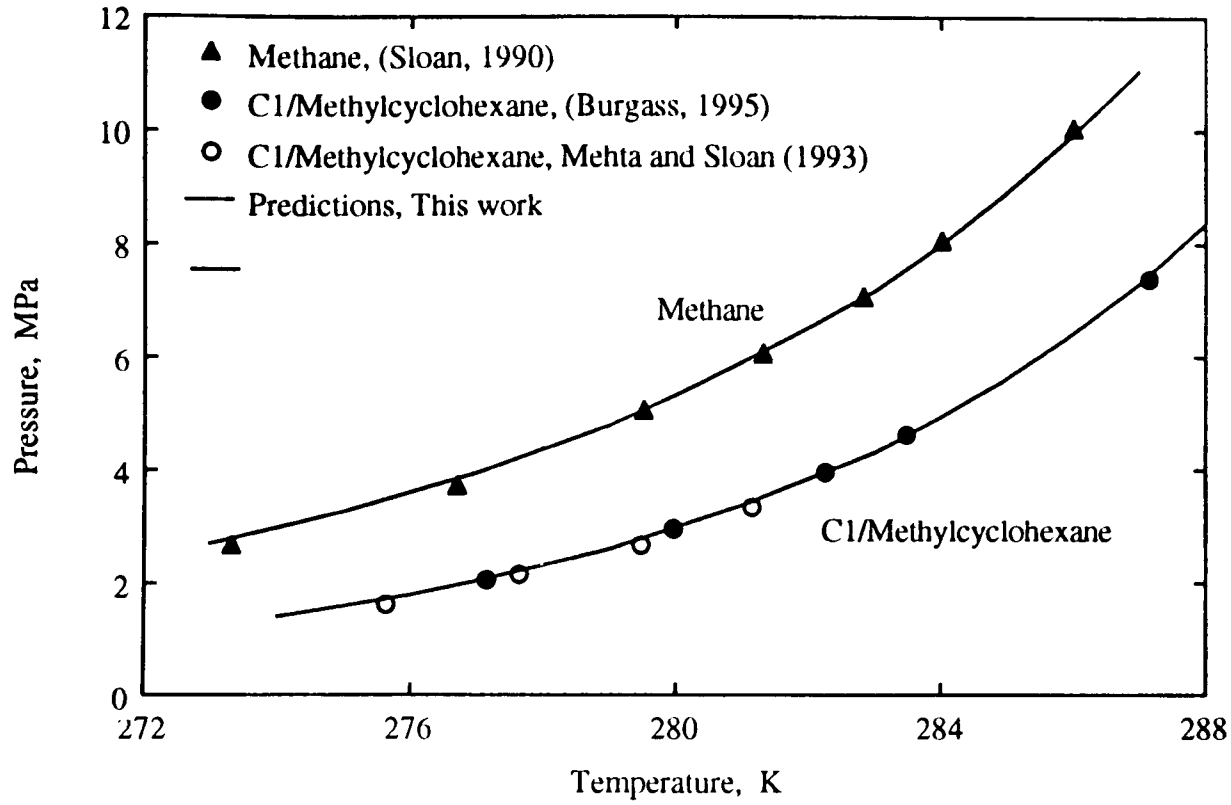

Figure-4.33 Dissociation conditions of methane, and methane+ methylcyclohexane (MCH) hydrates.

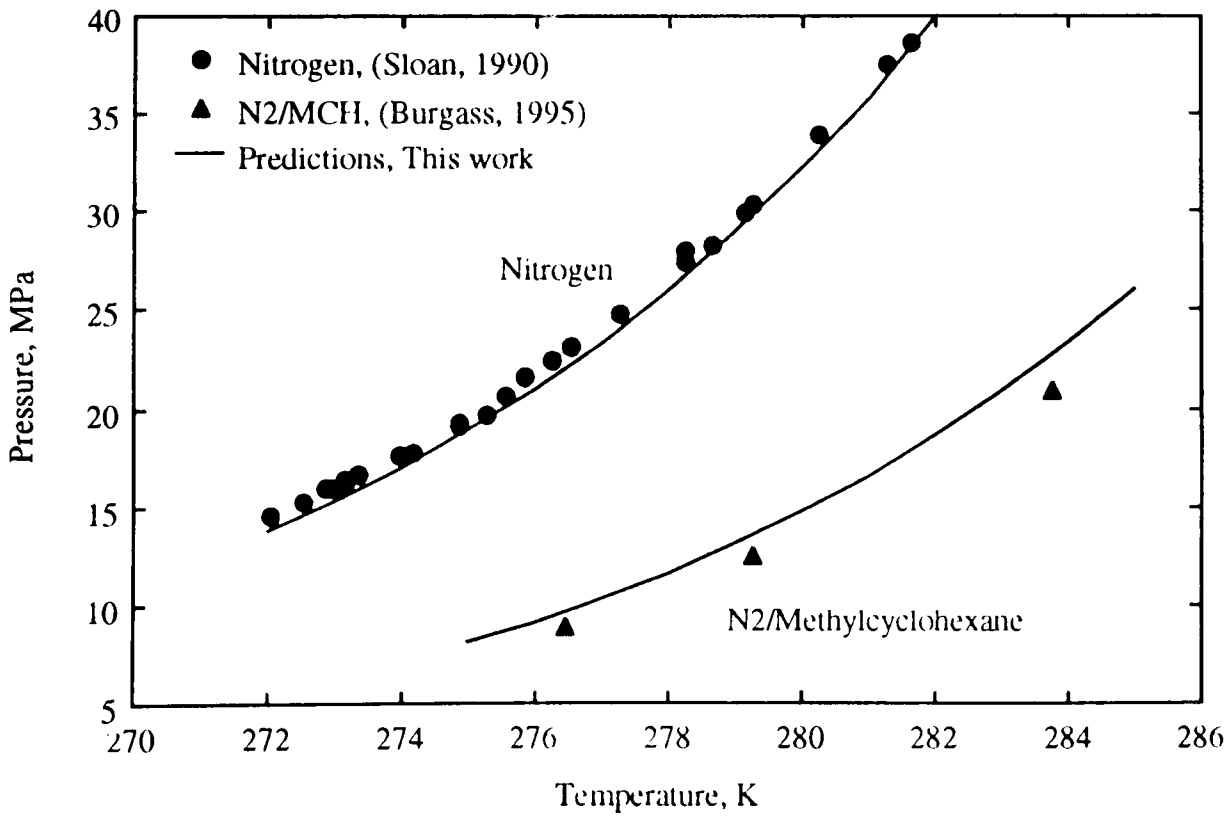

Figure-4.34 Dissociation conditions of nitrogen, and nitrogen+ methylcyclohexane (MCH) hydrates.

CHAPTER-5

MODELLING ELECTROLYTE SOLUTIONS

5.1. INTRODUCTION

Many models have been developed that are able to predict the phase equilibria of mixtures containing both polar and non-polar compounds. This is usually done by either introducing complex mixing rules into a conventional cubic equation of state or by coupling the equation of state with an activity coefficient model. However, none of these models can take into account the presence of ions.

Numerous models have also been developed for predicting vapour-liquid in mixtures containing electrolytes (e.g., Sander *et al.*, 1986; Li and Nghiem, 1986, Macedo *et al.* 1990) but they do not include non-condensable gases. In addition, it is also well-known that the activity coefficient approach is not suitable for extension to high pressures. Few researchers, such as Aasberg-Petersen *et al.* (1991) and Zuo and Guo, (1991) divided the fugacity coefficient of each component in the liquid water phase into two terms: an equation of state (short-range interactions) term and a Debye-Hückel electrostatic (long-range interactions). Recently, Søreide and Whitson (1992) have modified the PR EoS for predicting CO_2, N_2, and H_2S solubility in NaCl brine.

In the model presented in section 2.6, fugacity coefficient of each non-electrolyte compound in saline water phase is divided into two parts; the fugacity coefficient

calculated from the equation of state and the electrostatic contribution. Recalling Equation-2.23:

$$ln\,\gamma_i^{DH} = \frac{2AM_m h_{is}}{B^3} f(BI^{1/2}) \qquad (2.23)$$

The electrostatic contribution term has an adjustable parameter, h_{is}, which can be interpreted as an interaction coefficient between the dissolved salt and a non-electrolyte component (water or gas). Aasberg-Petersen *et al.* used temperature and composition independent parameters for water-salt and gas-salt interaction coefficients. For optimising the water-salt coefficients, they used water vapour pressure depression data for 1 molar single electrolyte solutions at 373.15 K. They implemented two approaches for the optimisation of gas-salt interaction coefficients by using high pressure gas solubility data and low pressure salting out constants. They reported the water-salt interaction coefficients for two salts and gas-salt interaction coefficients for seven gases.

Experience in this study showed that the water-salt interaction coefficients are strong functions of salt concentration and cannot be regarded as being independent of salt concentration. In a recent publication (Tohidi *et al.*, 1993c), the above solubility model was modified slightly by expressing the water-salt interaction coefficient as a function of ionic strength and using the Valderrama (Valderrama, 1990) modification of the Patel and Teja (VPT) equation of state with the density dependent mixing rules (Avlonitis et al., 1994), instead of the ALS (Adachi *et al.*, 1983) equation with a volume dependent mixing rules, as used by Aasberg-Petersen *et al.*, (1991). The modified gas solubility model was combined with the Pitzer (Pitzer and Mayorga, 1973) activity model, and the conventional formulation for gas hydrates (Parrish and Prausnitz, 1972), to calculate the hydrate phase boundary for highly soluble gases.

In relation to efficient and economical pipeline design and operation, phase equilibria, as well as the boundary of hydrate formation with and without salts and other chemical

inhibitors must be precisely known. Available models for calculating the hydrate inhibition effect of salts either ignore gas solubility (Hammerschmidt, 1939, Englezos and Bishnoi, 1988) in the water-rich phase or take into account the solubility of gas in a single electrolyte (Englezos, 1992, Tohidi *et al.*, 1993c). The former cannot be used for systems containing high soluble gases and the latter is unable to model the hydrate inhibition effect of mixed electrolyte solutions, such as formation water, on reservoir fluids.

Aasberg-Petersen *et al.* (1991) were successful in predicting the solubilities of N_2, CH_4, CO_2, and a natural gas in single electrolyte solutions of NaCl and $CaCl_2$ at reservoir temperature (366 K to 398 K), but in their model there are the following shortcomings, particularly in relation to hydrate phase equilibria predictions:

- The original model was developed to predict gas solubility at reservoir conditions i.e. high temperatures, so it is not expected to predict vapour-liquid equilibria of electrolyte solutions at low temperatures.
- The original model is restricted to single electrolyte solutions and there is no provision for calculating vapour-liquid equilibria, including gas solubility in mixed electrolyte solutions.
- They determined the interaction coefficients for only two salts, whereas in practical cases, such as formation water, the solution consists of several salts.

A more rigorous and versatile model has been developed in this work to extend the model capabilities to handle lower temperatures, other salts, wider salt concentrations, and mixed electrolyte solutions. The optimisation water-salt and gas-salt interaction coefficients and extension of the model to mixed electrolyte solutions are described in details in the following sections.

5.2. WATER-SALT INTERACTION COEFFICIENT

The model described earlier in Chapter-2 has been used for modelling the effect of salt in fugacity calculations in the saline water phase. Rewriting equation (2.23) for water and salt:

$$\ln \gamma_w^{DH} = \frac{2AM_m h_{ws}}{B^3} f(BI^{1/2}) \qquad (5.1)$$

where h_{ws} is the water-salt interaction coefficient. In this work, h_{ws} is expressed as a function of salt concentration and temperature to widen its range of application (temperature and salt concentration) and to enable the model to perform other calculations, e.g. water freezing point depression, boiling point elevation and vapour pressure depression.

For optimising the water-salt interaction coefficients, two approaches were implemented. In the first approach, water vapour pressure data at different temperatures (generally 40-100 °C) and salt concentrations (2.5 Wt% to maximum value reported) have been used. In the second approach, only water vapour pressure depression data at 373.15 K and freezing point depression data are employed in the optimisation of the water-salt interaction coefficients.

5.2.1. Approach-1, Vapour Pressure Data at Different Temperatures

In this approach, only water vapour pressure depression data at different temperatures are used in determining the water-salt interaction coefficient. Both the VPT (Valderrama, 1990) and PR (Peng and Robinson, 1976) equations of state are employed, with close results. Although only the results of using the VPT EoS are presented here, the PR EoS could be used for all calculations in this work. Two mixing rules, known as classical and non-density dependent (NDD) (Appendix-A) mixing rules, can be used for all calculations, but NDD mixing rules gave better results, particularly for high soluble gases such as CO_2.

Two main sources of data were the International Critical Tables (1928) and CRC Handbook of Chemistry and Physics (1989). The data in the latter was limited to vapour pressure depression at 373.15 K and usually disagreed with those of the International Critical Tables, particularly at high salt concentrations. When this was the case, the more recent data reported in the CRC were used for the modelling. For some salts, such as NaF, the available data were not adequate. In such cases, the Pitzer's activity model (Pitzer and Mayorga, 1973, Tohidi *et al.*, 1993c) was used to calculate the necessary vapour pressure data. For some salts, it was necessary to smooth the experimental data before optimising the water-salt interaction coefficient.

In the following sections, the determination of the water-salt interaction coefficients is detailed for NaCl as an example.

Water-NaCl

Water vapour pressure depression data in the range of 40 to 110 °C from the *International Critical Tables of Numerical Data, Vol. III (1928),* and vapour pressure depression data at 373.15 K from the CRC *Handbook of Chemistry and Physics (1988-1989)* have been used for optimising the water-NaCl interaction coefficient with the VPT and PR EoS. The results of the two equations of state were very close. The optimised interaction coefficient for the VPT EoS are shown in Figure-5.1. The figure shows that different plots at different temperatures are almost parallel to each other. As shown in the figure, the interaction coefficient approaches -0.00785 (as reported by Aasberg-Petersen *et al.*, 1991) for 5-10 Wt% NaCl at 110 °C, which demonstrates that the range of application for the original interaction coefficient, is rather limited.

A similar approach has been implemented for other salts and based on the observed results, the following relation is proposed to express the water-salt interaction as a function of temperature and salt concentrations:

$$h_{ws} = (A + BT + Cw + Dw^2 + ETw)/1000 \qquad (5.2)$$

T is the temperature in K and w is the salt concentration in weight percent. A, B, C, D, and E are constants. The water-salt interaction coefficient for each salt was fitted to the above equation (using least square). The constants for each salt are reported in Table-5.1

Discussion

The main shortcoming of the above approach is the scarcity of experimental vapour pressure data at different temperatures and salt concentrations. This will limit the extension of the model to other salts present in the formation water.

The resulting model was used for predicting the freezing point depressions of single and mixed electrolyte solutions (as detailed in Chapter-6). Figure-5.2 shows experimental and predicted freezing points for NaCl aqueous solutions, as an example. Both VPT and PR EoS have been used. The predictions are in good agreement with the experimental data. Therefore, based on the thermodynamic consistency, freezing point depression data could be used in the optimisation of the interaction coefficient. In addition, the freezing point depression data is more relevant to hydrate calculations. On the other hand, it was the objective of this work to develop a model, capable of predicting vapour-liquid equilibria at high temperatures, as well as hydrate calculations. Based on the above discussion the second approach was developed. In this approach, only water vapour pressure depression data at 373.15 K and freezing point depression data are employed in the optimisation of the water-salt interaction coefficients. Needless to say that the above two sets of data are also more readily available compared to vapour pressure depression data at different temperatures.

5.2.2. Approach-2, Vapour Pressure Data at 373.15 K and Freezing Point Data

In this approach, the water-salt interaction coefficients for different salts (Equation-5.1) were determined by using the more readily available vapour pressure (at 373.15 K) and

freezing point depression data (CRC Handbook of Chemistry and Physics, 1989). Both sets of data were smoothed before being used in the optimisation. The resulting correlations were used to generate vapour pressure and freezing point data at 2.5 Wt% salt intervals which were further used to determine the interaction coefficients to match the smoothed data. Figures-5.3 and 5.4 show the water-salt interaction coefficients for NaCl and $CaCl_2$, as two examples. The values reported by Aasberg-Petersen *et al.* for these two salts are also presented in the above figures for comparison. As shown in the above figures, the Aasberg-Petersen *et al.* model is limited to medium salt concentrations and high temperatures.

Equation-5.2 is used to express the water-salt interaction as a function of temperature and salt concentrations. Table-5.2 presents the constants for this approach.

5.3. GAS-SALT INTERACTION COEFFICIENT

Solubilities of methane and carbon dioxide in NaCl, KCl, and CaCl2 aqueous solutions are investigated and modelled in this section. The choice of gases was based on the fact that the first gas is present in significant quantities in reservoir fluids and the second gas is highly soluble in aqueous solutions. In addition, the second gas is also present in many reservoir fluids and more importantly it is used as a means of EOR. The three salts were chosen according to their concentrations in formation water and the availability of experimental solubility data.

Experimental data on the solubility of different gases in single and mixed electrolyte solutions, particularly at low temperatures have been sparsely reported in open literature. The equilibrium cell of a hydrate rig (in this laboratory) has been used for generating CO_2 solubility data in NaCl, KCl, $CaCl_2$ aqueous solutions and their mixtures to provide adequate data (Burgass, 1995), particularly at low temperatures, for modelling and validation purposes. Experimental data reported in open literature on the solubility of CH_4 in the above single electrolyte solutions has been used for modelling purposes.

Before finding the gas-salt interaction coefficient, the model predictions for the solubility of methane or carbon dioxide in pure water was examined against experimental data. In both cases the model predictions were found good and there was no need to optimise the gas-water binary interaction parameters. Writing Equation-2.23 for gas and salt:

$$\ln \gamma_g^{DH} = \frac{2AM_m h_{gs}}{B^3} f(BI^{1/2}) \qquad (5.3)$$

here h_{gs} is the gas-salt interaction coefficient. Gas solubility data in single electrolyte solutions at different temperatures and salt concentrations have been used for the optimisation of the gas-salt interaction coefficient. In each case, the data has been smoothed and examined for thermodynamic consistency. Table-5.3 shows the sources of data for the optimisation of the gas-salt interaction coefficients.

The gas-salt interaction coefficients have been assumed to be independent of pressure and only functions of temperature and salt concentration. Writing Equation-5.2 for the gas-salt interaction coefficients:

$$h_{gs} = (A + BT + Cw + Dw^2 + ETw)/1000 \qquad (5.4)$$

The numerical values of A, B, C, D, and E for calculating the gas-salt interaction coefficients are given in the Table-5.4.

As an example, Figure-5.5 shows the optimised gas-salt interaction coefficient for CH4-NaCl based on the solubility data at different temperatures and salt concentrations. The Aasberg- Petersen *et al.* (1991) interaction coefficient for CH4-NaCl is also shown in the above figure with a horizontal line at 65.5. As the figure shows, the Aasberg-Petersen coefficient is only valid for high temperatures and medium salt concentrations, whereas expressing the gas-salt interaction coefficient as a function of temperature and salt concentrations will increase its range of application.

5.4. EXTENSION TO MIXED ELECTROLYTE SOLUTIONS

One of the shortcomings in the Aasberg-Petersen *et al.* (1991) model is its limitation to single electrolyte solutions. They addressed this problem in their paper *"A problem arises if the new model is to be used for predicting the solubility of a gas in a solution containing two or more dissolved salts."* They added *"To solve this problem, it would be necessary to develop suitable mixing rules for the determination of the gas-salt and water-salt interaction coefficient."* They suggested *"However, if most of the dissolved solid come from one salt, it may be safely assumed that the mixture contains only this salt at a concentration corresponding to the ionic strength of the solution."* Although this could provide acceptable results in some cases, a more robust and general approach is presented in the following section.

Two approaches were examined in order to find the fugacity coefficient of water in mixed electrolyte solutions from the parameters in single electrolyte solutions. In the first approach, the aim was to find a mixing rule to relate the interaction coefficients of mixed electrolyte solutions to those of single electrolyte solutions. After proposing a simple mixing rule and appropriate boundary conditions, water vapour pressure depression data in mixed electrolyte solutions were used to calculate the interaction coefficient for mixed electrolyte solutions. Very limited data is available on the vapour depression of water due to the presence of mixed electrolyte solutions. On the other hand, the available data are not at the required temperatures, concentrations or combinations. Thereof, it was decided to evaluate and use the Pitzer activity model (Tohidi *et al.*, 1993c) for generating water vapour pressure depression data at required temperatures, concentrations, and combinations. The activity model was found to be very successful in predicting the water vapour pressure depression of single and mixed electrolyte solutions. However, several attempts at correlating the interaction coefficient in mixed electrolyte solutions to those of single electrolyte solutions failed.

In the second approach, the aim was to find the activity coefficients (rather than the interaction coefficients) of mixed electrolyte solutions from activity coefficients of single electrolyte solutions. In the following sections the second approach is described.

As presented earlier in this chapter, the electrolyte contribution term (for water or gas), (γ_i^{EL} in Equation-2.23), could be calculated in single electrolyte solutions. Now the problem is how to relate the electrostatic contribution term of mixed electrolyte solutions to those of single electrolyte solutions. Patwardhan and Kumar (1986) used a newly defined parameter, Γ^*, called the overall reduced ionic activity coefficient, to characterise the overall non-ideality of aqueous solution of mixed electrolyte solutions. They also showed that Γ^* is simply related to the properties of single electrolyte solutions. They found the following relationship between the activity of water in a mixed electrolyte solution and that in single electrolyte solutions of the same ionic strength:

$$\log a_w = \sum_i^{ns} y_i \log a_{w,i}^0 \qquad (5.5)$$

where a_w is the activity of water in a mixed electrolyte solution, and $a_{w,i}^0$ represents the activity of a single electrolyte solution of the same ionic strength as that of the mixed electrolyte solution. i and y_i represent electrolyte, and ionic strength fraction of electrolyte i, respectively. It is worth noting that the Equation-5.5 does not contain any empirical constants and was found valid for the entire concentration range encountered in practice (Patwardhan and Kumar, 1986). The above approach was used to find the electrostatic contribution term for mixed electrolyte solutions from those of single electrolyte solutions. This approach was successful in modelling mixed electrolyte solutions.

5.5. CONCLUSIONS

In modelling electrolyte solutions, two different approaches were employed in determining the water-salt interaction coefficients. In the first approach, water vapour pressure depression data at different temperatures were used. In the second approach, the more readily available water vapour pressure depression data at 373.15 K and freezing point depression data were employed in the optimisation of the water-salt interaction coefficient. The gas-salt interaction coefficients have been optimised by using gas solubility measurements in single electrolyte solutions.

The model was extended to mixed electrolyte solutions using the Patwardhan and Kumar approach. As a result the aqueous solutions of NaCl, KCl, $CaCl_2$, Na_2SO_4, NaF, NaBr, $MgCl_2$, $SrCl_2$, $BaCl_2$ and their mixtures, have been modelled. In addition, the solubilities of two important gases, methane and carbon dioxide, in aqueous electrolyte solutions of NaCl, KCl, $CaCl_2$ and their mixtures, have been investigated and a new method for their predictions has been developed.

The developed solubility model could be used independently for providing more reliable gas solubility predictions in the presence of single and mixed electrolyte solutions in a wide range of temperature (260-420 K) and salt concentrations (up to saturation). Reliable information on gas solubility, particularly in saline water, is also required in a number of EOR processes, in the management of oil/gas reservoirs, and in acid stimulation/fracturing.

In the next chapter, the accuracy and validity of the developed model is examined against experimental data generated in this laboratory (Burgass, 1995) as well as those reported in the open literature.

****

Table-5.1. Constants in Equation-5.2 for calculating the water-salt interaction coefficients, approach-1.

	A	B	C	D	E
NaCl	-1.393E01	1.305E-02	1.621E-01	-8.987E-03	-1.171E-06
KCl	-1.418E01	1.634E-02	1.240E-01	-4.494E-03	-8.085E-07
$CaCl_2$	-5.986E00	8.057E-03	-3.575E-01	-2.281E-03	6.778E-04
Na_2SO_4	-8.739E00	1.701E-02	5.288E-03	-1.258E-03	2.593E-07
NaF	-1.475E01	1.919E-02	-1.263E-01	-7.681E-03	-3.554E-04
KBr	-1.538E01	1.850E-02	2.218E-01	-4.882E-03	-1.975E-04
$MgCl_2$	-6.038E00	7.954E-03	-5.034E-01	-1.050E-02	1.311E-03
$SrCl_2$	-8.633E00	1.683E-02	-9.000E-02	-1.644E-03	-2.547E-09
$BaCl_2$	-6.210E00	1.138E-02	-1.350E-01	1.767E-03	4.782E-07

Table-5.2. Constants in Equation-5.2 for calculating the water-salt interaction coefficients, approach-2.

	A	B	C	D	E
NaCl	-1.191E01	1.037E-02	-6.043E-02	-5.814E-03	3.861E-04
KCl	-1.279E01	1.385E-02	5.184E-02	-2.152E-03	1.436E-05
$CaCl_2$	-5.672E00	8.037E-03	-3.330E-01	-1.771E-03	5.800E-04
Na_2SO_4	-5.495E00	7.476E-03	-1.769E-02	-8.905E-04	1.083E-04
NaF	-1.482E01	1.758E-02	-3.657E-02	-5.514E-02	1.258E-03
KBr	-1.404E01	1.705E-02	1.471E-01	-1.657E-03	-2.851E-04
$MgCl_2$	-6.420E00	1.066E-02	-6.186E-01	-4.556E-03	-1.312E-03
$SrCl_2$	-6.591E00	1.327E-02	-2.334E-01	9.035E-04	1.555E-04
$BaCl_2$	-5.905E00	8.248E-03	-9.799E-02	-2.780E-04	1.423E-04

Table-5.3. Sources of data for gas-water interaction coefficient optimisation.

Gas-Salt	Source of data
Methane-NaCl	Michels *et al.*, 1936, also reported in IUPAC SDS†, pp. 117-119. O'Sullivan and Smith, (1970).
Methane-KCl	Stoessell and Byrne, 1982, also reported in IUPAC SDS†, p. 165. Ben-Naim and Yaacobi, 1974, also reported in IUPAC SDS†, p. 163.
Methane-$CaCl_2$	Michels *et al.*, 1936, also reported in IUPAC SDS†, p. 107. Blanco and Smith, 1978, also reported in IUPAC SDS†, p. 108.
CO_2-NaCl	Malinin and Savelyeva, 1972. Burgass, 1995, MSc Thesis, Heriot-Watt University
CO_2-KCl	Burgass, 1995, MSc Thesis, Heriot-Watt University
CO_2-$CaCl_2$	Malinin and Savelyeva, 1972. Prutton and Savage, 1945. Burgass, 1995, MSc Thesis, Heriot-Watt University

† IUPAC Solubility Data Series, Volume 27/28 Methane, 1987.

Table-5.4. Constants in Equation-5.4 for calculating the gas-salt interaction coefficients.

Gas-salt	A	B	C	D	E
C_1-NaCl	2.567E+2	-4.447E-1	-7.447E+0	8.202E-2	1.115E-2
C_1-KCl	1.989E+2	-4.754E-1	8.223E-1	-2.731E-2	2.068E-5
C_1-$CaCl_2$	9.915E+1	-1.414E-1	-5.017E-1	-8.176E-6	7.240E-6
CO_2-NaCl	2.157E+2	-5.179E-1	-5.563E+0	-1.663E-2	1.738E-2
CO_2-KCl	2.507E+2	-7.110E-1	-9.441E+0	3.230E-3	2.917E-2
CO_2-$CaCl_2$	7.831E+1	-1.463E-1	-2.631E-1	-4.413E-3	1.597E-3

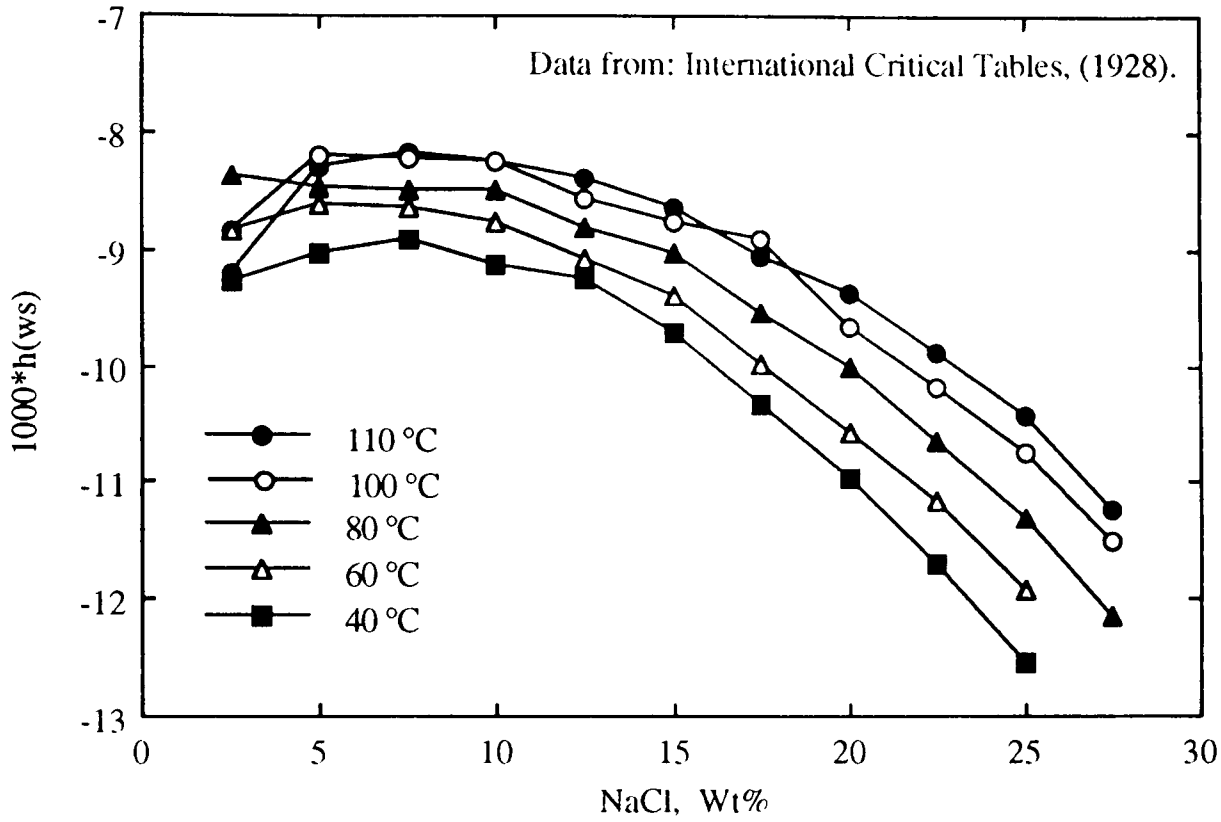

Figure-5.1 Water-NaCl interaction coefficients from vapour pressure data for the VPT EoS (Equation-5.2 and Table-5.1).

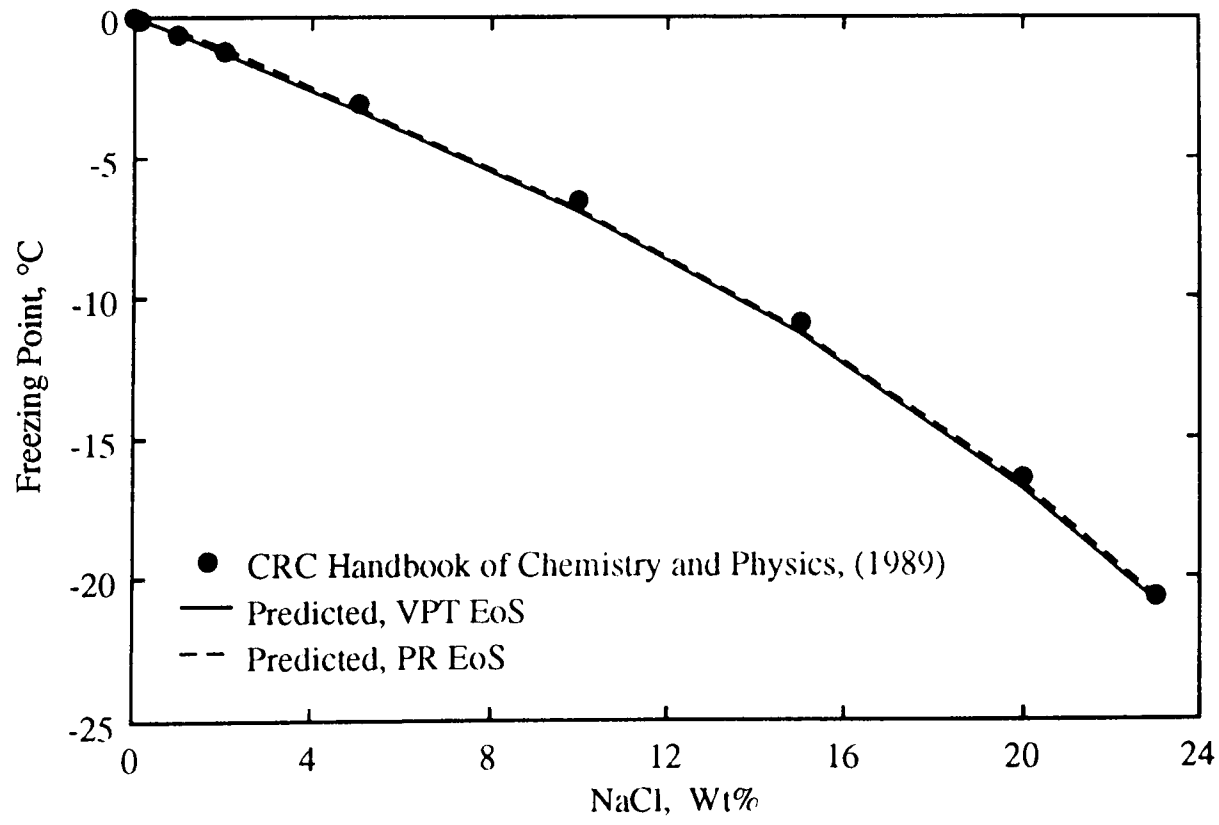

Figure-5.2 Experimental and predicted freezing points of NaCl aqueous solutions.

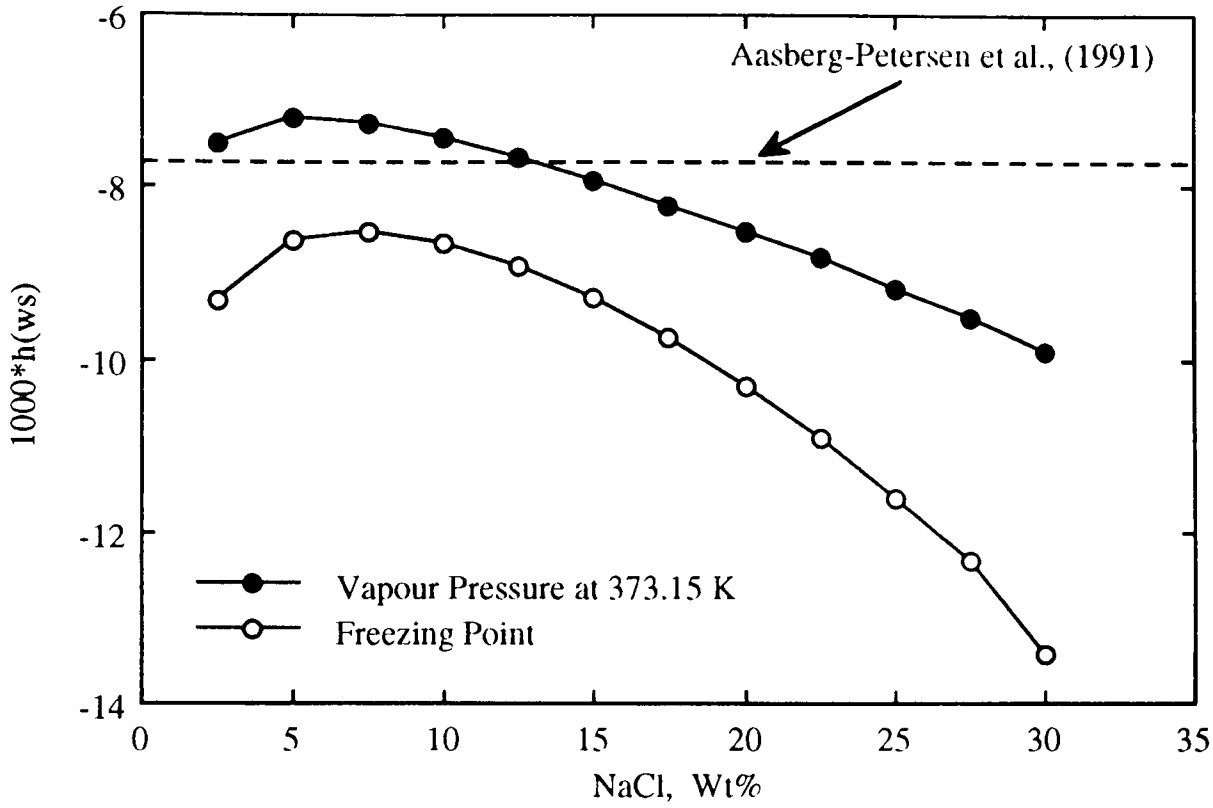

Figure-5.3 Water-NaCl interaction coefficients from vapour pressure at 373.15 K and freezing point data (Equation-5.2 and Table-5.2).

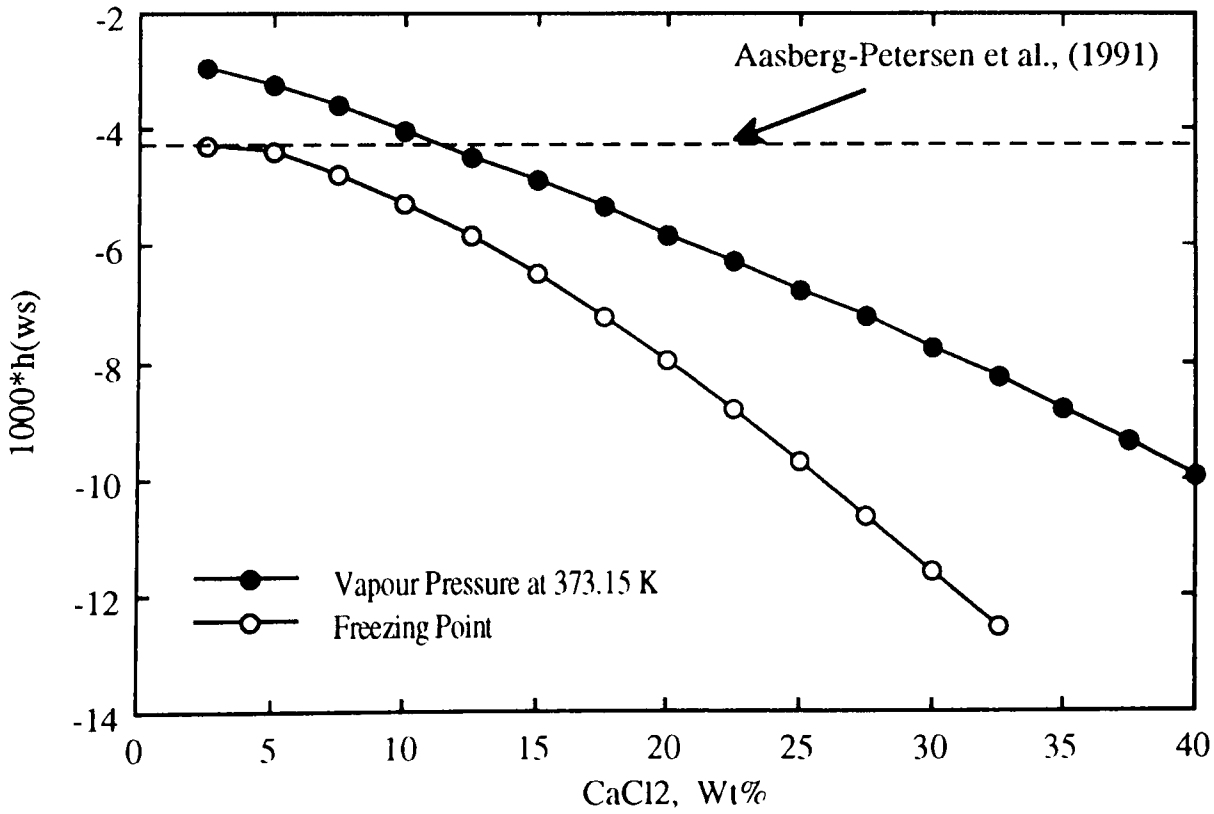

Figure-5.4 Water-CaCl2 interaction coefficients from vapour pressure at 373.15 K and freezing point data (Equation-5.2 and Table-5.2).

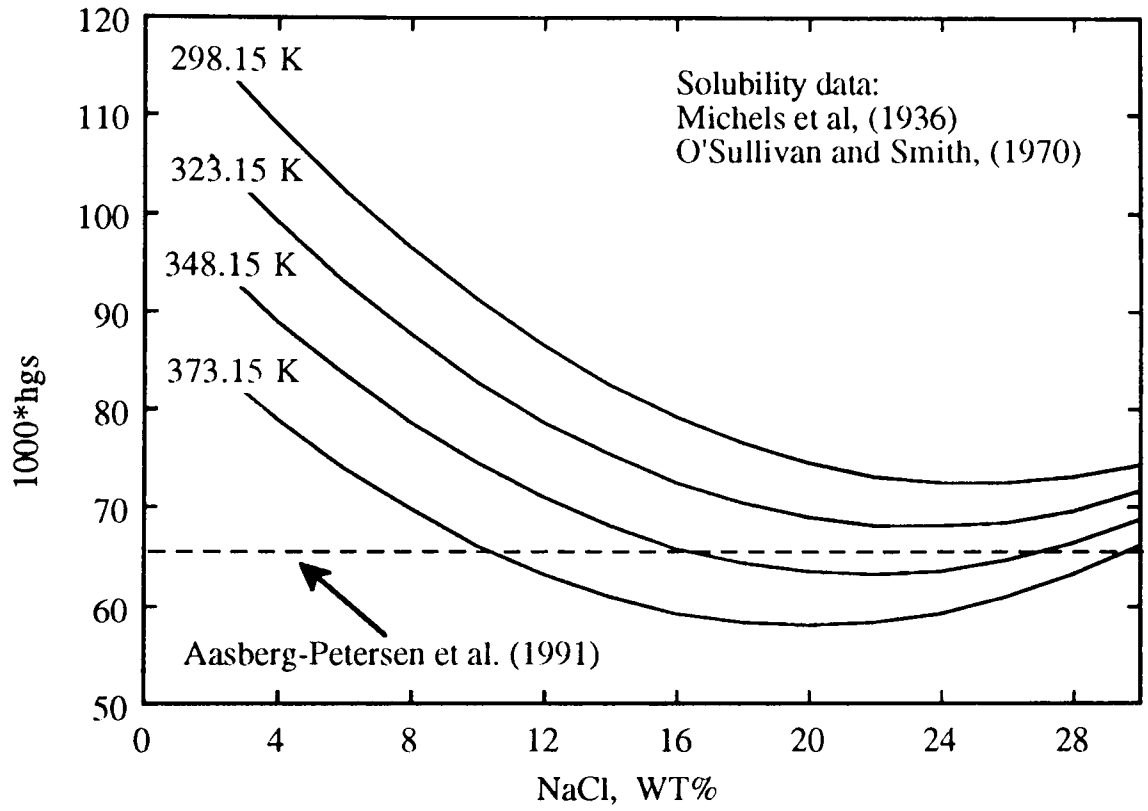

Figure-5.5 CH4-NaCl interaction coefficient as a function of temperature and salt concentration (Equation-5.4 and Table-5.4).

CHAPTER-6

VALIDATION OF THE MODEL

6.1. INTRODUCTION

As mentioned before, hydrate problems can be avoided by either operating at conditions outside hydrate region or transferring hydrates as slurry. In this study both options have been addressed. The first option which is widely accepted in the industry is largely dependent on the accurate determination of the hydrate phase boundary, whereas the success of the second option relies on predicting the amount of hydrates to be transferred.

The thermodynamic formulation presented in Chapter-2 simplifies the problem to finding a relationship for calculating the fugacity at different phases. In this study, all fluid phases are modelled with an EoS (both VPT and PR could be used), solid solution theory is used for modelling hydrate phases, and ice is regarded as sub-cooled liquid.

Hydrate phase equilibria is strongly dependent on the values of the Kihara potential parameters, representing guest-host interaction in hydrate lattice. As discussed in Chapter-3, a novel method has been used in the optimisation of the Kihara potential parameters. The other important factor in the accurate determination of hydrate phase boundary, is the effect of heavy hydrate formers. In Chapter-4, after modelling some of these compounds, their effects on hydrate phase boundary of methane and nitrogen have been investigated. Taking into account the effect of the heavy hydrate formers is expected to result in more reliable prediction for hydrate phase boundary of real reservoir

fluids. However, due to lack of experimental data it is not possible to investigate such an effect for the time being. Therefore, the effect of heavy hydrate formers has been ignored in all the predictions presented in this chapter.

Oil wellstreams generally contain saline water. The salts dissolved in the water-cut inhibit hydrate formation by shifting hydrate phase boundary. The hydrate inhibition effect of electrolyte solutions has been investigated in Chapter-5. A rigorous method has been used in modelling single and mixed electrolyte solutions, including gas solubility in saline water. The model is extended to mixed electrolyte solutions by using well established thermodynamic relations.

However, the fact that oil wellstreams may contain significantly higher water-cut than gas systems can prohibit an economical use of chemical inhibitors to prevent hydrate formation. In addition, methanol, which is largely added into hydrocarbon streams, is considered to be very harmful to the environment. For systems where the hydrate prevention approach is economically non-viable, using the growth modifiers, and the transfer of hydrates as slurry is an attractive option.

Although very little information on the growth modifiers has been released to the public domain, the general view is that these chemicals, due to their minute quantities, do not significantly affect the phase behaviour of hydrate-fluid systems, while they do affect the growth of hydrates. Most investigators are currently involved in the development and testing of growth modifying chemicals. However, we believe that the development and testing of a thermodynamic model for predicting the amount of hydrates to be transferred as slurry is equally important. The model presented in this work can be used to predict the amount and composition of different phases, particularly the amount of hydrates.

The extent of the validity and reliability of the model is investigated in this section by presenting some examples for each case. A wide range of experimental data has been

used in the validation of the model. The experimental data can be divided into the following groups:

Vapour pressure depression of single and mixed electrolyte solutions.

Freezing point depression of single and mixed electrolyte solutions.

Gas solubility in electrolyte solutions.

Hydrate inhibition effect of electrolyte solutions.

Comparison with commercial packages.

Flash calculations in presence of gas hydrates.

The reliability of the model in predicting the phase equilibria of electrolyte solutions is examined by the first three sets of experimental data. The other sets of data demonstrate the robustness of the model as a design tool for avoiding hydrate problems in sub-sea transmission lines. In relation to this study, they validate the optimisation of Kihara potential parameters, the effect of electrolyte solutions, and the effect of gas solubility on the hydrate phase boundary.

6.2. VAPOUR PRESSURE OF SINGLE AND MIXED ELECTROLYTE SOLUTIONS

In order to calculate the vapour pressure of single and mixed electrolyte solutions, bubble point calculations have been performed at different temperatures. None of the experimental data has been used in the optimisation of the gas-salt interaction parameters, so they can be regarded as independent data. Figures-6.1 to 6.5 present the experimental and predicted vapour pressure of aqueous KCl, $MgCl_2$, Na_2SO_4, KBr, and $BaCl_2$ single electrolyte solutions, respectively. The results are in good agreement with experimental data at different temperatures and even for high salt concentrations.

Figure-6.6 presents experimental (Sako *et al.*, 1985) and predicted vapour pressures of an aqueous mixed electrolyte solution of $CaCl_2$-$MgCl_2$. Again the results are in good agreement with the experimental data even at 400 K (127 °C).

Figures-6.7 and 6.8 present experimental (Fabuss and Korosi, 1966) and predicted vapour pressures of NaCl-KCl mixed electrolyte solution at 398.15 and 423.15 K (125 and 150 °C), respectively. The results of the predictions are in good agreement with the experimental data even for high temperatures.

Figures-6.9 and 6.10 show the experimental (Fabuss and Korosi, 1966) and predicted vapour pressures of NaCl-Na_2SO_4 mixed electrolyte solutions at 373.15 and 398.15 K (100 and 125 °C), respectively. Again, the results are in good agreement with the experimental data

Experimental (Kuschel and Seidel, 1985) and predicted vapour pressures of KCl-$MgCl_2$ mixed electrolyte solutions at 298.15 (25 °C) are shown in Figures-6.11 and 6.12 for two different ionic strength fractions of KCl. The good agreement between experimental and predicted vapour pressures is demonstrated.

6.3. FREEZING POINT OF SINGLE AND MIXED ELECTROLYTE SOLUTIONS

At freezing point the fugacity of water in ice phase is equal to that of the liquid water phase. For approach-1 (section 5.2.1), all freezing point data could be regarded as independent data, as none of them has been used in the optimisation of the water-salt interaction parameters. Figures-6.13 to 6.16 show the experimental and predicted freezing point of KCl, $CaCl_2$, SrCl2, and KBr single electrolyte solutions. For the first two salts, both equations of state (PR and VPT) have been used in predictions and the results are very close. The maximum error in predicting the freezing point is about 0.5 K.

Figures-6.17 and 6.18 show the experimental (Hall *et al.*, 1988) and predicted freezing point for NaCl-KCl mixed electrolyte solutions at two different weight ratios of NaCl. Good agreement is demonstrated in the figures.

Experimental (Gibbard and Gossmann, 1974) and predicted freezing points of NaCl-$MgCl_2$ mixed electrolyte solutions are presented in Figures-6.19 and 6.20. The predictions are very close to experimental data and the maximum error is less than 0.5 K.

A few freezing point measurements for mixed electrolyte solutions have been performed in this laboratory (Burgass, 1995). The experimental and predicted freezing point for different concentrations of single electrolyte solutions are reported in Table-6.1. As shown in the above table, the predictions, are in good agreements with experimental data, even for ternary salt solutions, and the maximum error is less than 0.1 K.

6.4. GAS SOLUBILITY IN ELECTROLYTE SOLUTIONS

Figure-6.21 presents experimental and predicted CO_2 solubility in NaCl single electrolyte solutions at different temperatures (298.15 to 348.15 K) and salt concentrations (0 to 22 Wt%). Englezos (1992) reported predictions for the above system at 298.15 K, which are also presented Figure-6.21, for comparison. Experimental and predicted CO_2 solubility in $CaCl_2$ aqueous solutions at 394.15 K and different salt concentrations is shown in Figure-6.22. Methane solubility in 1 and 4 molar NaCl solutions at 324.65 K is presented in Figure-6.23. As shown in the above figures, in all cases the predicted solubilities are in good agreement with the experimental data.

Predictions of CO_2 solubilities in electrolyte solutions are compared with the experimental data generated in this laboratory (Burgass, 1995). Tables-6.2 to 6.4 present the experimental (Burgass, 1995) and predicted CO_2 solubilities in NaCl, $CaCl_2$, and KCl single electrolyte solutions, respectively. As the above tables show, the predicted solubilities are in good agreement with the experimental data.

Experimental data on the solubility of CO_2 or methane in mixed electrolyte solutions are rather limited. Table-6.5 presents experimental (Burgass, 1995) and predicted CO_2 solubilities in NaCl, KCl, and $CaCl_2$ mixed electrolyte solutions. Experimental (Byrne and Stoessell, 1982) and predicted methane solubilities in mixed electrolyte solutions are shown in Table-6.6. In both tables the predicted gas solubilities in mixed electrolyte solutions are in good agreement with the experimental data. It is worth mentioning that none of the experimental data presented in Tables-6.5 and 6.6 has been used in any way in the optimisation of the model parameters.

6.5. HYDRATE INHIBITION EFFECT OF ELECTROLYTE SOLUTIONS

One of the objectives of this work was to develop a numerical model capable of predicting the hydrate free zone for pure, multicomponent, and real reservoir fluids in the presence of pure water and electrolyte solutions. Here, the model is examined against a wide range of experimental data from open literature and those generated in this laboratory (Burgass, 1995). Both VPT and PR equations of states with the two mixing rules (classical and the non-density dependent) can be used for hydrate calculations. However, the non-density dependent mixing rules are preferred to the classical mixing rules, when the solubility of gas in water is high.

This chapter could also be regarded as a validation for the optimisation of the Kihara potential parameters (Chapter-3), as the model predictions, particularly in the presence of pure water, depend on the accuracy of these parameters. For validation of the Kihara parameters, the model predictions for pure, binary, multi-component systems, and real reservoir fluids are compared with the experimental data. As detailed in Chapter-3 except selective sets of pure hydrate dissociation pressure data in the presence of pure water, none of the data presented in this chapter has been used in determining the parameters of the model. However, a comparison of the model predictions with experimental hydrate data of pure systems has been considered worthy mainly for two reasons. First, for gas components capable of forming both structures, pure component data were not the only

used data and the optimised parameters are not necessarily located at the FOB minimum of the simple hydrate of that gas. Second, since the simple gas hydrate data are supposed to be the most accurate data, and it was the objective of this work to improve the predictions for multi-component systems while keeping the accuracy of pure systems, it is worthy to examine how the objectives are met.

Methane Gas Hydrates

Experimental (de Roo *et al.*, 1983) and predicted dissociation conditions for methane gas hydrates in NaCl aqueous solutions are presented in Figure-6.24. Two cases have been investigated, i.e. ignoring, and taking into account the gas solubility in saline water. As shown in the figure, in the case of methane, due to its low solubility in water, the gas solubility does not have a significant effect on methane hydrate phase boundary. The experimental and predicted dissociation conditions are in good agreement, with the exception of very high salt concentrations.

Experimental (Dholabhai *et al.*, 1991) data on two binaries and a synthetic sea water comprised of eight electrolytes have been used to examine the model in mixed electrolyte solutions. Experimental and predicted dissociation conditions of methane hydrates in the above systems are presented in Figures-6.25 to 6.27. All of the above systems are in the three phase (liquid water rich, vapour, solid gas hydrate) region and good agreement between experimental and predicted data is demonstrated.

Ethane Gas Hydrates

Hydrate conditions for ethane simple gas hydrates in the presence of NaCl single electrolyte solutions are used to examine the reliability of the model. Experimental (Englezos and Bishnoi, 1991) and predicted dissociation conditions for NaCl, KCl, and $CaCl_2$ single electrolyte solutions are shown in Figure-6.28. The predictions show some deviation from the experimental data only at 20 Wt% NaCl. Referring to Figure-6.57 and the discussion on visual techniques, it is believed that the literature data for 20 Wt% NaCl

are in error and the data produced in this laboratory (Burgass, 1995), as conferred with the predictions, have better accuracy.

Figures-6.29 to 6.31 present the experimental (Englezos and Bishnoi, 1991) and predicted ethane hydrate dissociation conditions in binary and multi-salt mixed electrolyte solutions. The results of the predictions are in very good agreement with the experimental data. It is worth mentioning that all above systems are in the L_1-V-H three phase region.

Propane Gas Hydrates

The predictions of the model for propane hydrate points are compared with the literature data (Bishnoi and Dholabhai, 1993) for binary and ternary mixed electrolyte solutions in Figure-6.32 and very good agreement is demonstrated.

Propane hydrate points in a six component synthetic sea water, reported by Bishnoi and Dholabhai (1993), are compared with the model predictions in Figure-6.33. Despite the complexity of the system, the model is very successful in predicting the hydrate dissociation points.

Figure-6.34 presents experimental and calculated propane hydrate dissociation conditions in the presence of North Sea brine. The experimental data are generated in this laboratory (Burgass, 1995), and the predictions of the model are in good agreement with them.

A relatively high concentration mixed electrolyte solution, representing Forties formation water (Table-6.7), was used to examine the reliability of the model in predicting propane hydrate dissociation conditions. Experimental and predicted hydrate points are presented in Figure-6.35 and good agreement is demonstrated.

In all of the above systems, C_1, C_2, and C_3, have relatively low solubility in the water rich phase and both modes of calculation, i.e. ignoring gas solubility or taking into account the gas solubility due to the presence of salts, produced good results. In the next section, the model predictions are compared with the experimental data for systems containing highly water soluble gases.

CO_2 Gas Hydrates

Figure-6.36 presents experimental (Larson, 1955) and calculated hydrate dissociation conditions for CO_2 hydrates in the presence of distilled water and 1 molar NaCl solution. Three cases have been studied here, ignoring gas solubility in the water-rich phase, ignoring the change in gas solubility due to the presence of salts (assuming that the gas solubility in saline water is the same as that in pure water), and finally taking into account the change in gas solubility due to the presence of salts. *As shown in the above figure, the gas solubility model improves the predictions significantly, whereas ignoring the gas solubility produces the worst results.*

Englezos (1992) reported 57 experimental data for CO_2 hydrates in the presence of NaCl solutions, measured by Vlahakis *et al.* (1972). The data are at different temperatures and salt concentrations, so it is not possible to present all of them graphically. However, the average absolute deviation between the 57 Vlahakis' experimental measurements and the predictions of this model were found to be 3.1% compared to 7.2%, reported by Englezos (1992). The maximum absolute deviation was 7.2% at 275.3 K and 10.32 Wt% NaCl, compared to a maximum deviation of 14.8% at 277.2 K and 10.2 Wt% NaCl reported by Englezos (1992). Figure-6.37 is a graphical representation of some of the Vlahakis' experimental data and the predictions both by this model and by the model presented by Englezos (1992) which proves the superiority of the model developed in this study.

Dholabhai *et al.* (1993) reported experimental measurements for CO_2 hydrates in the presence of single and mixed electrolyte solutions. In their paper they presented an

empirical correlation with fitting constants for different systems by matching experimental data. More recently, Englezos and Hall (1994), presented experimental measurements for CO_2 hydrates in the presence of NaCl and $CaCl_2$ single electrolyte solutions and employed the model presented by Englezos (1992) for predictions. Figure-6.38 shows the above experimental data on CO_2 hydrates in the presence of $CaCl_2$ single electrolyte solutions alongside the predictions of the model presented in this work. There is some disagreement between the two sources of data, that is, the data reported by Dholabhai *et al.* (1993) at 9.99 Wt% $CaCl_2$ are at slightly higher pressures, compared to the data measured by Englezos and Hall (1994) at 10.57 Wt% CaCl2, whereas a reverse trend is expected. The predictions are in good agreement with the data presented by Englezos and Hall (1994). The model slightly under-predicts the hydrate dissociation pressures for the data reported by Dholabhai *et al.* (1993). However, the maximum error in predicting the potential hydrate formation temperature is less than 1 K for all cases.

Experimental (Dholabhai *et al.*, 1993) and predicted CO_2 hydrates dissociation conditions in a multi-salt synthetic sea water are depicted in Figure-6.39. Despite the complexity of the sea water, the predictions are in good agreement with the experimental data.

All of the above systems were simple gas hydrates. In the next section, the hydrate calculations for more complicated systems, composed of two binaries, a multi-component gas mixture, and finally real reservoir fluids, are presented.

Methane/CO_2 Gas Hydrates

Dholabhai *et al.* (1994) have reported experimental data on the hydrate inhibition effect of single and mixed electrolyte solutions on methane and CO_2 binary mixtures. Figure-6.40 shows experimental and predicted hydrate dissociation conditions for 50 mole% methane + 50 mole% CO_2 binary mixture in the presence of two binary electrolyte solutions, whereas, Figure-6.41 shows the hydrate phase boundary for 80 mole% methane

+ 20 mole% CO_2 binary gas mixture in the presence of a ternary mixed electrolyte solution. In the above two figures three different cases were studied which proved that the gas solubility model can improve the reliability of hydrate phase boundary calculations.

Multi-Component Gas Mixtures

The multicomponent gas mixture, the composition of which given in Table-6.8 has been used to generate hydrate phase boundary data in the presence of both pure water and Forties formation water (Table-6.7). Experimental and predicted hydrate dissociation conditions for the above gas mixture is presented in Figure-6.53. As shown in the figure, predictions are in good agreement with the experimental data and the maximum error in predicting the potential hydrate formation temperature is less than 1 K. The two points showing the cell conditions for compositional tests are discussed later.

Black Oil Sample

Figure-6.42 shows the experimental (Appendix-B) and predicted dissociation conditions for a black oil sample (composition in Table-6.8) in the presence of pure water and a synthetic formation water (Table-6.7). In the black oil sample all compounds heavier than normal hexane were grouped together as normal tetradecane to match its bubble point which was 9.411 MPa at 373.15 K. This is a four phase system in which liquid water, liquid hydrocarbon, vapour , and gas hydrates are in equilibrium. The results are in good agreement with the experimental data, which further proves the reliability of the model for highly complex systems.

The experimental (Appendix-B) and predicted dissociation conditions for the above black oil in the presence of Forties formation water (Table-6.7) and Forties formation water plus 8.67 Wt% methanol are presented in Figures-6.43 and 6.44. This experiment duplicates a real scenario where the inhibition effect of formation water is not sufficient

to avoid hydrate formation and methanol is added to the system. Despite the complexity of the system, the model predictions are in good agreement with the experimental data.

Also in Figures-6.42 to 6.44, the two approaches in determining the water-salt interaction coefficients (section-5.2) are compared with each other. The results demonstrate the good agreement between the two approaches, as expected.

6.6. COMPARISON WITH COMMERCIAL PACKAGES

Notz *et al.*, (1991) have recently reported experimental hydrate data on a produced gas, a gas-condensate, and a black oil sample with pure water, 20 Wt% NaCl, formation brine , methanol and methanol plus formation brine. The compositions of the above fluids is reported in Table-6.9, and the formation brine is reported to contain approximately 26,000 ppm TDS: 23,800 ppm NaCl, 400 ppm KCl, 1500 ppm HCO_3^-, 260 ppm Ca and 50 ppm Mg. They have also examined the reliability of four commercially available models. The commercial models have used empirical formulae for predicting the inhibition effect of methanol or NaCl, but none had the option of predicting the inhibition effect of reservoir brine or reservoir brine plus methanol (Notz *et al.*, 1991). The thermodynamic model developed in this study was evaluated against the above literature data and compared with the results predicted by other models.

Figure-6.45 presents the experimental and predicted hydrate conditions for the produced gas with distilled water and 20 Wt% NaCl solution. All of the predicted results, except that at 20 Wt% NaCl, are in acceptable agreement with the experimental data.

The experimental and predicted hydrate dissociation conditions for the gas-condensate sample with distilled water and in the presence of 8 Wt% methanol solution are presented in Figures-6.46 and 6.47, respectively. For the phase behaviour model, the heavy end of the gas-condensate was characterised as normal tridecane to match the measured molecular weight of C_7^+. A good agreement is demonstrated.

Figures-6.48 and 6.49 depict hydrate dissociation conditions for the black oil sample with distilled water and with 8 Wt% methanol solution, respectively. The predicted results are also presented in the above figures. The heavy end of the black oil was characterised as normal pentadecane to match the reported molecular weight of the C_7^+ fraction. All the models predict the experimental results with an acceptable accuracy.

Figures-6.50 and 6.51 show hydrate dissociation conditions for the above gas-condensate and black oil, respectively, with pure water and 8 Wt% methanol. The model predictions for the above systems with distilled water, reservoir brine, 8 Wt% methanol, and 8 Wt% methanol plus reservoir brine are also presented in the above figures. The experimental data on the above fluid systems with brine and methanol plus brine are not shown in the above figures as they were reported mistakenly equal to those of distilled water and 8 Wt% methanol, respectively by Notz *et al.* (1991). No predictions by the commercial packages were reported for these systems (Notz *et al.*, 1991).

In the above comparison the model developed in this work was found as reliable as, if not superior than, the four commercial packages, with the extra benefit of thermodynamic consistency. The model showed its capability in calculating the hydrate free zone for complex systems where methanol plus formation water were present. None of the commercial models are reported to be able to predict the hydrate free zone in the presence mixed electrolyte solutions, or the combined effect of methanol and formation water.

Almost in all cases the model over-predicted hydrate dissociation pressure, particularly for data presented by Notz *et al.*, (1991), which might be due to non-equilibrium conditions. Notz *et al.*, (1991) reported a typical time cycle of 10 hours for each cooling and heating cycle used to measure a hydrate point. It has been shown that the required time to attain equilibrium could be as high as several days at some conditions (Tohidi *et al.*, 1994).

6.7. FLASH CALCULATIONS IN THE PRESENCE OF GAS HYDRATES

There is very little information available in the literature on the amount and composition of the phases in systems with hydrates (Dharmawardhana *et al.*, 1980, Holder *et al.*, 1984), reflecting the difficulty of isolating and sampling different phases. Burgass (1995) has conducted a series of compositional tests in the presence of gas hydrates. He initially investigated the formation of hydrates in a number of binary mixtures. For both practical and theoretical reasons, xenon was chosen as one of the components of the binary mixtures used in the compositional work (Burgass, 1995).

Burgass (1995) performed compositional studies for three binary systems C_1/Xe, C_2/Xe (structure-I) and C_3/Xe (structure-II) with distilled water to generate information on the amount and composition of hydrates. Later, the method was successfully adapted to propane in the presence of electrolyte solutions, a multi-component gas mixture in the presence of pure and Forties formation water (Table-6.7), and a North Sea gas-condensate in the presence of pure water and methanol solution (Burgass, 1995).

The experimental and predicted dissociation conditions for a typical C_1/Xe mixture are presented in Figure-6.52 and good agreement is demonstrated. The results for the compositional test on the C_1/Xe binary are reported in Table-6.10. The model slightly over-predicts the amount of hydrates formed. The predicted composition of different phases and the amount of vapour phase are in good agreement with the experimental data.

The results of compositional tests on the amount of propane hydrates formed in the presence of single and mixed electrolyte solutions are presented in Table-6.11. Although the system was found to be very sensitive to P and T, the results are in good agreement with the experimental data, with the exception of the 20.03 Wt% NaCl solution. As presented in column-6 and 7 of the Table-6.11, the experimental and predicted salt concentrations in the free water are 21.324 and 22.178 Wt%, respectively. Column-10 of this table shows an error of 54%. Considering the high concentration of NaCl and the

low temperature, it is our opinion that a significant proportion of this error is due to the precipitation of NaCl.

The results for real reservoir fluids, including a gas mixture and a North Sea gas-condensate with pure and formation water and methanol, are presented next. The composition of the gas mixture and the gas-condensate is given in Table-6.8. The gas-condensate has a dew point of 42.62 MPa at 377.15 K. Table-6.7 presents the composition of Forties formation water.

Figure-6.53 shows the experimental and predicted dissociation conditions for the dry gas mixture in the presence of pure water and Forties formation water. The maximum error in predicting the potential hydrate formation temperature is less than 0.5 K. The equilibrium conditions for the two compositional tests on the gas mixture are also presented in the above figure, and are 0.65 MPa and 1.0 MPa inside the hydrate region for pure water and formation water, respectively.

Table-6.12 presents the results of the compositional tests on the gas mixture in the presence of pure water in the L_1-H-V three phase region. The predicted amount and composition of the vapour phase are in good agreement with the experimental values. The experimental and predicted compositions of the gas in hydrates are in acceptable agreement with the exception of C_2 and CO_2. The reason for this discrepancy is not yet clear, though it could be due to experimental error, or error in calculating the C_2 solubility in the free water. Comparison between the composition of the vapour phase and the gas in hydrates shows that, although the concentrations of light compounds of C_1 and CO_2 are lower in the hydrate gas, the concentrations of intermediates are significantly higher than those in the vapour phase. In the case of C_3, the concentration has increased from 1.67 to 17.29 mole%.

Table-6.13 presents the results of the compositional test on the dry gas mixture in the presence of Forties formation water (Table-6.7). The experimental and predicted compositions of the vapour phase are in very good agreement, with some deviations in the concentration of C_3. This could be due to the collection of some hydrate particles during the sampling of the vapour phase. Note that the concentration of C_3 in the hydrates is significantly higher than that of the equilibrium vapour phase. The experimental and predicted amount of vapour in equilibrium with other phases are in good agreement. Considering the experimental and predicted composition of gas in hydrates, again the largest deviations are in C_2 and CO_2, and the experimental result for the latter was not reliable. This table also shows that the experimental and predicted amount of hydrate phase are in good agreement.

Figure-6.53 shows some deviations between the experimental and predicted dissociation conditions of the gas mixture in the presence of Forties formation water. This paragraph examines the effect of such error in predicting the hydrate phase equilibrium line on the results of the compositional test. Figure-6.53 shows that the predicted dissociation pressures at the cell equilibrium temperature for Forties formation water is 0.15 MPa higher than the measured value. Implementing that deviation by calculating the equilibrium at 0.15 MPa higher than the test pressure, the mole percent of the vapour and hydrate phases will be 15.20 and 10.41, respectively. This reduces the deviation between the measured and predicted mole percents of vapour and hydrate phases from 0.29 and 0.67 to 0.14 and 0.45, respectively.

The gas-condensate heavy end was characterised as normal hexadecane by matching the predicted and measured dew points. Figure-6.54 presents the hydrate dissociation conditions for the gas-condensate in the presence of pure water and 30.5 Wt% methanol solution. The predicted dissociation conditions are in good agreement with the experimental values and the maximum error in predicting the potential hydrate formation temperature is about 1 K. In order to predict the amount of hydrates formed within the

hydrate region, the model was initially tuned by matching the dissociation pressure to measured values by adjusting the concentration of the inhibitors. A 29 Wt% methanol solution resulted in a predicted dissociation pressure of 4.351 MPa compared to the experimental value of 4.185 MPa at 272.15 K. The equilibrium conditions for the two compositional tests for the gas-condensate in the four phase L_1-L_2-H-V region are also shown in the figure, and are 0.45 MPa and 0.63 MPa inside the hydrate region for pure water and the 29 Wt% methanol solution, respectively. The predicted and measured results of the compositional tests on the gas-condensate in the presence of water and methanol are presented in Table-6.14. Calculated vapour compositions, mole percent vapour and the amount of water converted to hydrates are in good agreement with the experimental data.

Visual Technique and Electrolyte Solutions

The hydrate formation condition depends on many factors (e.g. the degree of sub-cooling, the history of water, the presence of foreign materials). Therefore, the experimental determination of the hydrate phase boundary is performed by measuring the hydrate dissociation (rather than formation) conditions (pressure and temperature). Two different methods, i.e. pressure search or temperature search, are used in the determination of hydrate dissociation conditions. In the pressure search method, the cell temperature is kept constant and the pressure is adjusted, till only a small amount of hydrates are present in the cell. The temperature and pressure are then recorded as one point on hydrate phase boundary. A typical pressure search method, as reported by Dholabhai *et al.* (1993, 1994), is as follows:

"Approximately 115 cm^3 of the solution (water-rich phase) was charged into the cell, and the solution was cooled down to the required temperature. Once the desired temperature was reached, the pressure in the cell was increased beyond the expected equilibrium value by introducing the gas from the cylinder. When the hydrates were formed, the pressure was reduced to a value slightly less than the expected equilibrium pressure by

venting out the excess gas. The system was then left to equilibrate. If the temperature and pressure of the system remained constant for 3-4 hours with a negligibly small quantity of the hydrates present in the solution, the constant pressure and temperature were taken as the equilibrium conditions and the experiment was terminated. If the system pressure was higher than the equilibrium pressure, then the pressure was readjusted to a lower value. On the other hand, if all the hydrates were decomposed, then the hydrates were formed again as described above, the pressure was adjusted to a value slightly higher than that at which all the hydrates had decomposed, and the observation was continued."

The above pressure search method has several shortcomings, such as:

- It cannot be applied to liquid hydrocarbon systems.
- For gas mixtures, it is difficult to specify the composition of the feed and only the vapour phase composition can be measured. It is also impossible to perform a test for a given composition. Therefore, purging the vapour phase (for reducing the system pressure) will change the overall feed composition, since the vapour composition will change upon hydrate formation.

In order to overcome the above shortcomings, the pressure search method could be modified by avoiding the removal or addition of gas, and adjusting the pressure by other means (using mercury or a variable volume cell), which is beyond the interest of this discussion.

In addition to the above, there are two more shortcomings in the above procedure. Firstly, the amount of the water-rich phase is significant and 3-4 hours time for achieving equilibrium could be insufficient in some cases. In a recent publication (Tohidi *et al.*, 1994), it was shown that the time required for achieving the equilibrium is a direct function of the amount of water used in the experiment. However, the amount of water should be enough to allow the formation of a sufficient amount of gas hydrates.

Secondly, only visual techniques can be used in determination of the hydrate dissociation pressure. As discussed later in this section, the visual techniques could be seriously misleading in electrolyte solutions.

The other widely used method is the so-called temperature search technique. In this method, after loading the cell, the cell temperature is lowered to allow the gas hydrates to form. Then the temperature is raised stepwise and the hydrate dissociation pressure is determined by visual or/and graphical methods. A typical temperature search method is described in the following paragraph (Tohidi *et al.*, 1994):

"Once the cell was charged with water (approximately 20 grams) and the test gas, the temperature was lowered to form hydrates (with the cell content being mixed). Their formation was confirmed by a rapid pressure drop. The temperature was raised stepwise, allowing at least 3 hours for equilibrium to be reached at each temperature. The temperature and pressure were logged continuously and the equilibrium data was plotted on a scatter-gram. The point at which the slope of the P=f(T) curve sharply changed was considered as the hydrate dissociation point." Figure-6.55 shows typical results from temperature search method and the graphical technique in determining the hydrate dissociation point. As shown in the figure, after sufficient cooling the pressure drops significantly upon hydrate formation. The temperature is increased stepwise, allowing sufficient time at each step. As hydrates dissociate, gas is released to the vapour phase and the pressure increases gradually. In this case, the pressure drops again due to the formation of structure-H hydrates and when all hydrates dissociate the pressure increase trend changes slope sharply. The point of sharp change in the slope of P vs T plot is the point where last hydrate crystal dissociates is one point on the hydrate phase boundary.

Therefore, the techniques in finding the hydrate dissociation points can also be divided into two groups, i.e. visual and graphical. In the visual techniques, the dissociation point

is the point at which a small amount of gas hydrate is present. This negligibly small amount is, in fact, left to individual judgement. In addition, most hydrate cells (Dholabhai *et al.*, 1993, 1994) have windows for visual observation, and there could be some hydrates present in other places (not visible through the window). However, the graphical techniques have their own shortcomings, e.g. they are not applicable to cases with no vapour phase, and the amount of water in the cell and the time for achieving equilibrium are more important (Tohidi *et al.*, 1994).

In the visual techniques, the presence of a negligible amount of hydrates, means that the system is inside the hydrate phase boundary, as some hydrates are present. In normal cases where there is no salt (or any other inhibitor) in the water-rich phase, this deviation from the hydrate phase boundary is usually negligible. However, this is not the case for electrolyte solutions as the deviation from the hydrate phase boundary increases with the salt concentration and is significant for concentrated salt solutions. In this section, it is shown that using visual techniques for measuring the hydrate dissociation condition in the presence of electrolyte solutions could be misleading. Generally in saline water (particularly high salt concentrations), the formation of any gas hydrates will increase the salt concentration in the free water, as salt is excluded from hydrate structure. This inhibits the formation of more hydrates, so the system has to be cooled down again, in order for more hydrates to be formed.

Using the pressure search method and visual techniques, Dholabhai *et al.*, (1993) measured the dissociation conditions for CO_2 simple gas hydrates in the presence of aqueous NaCl solutions, as presented in Figure-6.56. The model predictions (taking into account the change in the gas solubility due to the presence of the electrolyte) are also presented in the above figure. The predictions deviate from experimental data as a function of salt concentration and pressure, i.e. the deviations increase with increasing salt concentration or pressure. We want to show that some of the deviations are due to the error induced in hydrate phase boundary measurement by visual techniques.

Table-6.15 presents the hydrate phase fraction for CO_2 (10% CO_2 + 90% water in the feed) gas hydrates in the presence of different salt concentrations. In doing so, referring to Figure-6.56 a horizontal line is passed at P=2 MPa and the approximate hydrate dissociation temperature has been found for different salt concentrations. These temperatures are used to calculate the hydrate dissociation pressure, P. The temperature is reduced by 0.5 K and flash calculations are performed, the results of which are presented in Table-6.15. In other words, Table-6.15 shows the hydrate phase fraction at the points which are 0.5 K inside hydrate phase boundary for different salt concentrations.

In Table-6.15 column-2 shows the approximate hydrate dissociation temperatures at 2 MPa pressure for 3, 5, 10, 15, and 20 Wt% NaCl solutions (column-1), respectively (also shown graphically in Figure-6.56). Column-3 presents the hydrate dissociation pressure corresponding to the temperatures of column-2 for different salt concentrations. Assuming 0.5 K sub-cooling and a feed of 10% CO2, the system is flashed at P and T (columns-3 and 4). The Hydrate (H), Water (W), and Vapour (V) phase fractions are reported in columns-5 to 7. Finally, column-8 shows the resulting salt concentrations in the water-rich phase. The results in column-5 are very interesting and agree with the previous observations. As shown in column-5, for 0.5 K sub-cooling the hydrate phase fractions would be 0.29, 0.20, 0.11, 0.06, and 0.04 for 3, 5, 10, 15, and 20 Wt% NaCl solutions, respectively. Consequently, if a phase fraction of 0.05 is necessary to detect the hydrate dissociation conditions by visual techniques, more sub-cooling is needed at high salt concentrations.

The above argument proves that visual techniques are not suitable for high salt concentrations and they may lead to serious errors. One may argue that a phase fraction of 0.05 for hydrates is far too much and one must be able to detect much smaller amounts of hydrates visually. As mentioned earlier, most hydrate cells designed for visual determination of the hydrate phase boundary, have small windows for safety reasons (in

this particular case the cell was equipped with two marine-type windows) and it is not possible to see everywhere in the cell. In addition, when the system is close to the dissociation point, significant amount of hydrates could be present in the form of small particles dispersed in the water phase.

As mentioned before (also shown in Figure-6.56), the deviation between experimental and calculated hydrate points increases as pressure increases. In the above experiment, higher pressures are equivalent to a higher mole fraction of CO_2 in the feed, as the amount of water was about 115 cm^3 in all cases. The mole percent of CO_2 is assumed to be 5, 10, and 15 for 1, 2, and 3 MPa pressure, respectively. Obviously, these are approximate calculations, as more accurate information on the cell volume and the amount of water is required to calculate the amount of CO_2 in the feed at any given P and T. However, the approximation can show the trend. Table-6.16 shows the amount of hydrates formed for 0.5 K sub-cooling at different pressures and in the presence of 20 Wt% NaCl solution.

As shown in column-5 of the above table, the amount of hydrate formed for 0.5 K sub-cooling will decrease with an increase in pressure (amount of CO_2), so more sub-cooling is required at high pressures compared to low pressures for each salt concentration. Therefore, using visual techniques will lead to more error at higher pressures, as shown in Figure-6.56. This might explain the deviation in the experimental and predicted hydrate phase boundaries in Figures-6.28 and 6.38.

Figure-6.57 shows the experimental and predicted inhibition effect of NaCl aqueous solutions for ethane simple hydrates. Two sets of experimental data have been reported by Englezos and Bishnoi, (1991), and Burgass, (1995) for 20 Wt% NaCl concentration. The two sets of experimental data do not agree with each other, and the model predictions are closer to those reported by Burgass, (1995). It is interesting to know that Englezos

and Bishnoi have used visual techniques, whereas Burgass has used graphical method. The error in the first set of data could be due to the error induced by visual techniques.

6.8. CONCLUSIONS

Despite the wide range of temperature, salt concentrations, and type of data, the model was found to be very successful in predicting the phase behaviour of electrolyte solutions, i.e. water vapour pressure and freezing point depressions due to the presence of salts, and gas solubility in saline water.

Particular attention was given to the hydrate inhibition effect of electrolyte solutions as this was the main objective of this work. As shown in this chapter, the model is able to predict the hydrate inhibition effect of saline water on all synthetic and real reservoir fluids, including gas mixtures, gas-condensate samples, and black oil samples. The model was also successful in predicting the combined inhibition effect of a formation water plus methanol. Comparison of the model with 4 commercial packages showed that the developed model is as reliable as, if not superior to them and also benefits from thermodynamic consistency. In addition, none of the commercial packages is reported to be able to predict the hydrate inhibition effect of mixed electrolyte solutions and combined effect of methanol and formation water.

In relation to the amount of hydrates formed, synthetic and real reservoir fluids, including a dry gas and a gas-condensate, in different production scenarios, such as in the presence of condensed water, methanol, or formation water, have been investigated. The model predictions are compared with the experimental data and good agreement is demonstrated.

The ability of predicting the amount of hydrates in the presence of electrolyte solutions, showed that visual techniques are not suitable for determining the phase boundary in the presence of electrolyte solutions, particularly at high salt concentrations and pressures.

Validation of the Model

Comparison of the predicted results by the model with different sets of experimental data suggests that the model can be used as a reliable design tool in the production and transportation of reservoir fluids in the presence of condensed water, formation water, methanol, and methanol plus formation water.

****

Table-6.1. Experimental and calculated freezing point depressions for binary and ternary salt solutions.

Wt%					
NaCl	KCl	$CaCl_2$	$MgCl_2$	Experimental freezing point depression K. (±0.005)	Predicted freezing point depression K.
0.50	0.50	-	-	0.522	0.434
1.00	1.00	-	-	1.048	1.027
2.00	2.00	-	-	2.120	2.248
0.50	-	0.38	-	0.463	0.365
1.00	-	0.75	-	0.924	0.865
2.00	-	1.51	-	1.768	1.930
0.50	-	-	0.23	0.416	0.329
1.00	-	-	0.47	0.830	0.789
2.00	-	-	0.94	1.685	1.757
0.30	0.33	-	0.16	0.434	0.318
0.66	0.66	-	0.31	0.866	0.799
1.33	1.33	-	0.63	1.751	1.793

Table-6.2. CO_2 solubility in NaCl solutions.

Wt%	T, K	P, MPa	mole%, Exp	mole%, Pred
10.0	274.1	1.752	1.20	1.18
10.0	268.2	1.105	0.97	0.96
15.0	274.1	1.857	1.00	1.03
15.0	268.3	1.162	0.79	0.83

Table-6.3. CO_2 solubility in $CaCl_2$ solutions.

Wt%	T, K	P, MPa	mole%, Exp	mole%, Pred
7.05	273.2	1.675	1.36	1.36
7.05	266.4	0.910	1.00	1.01
13.65	273.2	2.027	1.28	1.18
13.65	266.4	1.076	0.82	0.87

Table-6.4. CO_2 solubility in KCl aqueous solutions.

Wt%	T, K	P, MPa	mole%, Exp	mole%, Pred
5.0	298.2	4.937	1.96	1.96
5.0	323.2	5.033	1.31	1.31
5.0	348.2	5.130	1.02	0.98
10.0	298.1	4.826	1.77	1.76
10.0	323.2	4.840	1.17	1.19
10.0	348.3	4.930	0.91	0.90
15.0	298.2	4.688	1.61	1.61
15.0	323.2	4.537	1.04	1.05
15.0	348.4	4.930	0.82	0.84
20.0	298.2	4.799	1.51	1.54
20.0	323.2	4.971	1.03	1.03
20.0	348.2	4.688	0.73	0.72
7.0	273.2	1.317	1.27	1.26
7.0	266.5	0.855	1.06	1.07
14.0	273.2	1.882	1.52	1.50
14.0	266.5	1.172	1.26	1.24

Table-6.5. Experimental and predicted CO_2 solubility in mixed electrolyte solutions.

NaCl, Wt%	KCl, Wt%	$CaCl_2$, Wt%	T, K	P, MPa	mole%, Exp	mole%, Pred
1.99	1.99	1.99	273.2	1.544	1.34	1.37
1.99	1.99	1.99	298.1	1.606	0.66	0.71
2.99	2.99	2.99	273.2	1.558	1.22	1.24
2.99	2.99	2.99	298.1	1.620	0.66	0.65

Table-6.6. Experimental and predicted CH_4 solubility in mixed electrolyte solutions.

NaCl, Wt%	KCl, Wt%	$CaCl_2$, Wt%	T, K	P, MPa	mole%, Exp	mole%, Pred
-	-	-	298.15	3.795	0.087	0.084
5.158	6.580	-	298.15	3.795	0.051	0.047
4.997	-	9.491	273.2	1.558	0.039	0.037

Table-6.7. Composition of synthetic and Forties formation water.

	Synthetic Formation Water	Forties Formation Water
Salt	Wt%	Wt%
NaCl	8.460	6.993
$CaCl_2$	3.043	0.735
$MgCl_2$	0.865	0.186
KCl	-	0.066
$SrCl_2$	-	0.099
$BaCl_2$	-	0.036

Table-6.8. Composition (mole%) of gas mixture, gas-condensate, and black oil.*

Component	Gas Mixture	Gas-condensate†	Black Oil¥
N2	0.72	0.58	-
CO_2	1.31	2.38	-
C_1	85.93	73.95	23.08
C_2	6.75	7.51	4.09
C_3	3.13	4.08	6.09
i-C_4	0.71	0.61	2.18
n-C_4	0.88	1.58	4.51
i-C_5	-	0.50	2.33
n-C_5	0.57	0.74	3.31
C_{6s}	-	0.89	4.30
C_7^+	-	7.19	50.11

* Data from R. W. Burgass, (1995).

† A bottom hole sample with the dew point of 42.62 MPa at 377.15 K.

¥ Bubble point was measured as 9.411 MPa at 373.15 K.

Table-6.9. Composition (mole%) of produced gas, gas-condensate, and black oil.*

	Produced Gas	Gas-condensate	Black Oil
CO_2	0.18	1.34	1.93
C_1	87.76	77.24	49.25
C_2	5.49	7.61	9.58
C_3	3.48	3.69	7.21
i-C_4	-	0.56	1.06
n-C_4	3.09	1.40	3.50
i-C_5	-	0.03	0.05
n-C_5	-	0.89	2.45
C_6s	-	0.67	2.18
C_7^+	-	6.57	22.79
Fluid MWt	19.1	30.7	68.0
C_7^+ MWt	-	174	204
C_7^+ Sp. Gr.	-	0.8096	0.8350

* Data from Notz *et al.*, (1991).

Table-6.10. Experimental and predicted equilibrium phase mole fractions and phase compositions (mole fractions) for C1/Xe gas hydrates in the L1-H-V region.

Cell conditions at equilibrium T=286.05 K, P=2.406 MPa

	Methane	Xenon	Water
Feed	0.0858	0.0286	0.8856
	Phase compositions		
	Methane	Xenon	Water
	Vapour		
Exp	0.7941	0.2059	-
Pred	0.8089	0.1904	0.0007
	Hydrate		
Exp	0.0379	0.1039	0.8582
Pred	0.0375	0.1056	0.8569
	Phase mole fractions		
	Vapour	Hydrate	Water
Exp	0.1044	0.0676	0.8280
Pred	0.1016	0.0843	0.8141

Table-6.11. Feed composition, equilibrium conditions, and results of compositional tests for C_3 hydrates in the presence of electrolyte solutions.

1	2	3	4	5	6	7	8	9	10
Salt(s)	Wt% salt original solution	T_{eq}, K	P_{eq}, MPa	C_3, mole %	Exp. Wt% of salt in free water	Pred. Wt% of salt in free water	Exp. Hyd. phase fraction	Pred. Hyd. phase fraction	100 (H_{pre}-H_{exp})/ H_{exp}
$CaCl_2$	7.274	272.15	0.317	3.248	8.533	8.607	*0.163*	*0.171*	5.224
$CaCl_2$	11.343	269.35	0.310	3.639	12.265	12.276	*0.088*	*0.087*	-1.068
$CaCl_2$	15.121	265.95	0.324	3.783	16.346	16.217	*0.089*	*0.810*	-9.154
NaCl	3.078	273.15	0.255	2.968	3.914	3.958	*0.226*	*0.236*	4.393
NaCl	20.03	260.05	0.283	3.646	21.324	22.178	*0.080*	*0.124*	53.868
KCl	9.976	270.75	0.290	3.834	12.245	12.184	*0.210*	*0.205*	-2.279
KCl	15.067	268.55	0.296	4.777	16.829	16.865	*0.125*	*0.126*	1.180
NaCl $CaCl_2$	4.820 3.710	271.15	0.324	2.940	5.589 4.301	5.607 4.316	*0.154*	*0.158*	2.088
NaCl KCl	5.109 5.109	270.15	0.296	3.107	5.863 5.863	5.870 5.870	*0.149*	*0.148*	-0.448

Table-6.12. Results of compositional tests on multi-component gas mixture in the presence of pure water.

	Cell condition at equilibrium, T=284.8 K, P=3.591 MPa Moles water/moles gas mixture=5.029			
	Composition (mole%) of vapour phase and gas released from hydrates on a nitrogen and water free basis			
Component	Vapour Exp.	Vapour Pred.	Hydrate Exp.	Hydrate Pred.
CO_2	1.68	1.24	0.37	0.65
C_1	88.57	89.21	67.89	63.52
C_2	6.47	6.20	8.63	12.34
C_3	1.67	1.60	17.29	17.35
i-C_4	0.29	0.32	4.54	4.29
n-C_4	0.80	0.79	1.28	1.85
n-C_5	0.52	0.64	-	-

Experimental and predicted mole % of equilibrium phases		
Phase	Experimental	Predicted
Vapour	14.85	14.88
Hydrate	11.63*	12.28
Water	73.52	72.84
Moles of gas in hydrates	0.022	0.022

* Calculated by assuming 100% cage occupancy and using measured volume of gas in hydrates. Measurement for water bonded into hydrates failed due to the contamination in the free water sample.

Table-6.13. Results of compositional tests on multi-component gas mixture in the presence of Forties formation water.

	Cell condition at equilibrium, T=284.5 K, P=5.366 MPa Moles water/moles gas mixture=4.987			
	Composition (mole%) of vapour phase and gas released from hydrates on a nitrogen and water free basis			
Component	Vapour Exp.	Vapour Pred.	Hydrate Exp.	Hydrate Pred.
CO_2	1.28	1.23	-	0.63
C_1	87.43	88.47	69.90	65.00
C_2	6.47	6.42	8.54	11.31
C_3	3.04	1.99	16.69	17.35
i-C_4	0.40	0.42	3.73	4.24
n-C_4	0.85	0.84	1.14	1.47
n-C_5	0.53	0.63	0	0

Experimental and predicted mole % of equilibrium phases		
Phase	Experimental	Predicted
Vapour	15.06	15.35
Hydrate	9.96	9.29
Water	74.98	75.36
Moles gas released from hydrates	0.019	0.016

Table-6.14. Comparison of experimental and calculated equilibrium vapour phase compositions (mole%) and moles water converted to hydrate for gas-condensate.

	Pure Water		Water/Methanol	
	T=283.25 K, P=2.848 MPa Moles water/moles gas-condensate=13.354		T=270.22 K, P=4.027 MPa Moles water/moles gas-condensate=3.632	
Component	Experimental	Predicted	Experimental	Predicted
N_2	0.65	0.74	0.96	0.72
CO_2	1.76	2.08	1.99	2.30
C_1	86.46	86.76	86.88	86.76
C_2	7.29	7.17	6.92	7.12
C_3	2.03	1.92	1.94	2.17
i-C_4	0.21	0.21	0.20	0.21
n-C_4	0.69	0.72	0.41	0.48
i-C_5	0.13	0.13	0.05	0.07
n-C_5	0.15	0.15	0.08	0.08
C_6^+	0.63	0.07	0.44	0.03
MeOH	-	-	0.13	0.04
H_2O	-	0.05	-	0.01
Mole% vapour	5.30	5.26	13.68	14.57
Moles of water converted to hydrates	0.042 (± 0.007)	0.046	0.048 (± 0.005)	0.046

Table-6.15. Flash calculations in the presence of CO_2 gas hydrates at different NaCl concentrations.

1	2	3	4	5	6	7	8
Wt%	Hyd. Temp, K	Hyd/Flash Press, MPa	Flash Temp, K	*H, Phase Frac.*	W, Phase Frac.	V, Phase Frac.	Final Salt Wt%
3.0	276.0	2.002	275.5	*0.296984*	0.655789	0.047227	4.41
5.0	275.0	1.974	274.5	*0.204920*	0.735272	0.059808	6.14
10.0	272.8	1.990	272.3	*0.106782*	0.819038	0.07418	11.01
15.0	270.0	1.972	269.5	*0.062334*	0.856179	0.081487	15.80
20.0	266.5	1.973	266.0	*0.039620*	0.874759	0.085622	20.62

Table-6.16. Flash calculations in the presence of CO_2 gas hydrates at 20 Wt% NaCl solution and different pressures.

1	2	3	4	5	6	7	8
App. P, MPa	Hyd. Temp., K	Hyd/Flash Press, MPa	Flash Temp., K	*H, Phase Frac.*	W, Phase Frac.	V, Phase Frac.	Final Salt Wt%
1	260.5	1.007	260.0	*0.042527*	0.919805	0.037668	20.634
2	266.5	1.973	266.0	*0.039620*	0.874759	0.085622	20.622
3	269.5	2.866	269.0	*0.036838*	0.828419	0.134743	20.612

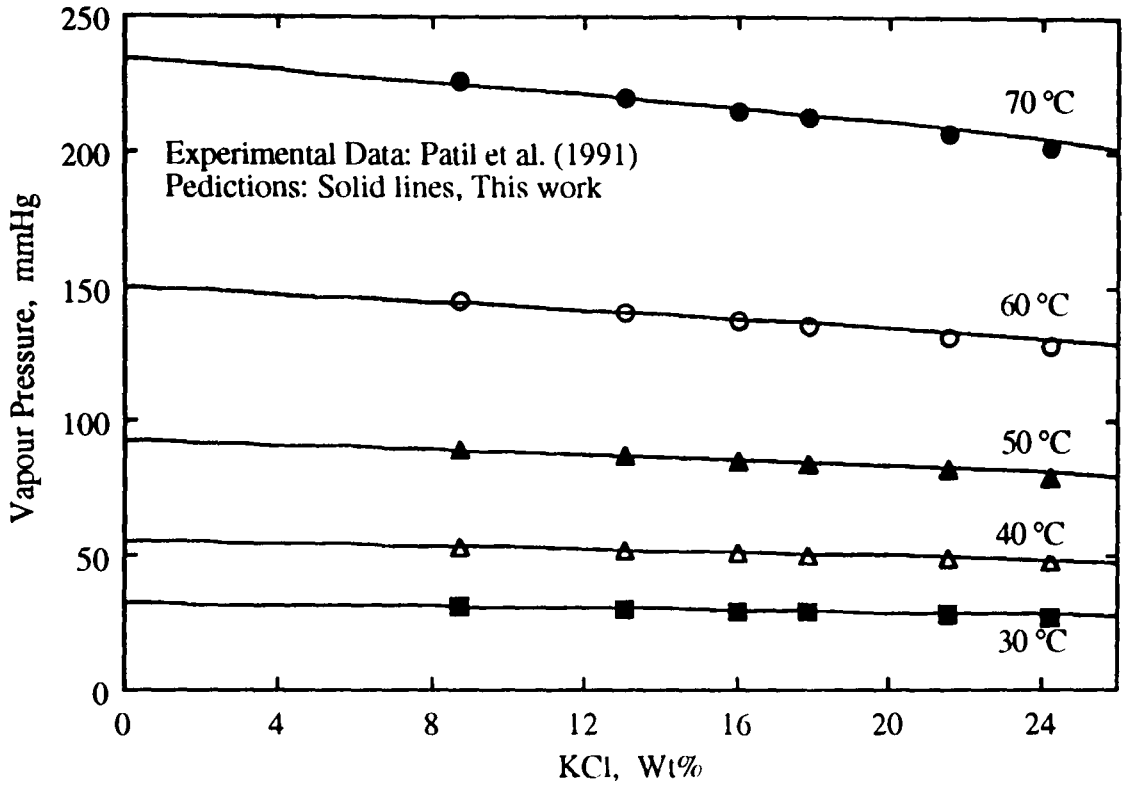

Figure-6.1 Experimental and calculated vapour pressure for KCl solutions.

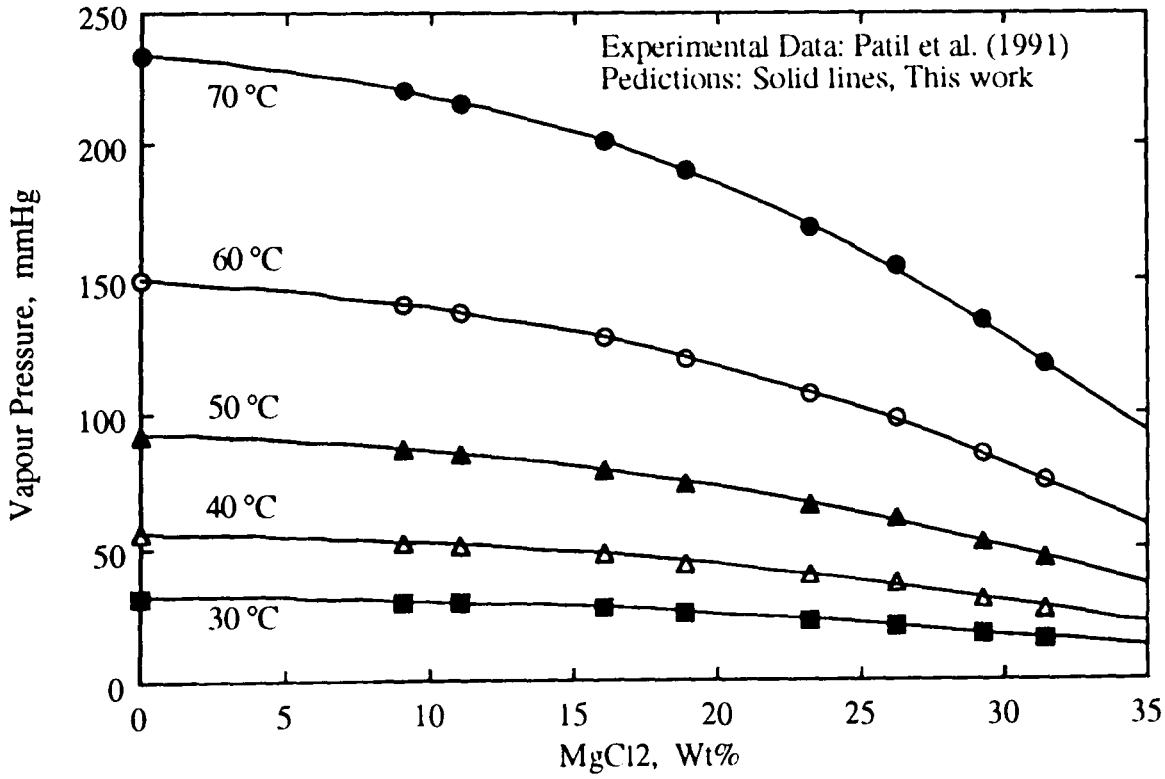

Figure-6.2 Experimental and predicted vapour pressure for MgCl2 solutions.

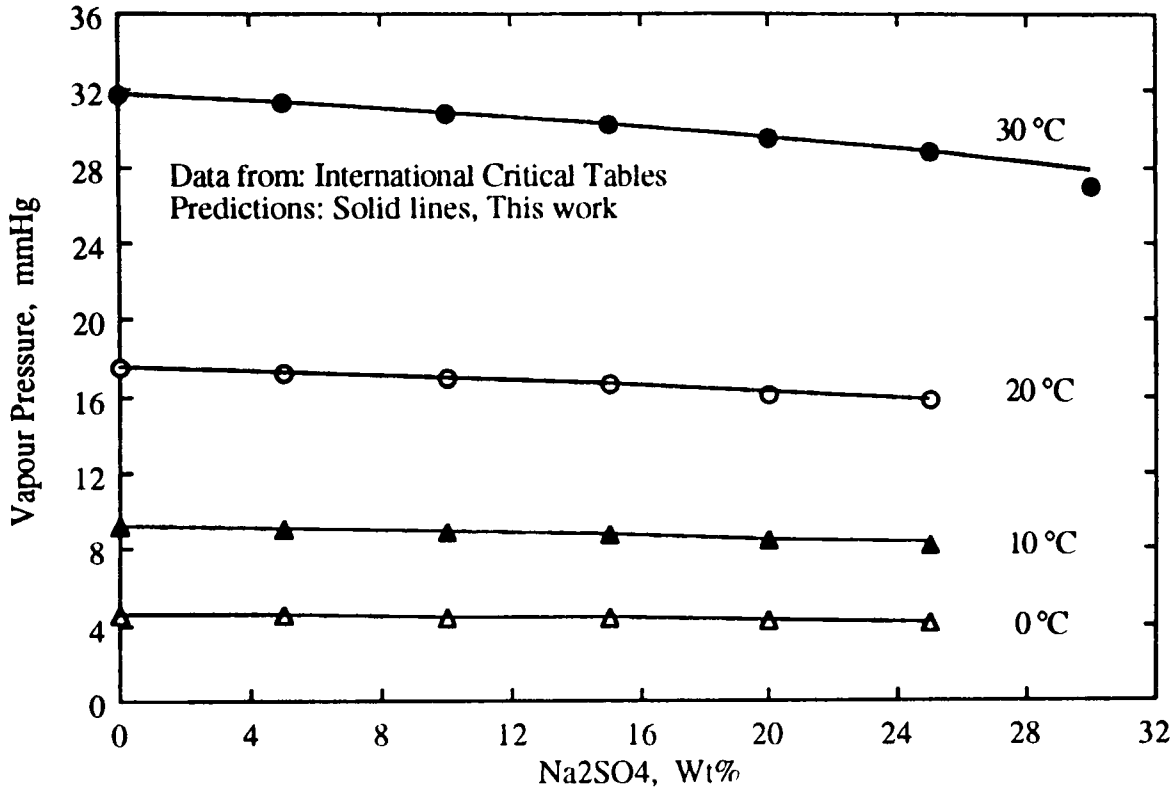

Figure-6.3 Vapour pressures of Na2SO4 aqueous solutions.

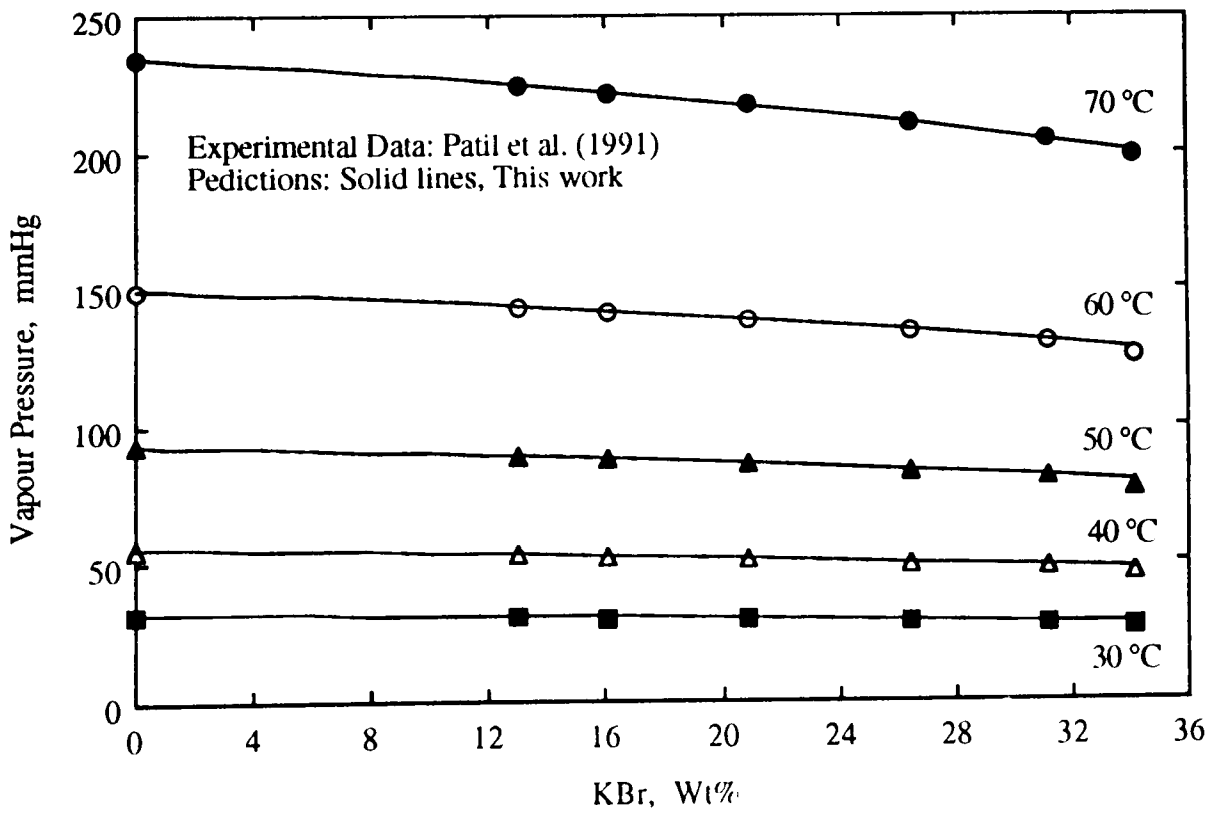

Figure-6.4 Vapour pressures of KBr aqueous solutions.

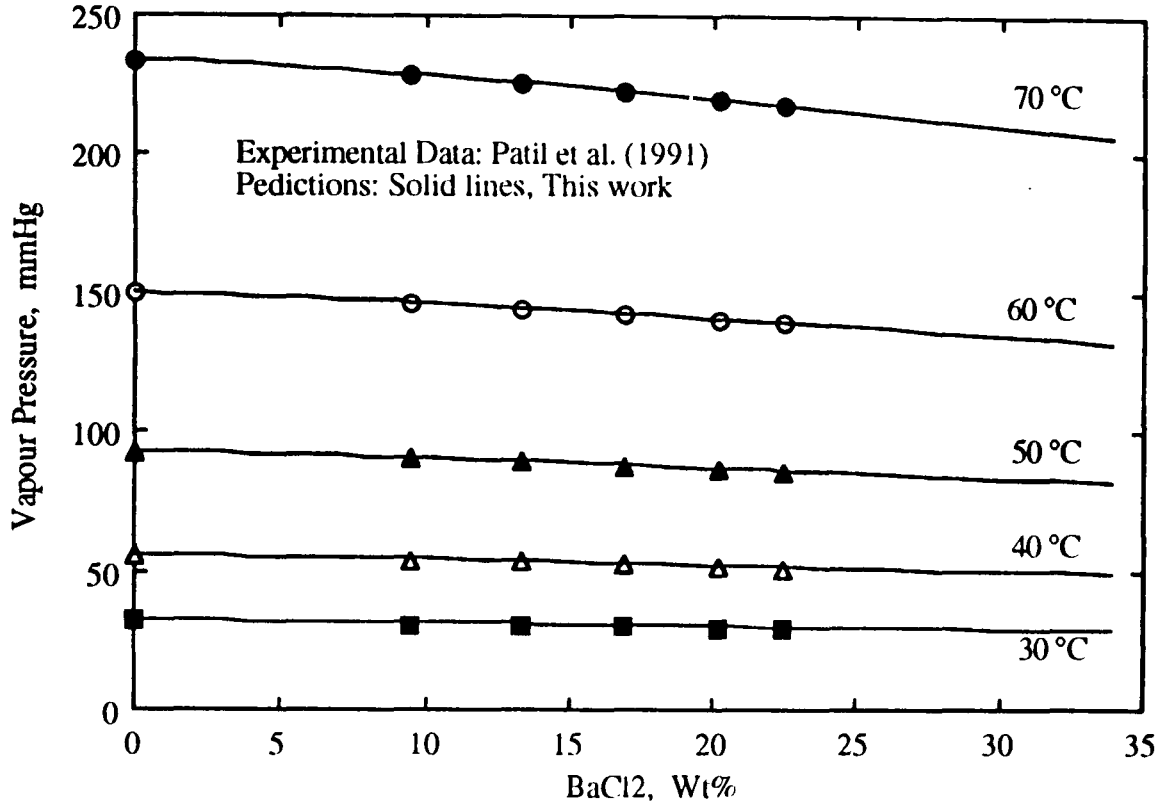

Figure-6.5 Vapour Pressures of BaCl2 aqueous solutions.

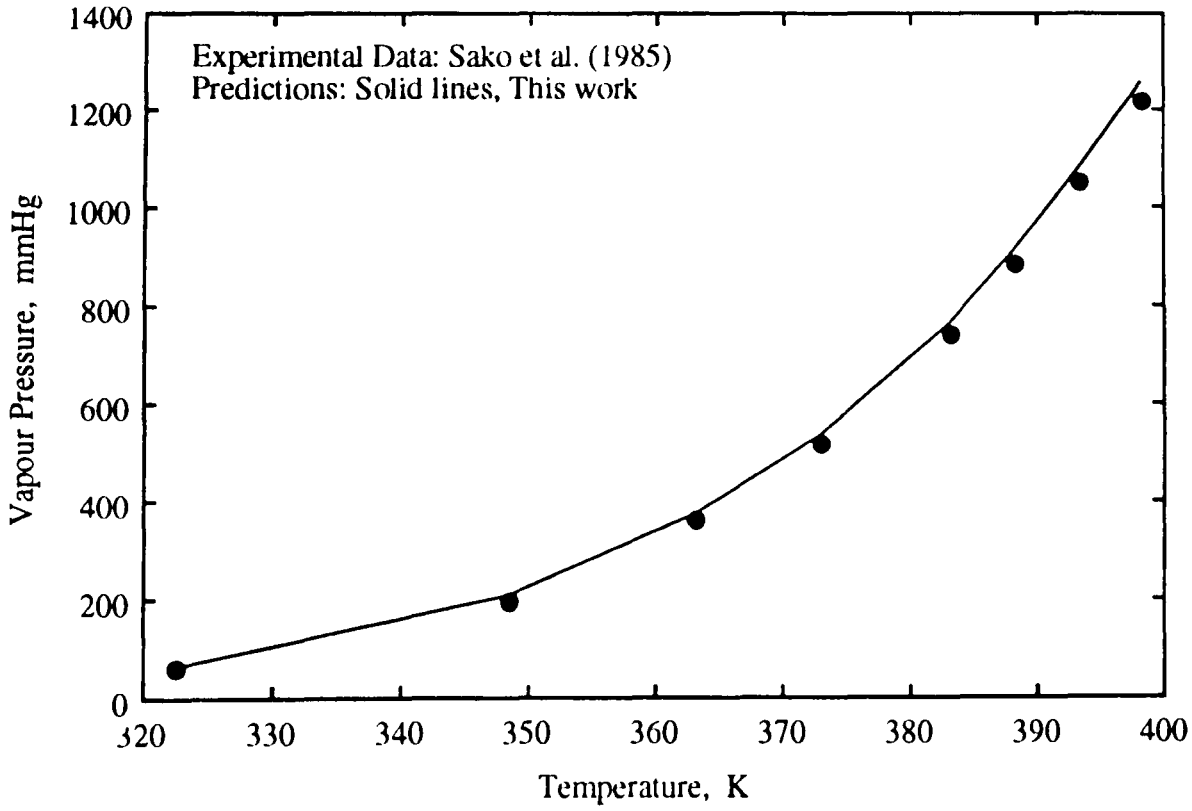

Figure-6.6 Vapour pressures of aqueous solutions containing 1.057 mol/kg MgCl2 and 2.905 mol/Kg CaCl2.

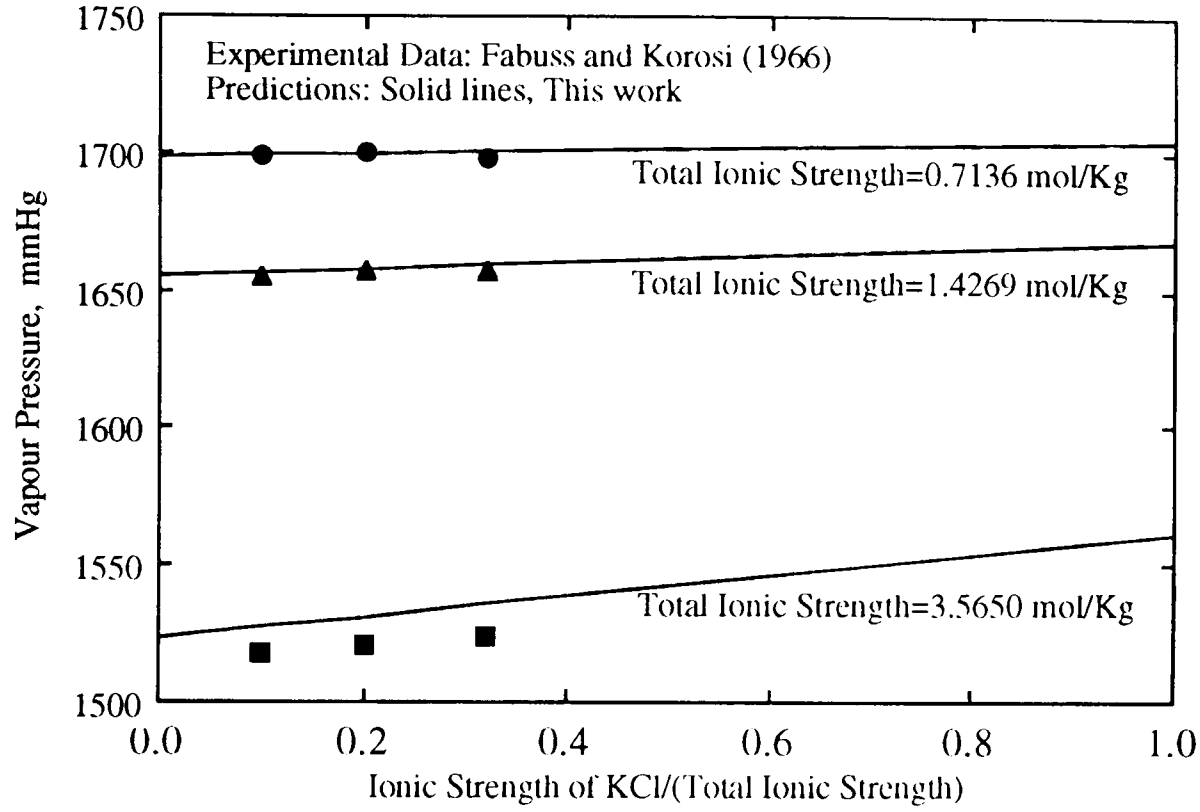

Figure-6.7 Experimental and predicted vapour pressure of NaCl-KCl aqueous solutions at 398.15 K (125 °C).

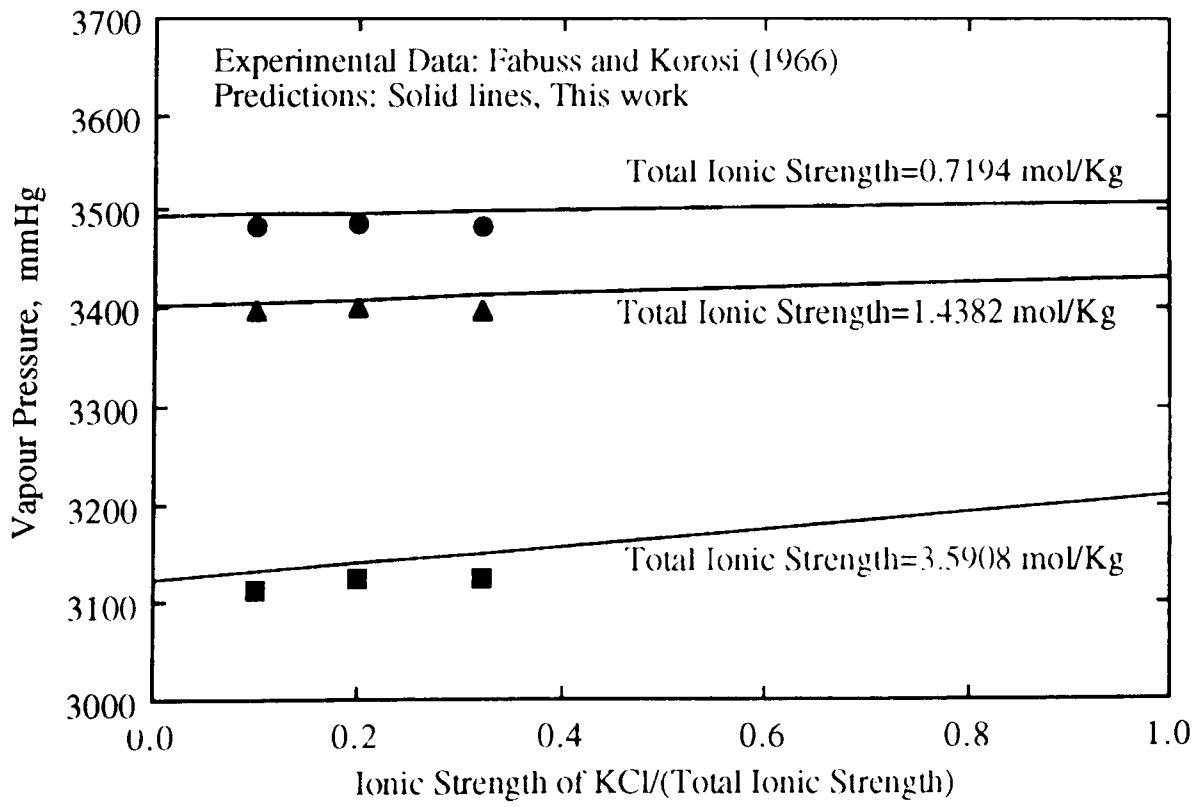

Figure-6.8 Experimental and predicted vapour pressure of NaCl-KCl aqueous solutions at 423.15 K (150 °C).

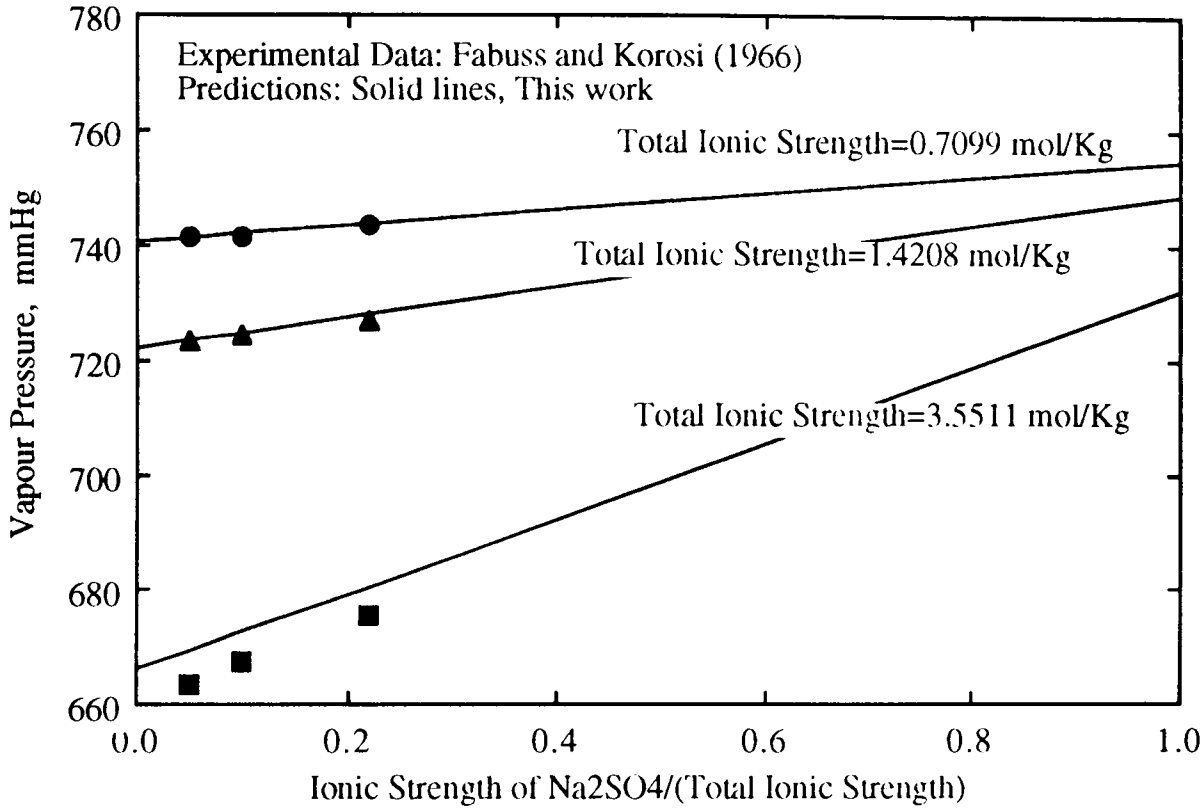

Figure-6.9 Experimental and predicted vapour pressure of NaCl-Na2SO4 aqueous solutions at 373.15 K (100 °C).

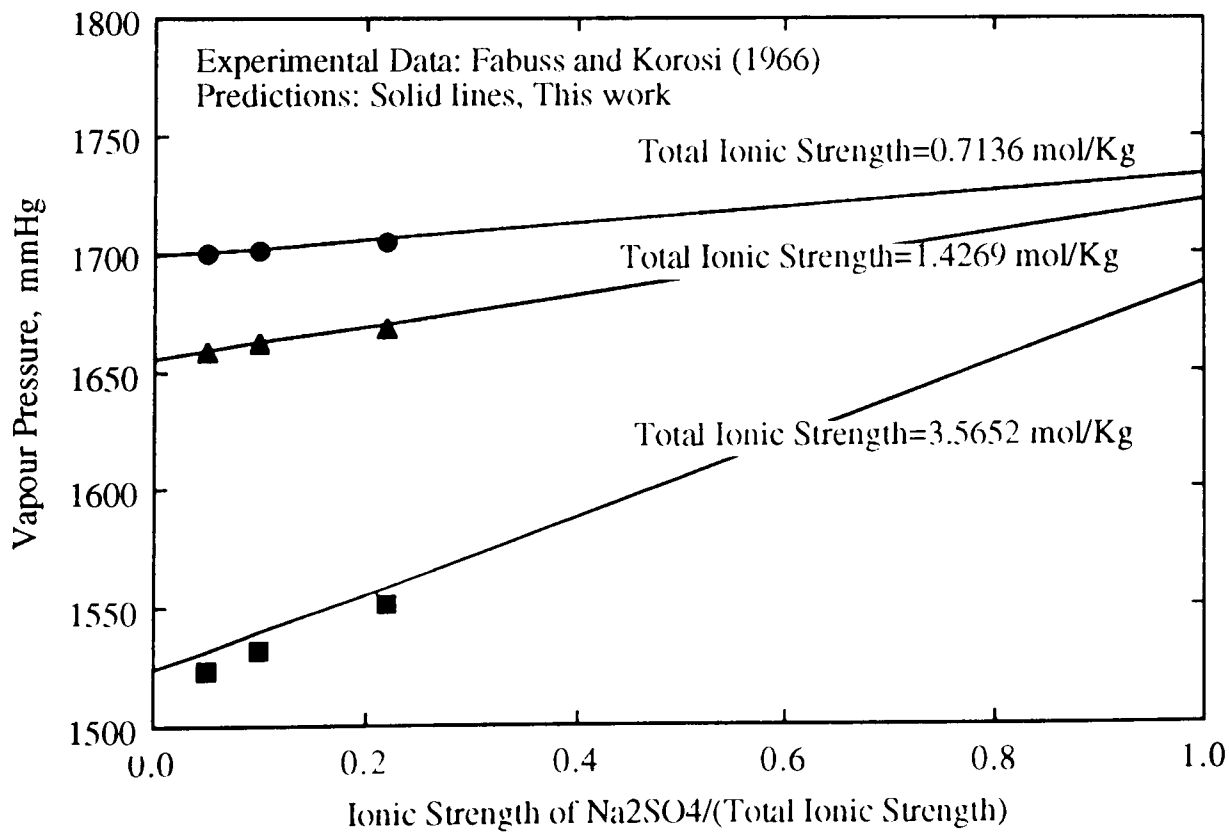

Figure-6.10 Experimental and predicted vapour pressure of NaCl-Na2SO4 aqueous solutions at 398.15 K (125 °C).

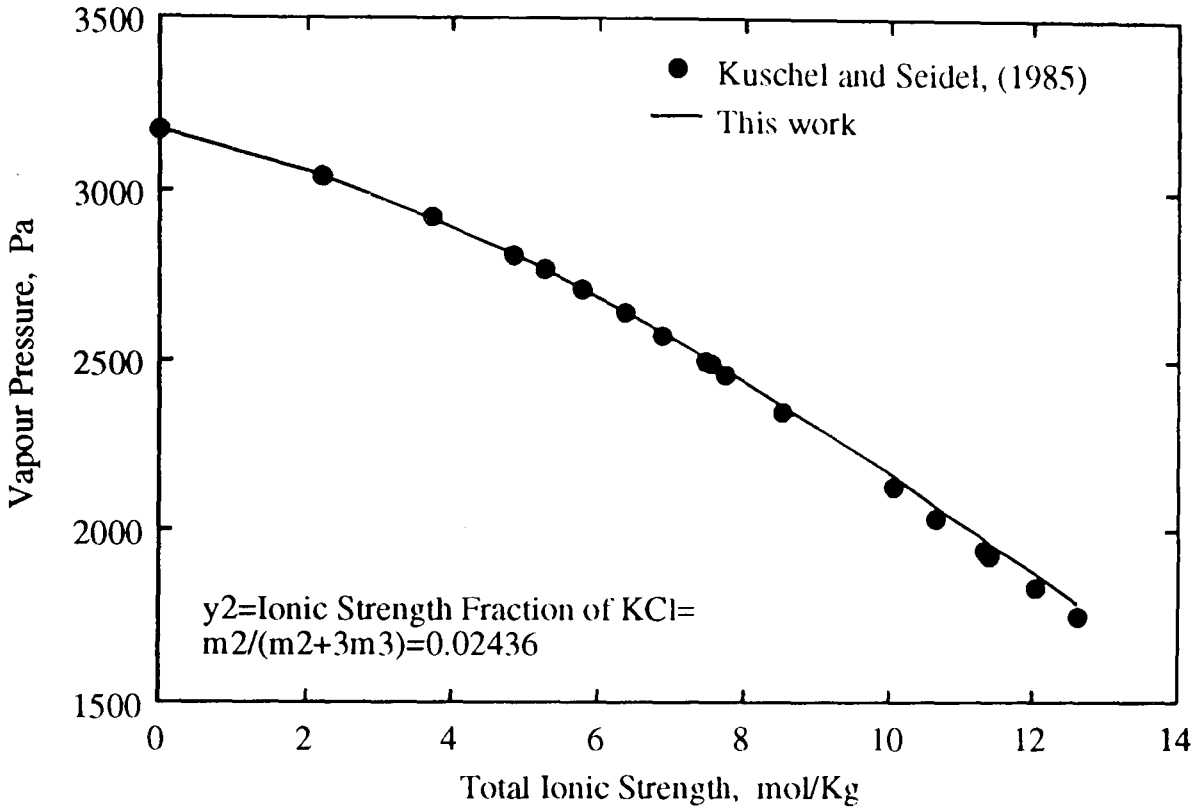

Figure-6.11 Experimental and predicted vapour pressure of KCl-MgCl2 mixed electrolyte solutions at 298.15 K (25 °C).

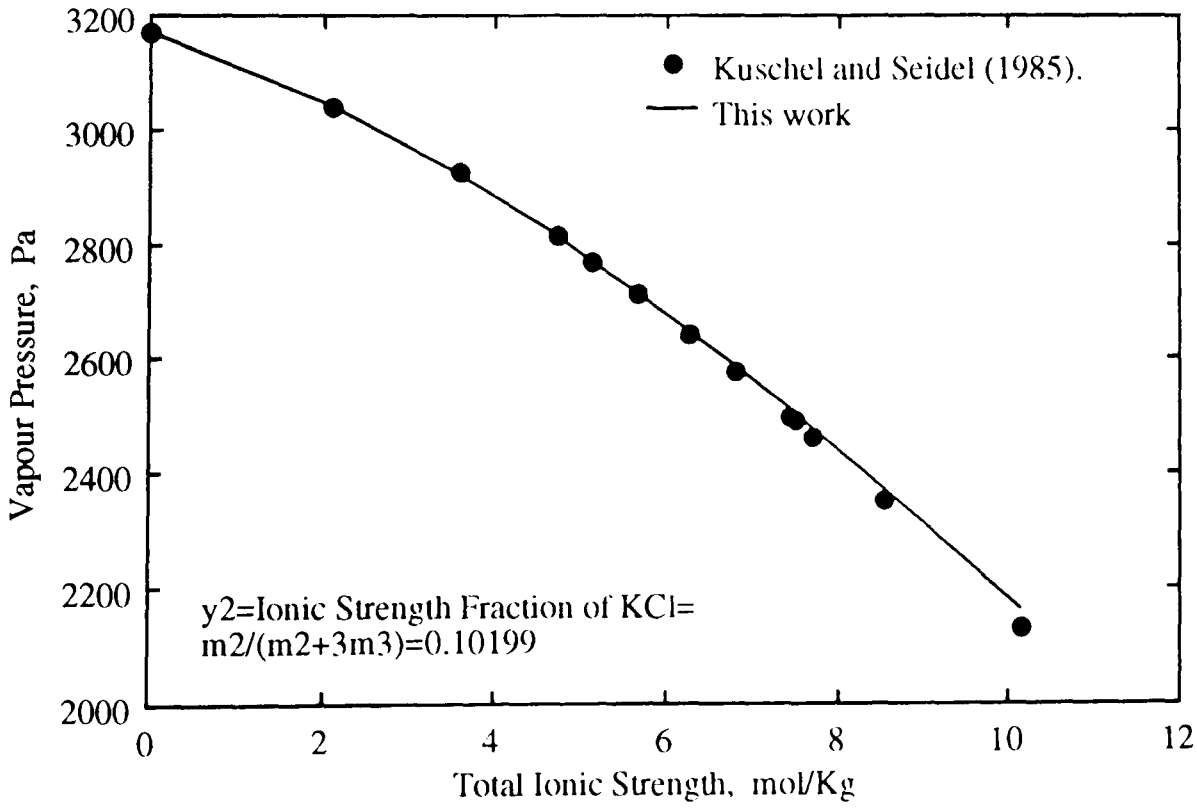

Figure-6.12 Experimental and predicted vapour pressure of KCl-MgCl2 mixed electrolyte solutions at 298.15 K (25 °C).

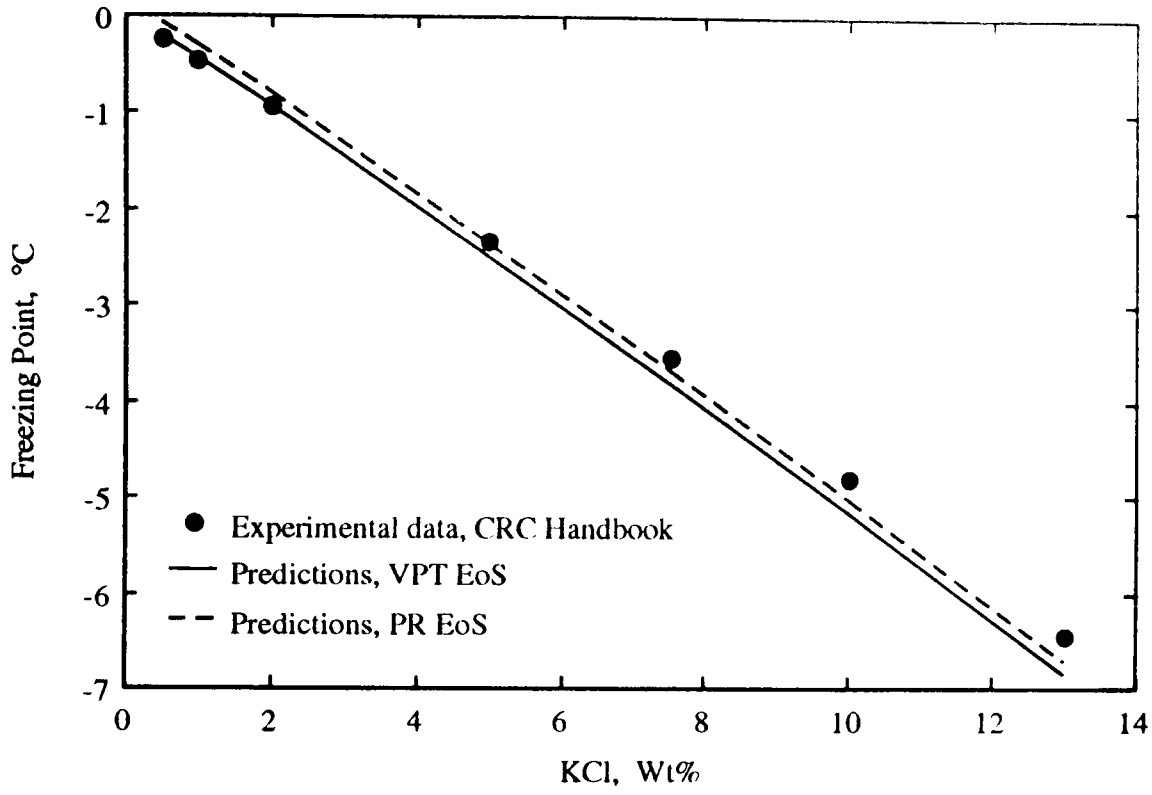

Figure-6.13 Experimental and predicted freezing points of KCl aqueous solutions.

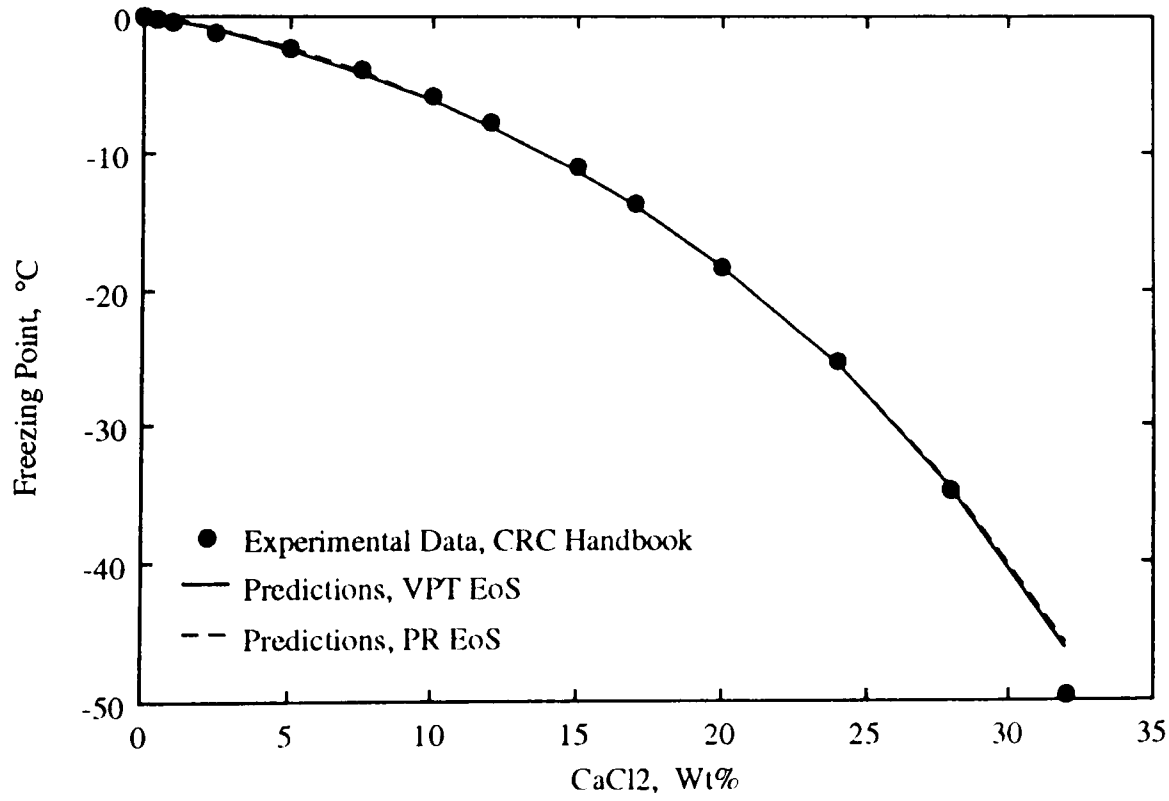

Figure-6.14 Experimental and predicted freezing points of CaCl2 aqueous solutions.

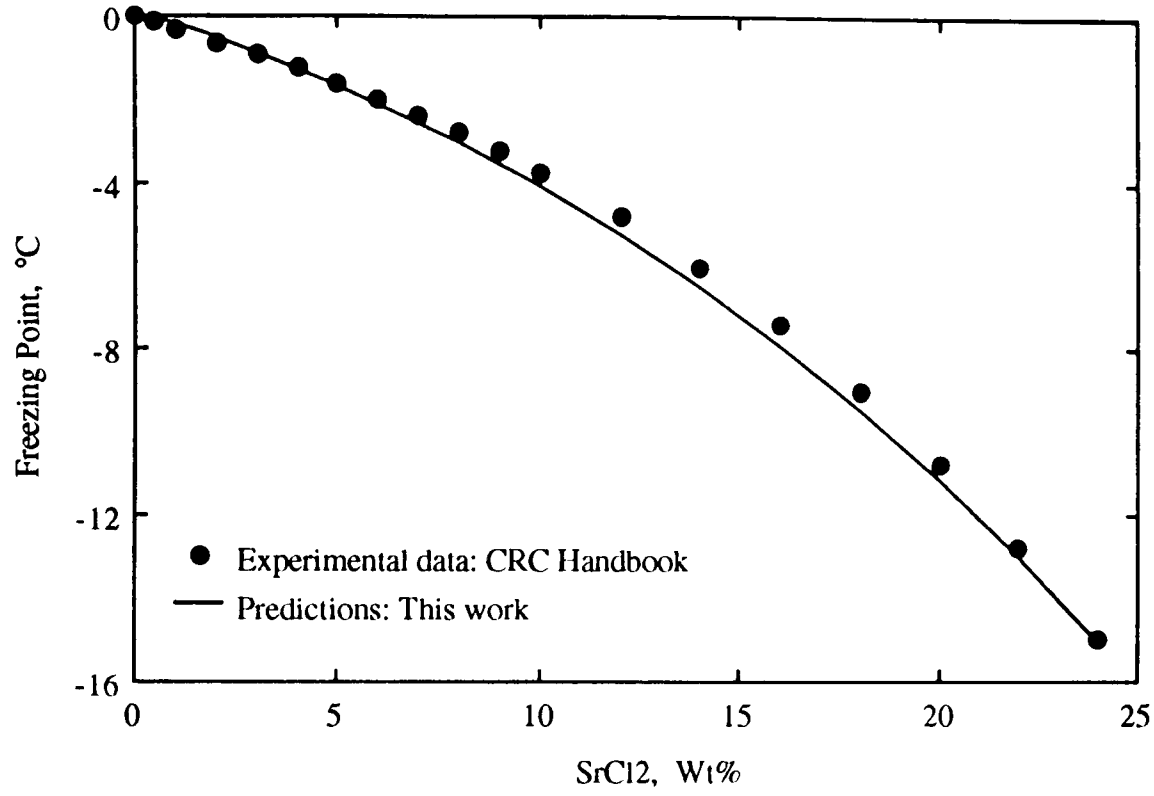

Figure-6.15 Freezing points of SrCl2 aqueous solutions.

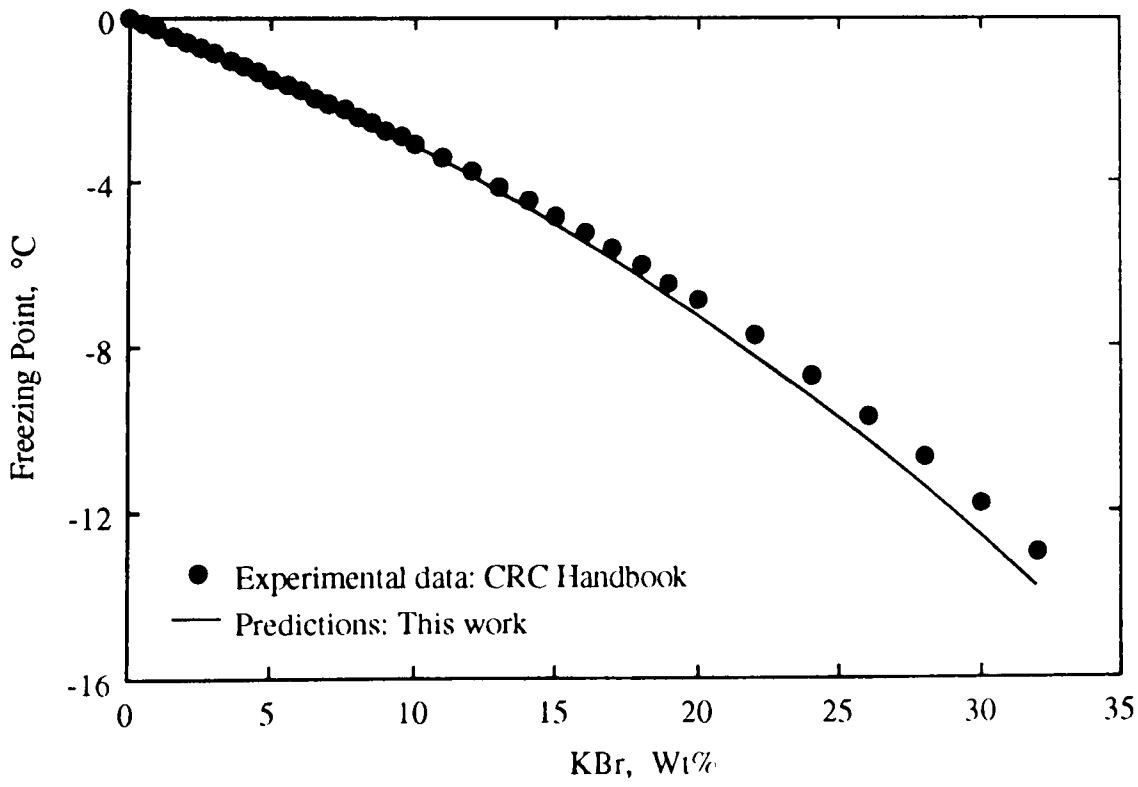

Figure-6.16 Freezing points of KBr aqueous solutions.

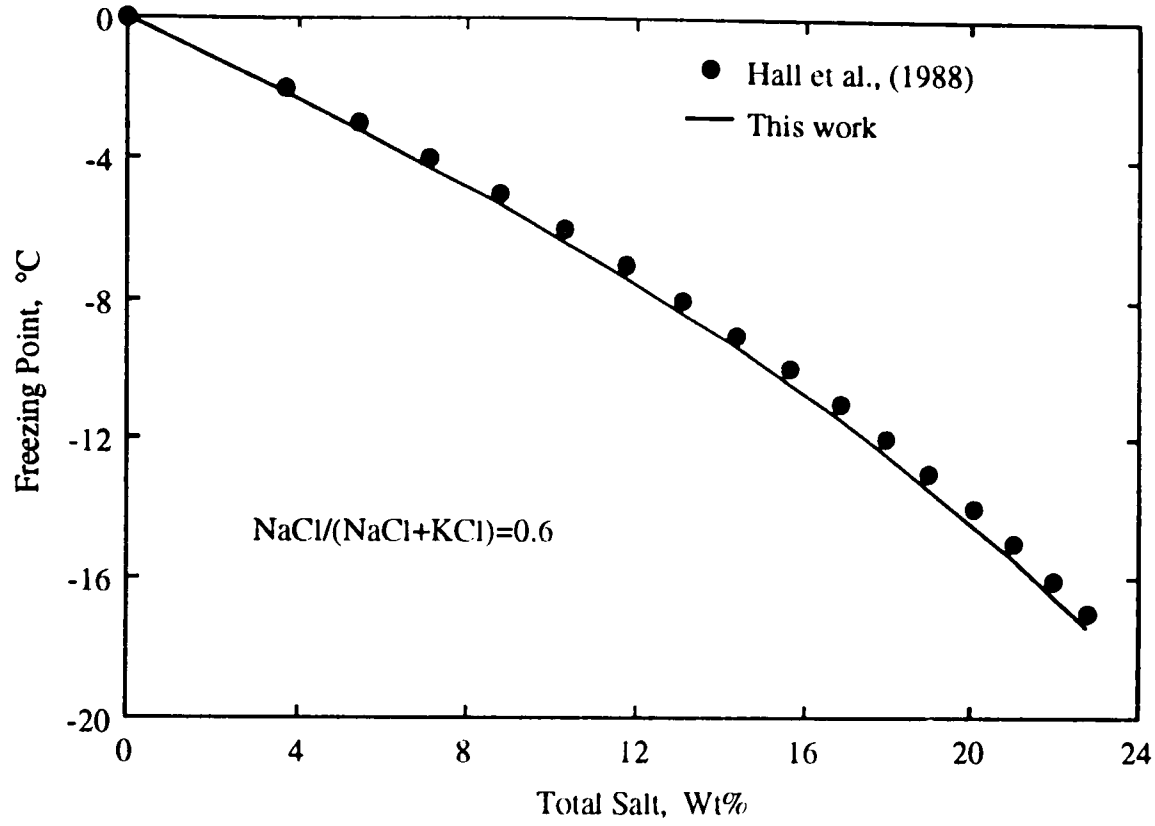

Figure-6.17 Freezing points of NaCl-KCl aqueous solutions.

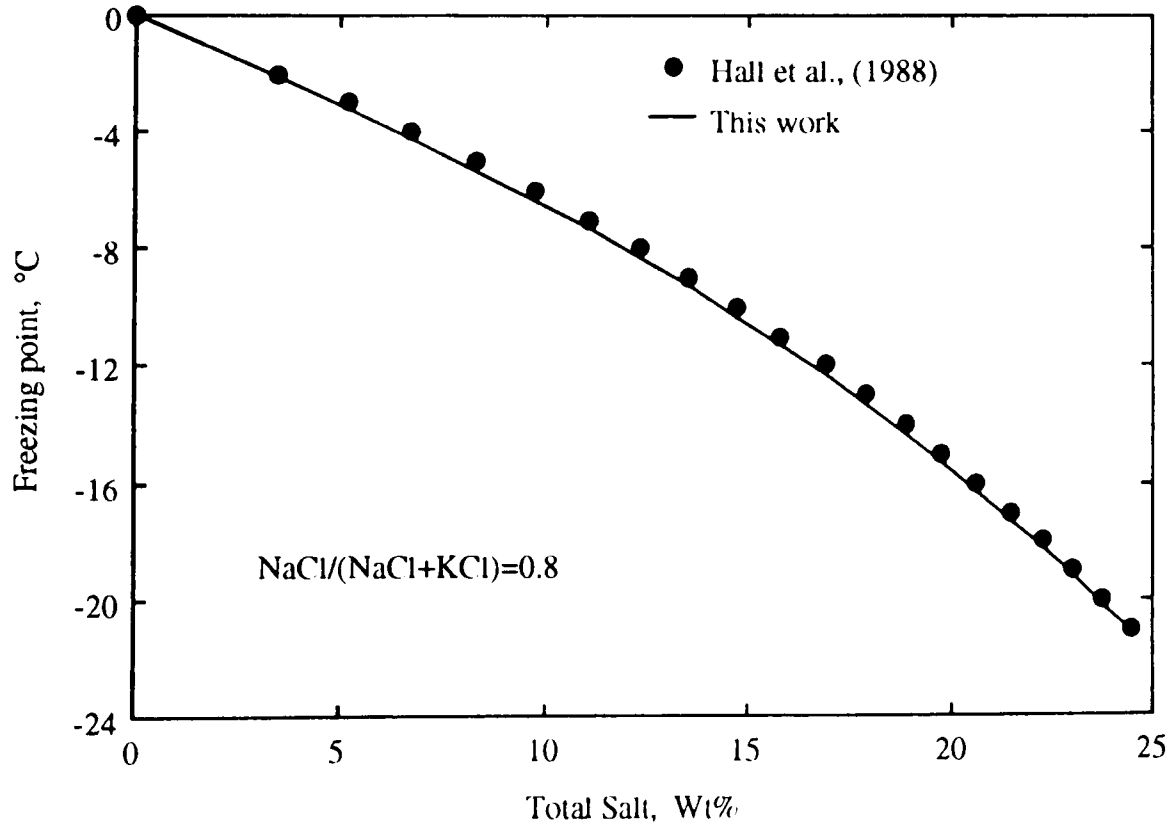

Figure-6.18 Freezing points of NaCl-KCl aqueous solutions.

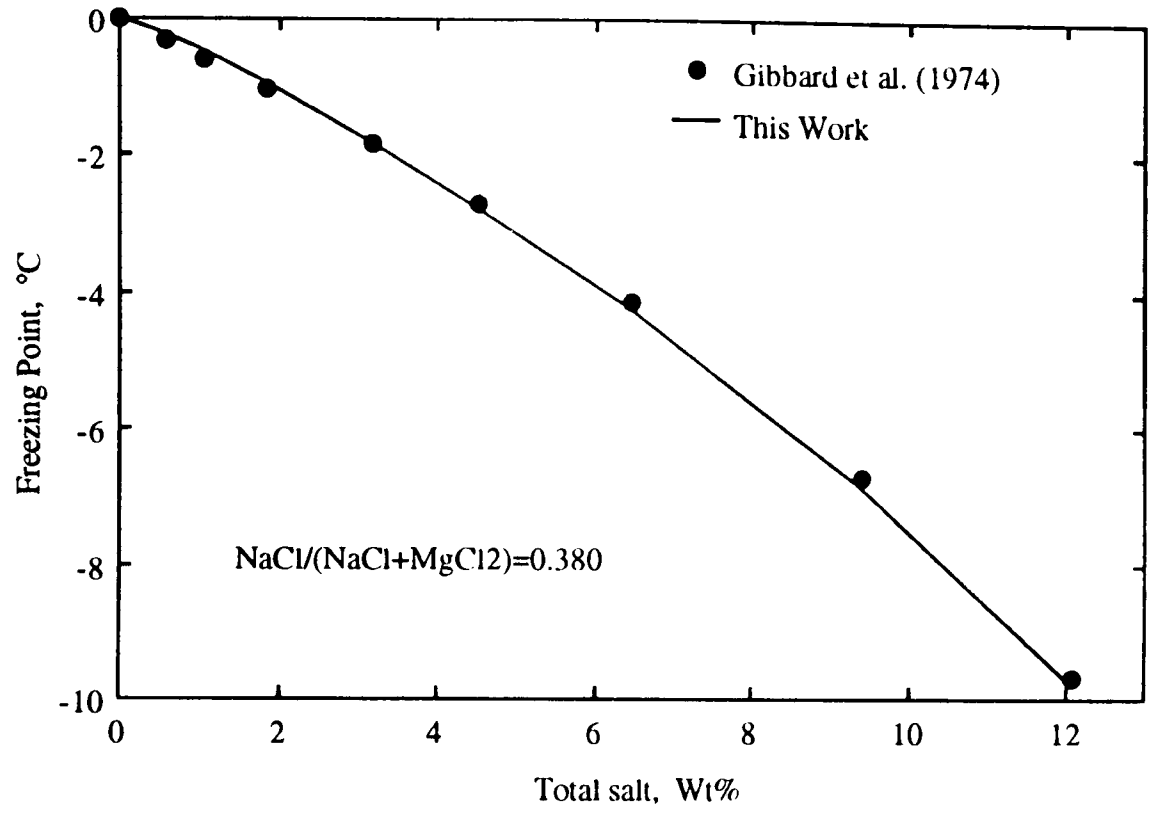

Figure-6.19 Freezing points of NaCl-MgCl2 aqueous solutions.

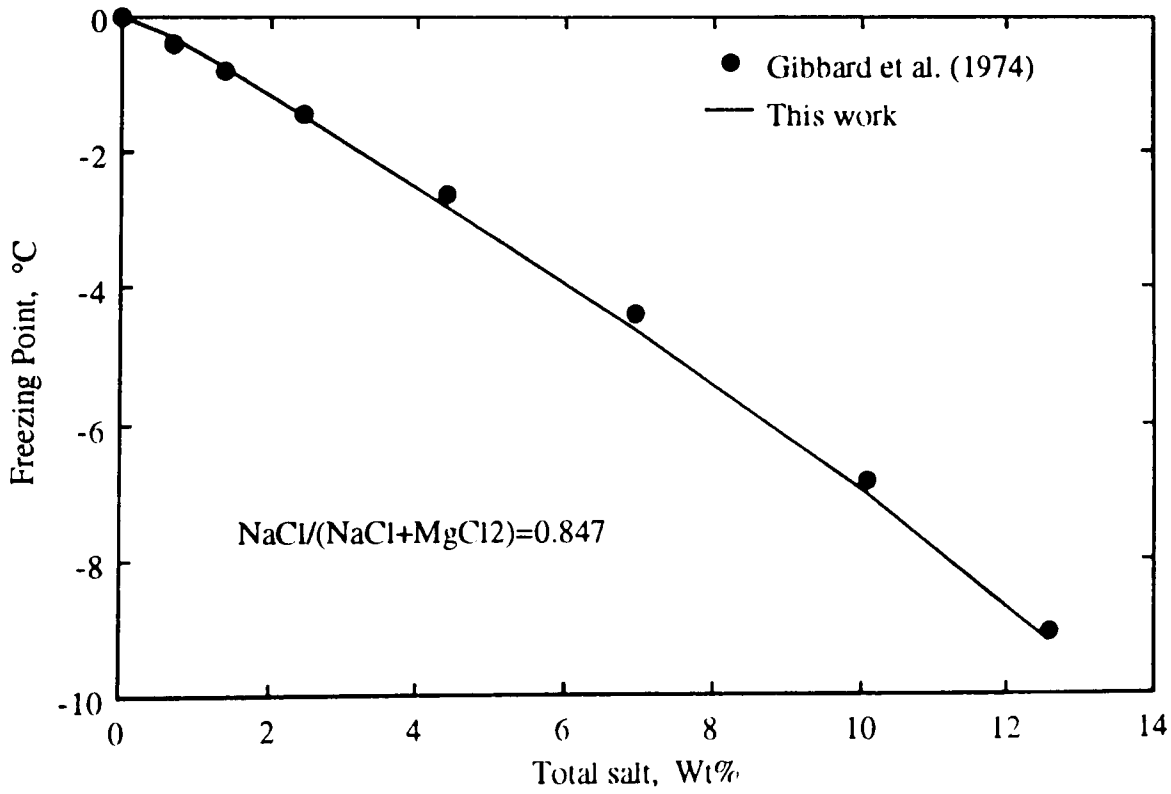

Figure-6.20 Freezing points of NaCl-MgCl2 aqueous solutions.

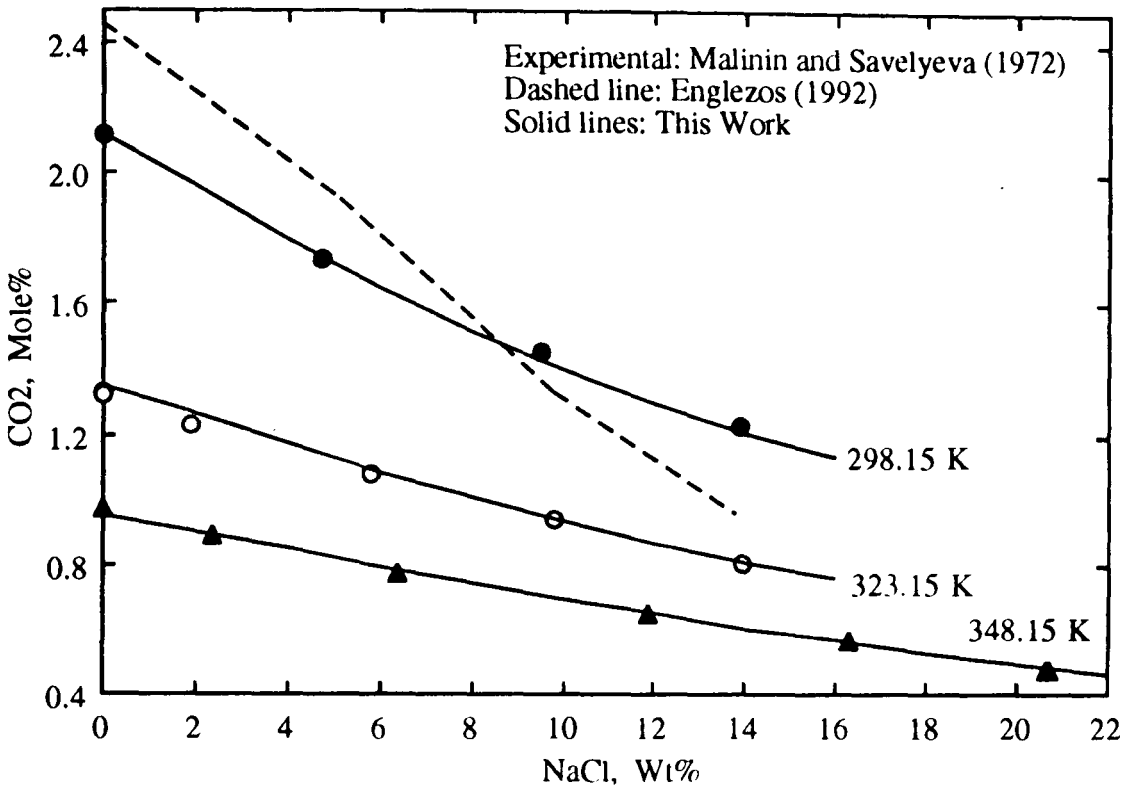

Figure-6.21 Experimental and predicted solubility of CO2 in aqueous solution of NaCl at 4.795 MPa.

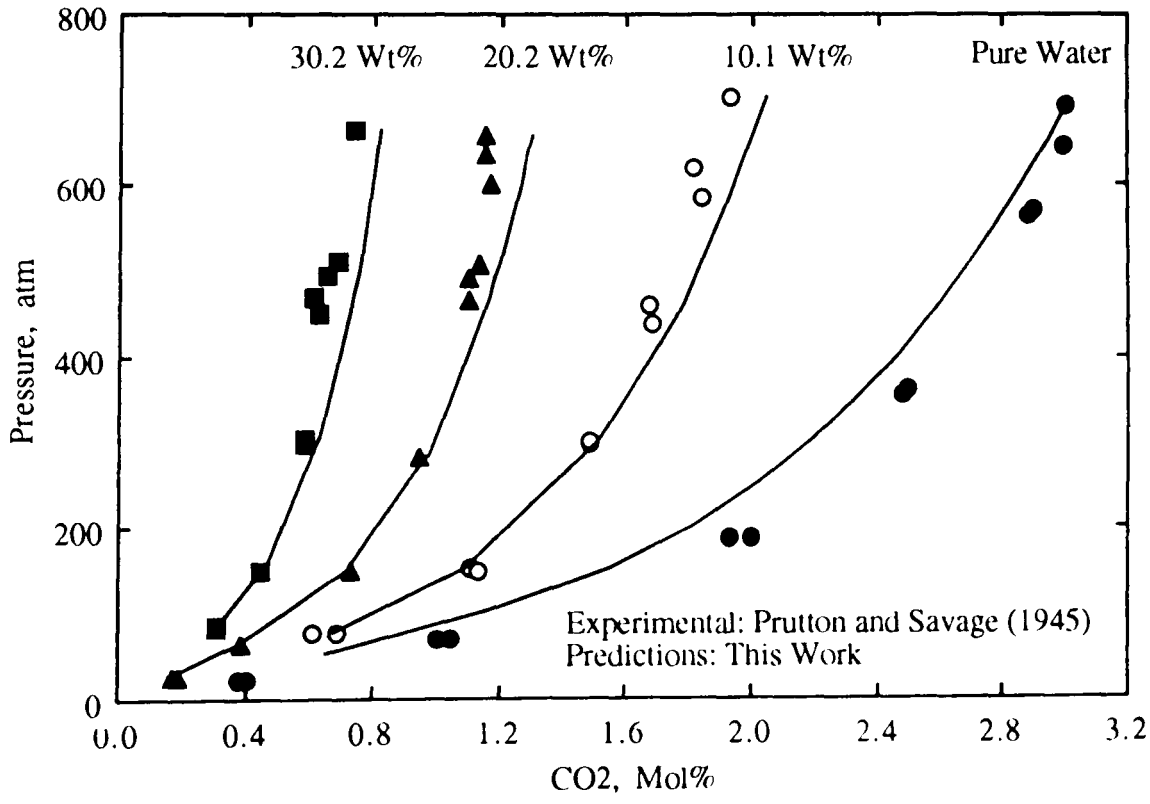

Figure-6.22 Experimental and predicted CO2 solubility in CaCl2 solutions at 394.15 K.

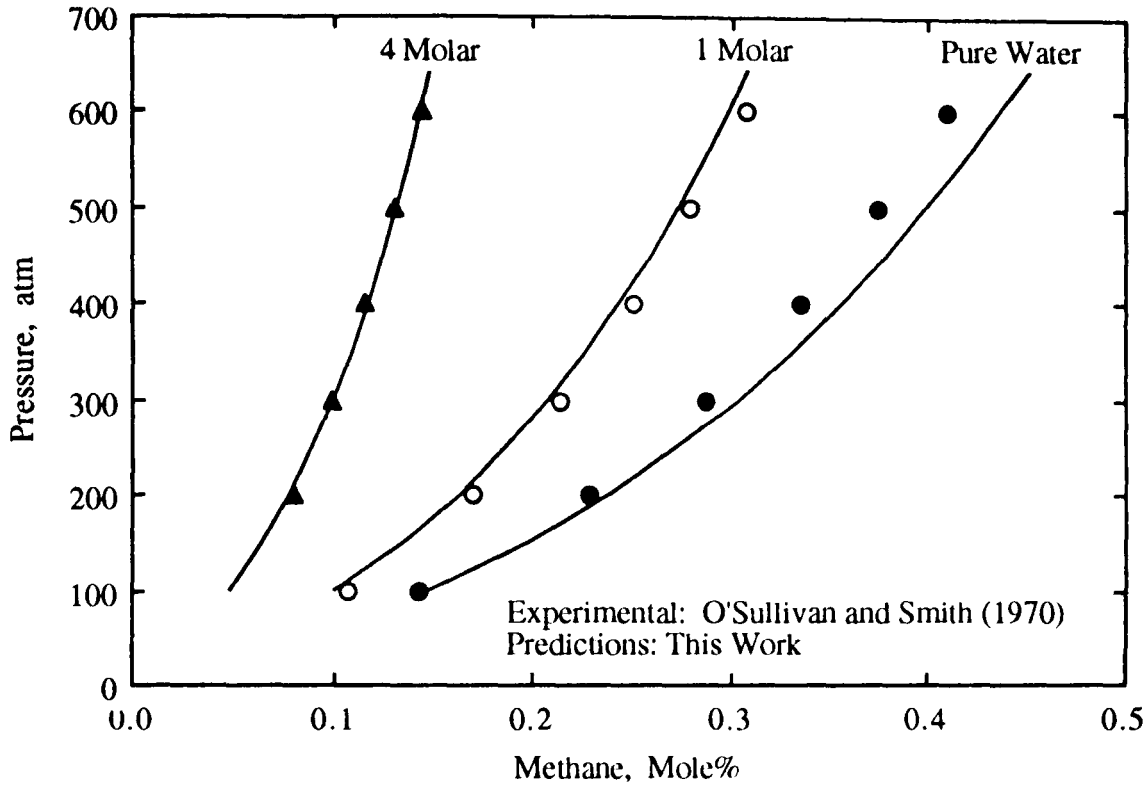

Figure-6.23 Experimental and predicted solubility of methane in NaCl solutions at 324.65 K.

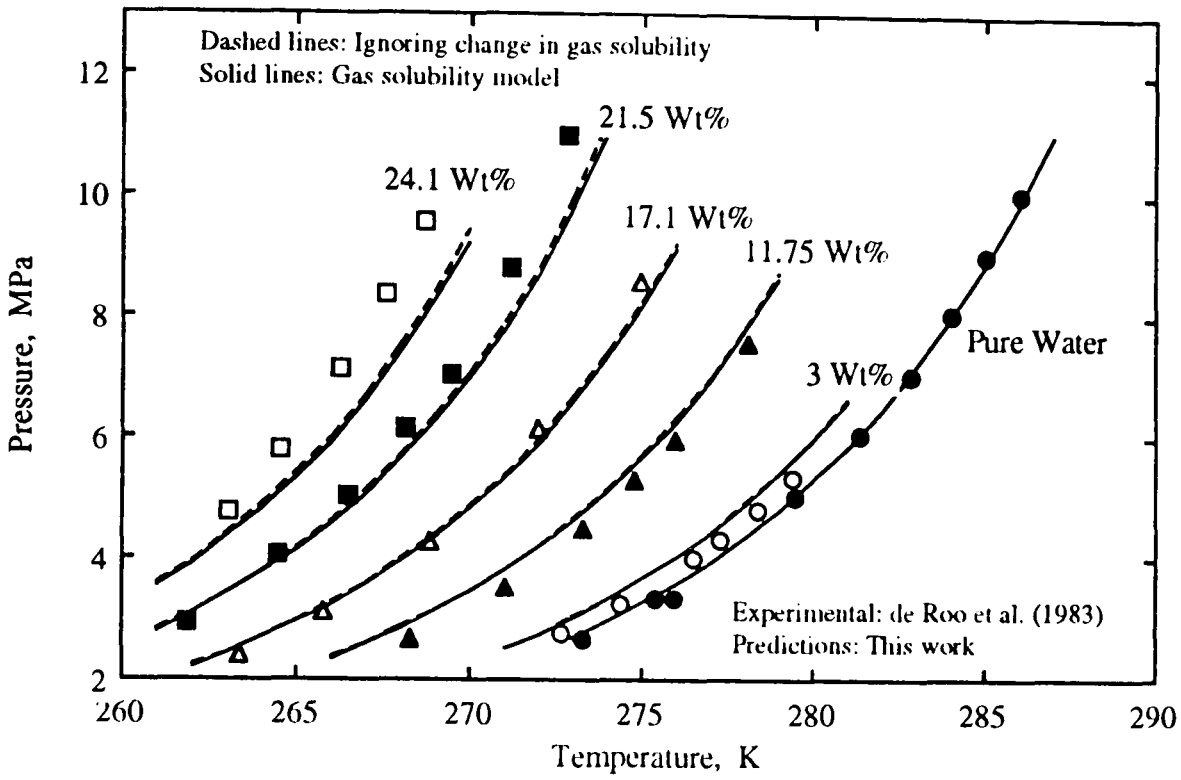

Figure-6.24 Experimental and predicted dissociation conditions of methane hydrates in the presence of NaCl aqueous solutions.

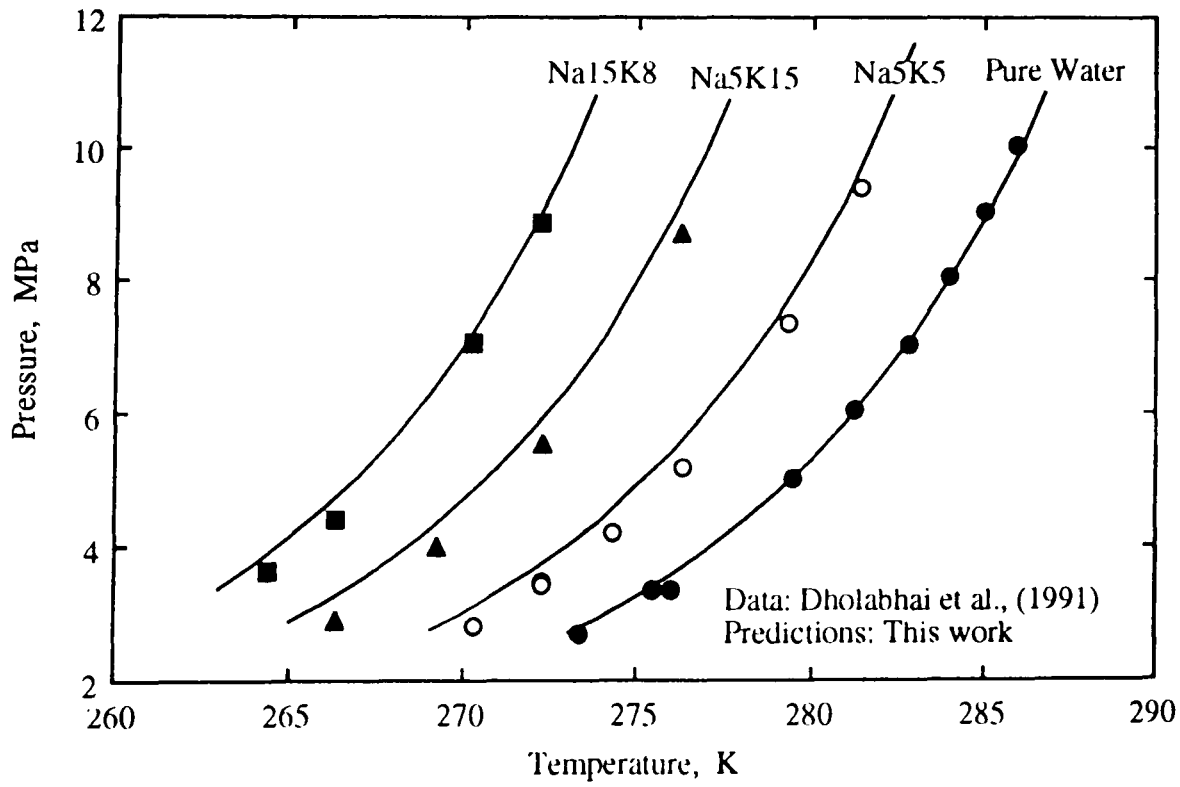

Figure-6.25 Experimental and predicted dissociation conditions of methane hydrates in aqueous solutions of (NaCl+KCl).

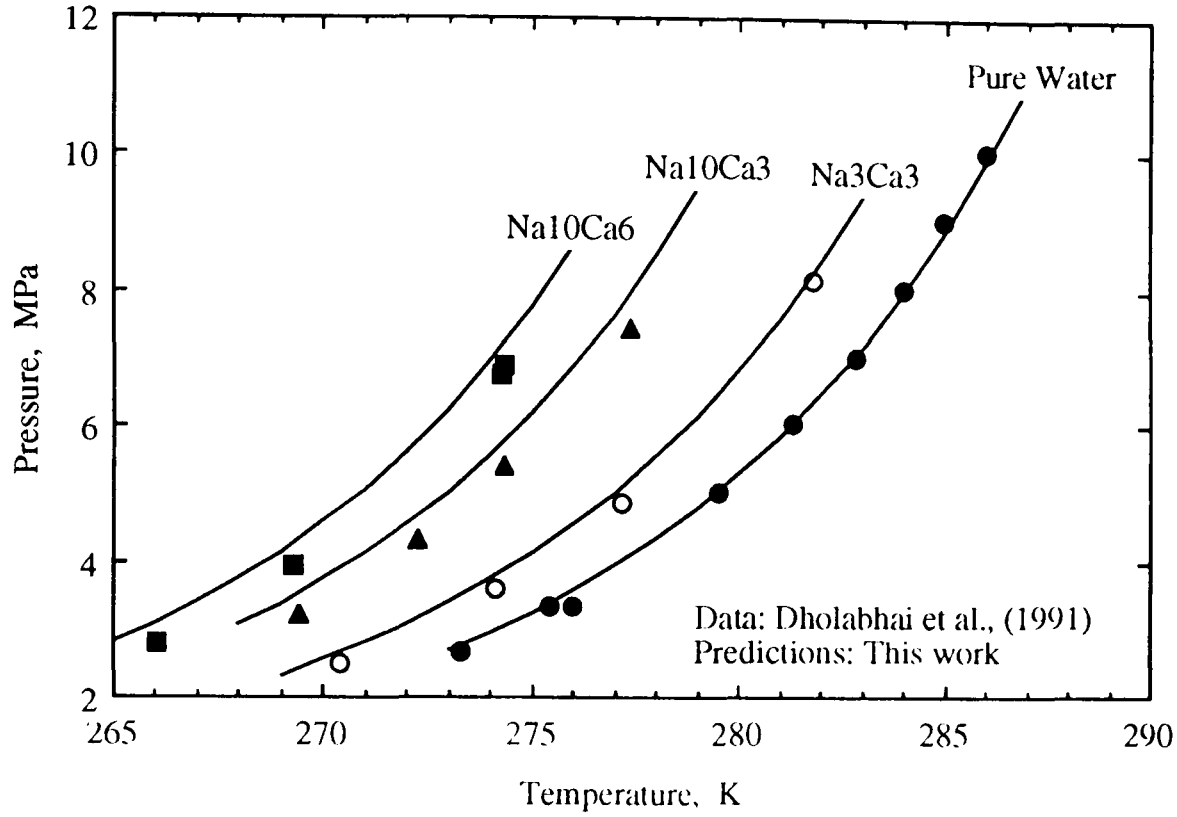

Figure-6.26 Experimental and predicted dissociation conditions of methane hydrates in aqueous solutions of (NaCl+CaCl2).

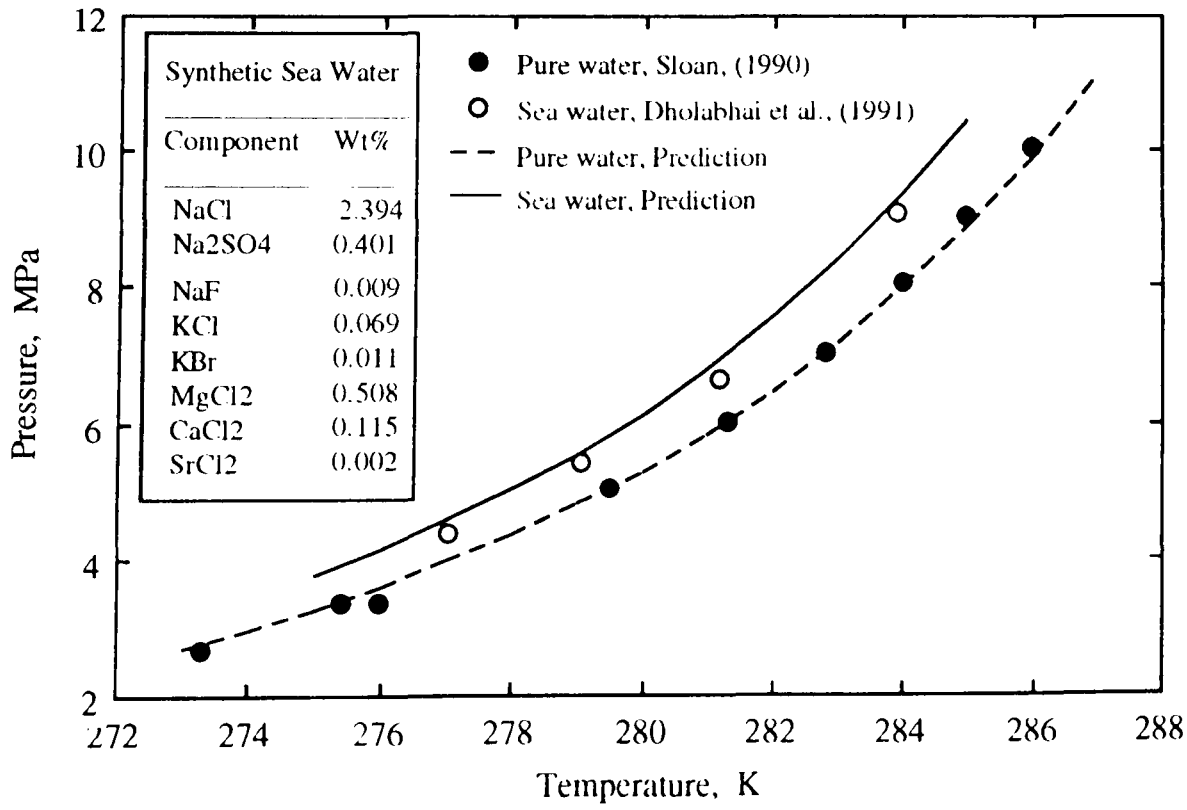

Figure-6.27 Experimental and calculated methane hydrate dissociation conditions in a synthetic sea water.

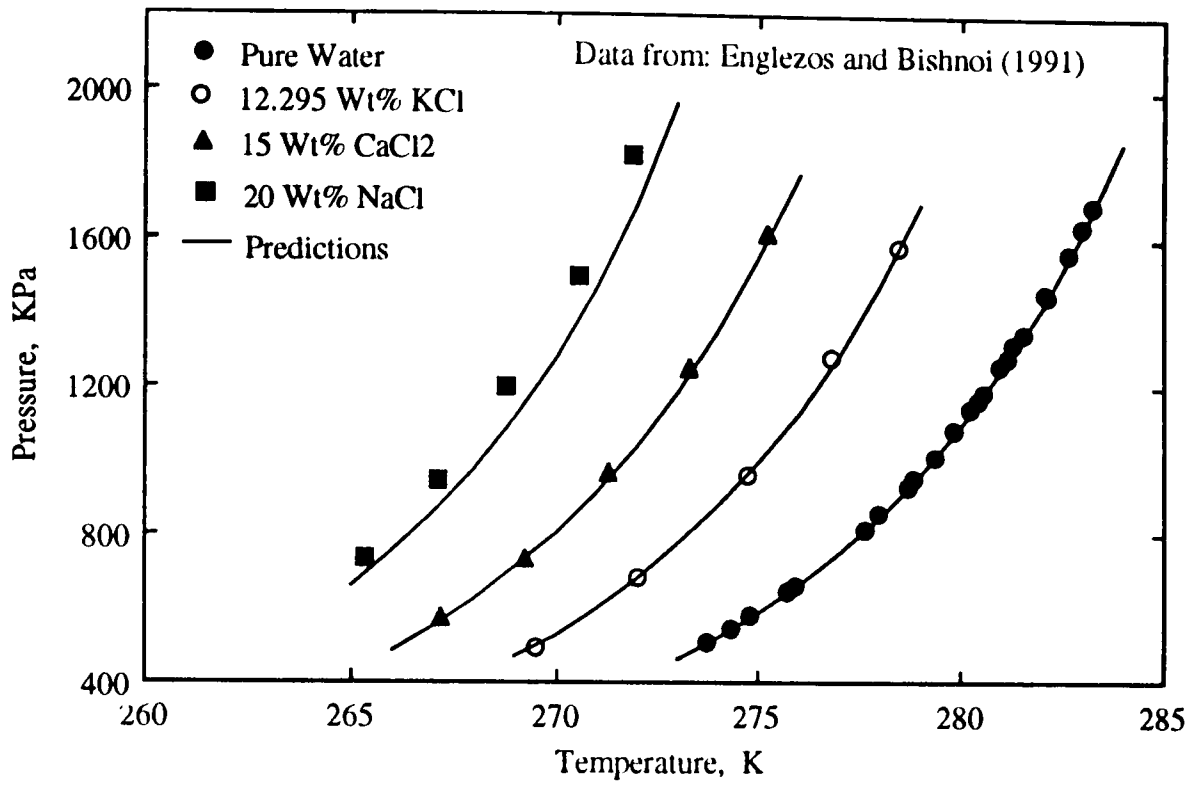

Figure-6.28 Experimental and predicted dissociation conditions for ethane hydrates in aqueous single electrolyte solutions.

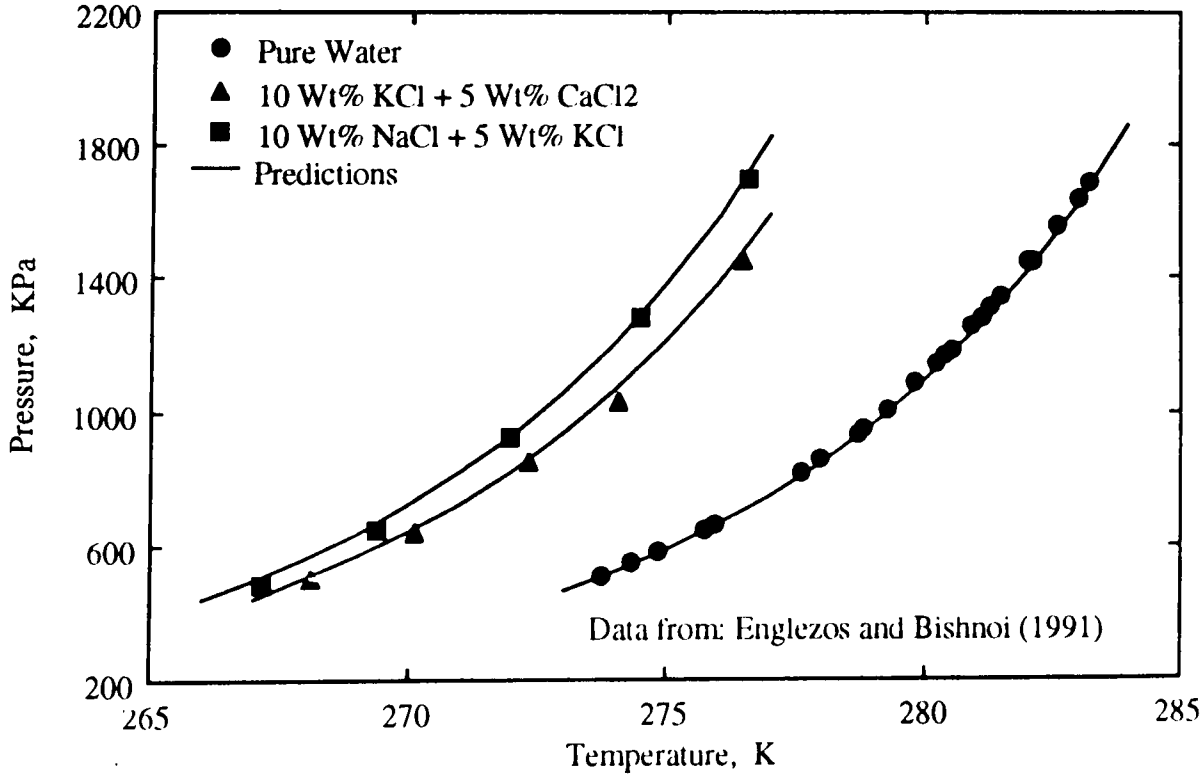

Figure-6.29 Experimental and predicted dissociation conditions for ethane hydrates in aqueous mixed electrolyte solutions.

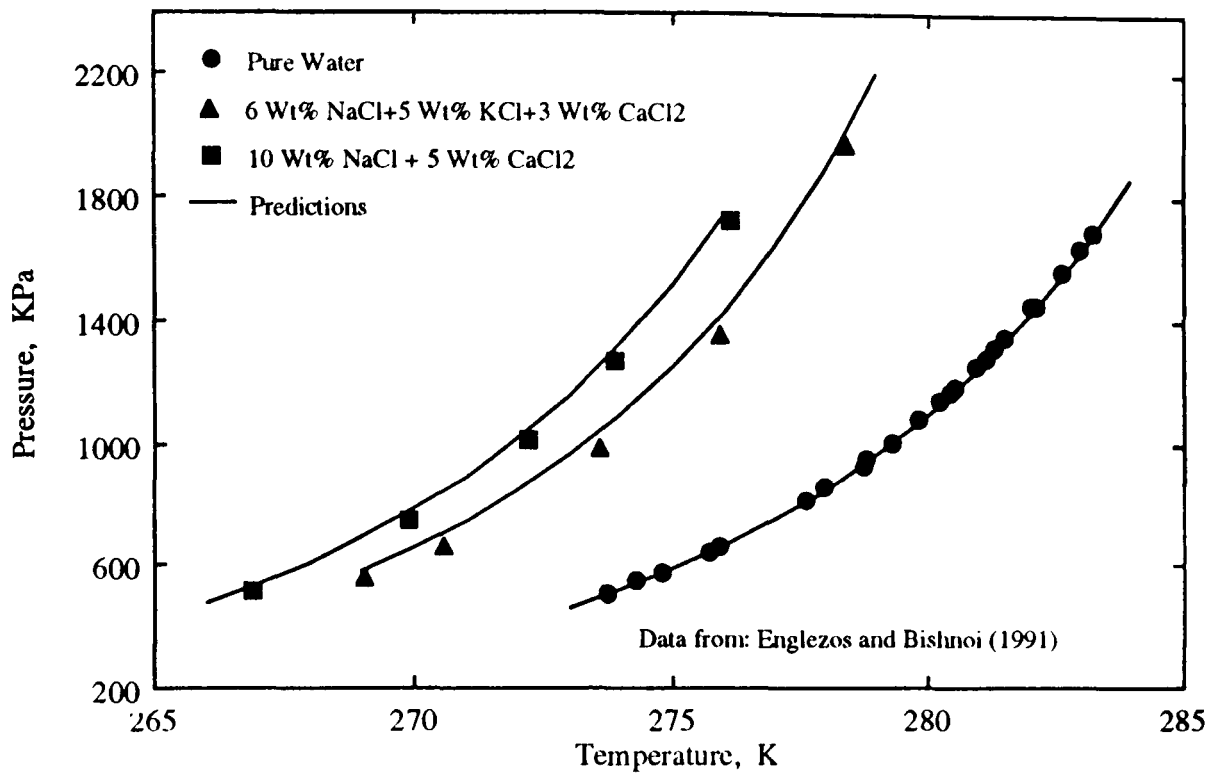

Figure-6.30 Experimental and predicted dissociation conditions for ethane hydrates in aqueous mixed electrolyte solutions.

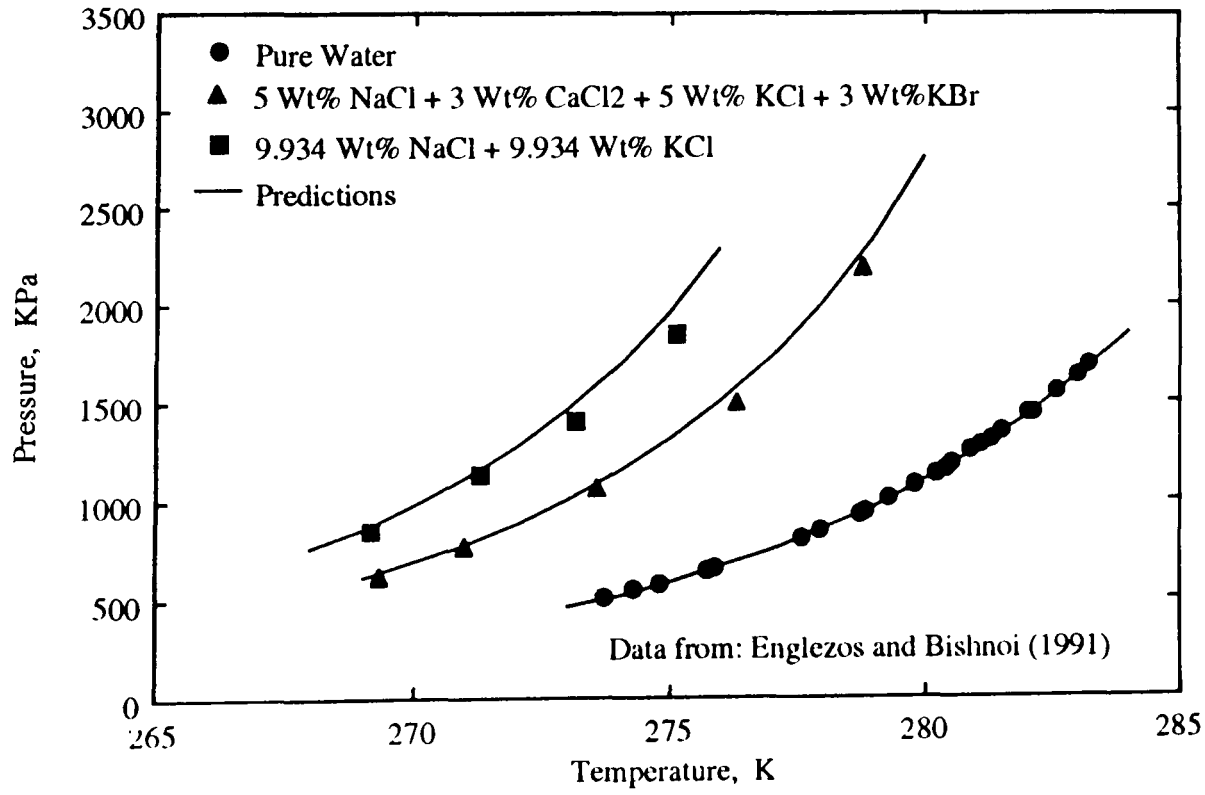

Figure-6.31 Experimental and predicted dissociation conditions for ethane hydrates in aqueous mixed electrolyte solutions.

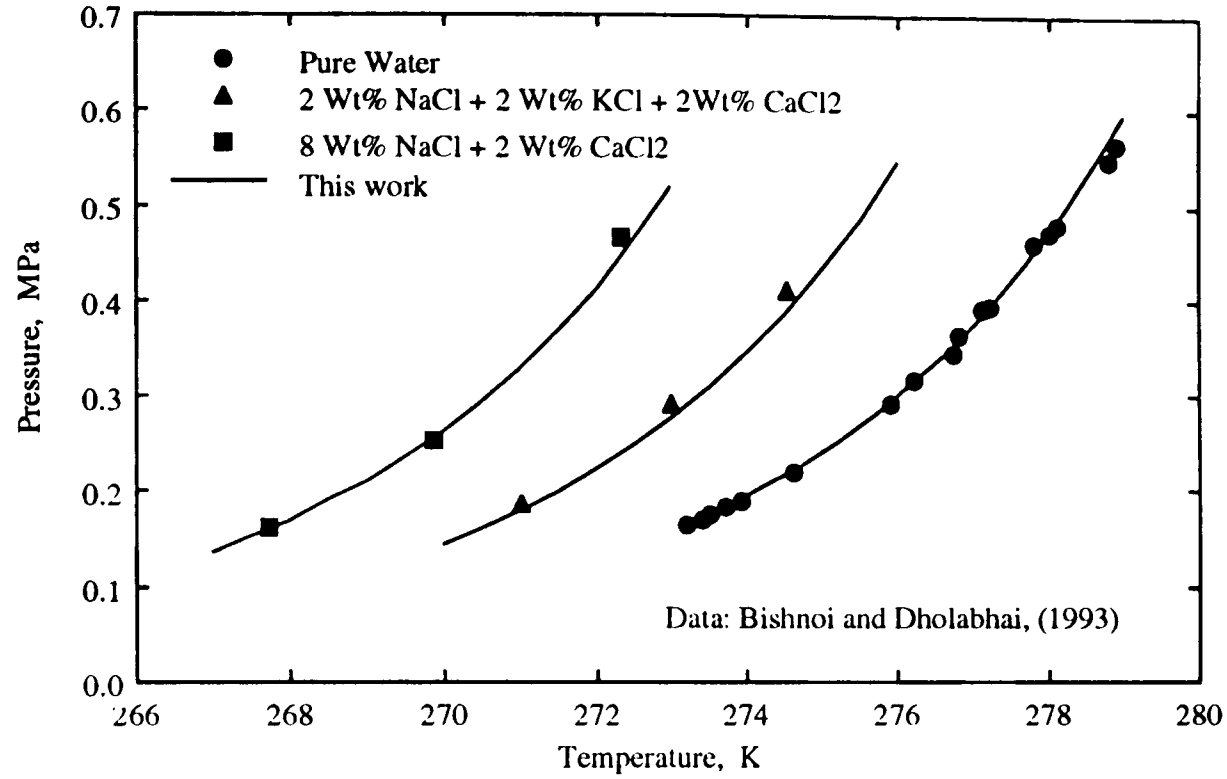

Figure-6.32 Dissociation conditions for propane hydrates in the presence of mixed electrolyte solutions.

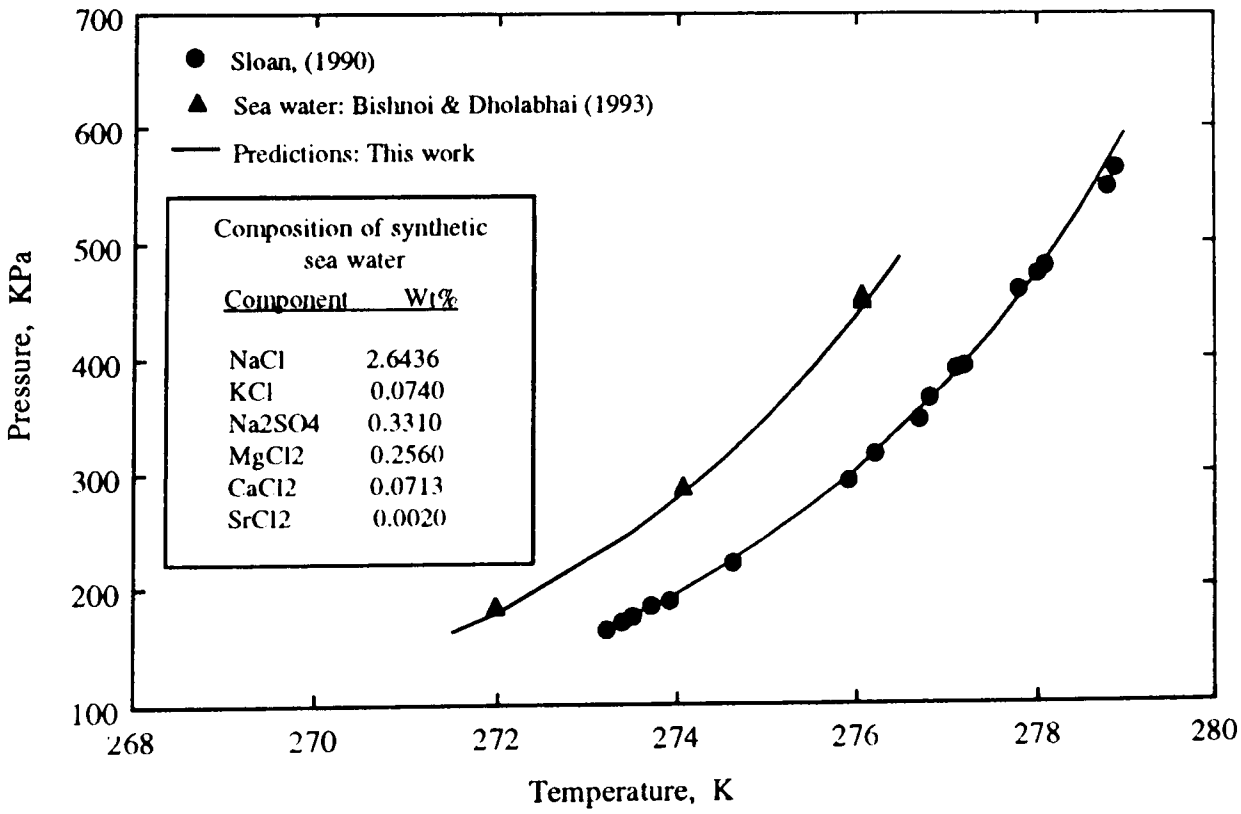

Figure-6.33 Experimental and calculated propane hydrate dissociation conditions in a synthetic sea water.

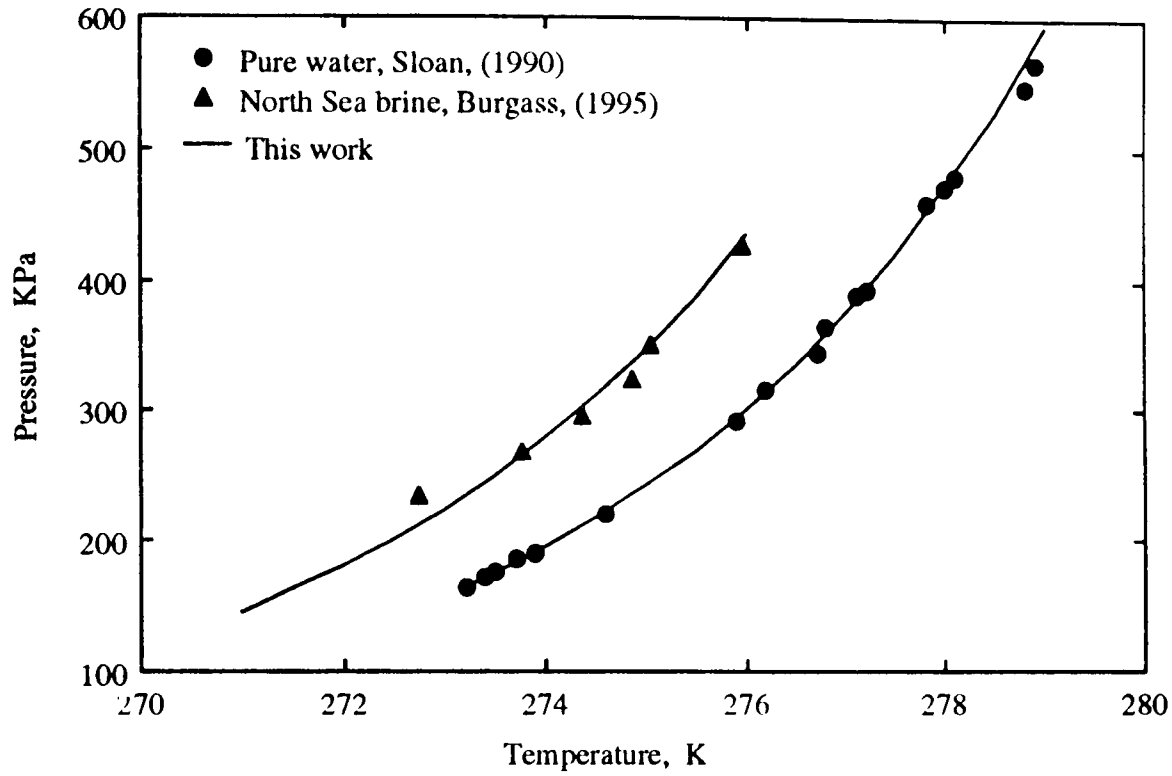

Figure-6.34 Experimental and calculated propane hydrate dissociation conditions in the presence of North Sea brine.

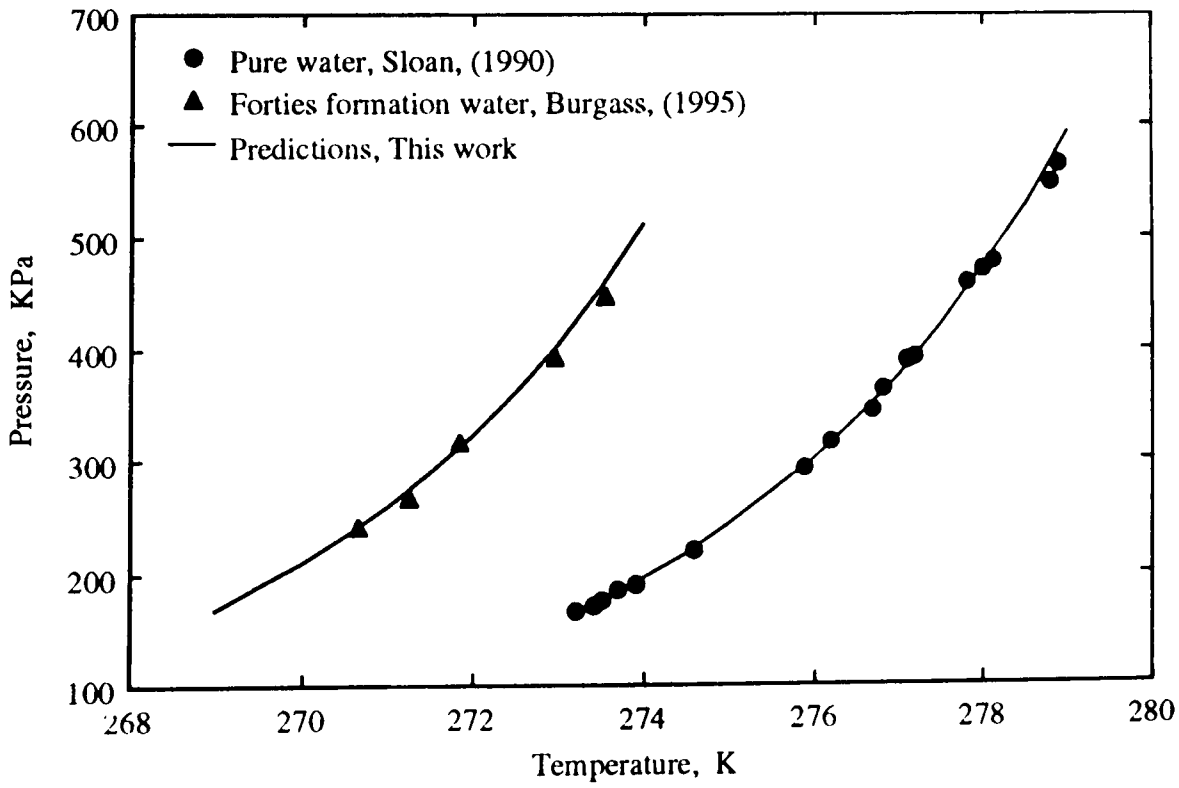

Figure-6.35 Dissociation conditions for propane hydrates in the presence of Forties formation water.

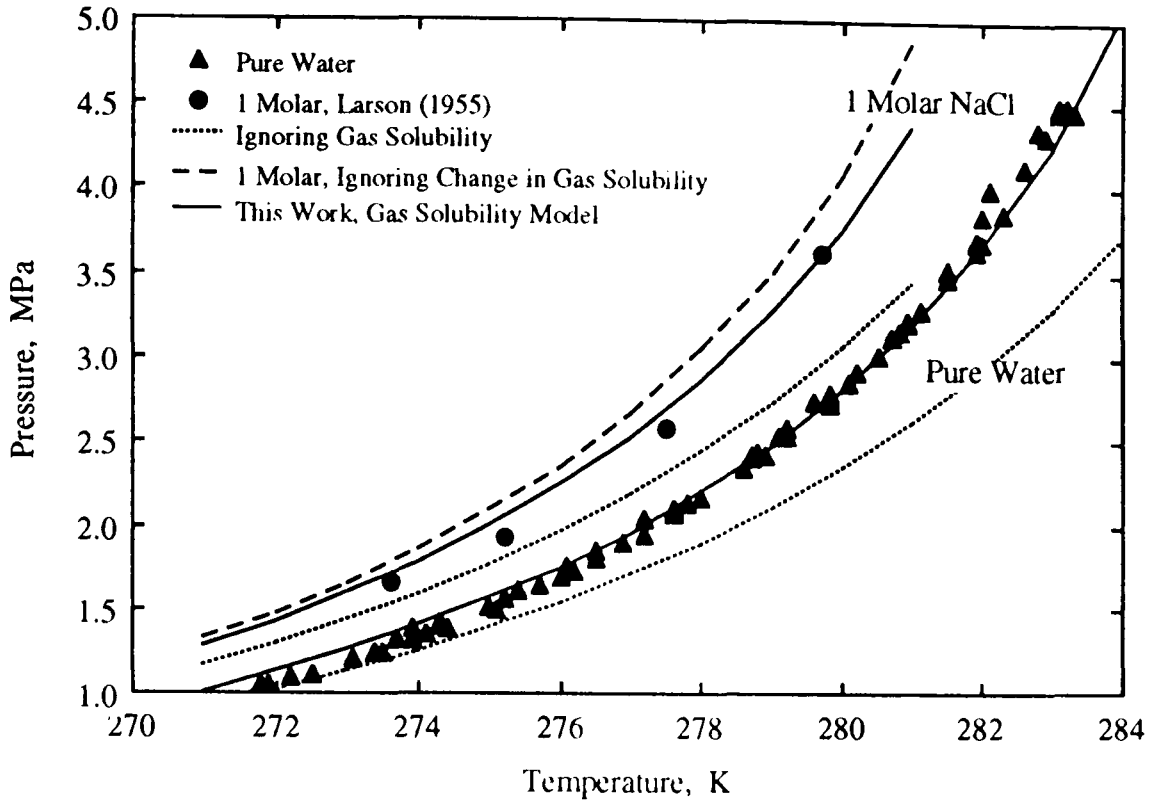

Figure-6.36 Experimental and predicted CO2 hydrate dissociation conditions in the presence of NaCl aqueous solution.

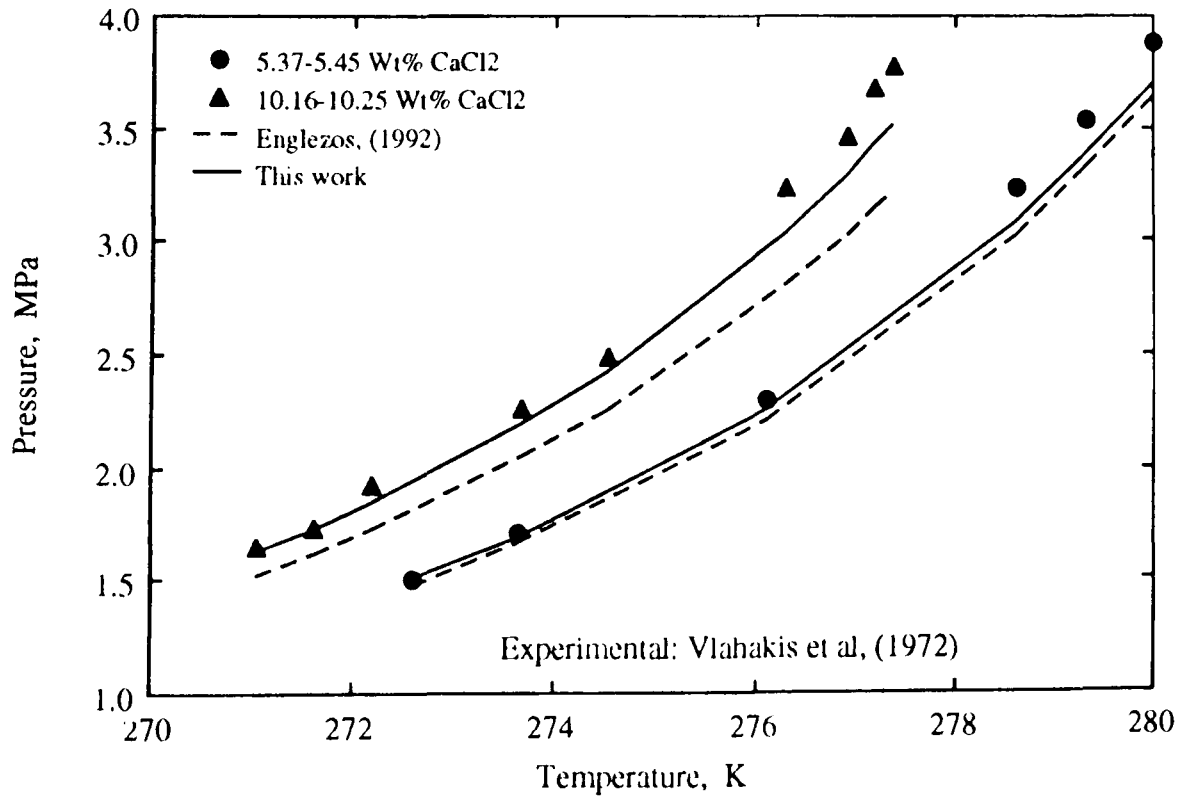

Figure-6.37 Experimental and predicted CO2 hydrate dissociation conditions in the presence of NaCl aqueous solution.

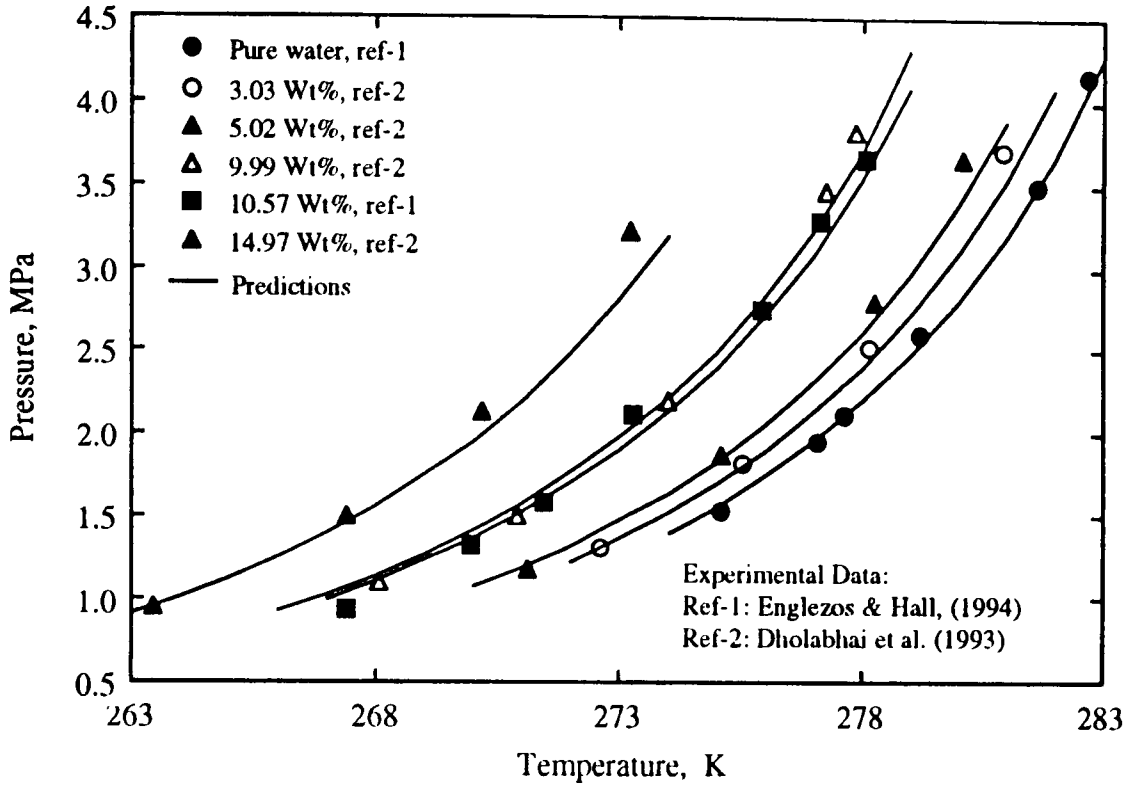

Figure-6.38 CO2 hydrate dissociation conditions in the presence of CaCl2 aqueous solution.

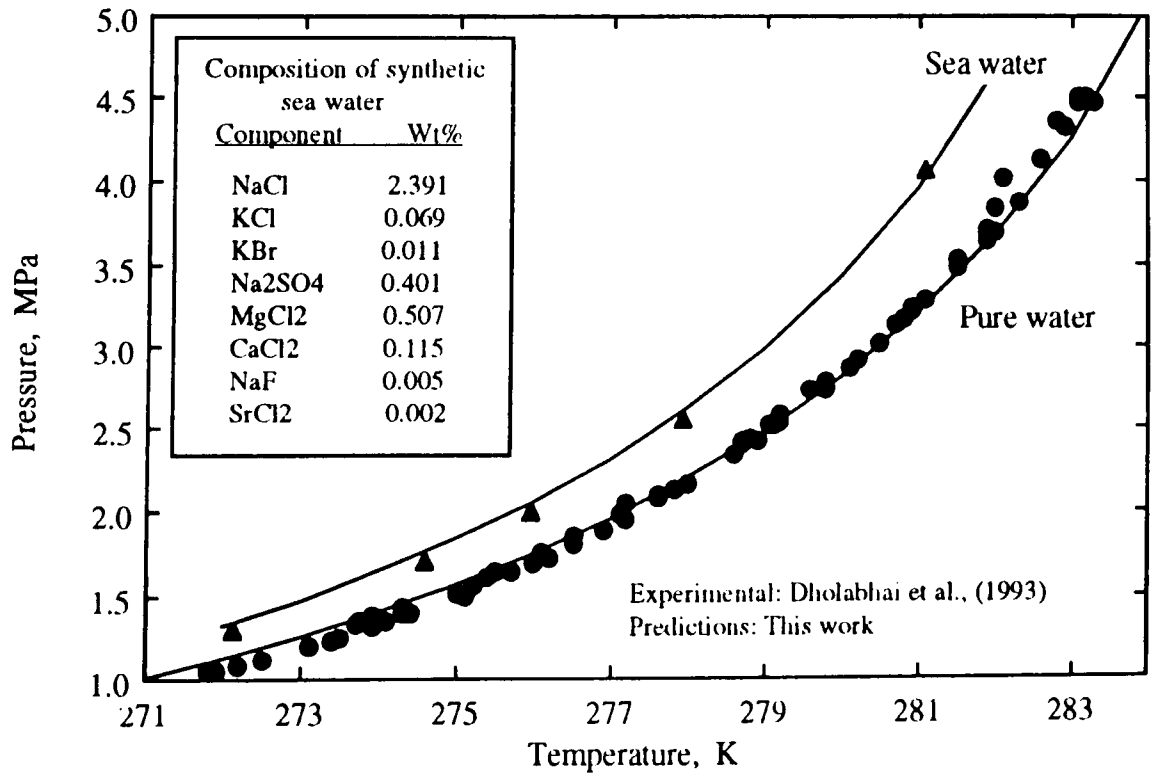

Figure-6.39 Dissociation conditions for CO2 hydrates in the presence of synthetic sea water.

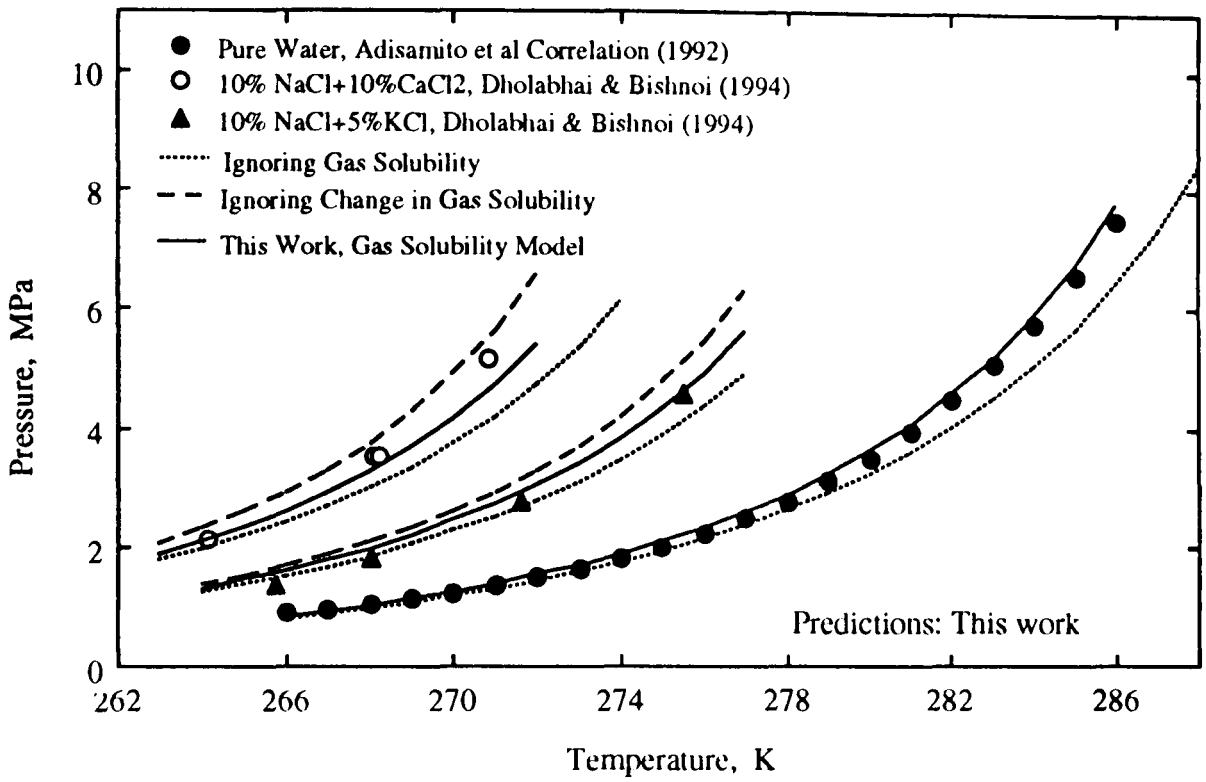

Figure-6.40 Hydrate dissociation conditions for 50% C1+50% CO2 mixture in mixed electrolyte solutions.

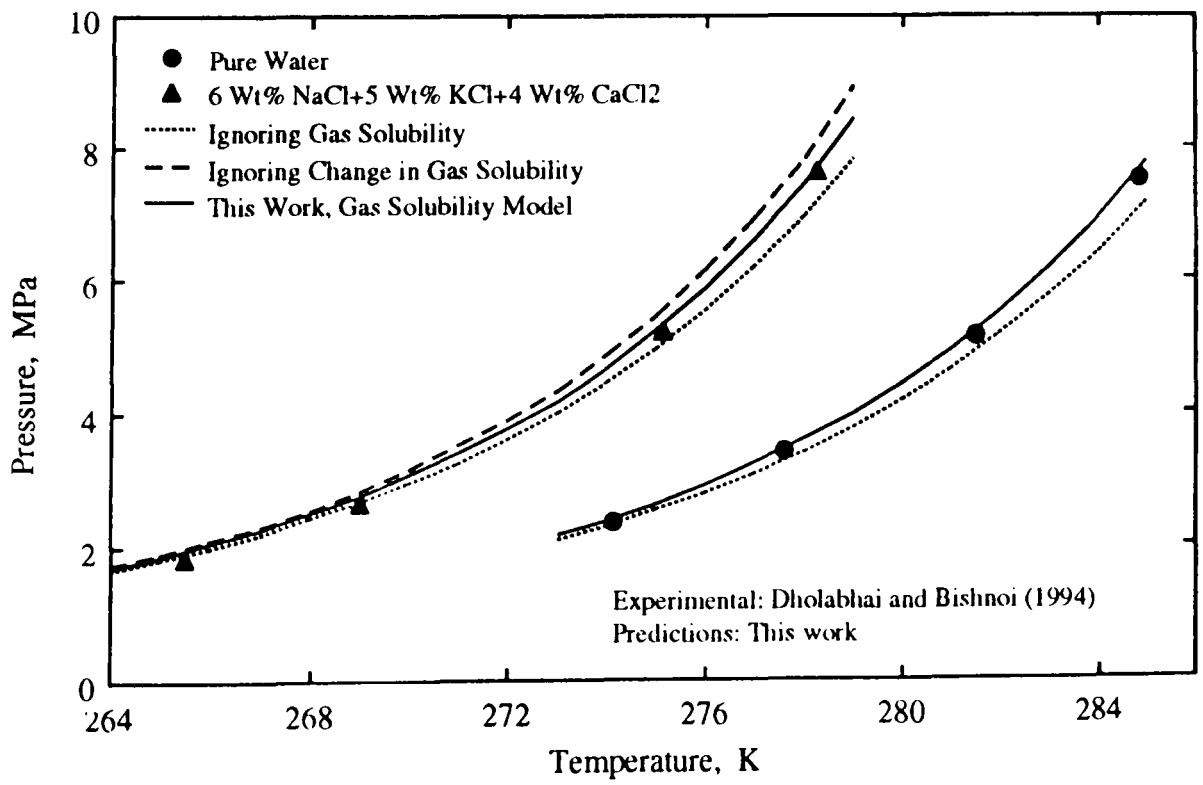

Figure-6.41 Hydrate dissociation conditions for 80% C1+20% CO2 mixture in mixed electrolyte solution.

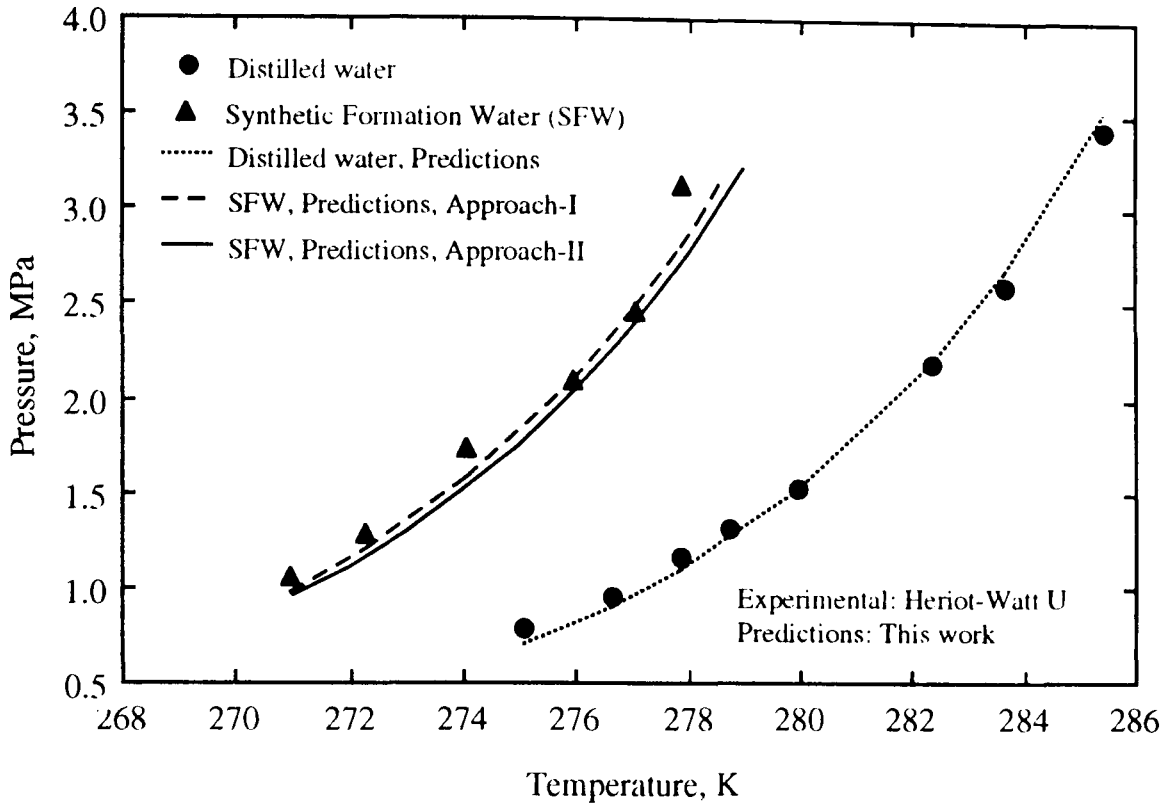

Figure-6.42 Hydrate dissociation conditions for the black oil.

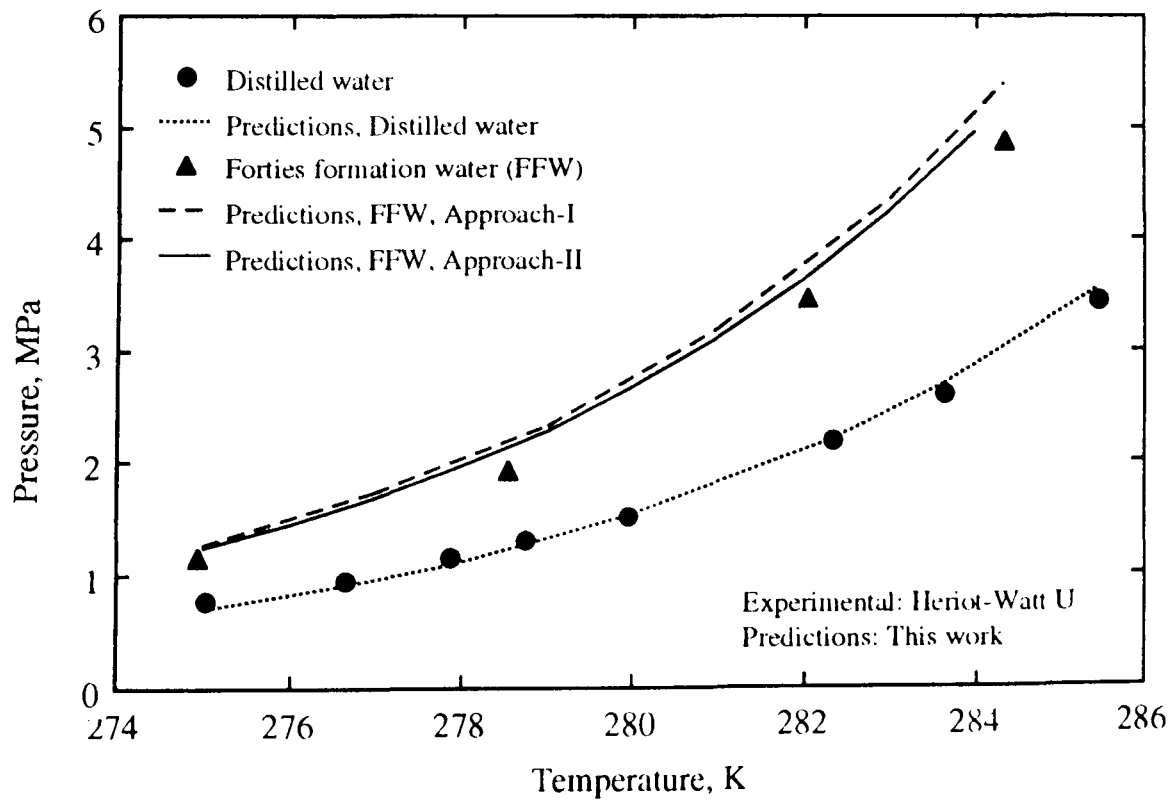

Figure-6.43 Hydrate dissociation conditions for the black oil, Forties formation water.

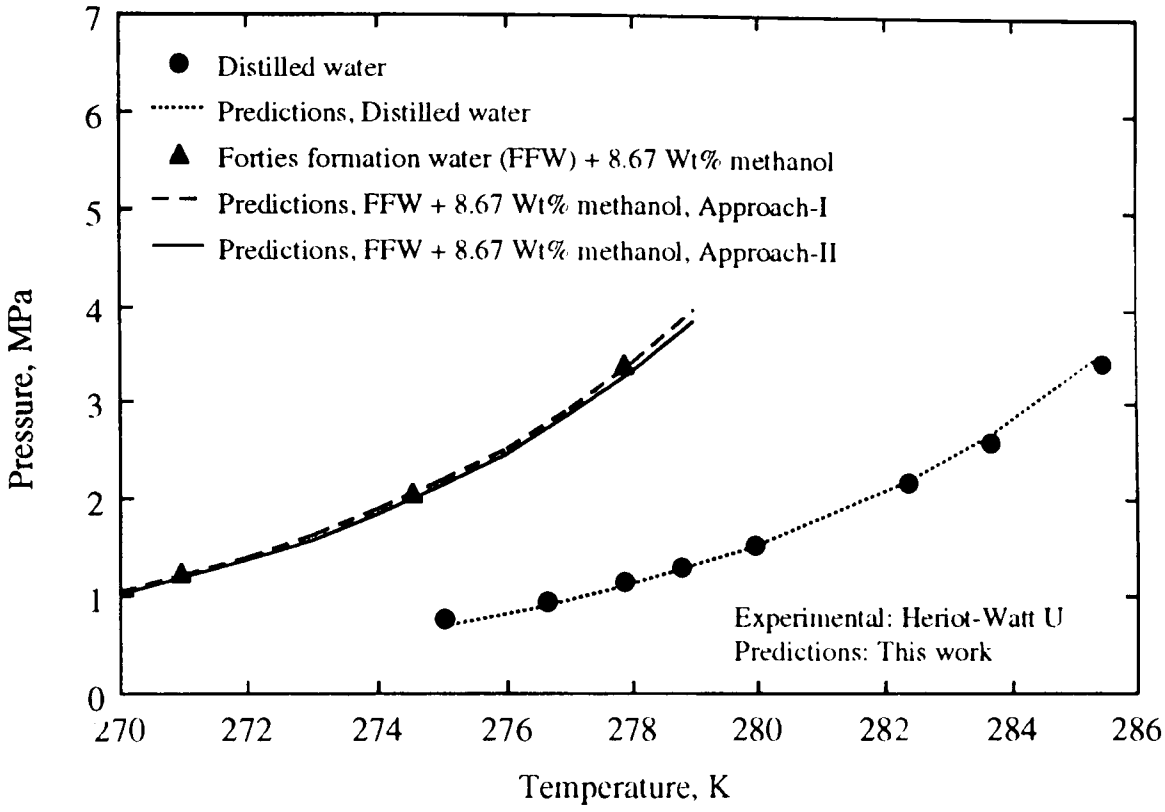

Figure-6.44 Hydrate dissociation conditions for the black oil, Forties formation water plus methanol.

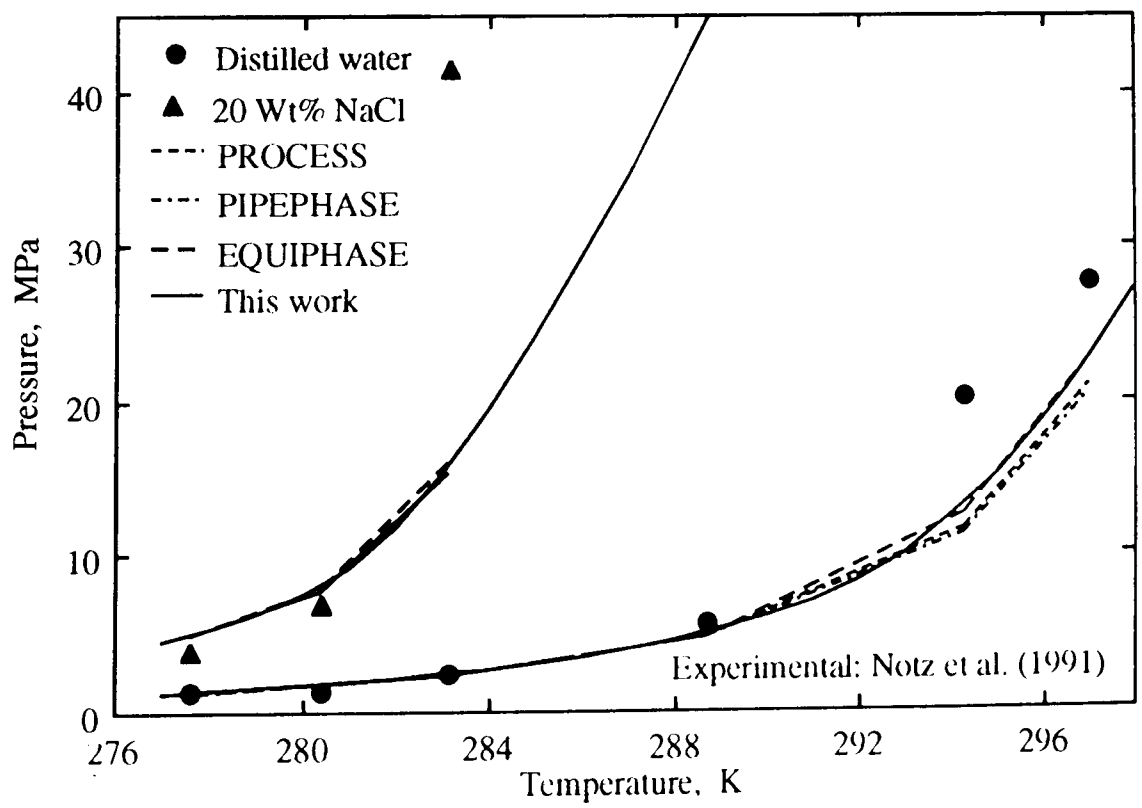

Figure-6.45 Hydrate dissociation conditions for produced dry gas.

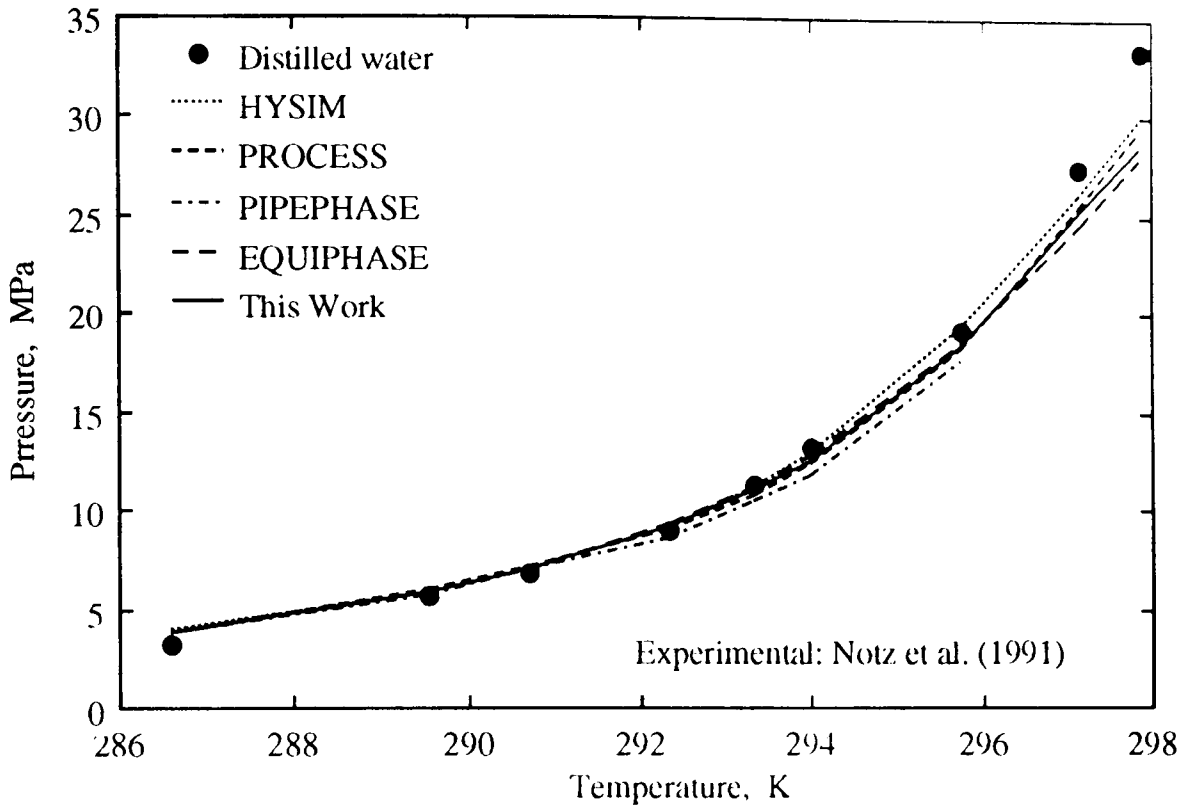

Figure-6.46 Hydrate dissociation conditions for the gas condensate.

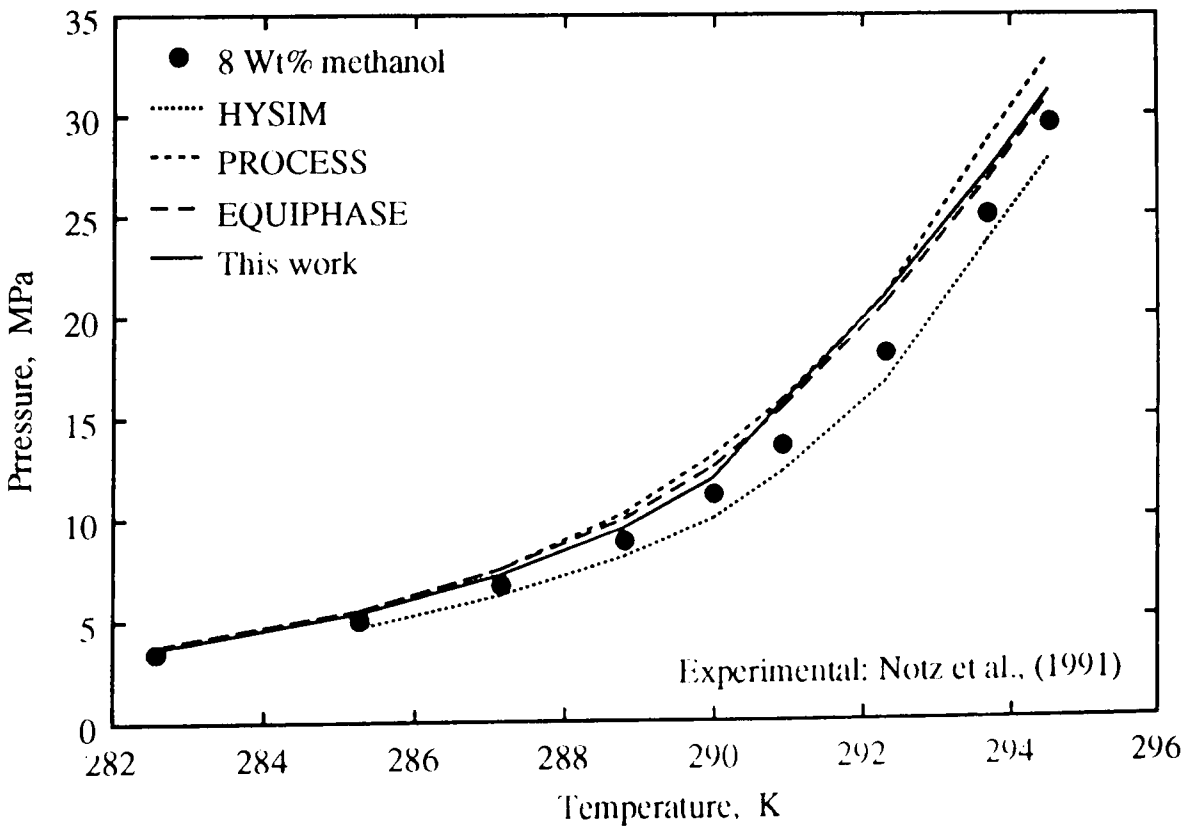

Figure-6.47 Hydrate dissociation conditions for the gas condensate in the presence of methanol.

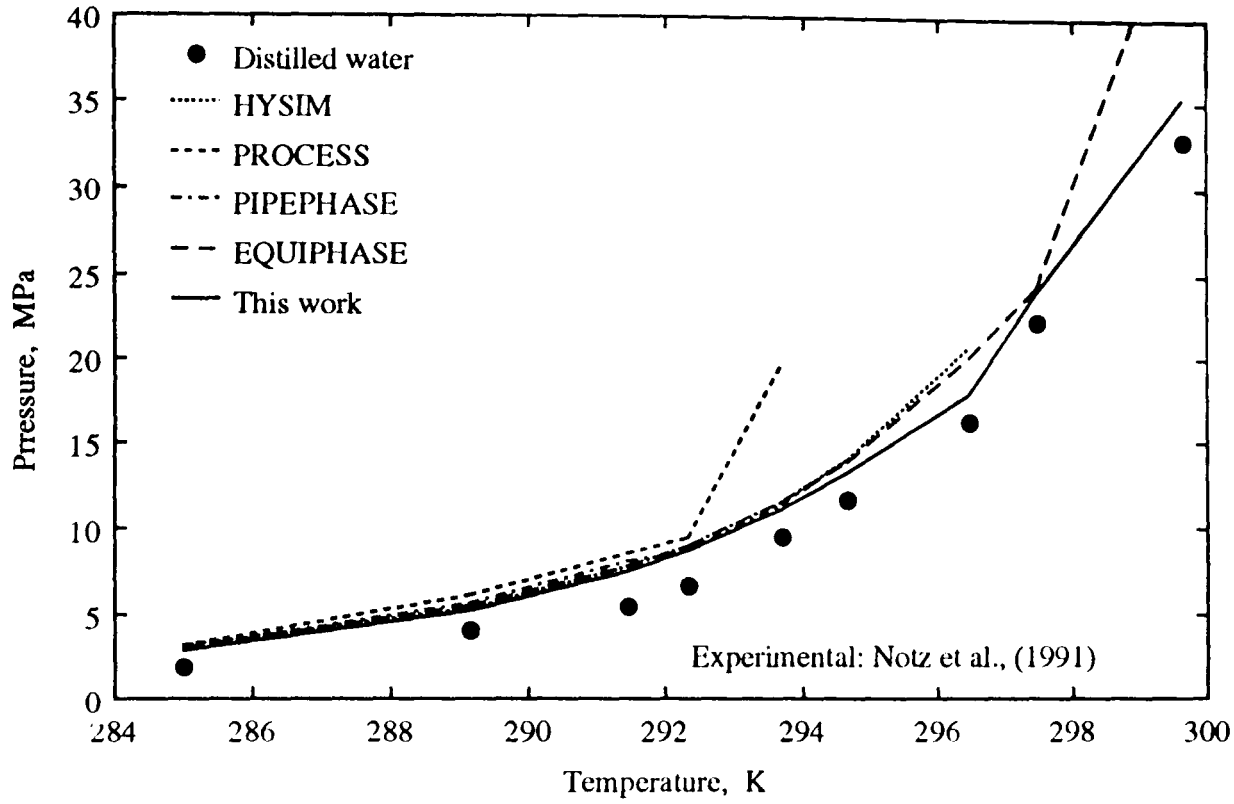

Figure-6.48 Hydrate dissociation conditions for the black oil.

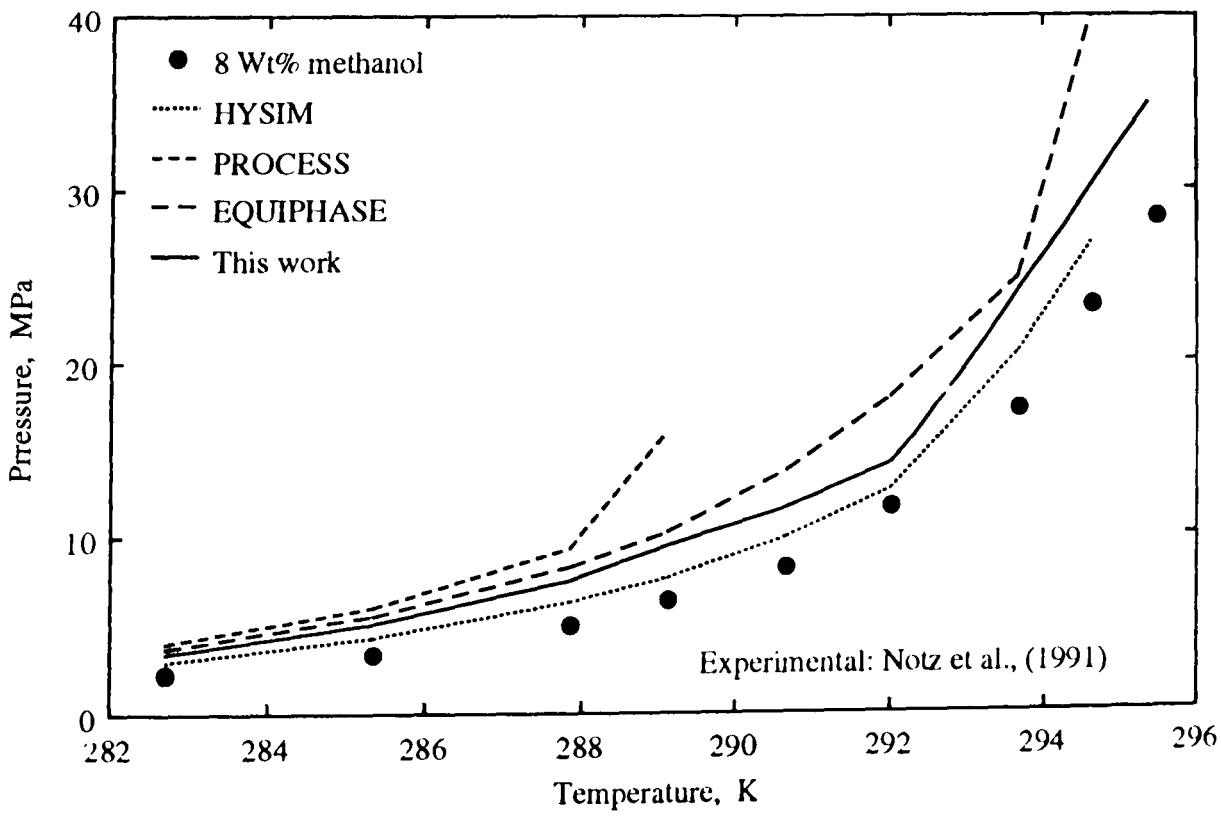

Figure-6.49 Hydrate dissociation conditions for the black oil in the presence of methanol.

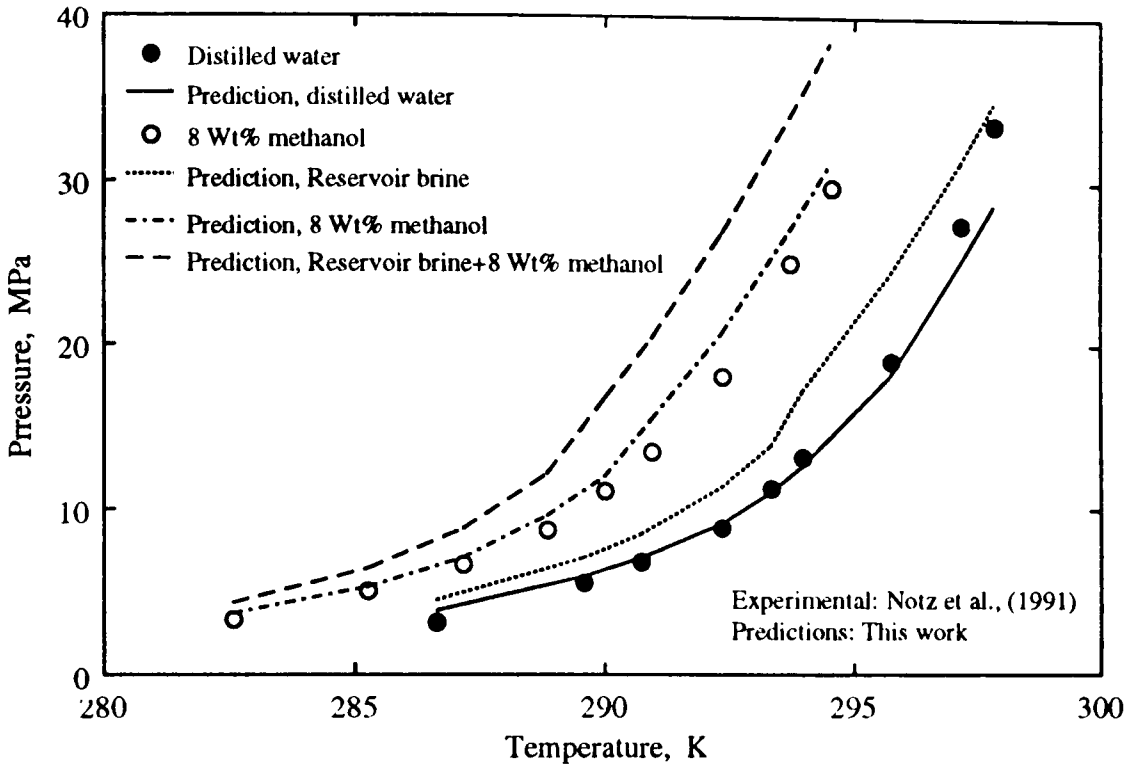

Figure-6.50 Experimental and predicted dissociation conditions for the gas condensate.

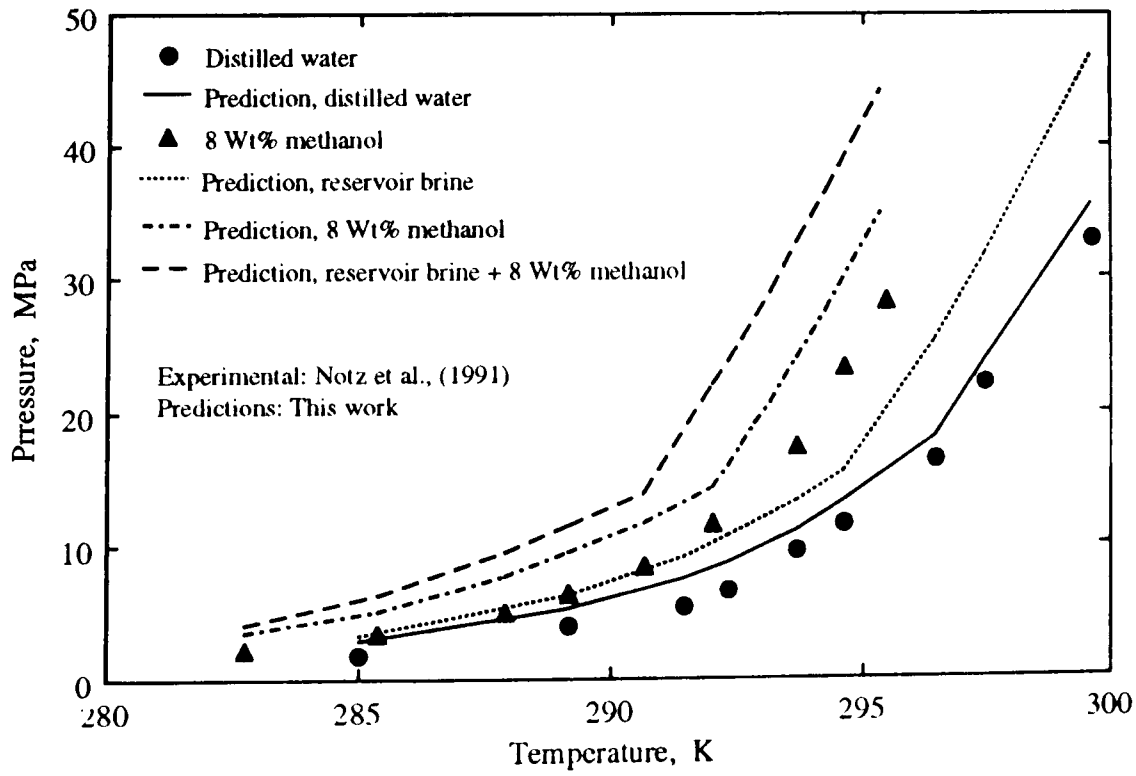

Figure-6.51 Experimental and predicted dissociation conditions for the black oil.

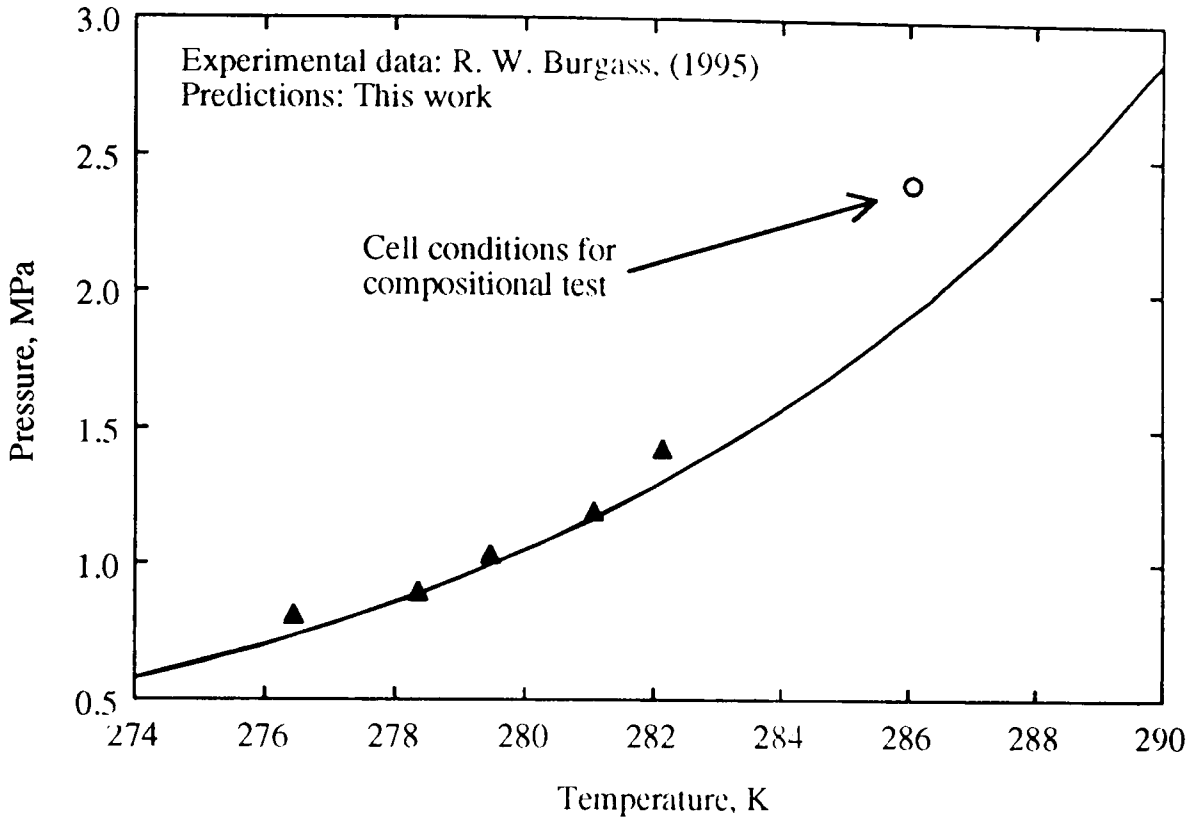

Figure-6.52 Experimental and predicted hydrate dissociation conditions of C1/Xe binary (Table-6.10).

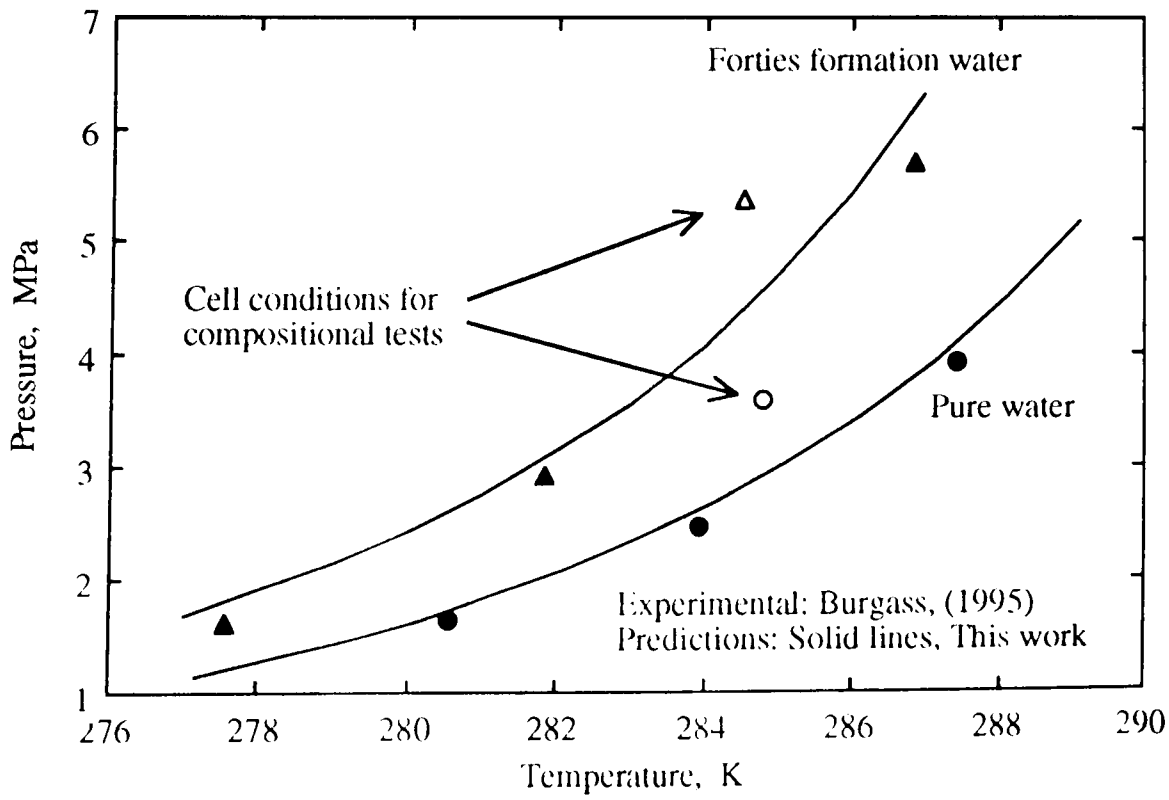

Figure-6.53 Hydrate dissociation conditions for the dry gas mixture (Table-6.8).

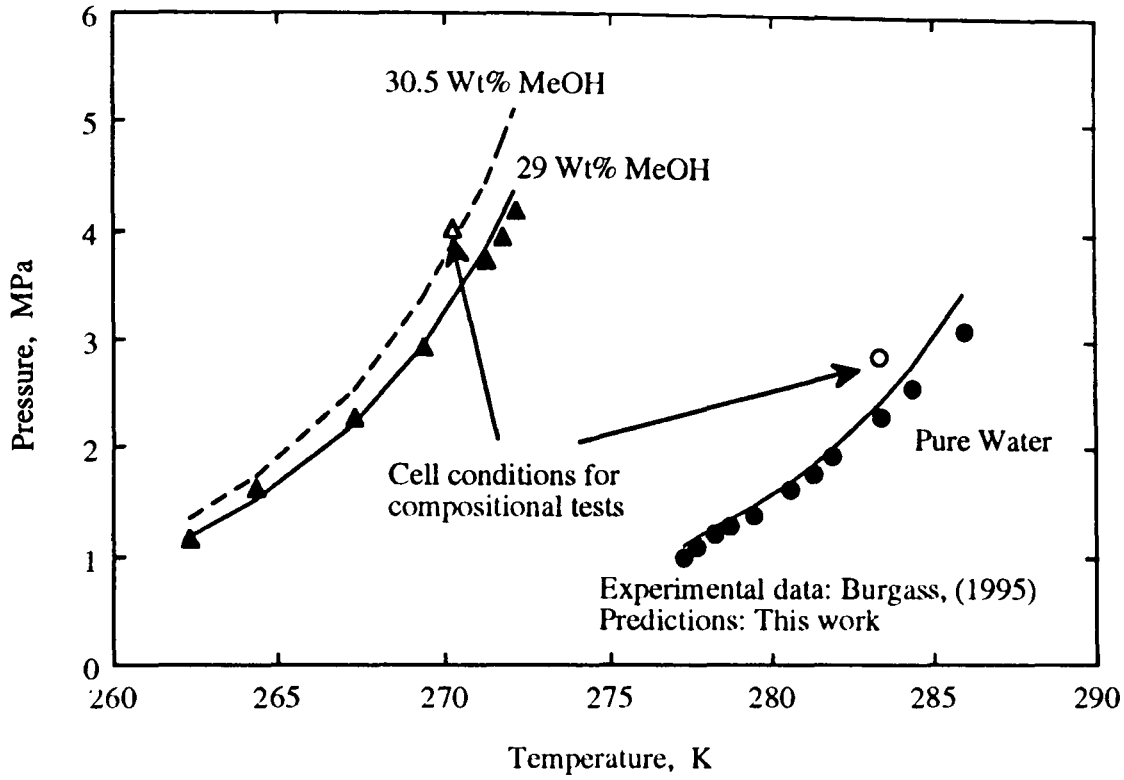

Figure-6.54 Experimental and predicted hydrate dissociation conditions of the gas condensate.

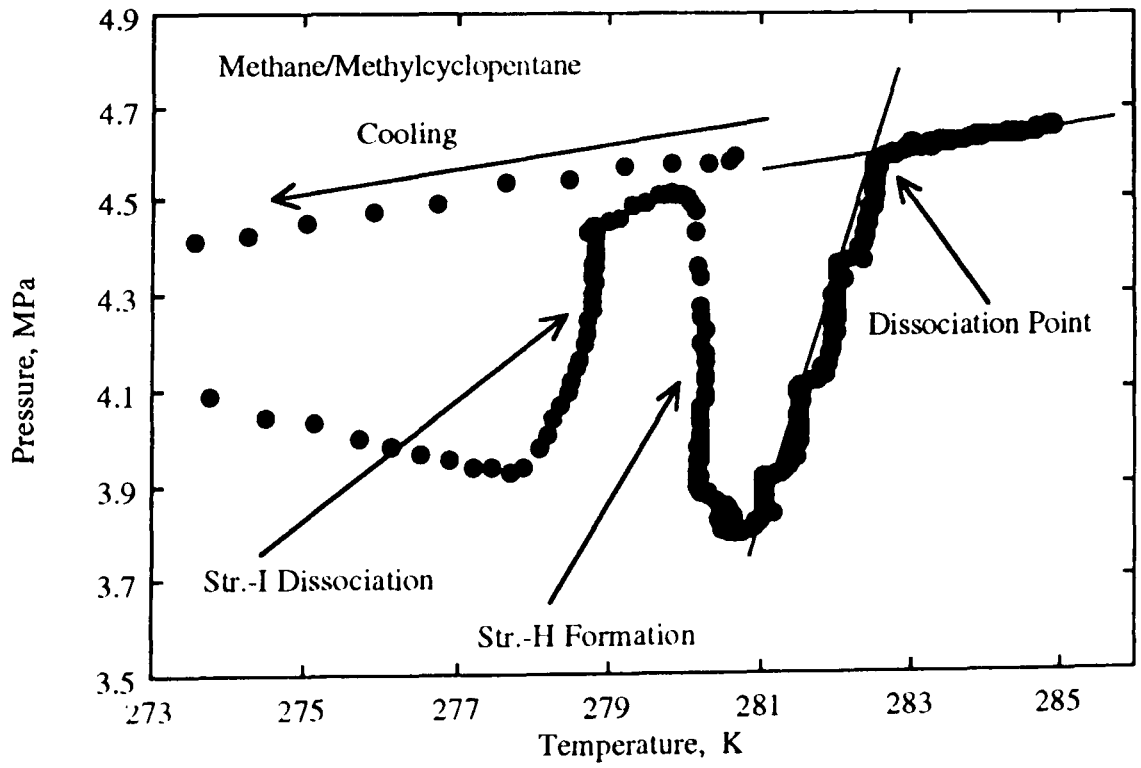

Figure-6.55 Graphical method used in determining dissociation condition of hydrates.

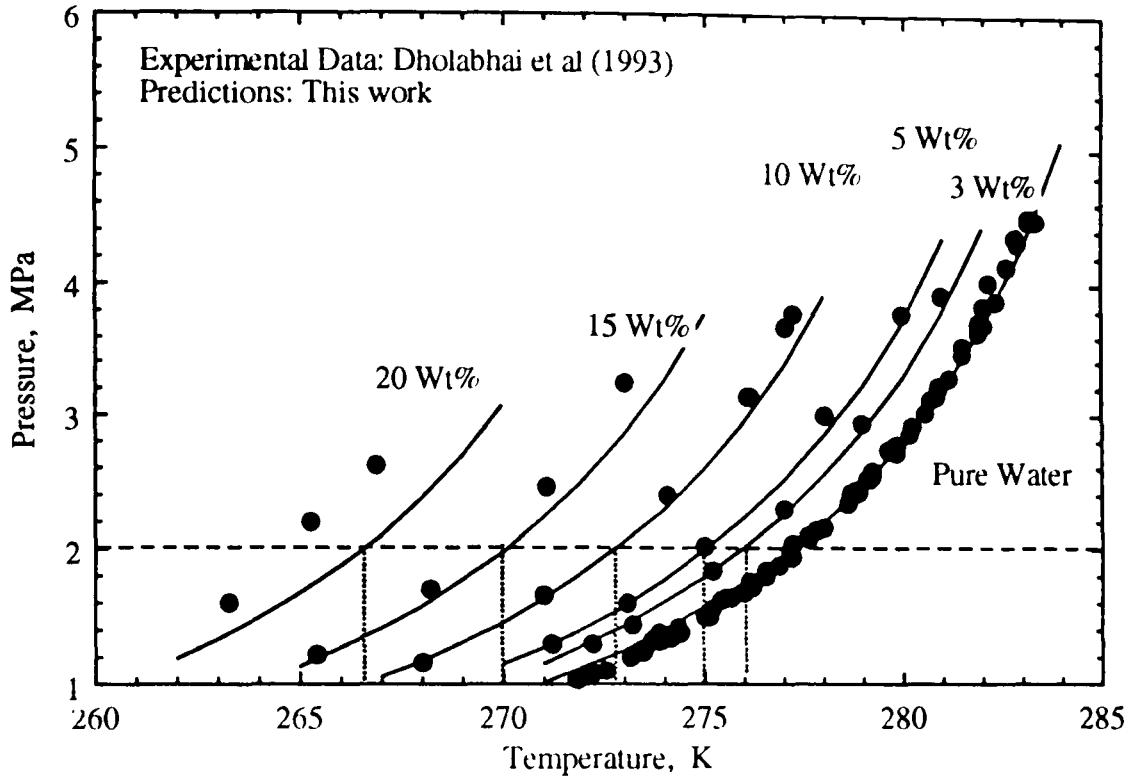

Figure-6.56 Dissociation conditions for CO2 hydrates in the presence of NaCl single electrolyte solutions.

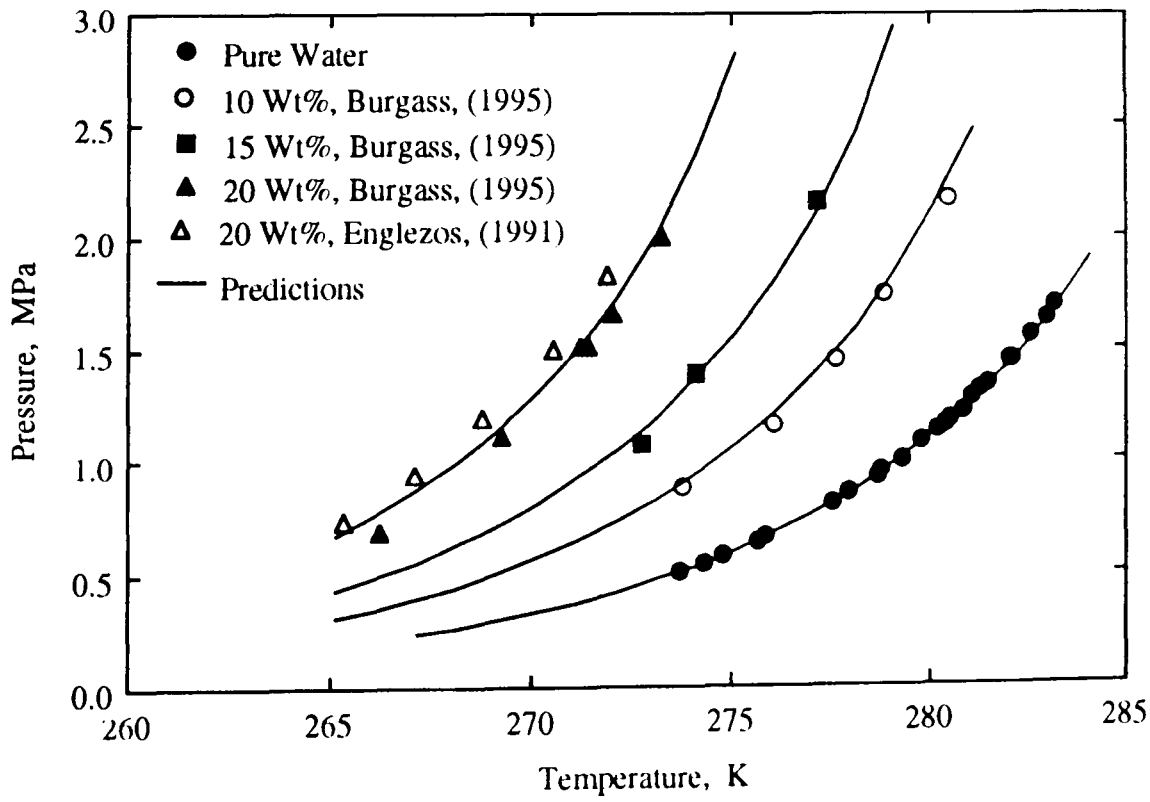

Figure-6.57 Experimental and predicted dissociation conditions of ethane hydrates in the presence of NaCl aqueous solutions.

CHAPTER-7

CONCLUSIONS AND RECOMMENDATIONS FOR FUTURE WORK

7.1 CONCLUSIONS

Thermodynamic Description of the Phases

In Chapter-2 the two approaches to the hydrate phase equilibria, namely, conventional and the general multi-phase flash (GMPF) have been briefly discussed. An equation of state (PR or VPT) has been used in modelling all fluid phases (vapour, liquid hydrocarbon, and water-rich). Hydrate phases (structure-I, II, and H) have been modelled by the ideal solution theory, and ice has been treated as a sub-cooled liquid.

For both EoS, the water vapour pressure data has been used in the temperature range of 258.15 K to 374.15 K (instead of the conventional approach of using water vapour pressure data from boiling point to the critical point) to optimise the water parameters. This modification significantly improved the calculated fugacity at low temperatures, particularly for the PR EoS.

The correlation for calculating the ice vapour pressure was also improved by the use of ice vapour pressure data in the range of 183.15 to 273.15 K (-90 to 0°C). The latest data on ice volume was employed in developing a new correlation.

Determination of the Kihara Parameters

In Chapter-3 the Kihara potential parameters were determined for common hydrate formers, i.e. methane, ethane, propane, i-butane, n-butane, carbon dioxide, hydrogen sulphide, and nitrogen. A number of methods were applied to determine a consistent and unique set of potential parameters for the above hydrate forming gases. In doing so, xenon was first used as a key component to optimise the parameters for other gases. This attempt was partially successful. Later propane was used as the key component and the Kihara parameters of methane, ethane, carbon dioxide, hydrogen sulphide, nitrogen, and xenon were optimised by using the data of both structures. For determining the Kihara parameters for other compounds, the conventional minimisation of the objective function was employed. The following conclusions can be drawn from the application of the above methodology.

(1) The potential parameters of molecules capable of forming only one hydrate structure as simple hydrates cannot be determined from their hydrate dissociation pressure data alone. Though a solution to the optimisation problem may be found, this solution can be shown to be non-unique. More importantly, the so-obtained "optimum" solution, when applied to multicomponent systems may lead to incorrect predictions.

(2) If compositional data of simple hydrates, indicating the cage occupancy ratios, are available then the proper potential parameters can be identified. The weak point of this method is that it requires highly accurate compositional data which are hard to generate.

(3) An alternative method was developed for the determination of the Kihara potential parameters of hydrate formers which enter two structures. This method is practically useful when accurate compositional data are not available. As we demonstrated it is possible to locate accurately the unique set of potential parameters by using the plots of optimised pairs in two structures.

(4) The above technique is not applicable for the determination of the potential parameters of components forming only one hydrate structure. They could be optimised using the binary data with other compounds, and minimising the difference between experimental and predicted dissociation pressures.

(5) The above approach gives a unique opportunity for determining the Kihara potential parameters for compounds, such as cyclopropane, that form simple gas hydrates and change hydrate structure with temperature. For example, cyclopropane changes hydrate structure from I to II as a function of temperature. Hypothetically, it must be possible to find the optimised set of Kihara parameters by using the dissociation pressure data for the two hydrate structures.

(6) Low temperature (100 K) X-ray diffraction shows that nitrogen forms structure-II gas hydrates. However, this study suggests that nitrogen may form structure-I gas hydrates in the L_1-V-H region.

Modelling the Heavy Hydrate Formers

Until recently, n-butane was regarded as the heaviest compound capable of hydrate formation and anything heavier than that as a non-hydrate former. Recent studies, particularly after the discovery of structure-H gas hydrates, showed that compounds as heavy as methylcyclohexane are capable of hydrate formation. This could have significant effect on the hydrate phase boundary and phase equilibria for oil and gas-condensate streams which contain significant amounts of these intermediate/heavy compounds.

In Chapter-3, some of these heavy hydrate formers (HHF) forming structure-II and H have been modelled. Their mutual solubilities with water and the vapour-liquid equilibria data with methane and nitrogen were employed to find the binary interaction parameters (BIP). Finally, using hydrate dissociation pressure data, the Kihara parameters for the

HHF were optimised. A number of conclusions can be drawn, as a result of the above work.

(1) The phase behaviour of heavy hydrate formers-water systems can be modelled with a cubic equation of state with non-random mixing rules. Non-density dependent mixing rules have been used in this work which resulted in a good agreement between the predicted and experimental data.

(2) The hydrate model for the HHF has been successfully validated against independent data. The HHF significantly reduced the hydrate free zone for the systems studied in this work. This shows that the effect of HHF in the determination of the hydrate phase boundary cannot be ignored.

Modelling Electrolyte Solutions

In Chapter-5, single and mixed electrolyte solutions and gas solubility in saline water were modelled. To take into account the effect of salts in water-rich phase, the EoS has been combined with the Debye-Hückel electrostatic term. The electrostatic term has one adjustable parameter, and represents the interaction between salt and a non-electrolyte (water or gas).

Two approaches have been implemented in determining the water-salt interaction coefficients. First, water vapour pressure depression data was used at different temperatures and salt concentrations. The main difficulty with this approach is the lack of reliable experimental data. The resulting parameters were used to predict the freezing point of different electrolyte solutions. The good agreement between the predictions and the experimental data, encouraged the use of more readily available freezing point depression data. In the second approach, only water vapour depression pressure data at 373.15 K and freezing point data for single electrolyte solutions were used in the optimisation of the water-salt interaction coefficients.

The gas solubilities in single electrolyte solutions have been used in finding the gas-salt interaction coefficient. In all cases, the interaction coefficients were considered to be a function of temperature and salt concentration. The model has also been extended to mixed electrolyte solutions. The main conclusions are as follows:

(1) The electrolyte solutions could be modelled by adding an electrostatic term to EoS. The model used in this study has only one adjustable parameter, representing the interaction between the salt and non-electrolytes.

(2) The two approaches used in the optimisation of the water-salt interaction coefficients produced similar results. The second approach, however, is preferred as it uses only two readily available sets of data, i.e. vapour pressure depression at 373.15 K and freezing point depression of single electrolyte solutions.

(3) The gas solubility model could be used independently to calculate the gas solubility in saline water over a wide range of temperature (260-420 K) and salt concentration, e.g. low temperature hydrate phase equilibria or high temperature gas solubility in formation water calculations.

(4) As a result of the extension of the model to mixed electrolyte solutions and its rigorous thermodynamic approach, the model could be used in more realistic production scenarios, e.g. hydrate phase boundary for oil in the presence of formation water or formation water plus methanol.

Validation of the Model

In Chapter-6, a wide range of experimental data have been used in the validation of the model. Also, the validation is planned to show the capabilities of the model as a design tool for sub-sea transmission lines and process facilities. In doing so, the two approaches, in avoiding hydrate problems, i.e. avoiding hydrate formation or transferring them as

slurry, are addressed. Therefore, first the accuracy of the model in predicting the hydrate phase boundary is examined and then the predicted amount of hydrates (to be transferred as slurry) is compared with the limited available experimental data.

All the data used in the validation of the model, with the exception of the gas solubility in single electrolyte solutions, were independent data. These data include, the vapour pressure and freezing point of aqueous electrolyte solutions, the gas solubility in saline water, the hydrate inhibition effect of electrolyte solutions, and the amount and composition of different phases in the presence of gas hydrates. The model was also compared with four leading commercial packages. The following conclusions can be drawn:

(1) The model developed in this work is able to predict vapour pressure and freezing point depression of aqueous single and mixed electrolyte solutions over a wide range of temperature and salt concentrations.

(2) The model reliably predicts the gas solubility in electrolyte solutions over a wide range of temperature and salt concentrations.

(3) The close agreement between experimental and predicted hydrate phase boundary for different types of synthetic and real reservoir fluids (particularly in the presence of pure water) demonstrates the success of the method used in the optimisation of the Kihara potential parameters.

(4) The hydrate inhibition effect of single and mixed electrolyte solutions has been modelled successfully, as demonstrated by comparing the experimental and predicted results. These include, predicting the hydrate phase boundary for pure, binary, multi-component gas mixture, gas-condensate and black oil in the presence of single and mixed electrolyte solutions, methanol, and methanol plus formation water.

(5) In predicting the hydrate phase boundary for real reservoir fluids, i.e. a produced gas, a gas-condensate, and a black oil sample, the model predictions were compared with literature experimental data and four leading commercial packages. The results showed that the model is as good as, if not superior to the commercial packages, with the extra benefit of thermodynamic consistency. None of the commercial packages is reported to be able to calculate the combined effect of methanol and formation brine, which could be a real production scenario when the inhibition effect of the formation water is not adequate and methanol should be added to suppress hydrate formation.

(6) In relation to the transfer of gas hydrates as slurry, the main information required for the design and operations of pipelines might be the amount of hydrates to be transferred. The developed model was employed to predict the amount of hydrates to be transferred (and the composition of different phases) for pure, binary, multi-component gas mixture, gas-condensate, in the presence of pure water, single electrolyte solutions, formation water, and methanol. The predictions were compared with the available experimental data which demonstrated the reliability of the model.

(7) In determining the hydrate dissociation point, two techniques are currently in use, i.e. visual and graphical. The ability of calculating the amount of hydrates in the presence of electrolyte solutions showed that, while the two techniques produce similar results in the presence of pure water; the visual technique could be misleading in the presence of electrolyte solutions. The results showed that the deviation increases with an increase in salt concentration and system pressure.

7.2. RECOMMENDATIONS FOR FUTURE WORK

Thermodynamic Description of Fluid Phases

Both the VPT and PR EoS could be used in the fugacity calculations. However, the PR EoS is limited to the classical mixing rules. The adaptation of non-random mixing rules in the PR EoS should improve the prediction of phase equilibria in the presence of water.

Liquid-Liquid equilibria for HHF and water showed that the non-density dependent mixing rules cannot predict the HHF solubilities in water at high temperatures accurately. This shortcoming, though not of significant importance for predicting hydrate phase equilibria, could be further investigated for improving the mixing rules.

For gas and gas-condensate streams, injection of methanol is the current practice for inhibiting hydrate formation or decomposing hydrate blockage. The above streams, particularly gas-condensate, contain significant amounts of the HHF. More experimental and numerical work is required to determine the HHF-methanol BIP and to model the HHF/water/methanol system.

In relation to modelling electrolyte solutions, new salts could be added to the library (NaCl, KCl, $CaCl_2$, $MgCl_2$, $SrCl_2$, KBr, NaF, $BaCl_2$, and Na_2SO_4). More importantly, it will be interesting to present salts as ions, as the formation water composition is normally reported in the form of cations and anions, and not individual salts. This approach could be further improved by modelling ions in the EoS formulation, which gives the ability of predicting the possible salt precipitation.

The present gas solubility predicts methane and carbon dioxide solubility in single or mixed electrolyte solutions of NaCl, KCl, and $CaCl_2$. The solubility model could be further improved to include other salts and gases. Immediate candidates could be ethane, nitrogen, hydrogen sulphide among gases, and $MgCl_2$, $BaCl_2$ among salts.

Hydrate Model

In relation to the optimisation of the Kihara potential parameters, there are several areas for further development. After the discovery of structure-H gas hydrates, the hydrate formers could be divided into the following groups:

Group-I, small molecules (methane, ethane, nitrogen, carbon dioxide etc.) which can enter all three hydrate structures.

Group-II, medium size molecules (propane, i-butane, n-butane, benzene etc.) which can enter structure-II and structure-H gas hydrates.

Group-III, large molecules (methylcyclopentane, methylcyclohexane, etc.) which can enter only structure-H gas hydrates.

For optimising the Kihara parameters for group-I, several approaches are possible. For example, the novel method proposed in this work could be used to determine the Kihara potential parameters for compounds (such as cyclopropane) which form simple gas hydrates and change hydrate structure (I to II) with temperature. Hypothetically, it could be possible to determine the optimised set of Kihara potential parameters by intersecting the ε/κ vs σ^* plots obtained from dissociation pressure data. One can choose one of the following approaches to optimise the Kihara potential parameters for the group-I compounds:

(1) Use cyclopropane as a key compound and determine the Kihara parameters for the group-I compounds. This approach requires experimental dissociation pressure data for binaries of cyclopropane/group-I hydrate formers in structure-II.

(2) Ethane/propane binaries are reported to form both hydrate structures-I and II gas hydrates (Holder and Hand, 1982), depending on the relative concentrations. Therefore, if we determine the Kihara parameters for ethane (using its structure-II binaries with cyclopropane), it would be possible to optimise the Kihara parameters for propane, using the intersection of the plots for the two hydrate structures. In optimising the Kihara parameters for other compounds, propane could be used as the key compound. This approach needs only experimental data for the ethane/cyclopropane binaries.

(3) Use propane/cyclopropane binary dissociation data to optimise the Kihara parameters for propane. This approach might not be successful, as it does not cause any structural change for propane. However, it can provide more reliable parameters for propane.

For Group-II, as mentioned in Chapters-3 and 4, the conventional minimisation of the objective function has been used in determining the Kihara potential parameters, as it is not possible to use the method proposed in this work. After the discovery of structure-H hydrates, it might be possible to use structure-H hydrates for further development of the above method.

Ripmeester et al. (1991) have reported that cyclopentane forms structure-II simple gas hydrates. Burgass (1995) has reported that cyclopentane shows signs of structural change in its binaries with methane or nitrogen. Regarding the size of cyclopropane it is unlikely that this compound could form structure-I gas hydrates. Therefore, the change in structure could be either from II to H, or from II to an unknown hydrate structure. Both possibilities are very interesting. If the change in hydrate structure is from II to H, after determining the Kihara parameters for methane or nitrogen (say using cyclopropane as key compound), it could be possible to determine the parameters for cyclopentane by intersection of the plots for the two hydrate structures, i.e. II and H. The structure-H dissociation pressure data for methane (or nitrogen)/cyclopentane/group-II ternaries could then provide enough information to find the ε/κ vs σ^* plot in structure-H for group-II compounds.

If cyclopentane is forming an unknown hydrate structure, the ε/κ vs σ^* plot for cyclopentane in methane/cyclopentane/methylcyclohexane ternary is expected to show a different pattern to that of methane/cyclopentane structure-H. The change of hydrate structure to H for cyclopentane is questionable, mainly because cyclohexane, which is larger than cyclopentane, is reported to form structure-II gas hydrates (Ripmeester et al.,

1991) and does not change structure (Burgass, 1995), whereas one expects cyclohexane to change structure to H at lower temperatures compared to cyclopentane. For a thorough investigation on the possibility of change in hydrate structure and formation of any new hydrate structure, one might consider to study cyclopropane (I and II), cyclobutane (II), cyclopentane (II and ?), and cyclohexane (II).

In relation to group-III, although the FOB vs σ^* plot for methylcyclohexane showed a sharp minimum (Chapter-4) and this could be the case for other compounds in this group, the compositional data on cage occupancy might be necessary to find the unique set of Kihara potential parameters for compounds in this group. However, it is not possible to do any accurate modelling for structure-H gas hydrates before determining its crystal structure. This area warrants further experimental and modelling investigations.

Finally the results of this work showed that nitrogen is likely to form structure-I gas hydrates in the L_1-V-H region. This needs further experimental and theoretical investigations. Some other compounds, such as oxygen, reported to form structure-II gas hydrates by X-ray diffraction at 100 K (Davidson et al., 1986), may also change structure at higher temperatures.

In relation to heavy hydrate formers, more experimental and modelling work is necessary. Firstly, one should see the effect of the HHF on hydrate phase boundary and phase equilibria of real reservoir fluids. Most real fluids are assumed to form structure-II gas hydrates. Therefore, it would be interesting to distinguish the effect of the new HHF and change in hydrate structure (say from II to H) on the hydrate phase boundary. Secondly, more experimental and modelling work are necessary to model the most important HHF. Cyclopentane is of particular interest for any future work, both for the possibility of change in hydrate structure and the largest shift observed in the hydrate phase boundary (Burgass, 1995). As mentioned earlier, the determination of reference properties and

definitive hydrate structure for structure-H hydrates are crucial for any future modelling work.

More experimental work on the amount and composition of equilibrium phases in heterogeneous systems containing gas hydrates is required. These data could be used in further improvement and validation of the model. Furthermore, the compositional data are valuable in improving the conventional K-value charts. We have noticed some deviations between the experimental and predicted amount of methanol and ethane in vapour and hydrate phases, respectively. It might be possible to use the compositional data to improve the model.

APPENDIX-A

EQUATIONS OF STATE AND MIXING RULES

A.1. INTRODUCTION

Equations of State (EoS) represent the relation existing between the temperature, T, and pressure conditions, P, the volume occupied, V, and the quantity of material, N. They can be divided in two categories: closed type analytical expressions of the type:

$$f(P,T,V,N) = 0 \tag{A.1}$$

and open ended series, or virial equations, where the compressibility factor is given as a power series in the reciprocal molar volume, *1/v:*

$$Z = \frac{Pv}{RT} = 1 + \frac{B}{v} + \frac{C}{v^2} + \frac{D}{v^3} + \ldots \tag{A.2}$$

In the above equation, B is the second virial coefficient, C is the third virial coefficient, D is the fourth, and so on. The virial equation of state is limited to gas phase only.

Most successful closed type equations of state are explicit in pressure and take a cubic form in terms of volume (or Z). The best-known example is the van der Waals EoS (1873). Cubic EoS may be classified according to the number of constants appearing in the equation. The van der Waals EoS contains two constants, and is known as the two parameter EoS. In this work the popular Peng-Robinson (1976) EoS and the well proven

(Danesh *et al.*, 1991) Valderrama (Valderrama, 1990) modification of the Patel and Teja EoS have been used in calculating the fugacity in all fluid phases.

The semi-empirical cubic EoS have in general been developed by using pure component data. The application of these equations has been extended to multicomponent systems by defining mixing rules to evaluate the average parameters required in the EoS calculations. In this work two different mixing rules, namely, classical mixing rules and non-density mixing (NDD) rules have been used.

The objective of this appendix is to give a brief review of the above equations of state and mixing rules. Xu (1990), Danesh *et al.* (1991), and Avlonitis *et al.* (1994) have been consulted in writing this appendix and the materials are mainly quotations from the above references.

A.2. EQUATIONS OF STATE (EoS)

Almost all van der Waals type cubic EoS can be expressed by the following general form:

$$P = \frac{RT}{v-b} - \frac{a}{v^2 + uv + w} \tag{A.3}$$

where P, T, v, and R are the pressure, temperature, molar volume, and the universal gas constant, respectively. a and b, as initially proposed by van der Waals, represent the attractive pressure term and the thermal repulsive term, respectively. In a two parameter EoS, u and w are related to b, whereas in a three parameter EoS u and w are related to b and a third parameter c, or some properties such as acentric factor.

These parameters are related to the critical temperature and pressure by:

$$a = \Omega_a \alpha(T_r) \frac{R^2 T_C^2}{P_C} \tag{A.4}$$

$$b = \Omega_b \frac{RT_C}{P_C} \tag{A.5}$$

$$c = \Omega_c \frac{RT_C}{P_C} \tag{A.6}$$

$$u = \Omega_u \frac{RT_C}{P_C} \tag{A.7}$$

$$w = \Omega_w (\frac{RT_C}{P_C})^2 \tag{A.6}$$

Ω_a and Ω_b in a two parameter EoS or Ω_c in a three parameter EoS may be found by satisfying Equation-A.3 and the following two critical point conditions:

$$(\frac{\partial P}{\partial v})_{T_c} = 0 \tag{A.8}$$

$$(\frac{\partial^2 P}{\partial v^2})_{T_c} = 0 \tag{A.9}$$

The temperature function $\alpha(T_r)$ is generally expressed by:

$$\alpha(T_r) = [1 + m(1 - T_r^{0.5})]^2 \tag{A.10}$$

where the slope m is commonly correlated by the acentric factor ω in a polynomial form; T_r is the reduced temperature defined by T/T_c. The expression for the parameters of the above two equations of states and the original van der Waals EoS (for comparison) are given in Table-A.1.

Avlonitis *et al.* (1994) relaxed the correlation of $\alpha(T_r)$ of Valderrama (VPT EoS) for water and methanol and regressed a more specific correlation for temperatures up to the critical point:

$$\alpha(T_r) = \{1 + m[1 - (T_r)^{\Psi}]\}^2 \tag{A.11}$$

where for methanol m=0.76757, ψ=0.67933 and for water m=0.72318 ψ=0.52084. We extended the Avlonitis *et al.* (1994) approach to the PR EoS. Furthermore, we used water vapour pressure data in the range of 258.15 K to 374.15 K to find m and ψ for water in the PR and VPT EoS, as explained in Chapter-2. A brief discussion of the PR and VPT equations of states is given below:

Peng-Robinson EoS

The Redlich-Kwong great contribution was to introduce the square root of temperature in the attractive term in the EoS, but their equation cannot accurately predict the phase behaviour and volumetric properties. Peng and Robinson (1976) proposed a modified Redlich-Kwong equation of state (PR EoS) which is capable of predicting the liquid density as well as the vapour pressure in order to further improve VLE predictions.

Peng and Robinson used a similar form of $\alpha(T_r)$ as proposed by Soave (1972), but it was correlated by using vapour-pressure data from the normal boiling points to the critical point, whereas Soave only used the critical point and the calculated vapour pressure at T_r=0.7. Later they (Robinson and Peng, 1978) modified the correlation for m by improving the predictions for heavier compounds. The parameters of the PR EoS are given in Table-A.1.

Valderrama-Patel-Teja EoS

Patel and Teja (1982) developed a cubic equation of state (PT EoS) by introducing two substance dependent parameters which are obtained from the liquid density and vapour pressure data. They correlated the two parameters with the acentric factor, ω. The three parameter PT EoS has been shown to give satisfactory results for both vapour pressure and density, even for heavy and polar compounds. The acentric factor, ω, has been extensively used along with T_c and P_c to correlate the parameters of most equations of state. However, ω is a parameter representing the behaviour of a substance at low pressure range (T_r=0.7). Valderrama and Cisternas (1986) modified the PT EoS by using

the critical compressibility factor, Z_C, instead of the acentric factor, ω, to correlate the parameters of the PT EoS. Later, Valderrama (1990) introduced both the critical compressibility factor and the acentric factor as generalising parameters in the PT EoS. In doing so he argues that the use of four substance dependent generalising parameters (T_C, P_C, Z_C, and ω) results in better predictions of volumetric properties and vapour pressures of polar and non-polar fluids. Danesh *et al.* (1991) extensively tested the VPT EoS in complex reservoir fluids and demonstrated its superiority to other EoS in the prediction of volumetric properties, even without any binary interaction parameters for hydrocarbon systems. The parameters of the PR EoS are summarised in Table-A.1.

A.3. MIXING RULES

For mixtures, the composition must be taken into account in formulating the equation of state. Consequently, for a mixture, Equation-A.1 would be:

$$f(P,T,V,N_1,N_2,N_3,\ldots)=0 \qquad \text{(A.12)}$$

In practice it is assumed that a mixture with a given composition behaves like a *hypothetical pure* substance, for which the parameters are calculated from the individual pure component parameters and the composition of the mixture. The rules governing the calculation of a, b, c, for the hypothetical pure substance are known as mixing rules.

In the calculation of phase equilibria in systems containing only non-polar components, adequate results are obtained with the classical mixing rules. For mixtures where strongly polar components (such as water and methanol) interact with non-polar compounds (asymmetric mixtures), more complex mixing rules are needed. In the following sections, the classical mixing rules and non-density dependent (NDD) mixing rules (Avlonitis *et al.*, 1994) are explained. It is should be noticed that the non-conventional mixing rules are only available with the VPT EoS.

Classical Mixing Rules

In classical mixing rules, also called the conventional random van der Waals mixing rules, the parameters a, b, and c, for a mixture, are calculated from the following equations:

$$a = \sum_i \sum_j x_i x_j (a_i a_j)^{0.5} (1 - k_{ij}) \qquad \text{(A.13)}$$

$$b = \sum_i x_i b_i \qquad \text{(A.14)}$$

$$c = \sum_i x_i c_i \qquad \text{(A.15)}$$

where x_i is the mole fraction of component i and k_{ij} is the so-called *standard binary interaction parameter* (BIP) between component i and component j.

As the binary interaction parameter is determined by matching the predicted values with experimental data, it should be considered as a fitting parameter and be used with the corresponding EoS. Furthermore, the hydrocarbon-hydrocarbon interaction have been found to be insignificant and can safely be assumed to be equal to zero. The binary interaction parameters used in this work for the PR and the VPT EoS are listed in Tables-A.2 and A.3, respectively.

Non-Density Dependent (NDD) Mixing Rules

The three parameter equation of state proposed by Valderrama has been extended to asymmetric systems by the introduction of new non-density dependent mixing rules with cubic dependence of the attractive term. Avlonitis *et al.* (1994) separated the attractive term a of the VPT EoS into two parts:

$$a = a^C + a^A \qquad \text{(A.16)}$$

where a^C stands for the classic quadratic mixing rules and is given by Equation A.13. a^A represents the asymmetric contribution and should vanish when the system approaches

ideal behaviour, i.e. at high temperatures. It should also vanish when the asymmetric interactions become unimportant, i.e. when the concentration of non-polars in a polar-rich phase tend to zero. For thermodynamic consistency, the term a^A should be independent of pressure. The simplest possible mixing rule which satisfies the above requirements is (Avlonitis *et al.*, 1994):

$$a^A = \sum_p x_p^2 \sum_i x_i a_{pi} l_{pi} \qquad \text{(A.17)}$$

where p is the index of the polar component, $a_{pi} = (a_p a_i)^{1/2}$ and l_{pi} is a binary interaction parameter, which is a decreasing function of temperature:

$$l_{pi} = l_{pi}^o - l_{pi}^l (T - T_o) \qquad \text{(A.18)}$$

where l_{pi}^o and l_{pi}^1 are dimensionless constants expected to be positive and T_o is the ice point in K. These parameters have been obtained by forcing the agreement of the model to the binary data reported in the open literature. Table-A.4 presents a listing of the obtained binary interaction parameters.

Table-A.1. Parameters of the cubic equations of state.

Equation	Ω_a	Ω_b	Ω_u	Ω_w	m
VDW (1873)	27/64	1/8	0	0	0
PR (1978)	0.45724	0.07780	$2\,\Omega_b$	$-\Omega_b^2$	$0.3796+1.485\,\omega-0.1644\,\omega^2+0.01667\,\omega^3$
VPT (1990)	$0.66121-0.76105\,Z_c$	$0.02207+0.20868\,Z_c$	$\Omega_b+\Omega_c$ †	$-\Omega_b\,\Omega_c$	$0.46283+3.5823\,\omega Z_c+8.19417\,(\omega Z_c)^2$

† $\Omega_c = 0.57765 - 1.87080\,Z_c$

Table-A.2. The binary interaction parameters (k_{21}) used for the PR EoS†.

Component	Carbon dioxide	Nitrogen	Hydrogen sulphide	Water
Methane	0.094	0.035	0.100	0.512
Ethane	0.134	0.038	0.095	0.496
Propane	0.128	0.070	0.088	0.544
i-Butane	0.126	0.094	0.050	0.500
n-Butane	0.165	0.114	0.097	0.472
n-Pentane	0.141	0.088	0.047	0.470
n-Hexane	0.118	0.150	0.047	0.470
n-Heptane	0.110	0.142	0.047	0.470
n-Octane	0.150	0.120	0.030	0.470
Carbon dioxide	-	-0.022	0.165	-0.030
Nitrogen	-	-	0.063	0.430
Hydrogen sulphide	-	-	-	0.500

† Avlonitis, 1988.

Table-A.3. The standard binary interaction parameters (k_{21}) for the VPT EoS †.

Component	Carbon dioxide	Nitrogen	Hydrogen sulphide
Methane	0.092	0.035	0.080
Ethane	0.134	0.038	0.095
Propane	0.128	0.070	0.088
i-Butane	0.126	0.134	0.050
n-Butane	0.138	0.114	0.050
n-Pentane	0.141	0.088	0.047
n-Hexane	0.118	0.150	0.047
n-Heptane	0.110	0.142	0.047
n-Octane	0.110	0.150	0.030
Carbon dioxide	-	-0.036	0.088
Nitrogen	-	-	0.176

† Avlonitis *et al.* 1994.

Table-A.4. Interaction parameters for the NDD mixing rules †.

Component (1)	Methanol (2)			Water (2)		
	k_{21}	l^o_{21}	$l^l_{21} \times 10^4$	k_{21}	l^o_{21}	$l^l_{21} \times 10^4$
Methane	0.2538	0.7319	6.88	0.5028	1.8180	49.00
Ethane	0.0137	0.0519	21.7	0.4974	1.4870	45.40
Propane	0.0278‡	0.0779	0.00	0.5465	1.6070	39.30
i-Butane	0.1233	0.3029	17.60	0.5863	1.7863	37.40
n-Butane	0.1465	0.2917	0.00	0.5800	1.6885	33.57
n-Pentane	0.2528	0.7908	58.28	0.5525	1.6188	23.72
n-Hexane	0.2245	0.5607	17.54	0.4577	1.5730	31.41
n-Heptane	0.1461	0.4592	27.17	0.4165	1.5201	35.21
n-Octane	0.1403	0.5331	36.91	0.3901	1.5200	35.31
Xenon	-	-	-	0.2374	0.8870	47.50
Carbon dioxide	0.0510	0.0700	11.56	0.1965	0.7232	23.74
Nitrogen	0.2484	1.0440	7.22	0.4792	2.6575	64.46
Hydrogen sulphide	0.0694	0.1133	0.00	0.1382	0.3809	13.24
Methanol	0.0000	0.0000	0.00	-0.0789	-0.0149	0.00
Water	-0.0789	0.0835	0.00	0.0000	0.0000	0.00

† Avlonitis *et al.* 1994.

‡ For propane, k_{ij} is temperature dependent: $K_{pm}=0.0278+0.000911(T-To)$.

APPENDIX-B

EXPERIMENTAL DATA

Table-B.1 Experimental hydrate dissociation conditions for black oil in the presence of pure water and synthetic formation water.

Pure water		Synthetic formation water, Table-6.7	
Temp, K (±0.05 K)	Press, MPa (±0.007 MPa)	Temp, K (±0.05 K)	Press, MPa (±0.007 MPa)
275.05	0.779	270.95	1.055
276.65	0.958	272.25	1.289
277.85	1.158	274.05	1.737
278.75	1.310	275.95	2.103
279.95	1.531	277.05	2.461
282.35	2.193	277.85	3.130
283.65	2.599		
285.45	3.427		

Table-B.2 Experimental hydrate dissociation conditions for black oil (Table-6.8) in the presence of Forties formation water and Forties formation water + 8.67 Wt% methanol.

Forties formation water, Table-6.7		Forties formation water+8.67 Wt% methanol	
Temp, K (±0.05 K)	Press, MPa (±0.007 MPa)	Temp, K (±0.05 K)	Press, MPa (±0.007 MPa)
274.90	1.165	270.90	1.255
278.50	1.924	274.50	2.075
282.00	3.447	277.80	3.392
284.30	4.868	281.10	5.330

REFERENCES

Aasberg-Petersen, K., Stenby, E., and Fredenslund, A., "Prediction of High-Pressure Gas Solubilities in Aqueous Mixtures of Electrolytes", *Ind. Eng. Chem. Res.*, **30**(9), 2180-2185, (1991).

Adachi, Y., Lu, B. C-Y., Sugie, H., "A Four-Parameter Equation of State", *Fluid Phase Equilibria*, **11**, 29, (1983).

Adisasmito, S., Sloan, E. D., "Hydrates Of Hydrocarbon Gases Containing Carbon Dioxide", *J. Chem. Eng. Data*, **37**(3), 343-349, (1992).

Anderson, F. E., Prausnitz, J. M., "Inhibition of Gas Hydrates by Methanol", *AIChE J.*, **32**(8), 1321-1332, (1986).

Avlonitis, D. A., "Multiphase Equilibria in Oil-Water Hydrate Forming Systems", *MSc. Thesis*, Heriot-Watt University, (October 1988).

Avlonitis, D. A., Danesh, A., Todd, A. C., and Baxter, T., "The Formation of Hydrate in Oil-Water Systems", *Proceedings of the 4th International Conference on Multiphase Flow*, Nice, 15, (1989).

Avlonitis, D. A., Danesh, A., and Todd, A. C., "Heterogeneous Equilibria Calculations for Multicomponent Hydrate Forming Systems", *AIChE Spring National. Meeting*, Houston, (1991).

Avlonitis, D. A., "Thermodynamic of Gas Hydrate Equilibria", *PhD Thesis*, Heriot-Watt University, (1992).

Avlonitis, D., Danesh, A., and Todd, A. C., "Prediction of VL and VLL Equilibria of Mixtures Containing Petroleum Reservoir Fluids and Methanol with a Cubic EoS", *Fluid Phase Equilibria*, **94**, 181-216, (1994).

Behar, E., Delion, A-S., Sugier, A., and Thomas, M., "Plugging Control of North Sea Production Facilities by Hydrates", paper presented at International Conference on Natural Gas Hydrates, 20-24 June 1993, New Paltz, New York, USA, *the Annals of the New York Academy of Sciences*, **715**, 95-105, (1994).

Ben-Naim, A., and Yaacobi, M., *J. Phys. Chem.*, **78**, 175-178, (1974). Also IUPAC Solubility Data Series, Volume 27/28, Methane.

Bishnoi, R. J., Gupta, A. K., Englezos, P., and Kalogerakis, N., "Multiphase Equilibrium Flash Calculations for Systems Containing Gas Hydrates", *Fluid Phase Equilibria*, **53**, 97-104, (1989).

Bishnoi, P. R., and Dholabhai, P. D., "Experimental Study on Propane Hydrate Equilibrium Conditions in Aqueous Electrolyte Solutions", *Fluid Phase Equilibria*, **83**, 455-462, (1993).

Blanco, L. H., and Smith, N. O., "The High Pressure Solubility of Methane in Aqueous Calcium Chloride and Aqueous Tetraethylammonium Bromide. Partial Molar

Properties of Dissolved Methane and Nitrogen in Relation to Water Structure", *J. Phys. Chem.*, **82**, 186-191, (1978). IUPAC Solubility Data Series, Volume 27/28, Methane.

Burgass, R. W., "Experimental Investigation on Hydrate Equilibria of Reservoir Fluids Containing Salt and Intermediate/Heavy Compounds", *MPhil Thesis, Heriot-Watt University*, (1995).

Byrne, P. A., and Stoessell, R. K., *Geochim Cosmochim Acta*, **46**, 2395-2397, (1982). Also IUPAC Solubility Data Series, Volume 27/28, Methane.

Campbell, J. M., Gas Conditioning and Processing, *Campbell Petroleum Series Inc.*, Norman, OK, Vol. **2**, Chapter 17, (1976).

Carson, D. B., and Katz, D. L, "Natural Gas Hydrates", *Trans. AIME*, **146**, 150-158, (1941).

Cole, W. A., and Goodwin, S. P., "Flash Calculations for Gas Hydrates: A Rigorous Approach", *Chemical Engineering Science*, **45**(3), 569-573, (1990).

CRC Handbook of Chemistry and Physics, *CRC Press Inc.*, Boca Raton, Florida, (1988).

Danesh, A., Xu, D.-H, and Todd, A. C., "Comparative Study of Cubic Equations of State for Predicting Phase Behaviour and Volumetric Properties of Injection Gas Reservoir Oil Systems", *Fluid Phase Equilibria*, **63**, 259-278, (1991).

Danesh, A., Tohidi, B., Burgass, R. W., and Todd, A. C., "Benzene Can Form Gas Hydrates", *Trans. IChemE*, **71** (Part A), 457-459, (July 1993).

Danesh, A., Tohidi, B., Burgass, R. W., and Todd. A. C., "Hydrate Equilibrium Data of Methyl Cyclo-Pentane with Methane or Nitrogen", *Trans. IChemE*, **72** (Part A), 197-200, (March 1994).

Davidson, D. W., Handa, Y. P. and Ripmeester, J. A.,: "Xenon-129 NMR and Thermodynamic Parameters of Xenon Hydrate", *J. Phys. Chem.*, **90**, 6549-6552, (1986a).

Davidson, D. W., Handa, Y. P., Ratcliffe, C. I., Ripmeester, J. A., Tse, J. S., Dahn, J. R., Lee, F., Calvert, L. D., "Crystallographic Studies of Clathrate Hydrates. Part I.", *Mol. Cryst. Liq.*, **141**, 141-149, (1986b).

Davidson, D. W., Desando, S. R., Gough, S. R., Handa, Y. P., Ratcliffe, C. I., Ripmeester, J. A., Tse, J. S., "Some Structural Studies of Clathrate Hydrates", *Journal of Inclusion Phenomena*, **5**, 219-223, (1987).

Davy, H., "The Bakerian Lecture: On Some of the Combinations of Oxymuriatic Gas and Oxygene, and on the Chemical Relations of These Principles to Inflammable Bodies", *Philos. Trans. Royal Soc. London*, **101** (Part I), 1-35, (1811).

de Roo, J. L., Peters, C. J., Lichtenthaler, R. N., and Diepen, G. A. M., "Occurrence of Methane Hydrate in Saturated and Unsaturated Solutions of Sodium Chloride and Water in Dependence of Temperature and Pressure", *AIChE J.*, **29**(4), 651-657, (1983).

Deaton, W. M., and Frost, E. M., "Gas Hydrates in Natural Gas Pipe Lines", *Oil and Gas J.*, **36**(1), 75, (1937).

Dharmawardhana, P. B., Parrish, W. R., and Sloan, E. D., "Experimental Thermodynamic Parameters for the Prediction of Natural Gas Hydrate Dissociation Conditions", *Ind. Eng.* Chem. *Fundam.*, **19**, 410-414, (1980).

Dholabhai, P. D., Englezos, P., Kalogerakis, N., and Bishnoi, P. R., "Equilibrium Conditions for Methane Hydrate Formation in Aqueous Mixed Electrolyte Solutions", *The Canadian Journal of Chemical Engineering*, **69**, 800-805, (1991).

Dholabhai., P. D., Kalogerakis, N., and Bishnoi, P. R., "Equilibrium Conditions for Carbon Dioxide Hydrate Formation in Aqueous Electrolyte Solutions", *Journal of Chemical and Engineering Data,* **38**(4), 650-654, (1993).

Dholabhai, P. D., and Bishnoi, P. R., "Hydrate Equilibrium Conditions in Aqueous Electrolyte Solutions: Mixtures of Methane and Carbon Dioxide", *J. Chem. Eng. Data*, **39**(1), 191-194, (1994).

Elbishlawi, M., and Spencer, J. R., *Ind. Eng. Chem.*, **43**, 1811-1815, (1951). Also IUPAC Solubility Data Series, Volume-27/28, Methane.

Englezos, P., and Bishnoi, P. R.,: "Prediction of Gas Hydrate Formation Conditions in Aqueous Electrolyte Solutions", *AIChE J.*, **34**, 1718-1721, (1988).

Englezos, P., and Bishnoi, P. R., "Experimental Study on the Equilibrium Ethane Hydrate Formation in Aqueous Electrolyte Solutions", *Ind. Eng. Chem. Res.*, **30**(7), 1655-1659, (1991).

Englezos, P., "Computation of the Incipient Equilibrium Carbon Dioxide Hydrate Formation Conditions in Aqueous Electrolyte Solutions", *Ind. Eng. Chem. Res.*, **31**(9), 2232-2237, (1992).

Englezos, P. and Hall, S., "Phase Equilibrium Data on Carbon Dioxide Hydrate in the Presence of Electrolytes, Water Soluble Polymers and Montmorillonite", *The Canadian Journal of Chemical Engineering*, **72**, 887-893, (1994).

Ewing, G. I. Ionescu, I. G., "Dissociation Pressure and Other Thermodynamic Properties of Xenon-Water Clathrate", *J. Chem. Eng. Data*, **19**(4), 367-369, (1974).

Fabuss, B. M., and Korosi, A., "Vapour Pressures of Ternary Aqueous Solutions of NaCl, KCl, Na2SO4, and MgSO4 at concentrations and Temperatures of Interest in Desalination Processes", *Desalination*, **1**, 149-155, (1966).

Field, L. R., Wilhelm, E., Battino, R. J., *J. Chem. Thermodyn.*, **6**, 237, (1974). Also IUPAC Solubility Data Series, Volume-27/28, Methane.

Gibbard, H. F., and Gossmann, A. F., "Freezing Points of Electrolyte Mixtures. I. Mixtures of Sodium Chloride and Magnesium Chloride in Water", *Journal of Solution Chemistry*, **3**(5), 385-393, (1974).

GPSA Engineering Data Book, *Gas Processors Suppliers Association*, Tulsa, Oklahoma, USA, (1981).

Hall, D. L., Sterner, M., and Bodnar, R. J., "Freezing Point Depression of NaCl-KCl-H2O Solutions", *Economic Geology*, **83**, 197-202, (1988).

Hammerschmidt, E. G.., "Formation of Gas Hydrates in Natural Gas Transmission Lines", *Ind. Eng. Chem.*, **26**, 851, (1934).

Hammerschmidt, E. G.,: "Gas Hydrate Formations", *Gas*, **15**(5), 30, (1939).

Hobbs, P. V., Ice Physics, *Clarendon*, (1974).

Holder, G. D., Corbin, G, Papadopoulos, K. D, "Thermodynamic and Molecular Properties of Gas Hydrates from Mixtures Containing Methane, Argon, and Krypton", *Ind. Eng. Chem., Fundam.*, **19**, 282-286, (1980).

Holder, G. D., and Hand, J. H., "Multiple-Phase Equilibria in Hydrates from Methane, Ethane, Propane and Water Mixtures", *AIChE J.*, **28**(3), 440-447, (1982).

Holder, G. D., Malekar, S. T. and Sloan, E. D.,: "Determination of Hydrate Thermodynamic Reference Properties from Experimental Hydrate Composition Data", *Ind. Eng. Chem. Fundam.* , **23**, 123-126, (1984).

IUPAC Solubility Data Series, "Nitrogen and Air", Volume 10, *Pergamon Press, A., Wheaton & Co. Ltd.*, Exeter, Great Britain, (1982).

IUPAC Solubility Data Series, "Methane", Volume 27/28, *Pergamon Press, A., Wheaton & Co. Ltd.*, Exeter, Great Britain, (1987).

IUPAC Solubility Data Series, "Hydrocarbons water Sea water, Part-1, C_5-C_7", Volume 37, *Pergamon Press, A., Wheaton & Co. Ltd.*, Exeter, Great Britain, (1989).

Jhaveri, J., and Robinson, D. B., Can. J. Chem. Eng., **43**, 75, (1965). Also Sloan, E. D., (1990).

Katz, D. L., and Lee, R. L., Natural Gas Engineering, Production and Storage, *McGraw Hill*, New York, 197-230, (1990).

Kihara, T., "Virial Coefficient and Models of Molecules in Gases", *Reviews of Modern Physics*, **25**(4), 831-843, (1953).

Krichevskii, I. R. and Efremova, G. D., *Zhur. Fiz. Khim.*, **22**, 1116, (1948). Also IUPAC Solubility Data Series, Volume-10.

Kubota, H., Shimizu, K., Tanaka, Y., and Makita, T., "Thermodynamic Properties of R13 ($CClF_3$), R23 (CHF_3), R152a ($C_2H_4F_2$), and Propane Hydrates for Desalination of Sea Water", *Journal of Chemical Engineering of Japan*, **17**(4), 423-429, (1984).

Kuschel, F., and Seidel, J., "Osmotic and Activity Coefficients of Aqueous K_2SO_4-$MgSO_4$ and KCl-$MgCl_2$ at 25 °C", *Journal of Chemical and Engineering Data*, **30**, 440-445, (1985).

Larson, S. D., "Phase Studies of the Two-Component Carbon Dioxide-Water System Involving the Carbon Dioxide Hydrate", *PhD Dissertation*, University of Illinois, (1955).

Lederhos, J. P., Mehta, A. P., Nyberg, G. B., Warn, K. J., and Sloan, E. D., "Structure H Clathrate Hydrate Equilibria of Methane and Adamantane", *AIChE J.*, **38**(7), 1045-1048, (1992).

Li, Y., -K, and Nghiem, L. X., "Phase Equilibria of Oil, Gas and Water/Brine Mixtures from a Cubic Equation of State and Henry's Law", *Can. J. Chem. Eng.*, **64**, 486-496, (1986).

Lin, H-M., Sebastian, H. M., Simnick, J. J., Chao, K-C., *J. Chem. Eng. Data*, **24**, 146-149, (1979).

London, F., *Trans. Faraday Soc.*, **33**, 8, (1937).

Macedo, E. A., Skovborg, P., Rasmussen, P., "Calculation of Phase Equilibria for Solutions of Strong Electrolytes in Solvent-Water Mixtures", *Chem. Eng. Sci.*, **45**(4), 875-882, (1990).

Malinin, S. D., and Savelyeva, N. I., "The Solubility of CO_2 in NaCl and $CaCl_2$ Solutions at 25, 50, and 75 ° Under Elevated CO_2 Pressures", *Geochemistry International*, 410-418. Translated from *Geokhimiya* 1972, No 6, 643-653, (1972).

Marshal, D. R., Satio, S. Kobayashi, R., "Hydrates at High Pressures: Part I. Methane-Water, Argon-Water, and Nitrogen-Water Systems", *AIChE J.*, **10**(2), 202-205, (1964). Also Sloan, E. D., (1990).

McKoy, V., Sinanoglu, O., "Theory of Dissociation Pressures of Some Gas Hydrates", *J. Chem. Physics*, **38**(12), 2946-2956, (1963).

Mehta, A. P., and Sloan, E. D., "Structure H Hydrate Phase Equilibria of Methane+Liquid Hydrocarbon Mixtures", *J. Chem. Eng. Data*, **38**, 580-582, (1993).

Mehta, A. J., and Sloan, E. D., "Structure H Hydrate Phase Equilibria of Paraffins, Naphthenes, and Olefins with Methane", *J. Chem. Eng. Data*, **39**, 887-890, (1994a).

Mehta, A. J., and Sloan, E. D., "A Thermodynamic Model for Structure-H Hydrates", *AIChE J.*, **40**(2), 312-320, (1994b).

Menten, P. D., Parrish, W. R., and Sloan, E. D., "Effect of Inhibitors on Hydrate Formation", *Ind. Eng. Chem. Process Des. Dev.*, **20**, 399-401, (1981).

Michelsen, M. L., "The Isothermal Flash Problem. Part-I. Stability", *Fluid Phase Equilibria*, **9**, 1-19, (1982a).

Michelsen, M. L., "The Isothermal Flash Problem. Part-II. Phase-Split Calculation", *Fluid Phase Equilibria*, **9**, 21-40, (1982b).

Michel, S., Hooper, H. H., and Prausnitz, J. M., "Mutual Solubilities of Water and Hydrocarbons from an Equation of State. Need for an Unconventional Mixing Rule", *Fluid Phase Equilibria*, **45**, 173-189, (1989).

Michels, A., Gerver, J., and Bijl, A., *Physica*, **3**, 797-808, (1936). Also IUPAC Solubility Data Series, Volume 27/28, Methane.

Miller, P. and Dodge, B. F., *Ind. Eng. Chem.*, **32**, 434-438, (1940). Also IUPAC Solubility Series, Volume-10.

Notz, P. K., Burke, N. E., and Hawker, P. C., "Measurement and Prediction of Hydrate Formation Conditions for Dry Gas, Gas Condensate, and Black Oil Reservoirs", OTC 6745, paper presented at the 23rd Annual OTC in Houston, Texas, 6-9 May 1991, *Conference Proceedings*, 409-419, (1991).

O'Sullivan, T. D., and Smith, N. O., "The Solubility and Partial Molar Volume of Nitrogen and Methane in Water and in Aqueous Sodium Chloride from 50 to 125 ° and 100 to 600 Atm", *J. Phys. Chem.*, **74**(7), 1460-1466, (1970).

Parrish, W. R., and Prausnitz, J. M., "Dissociation Pressures of Gas Hydrates Formed by Gas Mixtures", *Ind. Eng. Chem. Process. Des. Develop.*, **11**(1), 26-35, (1972).

Patel, N. C., and Teja, A. S., "A New Cubic Equation of State for Fluids and Fluid Mixtures", *Chem. Eng. Sci.*, **37**, 463-473, (1982).

Patil, K. R., Tripathi, A. D, Pathak, G., and Katti, S. S., "Thermodynamic Properties of Aqueous Electrolyte Solutions. 2. Vapour Pressure of Aqueous Solutions of NaBr, NaI, KCl, KBr, KI, RbCl, CsCl, CsBr, $MgCl_2$, $CaCl_2$, $CaBr_2$, CaI_2, $SrCl_2$, $SrBr_2$, SrI_2, $BaCl_2$, and $BaBr_2$", *Journal of Chemical and Engineering Data*, **36**(2), 225-230, (1991).

Patwardhan, V. S., and Kumar, A., "A Unified Approach for Prediction of Thermodynamic Properties of Aqueous Mixed-Electrolyte Solutions. I. Vapour Pressure and Heat of Vaporisation", *AIChE Journal*, **32**(9), 1419-1428, (1986).

Peng, D-Y., and Robinson, D. B., "A New Two-Constant Equation of State", *Ind. Eng. Chem. Fundam.*, **15**, 59, (1976).

Perry's Chemical Engineers' Handbook, *McGraw-Hill Company*, Tokyo Japan, (1984).

Pitzer, K. S., and Mayorga, G., "Thermodynamics of Electrolytes II. Activity and Osmotic Coefficient for Strong Electrolytes with One or Both Ions Univalent", *J. Phys. Chem.*, **77**(19), 2300, (1973).

Pitzer, K. S. and Bradley D. J., "Thermodynamics of Electrolytes. 12. Dielectric Properties of Water and Debye-Hückel Parameters to 350 °C and 1 kbar", *J. Phys. Chem.*, **83**, 1599, (1979).

Prausnitz, J. M., Molecular Thermodynamics of Fluid-Phase Equilibria, *Prentice-Hall, Inc.*, Englewood Cliffs, New Jersey, USA, (1969).

Prausnitz, J. M., Lichtenthaler, R. N., de Azevedo, E. G., Molecular Thermodynamics of Fluid-Phase Equilibria, *Prentice-Hall, Inc.*, Englewood Cliffs, New Jersey, USA, (1986).

Prutton, C. F., Savage, R. L., "Solubility of Carbon Dioxide in Calcium Chloride-Water Solutions at 75, 100, 120 ° and High Pressures", *J. Am. Chem. Soc.*, **67**, 1550-1554, (1945).

Reamer, H. H., Sage, B. H., and Lacey, W. N., *Ind. Eng. Chem.*, **3**, 240-245, (1958). Also IUPAC Solubility Data Series, Volume-27/28, Methane.

Ripmeester, J. A. and Davidson, D. W.,: "^{129}Xe Nuclear Magnetic Resonance in The Clathrate Hydrate of Xenon", *Journal of Molecular Structure*, **75**, 67-72, (1981).

Ripmeester, J. A., Tse, J. S, Ratcliffe, C. I., and Powell, B. M.,: "A New Clathrate Hydrate Structure", *Nature*, **325**, 135-136, (1987).

Ripmeester, J. A., Ratcliffe, C. I., and McLaurin, G. E.,: "The Role of Heavier Hydrocarbons in Hydrate Formation", AIChE Spring Meeting, Session 44, Hydrates in the Gas Industry, (April 1991).

Robinson, D. B. and Peng, D-Y., "The Characterisation of the Heptane and Heavier Fractions for the GPA Peng-Robinson Programme", *GPA Research Report 28*, (1978).

Rojey, A. and A. Pierrot,: "Hydrates Control in Multiphase Flow", paper presented at IChemE SONG Conference, Hydrate 92, London, 24 June 1992, *Conference Proceedings*.

Saito, S., Marshal, D. R., Kobayashi, R, "Hydrates at High Pressures: Part II. Application of Statistical Mechanics to the Study of the Hydrates of Methane, Argon, and Nitrogen", *AIChE J.*, **10**(5), 734, (1964).

Sako, T., Hakuta, T., and Yoshitome, H., "Vapour Pressures of Binary (H_2O-HCl, -$MgCl_2$, And -$CaCl_2$) And Ternary (H_2O-$MgCl_2$-$CaCl_2$) Aqueous Solutions", *Journal of Chemical and Engineering Data*, **30**(2), 224-228, (1985).

Sander, B., Fredensland, A., and Rasmussen, P., "Calculation of Vapour-Liquid Equilibria in Mixed Solvent/Salt Systems Using an Extended UNIQUAC Equation", *Chem. Eng. Sci.*, **41**(5), 1171-1183, (1986).

Sloan, E. D., Clathrate Hydrates of Natural Gases, *Marcel Dekker Inc.*, New York, (1990).

Søreide, I, Whitson, C. H., "Peng-Robinson Predictions for Hydrocarbons, CO_2, N_2, and H_2S with Pure Water and NaCl Brine", *Fluid Phase Equilibria*, **77**, 217-240, (1992).

Soave, G., "Equilibrium Constants from a Modified Redlich-Kwong Equation of State", *Chem. Eng. Sci.*, **27**, 1197-1203, (1972).

Stoessell, R. K., Byrne, P. A., *Geochim Cosmochim Acta*, **46**, 1327-1332, (1982). Also IUPAC Solubility Data Series, Volume 27/28, Methane.

Tee, S. L., Gotoh, S., and Stewart, W. E., "Molecular Parameters for Normal Fluids", *I & EC Fundam.*, **5**(3), 363-367, (1966).

Tohidi, B., Burgass, R. W., Danesh, A., and Todd, A. C., "Gas Hydrate Formation and Inhibition Prediction", Proceedings of IChemE SONG Conference, Hydrate 92, London, 24 June 1992, *Conference Proceedings*.

Tohidi, B., Burgass, R. W., Danesh, A. and Todd, A. C. "Measurement and Prediction of Amount and Composition of Equilibrium Phases in Heterogeneous Systems Containing Gas Hydrates", presented at the *SPE student paper contest*, September 6, 1993, Aberdeen, Scotland, (1993a).

Tohidi, B., Burgass, R. W., Danesh, A. and Todd, A. C., "Hydrate Inhibition Effect of Produced Water, Part-1. Ethane and Propane Simple Gas Hydrates", presented at SPE Offshore Europe 93, September 7-10, 1993, Aberdeen, Scotland. Published in the *Conference Proceedings*, **1**, 255-264, (1993b).

Tohidi, B., Burgass, R. W., Danesh, A. and Todd, A. C., "Gas Hydrates Modelling, Effect of Gas Solubility in Saline Water", presented at International Non-Renewable Energy Sources Congress, December 26-30, 1993, Tehran, Iran. Published in *the Congress Proceedings*, 602-612, (1993c).

Tohidi, B., Burgass, R. W., Danesh, A. and Todd, A. C., "Gas Hydrates, Problem or Source of Energy", presented at International Non-Renewable Energy Sources Congress, December 26-30, 1993, Tehran, Iran. Published in *the Congress Proceedings*, 701-715, (1993d).

Tohidi, B., Burgass, R. W., Danesh, A. and Todd, A. C., "Experimental Study on the Causes of Disagreements in Methane Hydrate Dissociation Data", paper presented

Tee, S. L., Gotoh, S., and Stewart, W. E., "Molecular Parameters for Normal Fluids", *I & EC Fundam.*, **5**(3), 363-367, (1966).

Tohidi, B., Burgass, R. W., Danesh, A., and Todd, A. C., "Gas Hydrate Formation and Inhibition Prediction", Proceedings of IChemE SONG Conference, Hydrate 92, London, 24 June 1992, *Conference Proceedings*.

Tohidi, B., Burgass, R. W., Danesh, A. and Todd, A. C. "Measurement and Prediction of Amount and Composition of Equilibrium Phases in Heterogeneous Systems Containing Gas Hydrates", presented at the *SPE student paper contest,* September 6, 1993, Aberdeen, Scotland, (1993a).

Tohidi, B., Burgass, R. W., Danesh, A. and Todd, A. C., "Hydrate Inhibition Effect of Produced Water, Part-1. Ethane and Propane Simple Gas Hydrates", presented at SPE Offshore Europe 93, September 7-10, 1993, Aberdeen, Scotland. Published in the *Conference Proceedings*, **1**, 255-264, (1993b).

Tohidi, B., Burgass, R. W., Danesh, A. and Todd, A. C., "Gas Hydrates Modelling, Effect of Gas Solubility in Saline Water", presented at International Non-Renewable Energy Sources Congress, December 26-30, 1993, Tehran, Iran. Published in *the Congress Proceedings*, 602-612, (1993c).

Tohidi, B., Burgass, R. W., Danesh, A. and Todd, A. C., "Gas Hydrates, Problem or Source of Energy", presented at International Non-Renewable Energy Sources Congress, December 26-30, 1993, Tehran, Iran. Published in *the Congress Proceedings*, 701-715, (1993d).

Tohidi, B., Burgass, R. W., Danesh, A. and Todd, A. C., "Experimental Study on the Causes of Disagreements in Methane Hydrate Dissociation Data", paper presented

at International Conference on Natural Gas Hydrates, 20-24 June 1993, New Paltz, New York, USA, *Annals of the New York Academy of Sciences*, **715**, 532-534, (1994a).

Tohidi, B., Danesh, A., Burgass, R. W., and Todd, A. C., "Hydrates Formed in Unprocessed Wellstreams", SPE 28478, the SPE 69th Annual Conference and Exhibition, 25-28 September 1994, New Orleans, USA, Published in *the Conference Proceedings*, Π, 157-167, (1994b).

Tohidi, B., Danesh, A., Burgass, R. W., and Todd, A. C., "Phase Equilibria in the Presence of Saline Water Systems and Its Application to the Hydrate Inhibition Effect of Produced Water", SPE 28884, presented at the European Petroleum Conference, 25-27 October 1994, London, UK, Published in *the Conference Proceedings*, 169-177, (1994c)

Tohidi, B., Danesh, A., and Todd, A. C., "Modelling Single and Mixed Electrolyte Solutions and its Applications to Gas Hydrates", *Transactions of IChemE*, **73** (Part A), 464-472, May (1995a).

Tohidi, B., Danesh, A., Burgass, R. W., and Todd, A. C., "Measurement and Prediction of the Amount of Gas Hydrates", *proceedings of the BHR Group Conference, Multiphase 95*, 7-9 June 1995, Cannes, France, 519-537, (1995b).

Tohidi, B., Danesh, A., Burgass, R. W., and Todd, A. C., "Gas Solubility in Saline Water and Its Effect on Hydrate Equilibria", *Proceedings of the 5th International Offshore and Polar Engineering Conference (ISOPE-95)*, 11-16 June, the Hague, the Netherlands, (1995c).

Tohidi, B., Danesh, A., Burgass, R. W., and Todd, A. C., "Equilibrium Data and Thermodynamic Modelling of Cyclohexane Gas Hydrates", accepted for publication by *Chemical Engineering Science,* (1995d).

Tsonopoulos, C., and Wilson, G. M., "High-Temperature Mutual Solubilities of Hydrocarbons and Water Part I: Benzene, Cyclohexane and n-Hexane", *AIChE Journal*, **29**(6), 990-999, (1983).

Valderrama, J. O., and Cisternas L. A.: "A Cubic Equation of State for Polar and Other Complex Mixture", *Fluid Phase Equilibria*, **29**, 431-438, (1986).

Valderrama, J. O., "A Generalised Patel-Teja Equation Of State for Polar and Non Polar Fluids and Their Mixtures", *J. Chem. Eng. Japan*, **23**, 87, (1990).

van Cleef, A., and Diepen, G. A. M., *Rec. Trav. Chim.*, **79**, 582 (1960). Also Sloan, E. D., (1990).

van der Waals, J. H., and Platteeuw, J. C.,: "Clathrate Solutions", *Adv. Chem. Phys.*, **2**(1), 1-57, (1959).

Vlahakis, J. G., Chen, H. S., Suwandi, M. S., and Braduhn, A. J., "The Growth Rate of Ice Crystals: Properties of Carbon Dioxide Hydrate, A Review of Properties of 51 Gas Hydrates", Syracuse University Research and Development Report No. 830, prepared for the Office of Saline Water, *U.S. Dept. of the Interior,* Washington, DC, (1972).

von Stackelberg, M. and Müller, H. R., "Feste Gashydrate", *Z. fur Elektrochemie*, **58**, 25, (1954).

Xu, D-H, "Phase Behaviour Modelling of Hydrocarbon Systems for Compositional Reservoir Simulation of Gas Injection Process", *PhD Thesis*, Heriot-Watt University, (1990).

Zuo, Y-X. and Guo, T-M., "Extension of the Patel-Teja Equation of State to the Prediction of the Solubility of Natural Gas in Formation Water", *Chem. Eng. Sci.*, **46**, 3251-3258, (1991).